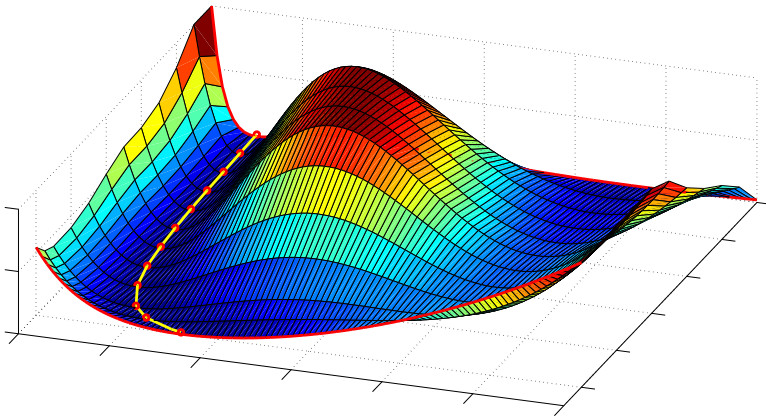




STRUCTURE AND CONVEXITY EXPLOITATION IN NONLINEAR CHEMICAL PROCESS MODELING AND ESTIMATION



Julián Eduardo Bonilla Alarcón

Dissertation presented in partial
fulfillment of the requirements for
the degree of Doctor
in Engineering

May 2011

STRUCTURE AND CONVEXITY EXPLOITATION IN NONLINEAR CHEMICAL PROCESS MODELING AND ESTIMATION

Julián Eduardo Bonilla Alarcón

Jury:

Prof. dr. ir. Paul Sas, voorzitter

Prof. dr. ir. Jan Van Impe, promotor

Prof. dr. ir. Bart De Moor, promotor

Prof. dr. Moritz Diehl, promotor

dr. ir. Filip Logist, promotor

Prof. dr. ir. A. C. P. M. Backx (TU/e)

Prof. dr. ir. Joos Vandewalle

Prof. dr. ir. Ilse Smets

Prof. dr. ir. Jan Degrève

Dissertation presented in partial
fulfillment of the requirements for
the degree of Doctor
in Engineering

May 2011

© Katholieke Universiteit Leuven – Faculty of Engineering
Department of Chemical Engineering
W. De Croylaan 46, B-3001 Leuven (Belgium)

Alle rechten voorbehouden. Niets uit deze uitgave mag worden vermenigvuldigd en/of openbaar gemaakt worden door middel van druk, fotocopie, microfilm, elektronisch of op welke andere wijze ook zonder voorafgaande schriftelijke toestemming van de uitgever.

All rights reserved. No part of the publication may be reproduced in any form by print, photoprint, microfilm or any other means without written permission from the publisher.

Legal depot number D/2011/7515/69
ISBN 978-94-6018-367-6

A mi madre y mis hermanos.

Foreword

I would like to thank the people that have been behind this work at the academic and personal levels. I thank prof. Alfonso Muñoz and the Automation Department at the Universidad de Ibagué, (Ibagué-Colombia), prof. De Keyser at Universiteit Gent and the founding project ALFA-LABIOPROC for facilitating my move to Europe to start my research in 2005. I Thank prof. Vandewalle and prof. De Moor for accepting me as a PhD student at ESAT/SCD in 2007, to prof. Van Impe for allowing me to move to his group at CIT/BioTeC to finish my PhD and to the founding project IUAP P6/04 (DYSCO).

I express my gratitude to prof. Diehl for the exciting discussions on optimization since the beginning of my PhD and to Dr. Logist for the inspiring comments on my work and the nice team-spirit he maintains at the office. I thank prof. Van Impe, prof. De Moor, prof. Diehl, Dr. Logist, prof. Backx (TU-Eindhoven), prof. Vandewalle, prof. Smets, prof. Degrève and prof. Sas (chairman), for being part of my evaluation committee, for the motivating comments on my work and the suggestions to improve the final version of this dissertation. I specially thank prof. Backx for taking the time to come from Eindhoven.

I express my appreciation to my colleagues at BioTeC and SMC for the enjoyable moments in both labs in the last four years. I also thank the administrative and technical personnel at BioTeC and SCD for making my particular administrative procedures easier. I express my gratitude to Alexandra, Carlos, Sandra, Anderson, Clara, Yves, Lia and Kristiaan for their friendship during these years in Belgium. I also thank Maaïke for her help and patience these last months. Last but not least I thank to the Latin community in Gent and Leuven for the laughs and the nice moments that made me feel at home.

Agradezco a mi familia en Colombia y mis hermanos Constanza y César por los mensajes de motivación durante estos años. Le doy gracias a Amparito por su entrega como madre, sus oraciones y por ser mi ejemplo de lo que se puede lograr cuando se trabaja con dedicación.

Julián E. Bonilla A.
Leuven, May 2011

Abstract

The field of chemical process estimation and control has been intensively explored in the last decades. However, novel applications, the demands required by strict safety regulations, tightening environmental standards, operating constraints and product quality specifications, generate more difficult and challenging situations. This stimulates the need of more sophisticated solutions than the ones that can be provided by traditional techniques alone. *(i)* Exploiting the process model structure along with *(ii)* methods to deal efficiently with estimation and control problems are of paramount importance to reduce the computational load that new techniques often demand. This dissertation explores these two aspects for a particular class of first principles dynamic models. On the one hand, structure exploitation is studied through a widely used input-affine chemical process, namely distillation. A rigorous model is developed for a packed distillation column, leading to large scale differential-algebraic equations (DAEs). It is shown that these DAEs can be reduced by constraints differentiation and algebraic manipulation, preserving the physical meaning of the states in the representation. This kind of models exhibits high differentiation index, making its simulation impossible with off-the-shelf solvers. Hence, a simple procedure, based on the model Jacobian structural properties, is proposed in order to reduce the index of the model. Moreover, the reduced index DAEs are cast such that sparse structures are obtained for simulation tasks, alleviating the computational load when solving the model. On the other hand, input/parameter-affine models are analyzed in the formulation of dynamic optimization problems (DOP). It is shown that a DOP using this kind of models, with convex cost and convex inequality constraints, can be approximated by a convex formulation. This approximation is performed by proposing a parametric optimization problem whose extremes correspond to the original nonconvex DOP and to a convex one. The method is used in the context of optimal control and parameter estimation, such that a simple 2-step approach is proposed as an alternative to the solution of the original nonconvex problem. In this form, the computational load involved in solving a parameterized DOP exactly, is reduced by a simple 2-step convex optimization method that leads to a nearly optimal solution.

Notation

List of symbols

α, β, \dots	Greek symbols, scalars
a, b, \dots	Scalars or vectors variables
A, B, \dots	Matrices
$P(\alpha)$	Parametric problem on α
\bar{x}	Reference or state measured trajectory
$\bar{\bar{x}}$	Noise free or perfect traceable trajectory
\mathcal{L}	Lagrangian function
\mathbb{R}	Set of real variables
$\mathbb{R}^{m \times n}$	Set of real matrices of size $m \times n$
\mathbb{N}	Set of strictly positive integers
$\mathcal{A}(w)$	Active set evaluated at w
\mathcal{C}^2	Space of twice continuous differentiable functions

Basic operations

x^T	Vector transpose
A^{-1}	Matrix inverse
$\ x\ _2$	2-norm of a vector
$\ x\ _Q$	Weighted 2-norm of a vector
$\nabla_w F^T$	Jacobian of F with respect to w
$\nabla_w^2 \mathcal{L}$	Hessian of \mathcal{L} with respect to w
$diag(x)$	Squared diagonal matrix with vector x as diagonal
$>, \geq,$	Scalar inequality
\succ, \succeq	Matrix inequality

Abbreviations

CIT	Chemische Ingenieurstechniken
CG	Conjugate gradient algorithm
CPE	Chemical process engineering
CSTR	Continuous stirred tank reactor
CVX-OP	Convex optimization problem
DAE	Differential-algebraic equation
DES	Differential equations solver
DMS	Direct multiple shooting
DOP	Dynamic optimization problem
DSS	Direct single shooting
FRBM	Full rate based model
KKT	Karush-Kuhn-Tucker
MPC	Model predictive control
NMPC	Nonlinear model predictive control
NLP	Nonlinear programming problem
OCP	Optimal control problem
ODE	Ordinary differential equation
OP	Optimization problem
PCG	Preconditioned conjugate gradient algorithm
PEP	Parameter estimation problem
QP	Quadratic programming problem
RBM	Rate base model
RHC	Receding horizon control
RORBM	Reduced order rate based model
SSE	Sum of squared errors
SOSC	Second order sufficient conditions
SQP	Sequential quadratic programming
s.t.	Subject to
a.e.	Almost everywhere

Contents

Contents	ix
List of Figures	xiii
List of Tables	xvii
1 General introduction	1
1.1 Motivation	1
1.2 Research objectives	3
1.3 Chapter by chapter overview	3
1.4 Contributions	6
2 Dynamic optimization: theory and numerical methods	9
2.1 Optimization problems	9
2.2 Optimality conditions	12
2.3 Solving nonlinear programming problems	15
2.4 Dynamic optimization problems	18
2.5 Direct methods for dynamic optimization	23
2.6 Conclusions	29

I	Model structure exploitation for simulation of separation processes	31
3	An equilibrium model for the CIT distillation column	33
3.1	Pilot plant description	33
3.2	Equilibrium based approach for distillation	35
3.3	Dynamic simulation	43
3.4	Sensitivity analysis of model parameters	45
3.5	Conclusions	48
4	A rate based model for separation in packed columns	53
4.1	The rate based model	55
4.2	Reduced order rate based model	60
4.3	Steady state model simulation	70
4.4	Steady state parameter estimation of the reduced order rate based model	87
4.5	Dynamic simulation	91
4.6	Conclusions	105
II	Convexity exploitation in dynamic optimization problems	109
5	A homotopy-based convex approximation of input-affine optimal control problems	111
5.1	A convex-homotopy based method for the solution of optimal control problems	112
5.2	Optimal control numerical example	120
5.3	Receding horizon control numerical example	125
5.4	Discussion of the homotopy approach	130
5.5	Conclusions	132

6 A near optimal solution to parameter estimation problems with parameter-affine dynamics embedded	133
6.1 Convexification of parameter estimation problems with parameter-affine models	133
6.2 A 2-step procedure for the solution of estimation problems with parameter-affine dynamics embedded	136
6.3 Automatic initialization for PEP in simultaneous optimization . .	143
6.4 Conclusions	152
7 General conclusions and future work	155
7.1 Concluding remarks	155
7.2 Future work	157
A Correlations for calculation of thermodynamic properties	161
A.1 Correlations for binary mixtures	161
A.2 Pure components properties and coefficients	174
A.3 Structural parameters for sulzer CY packing	175
A.4 List of properties and variables used in distillation models	178
Bibliography	179
Curriculum vitae	187
Publications by the author	187

List of Figures

1.1	General structure of the thesis.	4
2.1	Convex and non-convex optimization problems	10
2.2	Dynamic optimization problem classical scenarios.	20
2.3	Receding horizon control scenario.	22
2.4	Direct single shooting parameterization	25
2.5	Direct multiple shooting (DMS) parameterization	27
3.1	General layout of the distillation set-up at CIT	35
3.2	Equilibrium stage	37
3.3	Equilibrium model dynamic response to changes in the reflux and reboiler duty	46
3.4	Steady state profiles obtained from equilibrium model and real process	47
3.5	Change in reboiler temperature response due to changes in the process inputs	49
3.6	Change in top temperature dynamic profile due to changes in the process input	50
3.7	Norm (3.31) on the change of temperature and liquid composition with respect to the 12 equilibrium model parameters	51
4.1	Non-equilibrium stage in the rate based model.	54
4.2	Temperature profiles using the proposed initialization approach . .	73

4.3	System Jacobian for a 5 stages column using the FRBM	77
4.4	Steady state trajectories for the full rate based model	81
4.5	System Jacobian for a 5 stages column using the RORBM	82
4.6	Steady state trajectories using the RORBM	84
4.7	Norm on the sensitivity of some RORBM states with respect to model parameters	86
4.8	Boiling point diagram for the mixture of methanol-isopropanol using parameters initial values	88
4.9	Experimental data used for estimation	89
4.10	Fitted and validation results for the steady state PEP	92
4.11	Boiling point diagram for the mixture of methanol-isopropanol with optimized parameters	93
4.12	Incidence matrix for a 3 stages distillation system using the RORBM.	97
4.13	RORBM response to ± 10 percent changes in the reboiler duty and the reflux	100
4.14	Dynamic sensitivities of the bottom temperature with respect to model parameters	103
4.15	Dynamic sensitivities of the top temperature with respect to model parameters	104
4.16	Norm on the dynamic sensitivity of some RORBM with respect to model parameters	105
5.1	Some possible behaviors of the homotopy path in the space	120
5.2	Isothermal CSTR.	122
5.3	Steady state gain for the CSTR process for different values of the input concentration $C_{a,0}$	123
5.4	Original cost for the CSTR open loop optimal control problem.	124
5.5	Homotopy map for an OCP using a CSTR model	125
5.6	Behavior of the norm on $\ x_c - x\ _J^2$ as a function of the homotopy parameter.	126
5.7	Perfect traceable trajectory in the homotopy map for the OCP	126

5.8	Tracking and disturbance test for the NMPC applied to the CSTR	128
5.9	Computational demand for the studied test scenario with $N_u = 1$.	129
5.10	Optimal control trajectory provided by the optimization methods.	129
5.11	Computational cost for the studied test scenario in Figure 5.12 with increased control horizon $N_u = 30$.	130
5.12	Tracking and disturbance test for the NMPC applied to the CSTR with increased control horizon	131
6.1	Chaotic behavior of Lorenz attractor, $\sigma = 10$, $\beta = 8/3$ and $\rho = 28$ (a), and noisy data used for estimation (b).	135
6.2	Costs for different approaches $\sigma = 10$, $\beta = 8/3$. The data has been contaminated with noise in the range 100 to 150 Hz (left) and 400 to 450 Hz (right).	136
6.3	Cost functions generated by the PEP of a harmonic oscillator.	143
6.4	Sparsity patterns for the Jacobians in a multiple shooting parameterization.	145
6.5	Data set for the PEP of the Lotka-Volterra model.	146
6.6	Convergence results for the SGN method applied to the PEP in the Lotka-Volterra model.	148
6.7	Data for the formaldehyde-sodium p-phenol sulfonate reaction PEP.	150
6.8	Convergence results using the SGN method for the PEP in the numerical example	152

List of Tables

3.1	Summary of variables and equations involved in the equilibrium based model proposed in Diehl (2002).	42
3.2	Initial guess for parameters in the equilibrium model for the CIT column.	44
3.3	Manipulated variables in the CIT distillation setup.	44
4.1	Summary of variables and equations involved in the RBM proposed in Taylor and Krishna (1993).	61
4.2	Summary of variables and equations involved in the reduced order RBM.	69
4.3	Initial guess for parameters in the rate based model.	79
4.4	Nonlinear equation solver statistics when no information about the Jacobian pattern is provided in the FRBM.	80
4.5	Nonlinear equation solver statistics when the Jacobian pattern and its bandwidth are provided in the FRBM	80
4.6	Nonlinear equation solver statistics when no information about the Jacobian pattern is provided in the RORBM.	83
4.7	Nonlinear equation solver statistics when the Jacobian pattern and its bandwidth are provided in the RORBM.	83
4.8	Performance comparison between the full rate based model and the reduced rate based model when sparsity is exploited.	83
4.9	Steady state experiments used for identification and validation. . .	89
4.10	Initial and optimized parameters for the steady state RORBM. . .	90

4.11	Actuator related and vapor holdup parameters in the RORBM. . .	101
4.12	RORBM parameters and its influence on the dynamic and static response.	106
5.1	CSTR parameters and nominal conditions.	122
6.1	Optimum values for the PEP of the Lorenz attractor with $\rho = 28$. . .	136
6.2	Algorithm parameters for the Lotka-Volterra PEP using arbitrary and convex initialization approaches.	148
6.3	Reaction rates for the batch reaction of formaldehyde with sodium p-phenol sulfonate.	149
6.4	Algorithm parameters for the complex batch reaction PEP using arbitrary and convex initialization approaches.	151
A.1	Component parameters for the binary mixture.	175
A.2	Pure component coefficients for different properties of methanol CH_4O , ($i = 1$)	176
A.3	Pure component coefficients for different properties of isopropanol C_3H_8O , ($i = 2$)	177
A.4	Geometry parameters of Sulzer CY packing (Kister, 1992).	178

Chapter 1

General introduction

1.1 Motivation

A considerable amount of chemical process engineering (CPE) efforts are still oriented towards modeling and control of individual processing units, e.g., distillation columns, chemical reactors, heat exchangers among others. Although the field of chemical process engineering has been widely explored in the last four decades, the stringent demands required by strict safety regulations, tightening environmental standards, operating constraints and product quality specifications create more difficult and challenging problems (Lukszo et al., 2006), (Harold and Ogunnaike, 2000). These problems require more sophisticated solutions than the ones that can be provided by traditional techniques alone (Engell, 2007). Modeling, estimation and control are three key aspects in CPE. Detailed models for process simulation normally lead to an increased complexity in the formulation. Nevertheless, they are essential for e.g., experimental design, rapid evaluation of control techniques, decision-making and operator training tasks, among others. Certain degree of detail creates challenges at the level of the computational efficiency in solving those models. Particularly, in a field such as CPE, where detailed chemical and thermodynamic relations normally lead to nonlinear behavior and may be used in companion with a large number of equations and variables that describe the process. Grossmann and Westerberg (2000) highlight two of the major challenges in computational requirements for chemical process engineering, *(i)* the computation requirements increase with the problem size, and *(ii)* models might be used in a real-time environment where constraints in computation time are hard. Hence, the development of detailed models must be accompanied with computationally efficient methods to solve them. Moreover, when these models are intended to be used in more advance

online strategies, it is necessary to find an efficient problem representation so that computational constraints can be satisfied.

The first part of this dissertation concentrates on a very common unit operation in CPE, namely distillation, with the goal of developing a model that allows for detailed simulation while computationally efficient. Models for distillation exist in a wide range, but mainly divided in black box (Waller and Böling, 2005), (Karacan et al., 2007) and white box models. The latter are clearly differentiated in thermodynamic equilibrium, (Gani et al., 1986), (Skogestad, 1992), (Flatby et al., 1994), (Wittgens and Skogestad, 2000) and nonequilibrium based models (Khrishnamurthy and Taylor, 1985), (Kooijman, 1995), (Guo et al., 2004), (Kenig and Seferlis, 2009). Rigorous first principle models for distillation normally lead to large scale nonlinear differential-algebraic equations (DAEs). The large scale issue becomes more serious when nonequilibrium formulations are used, since the number of equations can easily triplicate the ones of an equilibrium based formulation. In this case, reduction of model complexity based on approximating physical properties is normally performed (Peng et al., 2003). Nevertheless, this stage-wise process exhibits a lot of structure due to the local interaction between variables of stages which are adjacent. Hence, it is possible to exploit first principles model structure in order to efficiently deal with the number of variables and equations used to describe the model dynamics.

In addition to the internal model structure, distillation columns along with continuous stirred tank reactors (CSTRs) and other dynamic processes, belong to a particular class of models, namely input-affine dynamic models. This feature can be exploited when formulating dynamic optimization problems (DOPs) (Kirk, 1970). DOPs with nonlinear models embedded and process constraints normally lead to *Nonlinear programming problems* (NLPs) (Nocedal and Wright, 2006), which, due to the nonlinear nature of the model, are inherently nonconvex (Boyd and Vandenberghe, 2006). Nonconvex problems are in general more difficult to solve and methods to solve them usually depend on local convex approximations e.g., *sequential quadratic programming* (SQP) methods. The advantages of using convex formulations lie not only in the fact that local solutions are global, but also in the feature that algorithms exhibit polynomial-time convergence, and that efficient methods to solve such convex problems are well developed (Karmarkar, 1984), (Nesterov and Nemirovski, 1995).

Additionally, there are other kinds of methods that attempt to tackle the nonconvex problem in a different form. On the one hand, some approaches are based on relaxation techniques that convexify the problem by iteratively finding convex upper and lower bounds (McCormick, 1976). The use of spatial Branch and Bound methods (B&B) (Horst and Tuy, 1996) combined with the convex relaxation of Bolza-type functionals has been proposed for the solution of parameterized nonconvex DOPs (Singer and Barton, 2006). Nevertheless, there is still a lot of ongoing work in improving the computational demand of B&B methods and

finding tighter convex relaxations to functionals with embedded dynamic equations (Chachuat et al., 2006). On the other hand, mathematicians and practitioners have realized that several nonconvex optimization problems may be reformulated so that the new formulation exhibits convexity (Boyd et al., 1998), (Demeulenaere et al., 2004), (Verscheure et al., 2009). This is performed by analyzing the structure of the DOP and/or reformulating the optimization problem in a different search space when possible.

Consequently, finding convex formulations of optimization problems and exploiting model structure are necessary steps to efficiently tackle problems that involve a large number of variables, problems that often appear in the field of chemical process engineering.

1.2 Research objectives

This research is organized around two major tasks:

- To *exploit structure* in optimization tasks involving large-scale first-principle models, in particular *distillation*.
- To *look for reformulations* of nonconvex dynamic optimization problems arising in chemical processing so that *convexity* can be exploited in a different form than by linearizing the model and the problem constraints.

1.3 Chapter by chapter overview

The thesis is divided into two main parts. The first part deals with rigorous models for a widely used input-affine chemical process, namely, distillation. The second part deals with convex formulations for dynamic optimization problems with input/parameter-affine dynamic systems. Figure 1.1 displays a general layout of the thesis structure. In the following, details of the different chapters are given.

Chapter 2 presents the concepts and methods used along the thesis. It starts with introducing optimization concepts highlighting the importance of dealing with convex optimization problems. The general dynamic optimization problem (DOP) is formulated, providing the differentiation between optimal control problems (OCP), parameter estimation problems (PEP) and receding horizon control (RHC). Direct approaches for the parameterization of DOPs are presented. In particular, details for single and multiple shooting parameterization are explained. Moreover, the nonlinear programming problem (NLP) resulting from the use of direct

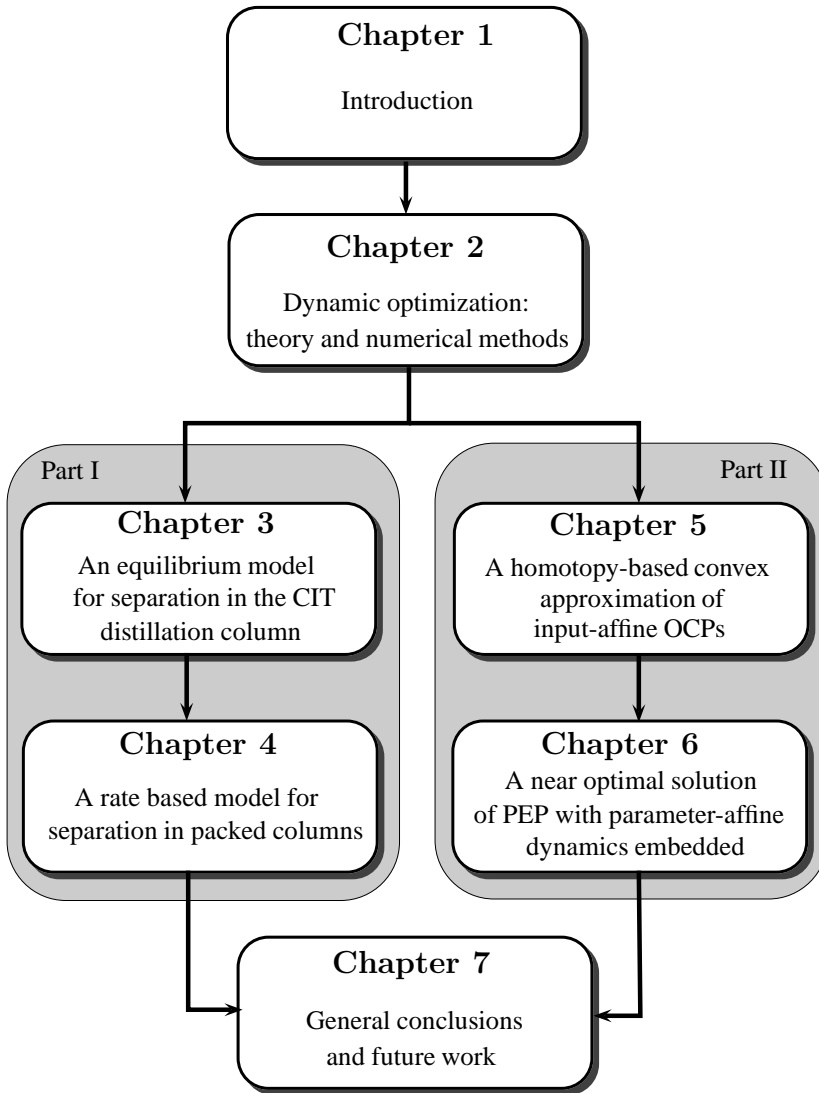


Figure 1.1: General structure of the thesis.

methods is introduced along with the necessary optimality conditions that a solution to this problem must satisfy. Numerical methods to solve the problem based on the differentiability of the functions in the NLP are presented at the end of the chapter. These methods are the bases for the programmed algorithms used in the second part of the thesis.

Part I: Model structure exploitation for simulation of separation processes

Part I deals with a particular kind of input-affine process that is widely used in the chemical industry, namely distillation. In this part, rigorous models for tray-based and packed columns are studied. The models are intended to be used for prediction and control of a real setup, installed at the *Department of Chemical Engineering (CIT)* at K.U.Leuven.

Chapter 3 presents a tray-based distillation model for the separation of a binary mixture in the CIT distillation column. The model is an adaptation of the system presented in Diehl et al. (2001) and Diehl (2002). The model based on differential-algebraic equations is presented along with the required thermodynamic correlations for the calculation of physical and chemical properties. Contrary to other models presented in literature, the DAE is formulated in terms of the dynamic variables composition, temperature and molar holdups. Hence, an analytical differentiation of energy balances is presented. A particular reorganization of model states is proposed in order to obtain sparse and banded Jacobian matrices for simulation and optimization. The observability of model parameters with respect to available measurements is studied through a sensitivity analysis.

Chapter 4 develops a rate based model (RBM) for distillation in packed columns. The model is cast as a set of DAEs. The large scale DAEs are reduced by differentiating part of the algebraic equations and algebraic manipulation. The origin of the higher index problem for this kind of models is analyzed and methods for reducing the high index for this particular system are proposed. It is shown that neglecting part of the dynamics allows for easy simulation of the large scale problem. A particular arrangement of model states and equations is proposed so that the model Jacobian is sparse and banded. This structure is exploited in the simulation and optimization task by off-the-shelf solvers. Finally, a sensitivity analysis of model parameters with respect to available measurements is presented indicating that a reduction in the search space for the PEP is possible.

Part II: Convexity exploitation in dynamic optimization problems

The second part of the thesis concerns convex approximations to dynamic optimization problems with input/parameter-affine dynamics embedded. This part is further divided into two chapters:

Chapter 5 presents a continuation method for the solution of nonconvex optimal control problems. The approach deals with a special class of OCP formulations where the dynamic system involved is control-affine and the objective is a penalty on deviations from a reference state trajectory. The nonconvex OCP is modified by introducing a penalized pseudo state and a homotopy parameter which gradually transforms the original problem into a convex one. Proofs of convergence of the parametric DOP to the convex and original OCP are provided. The method solves first the convex formulation and uses the result to initialize the solution of the next problem on the zero path, recovering the original OCP. Numerical examples are presented where the method outperforms a local optimization technique.

Chapter 6 introduces an initialization approach for parameter estimation problems (PEPs) involving parameter-affine dynamic models. By using the state measurements, the nonconvex PEP is modified so that a convex approximation to the original PEP is obtained. The modified problem is solved by convex optimization methods yielding an approximate solution to the original PEP. The approximate solution can be further refined by linearizing the original problem around the obtained minimum. An assessment of the distance between the real solution and the one provided by the linearization of the problem around the convex approximation is presented. The optimum obtained by the convex approximation is used to subsequently initialize a simultaneous Gauss–Newton (SGN) approach to the original nonconvex PEP. Comparative results for the SGN with arbitrary initialization and with the proposed approach are presented using benchmark examples in the chemical and biological fields.

Chapter 7: In this chapter general conclusions and future work are presented.

Appendix A Contains all the thermodynamic correlations required for the simulation of the distillation models used in Chapter 3 and Chapter 4.

1.4 Contributions

There are two major contributions in this dissertation, which are the basis of the division into two parts. On the one hand, model formulation, reduction and structure exploitation for simulation in distillation processes is developed in Chapters 3 and 4. On the other hand, in Chapters 5 and 6 convexification methods for DOP with input/parameter affine dynamics are developed. Details of these contributions are as follows:

- In Chapter 3 the first contribution of this dissertation is presented. It lies in the modification of an existing rigorous model for distillation in tray based columns using equilibrium and tray efficiencies. Although an existing model is presented in Diehl (2002), the model is fixed to a particular mixture and correlations are not easily found in literature. In the modified version presented here, all the correlations used for the calculation of thermodynamic properties are easily traced back to the existing literature so that the model can be used for separation of different kind of binary mixtures by simply modifying well-known correlation coefficients. This leads to an equilibrium model that can be easily adapted to new operating conditions. Moreover, the model is formulated so that sparsity can be exploited at the simulation level.
- In Chapter 4 a rigorous first principle Rate Based Model (RBM) for distillation in packed columns is formulated. A completely documented set of thermodynamic properties required for its simulation is provided. It is shown that a model reduction of around 30% in the number of algebraic variables is possible by simple algebraic manipulation and constraint differentiation. An analysis of the high index problem for this kind of system is performed, highlighting the origins of the problem and providing a simple solution by neglecting part of the fast dynamics of the process. Moreover, the reduced index model is formulated in such form that Jacobian matrices, needed for simulation and optimization tasks, have a sparse and banded structure that can be exploited by sparse linear algebra solvers. Finally, sensitivity analysis of the reduced state index-1 RBM is performed, indicating that with a limited set of measurements only a reduced set of its model parameters can be estimated. This leads to a reduced search space for the parameter estimation problem (PEP). Additionally, a novel set of parameter constraints for the RBM PEP is presented. This set of constraints is intended to be used in PEP so that the tuned model leads to state trajectories that are physically possible.

These contributions are reported in

- J. Bonilla, F. Logist, J. Degreve, B. De Moor, and J. Van Impe. A rate based model for distillation in packed columns: Sensitivity analysis and structure exploitation. *Submitted*, 2011.
- J. Bonilla, F. Logist, J. Degreve, B. De Moor, and J. Van Impe. A rate based model for distillation in packed columns: Dynamic simulation and the index problem. *Submitted*, 2011.
- J. Bonilla, F. Logist, B. De Moor, and J. Van Impe. Parameter estimation of a rigorous rate based model for distillation in packed columns. *In proceedings of the 18th World Congress of the International Federation of Automatic Control*, Milan-Italy, August 2011.

- In Chapter 5 it is shown that an *Optimal Control Problem* OCP with input-affine dynamics can be transformed through a particular homotopy, yielding a related convex OCP. The solution of this convex problem generates an approximation to the original nonconvex formulation, so that this solution can be used to initialize a new OCP on the path of minimizers of the parametric problem. Proofs of convergence of this parametric OCP to the original and its convex formulation are provided through Lemmata 5.1.1, 5.1.2 and 5.1.3 in Section 5.1. In addition, conditions for continuity of the path of minimizers between the convex solution and the solution of the original OCP are related to the KKT conditions of the parametric OCP in view of a well developed theory for homotopy methods (Watson, 2000).

These contributions are published in

- J. Bonilla, M. Diehl, F. Logist, B. De Moor, J. Van Impe, A convexity-based homotopy method for nonlinear optimization in model predictive control. *Optimal control applications and methods*, Vol 31 (5), p. 393–414, 2010.
- J. Bonilla, M. Diehl, F. Logist, B. De Moor, and J. Van Impe. A suboptimal solution to nonconvex optimal control problems involving input-affine dynamic models. *20th European Symposium on Computer Aided Process Engineering–ESCAPE20*, Ischia-Italy, 2010.
- In Chapter 6 the method presented in Chapter 5 is refined for PEPs. A novel approach to calculate the solution of nonconvex PEPs is proposed. The method only requires to solve sequentially two convex problems. It is shown in Theorem 6.2.2 that the distance between the near optimal solution and the optimal one is of second order in the size of the measurement and modeling errors. In addition, it is numerically illustrated that the method improves convergence when used with efficient simultaneous optimization routines. Contributions in this chapter are published in
 - J. Bonilla, M. Diehl, F. Logist, B. De Moor, J. Van Impe. An automatic initialization procedure in parameter estimation problems with parameter-affine dynamic models. *Computers and Chemical Engineering*, 34, 953–964, 2010.
 - J. Bonilla, M. Diehl, F. Logist, B. De Moor, and J. Van Impe. A convex approximation for parameter estimation involving parameter-affine dynamic models. *In Joint 48th IEEE Conference on Decision and Control and 28th Chinese Control Conference*, p. 4670–4675, Shanghai-China, December, 2009.
 - J. Bonilla, M. Diehl, B. De Moor, J. Van Impe. A nonlinear least squares estimation procedure without initial parameter guesses. *In Proceedings of the 47th IEEE Conference on Decision and Control* p. 5519–5524, Cancún-Mexico, December 2008.

Chapter 2

Dynamic optimization: theory and numerical methods

This chapter presents the basic concepts used throughout the document. In Section 2.1 basic concepts on optimization and convex optimization problems are given in order to show the advantages of dealing with convex problems. Section 2.2 presents the optimality conditions for optimization problems. Section 2.3 discusses classical methods used to solve the nonlinear programming problems obtained from the parameterization of dynamic optimization formulations. Section 2.4 introduces standard forms for the dynamic optimization problem obtained from optimal control and parameter estimation tasks. Section 2.5 presents direct methods for the solution of dynamic optimization problems, particularly single and multiple shooting. Those methods are the basis of the algorithms used in Chapter 6 for the efficient solution of parameter estimation problems. Conclusions to the chapter follow in Section 2.6.

2.1 Optimization problems

In this section the bases of optimization problems (OP) are presented. For a deep review the reader is referred to Boyd and Vandenberghe (2006) and Nocedal and Wright (2006). Features that lead to convexity in an OP are highlighted due to the advantages of convex formulations with respect to nonconvex ones.

An optimization problem

$$\text{NLP : } \min_w F(w) \quad \text{subject to} \quad \begin{cases} G_i(w) = 0, & i = 1, \dots, n_G, \\ H_j(w) \geq 0 & j = 1, \dots, n_H, \end{cases} \quad (2.1)$$

with $w \in \mathbb{R}^{n_w}$, $F \in \mathcal{C}^2 : \mathbb{R}^{n_w} \rightarrow \mathbb{R}$, $G \in \mathcal{C}^2 : \mathbb{R}^{n_w} \rightarrow \mathbb{R}^{n_G}$ and $H \in \mathcal{C}^2 : \mathbb{R}^{n_w} \rightarrow \mathbb{R}^{n_H}$, is a mathematical problem where it is required to find the best value of a variable w that lies in a predefined region Ω in the space of w . Optimization problems are, in general, defined by a cost $F(w)$ and a *feasible set* Ω . The feasible set is defined in (2.1) by the constraints imposed on the values of the optimization variable, i.e., each $w \in \Omega$ must satisfy the *equality constraints* $G_i(w) = 0$ and the *inequality constraints* $H_j(w) \geq 0$. The cost defines the function that needs to be minimized or maximized while the constraints define the limits of the search space for the optimization variable. There exist several types of cost functions, and feasible sets. However, a major classification is related to the complexity they imply when used in an OP. Assuming smooth cost functions and feasible sets, hence constraints, they can be classified in convex and nonconvex. Herein, these concepts are introduced formally since they are used in Chapters 5 and 6.

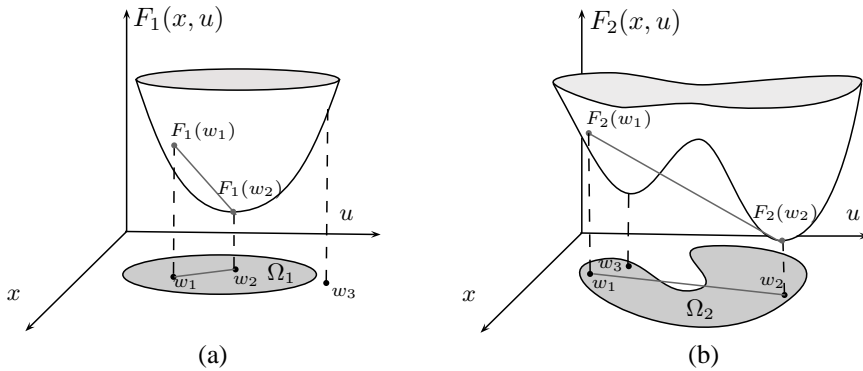


Figure 2.1: Convex (a) and nonconvex (b) optimization problems. The vector w has been defined as $w = [x, u]^T$.

Definition 2.1.1 (Convex set). A set Ω is called convex iff for every pair of points in Ω , Ω contains the straight line segment that joins those points.

The sets Ω_1 and Ω_2 in Figure 2.1(a) and (b) are examples of convex and nonconvex sets, respectively.

Definition 2.1.2 (Convex function). A real valued function, $F : \mathbb{R}^{n_w} \rightarrow \mathbb{R}$ in a domain which is a convex set, is convex iff for any two points w_1 and w_2 in the domain of F and any $\lambda \in [0, 1]$

$$F(\lambda w_1 + (1 - \lambda)w_2) \leq \lambda F(w_1) + (1 - \lambda)F(w_2), \quad (2.2)$$

i.e., the line segment that connects $(F(w_1), w_1)$ and $(F(w_2), w_2)$ must lie above the graph of $F(w)$. The functions F_1 and F_2 in Figure 2.1 are examples of convex and nonconvex functions, respectively.

Definition 2.1.3 (Convex optimization problem (Boyd and Vandenberghe, 2006)). A problem of the form (2.1) is convex, iff:

- $F(w)$ is a convex function,
- $-H_j(w)$ is a convex function¹,
- $G_i(w)$ is an affine map of w , i.e., $G_i(w) = a_i^T w + b_i$, $a_i \in \mathbb{R}^{n_w}$, $b_i \in \mathbb{R}$.

Remark 2.1.1. Nonlinearities in the inequality constraints and cost do not necessarily imply nonconvexity in the problem. In contrast to this, nonlinearity in the equality constraints directly makes the problem nonconvex.

Definition 2.1.4 (Feasible point). A point w in the domain of $F(w)$ is said to be feasible if it satisfies the constraints, i.e., $w \in \Omega$. Otherwise, it is called an infeasible point.

The point w_3 in Figure 2.1(a) corresponds to an infeasible point while w_1 and w_2 are feasible points.

Definition 2.1.5 (Infeasible optimization problem). An optimization problem is said to be infeasible if its feasible set is empty, i.e., there exist no value of w that satisfies all the constraints.

This is an important concept since by definition there exists no solution to an infeasible OP. However, by relaxing the OP, i.e., dropping or modifying constraints, feasibility can be regained.

The solution to an optimization problem can be classified as:

Definition 2.1.6 (Global solution). The point $w^* \in \Omega$ is said to be a global solution to the problem (2.1) iff $F(w^*) \leq F(w)$ for all $w \in \Omega$.

The point w_2 in Figure 2.1(b) corresponds to a global minimum to the optimization problem defined by $F_2(w)$ and Ω_2 .

¹The minus sign is introduced to be consistent with the notation used in this document.

Definition 2.1.7 (Local solution). The point $w^* \in \Omega$ is said to be a local solution of the problem (2.1) iff there exists a neighborhood S of w^* so that $F(w^*) \leq F(w)$ for all $w \in S \cap \Omega$.

The point w_3 in Figure 2.1(b) corresponds to a local minimum to the optimization problem defined by $F_2(w)$ and Ω_2 , since it is possible to choose an S around w_3 for which definition 2.1.7 holds.

The previous concepts clearly differentiate convex optimization problems (CVX-OP) from nonconvex ones. This differentiation is presented since CVX-OP exhibit several advantages with respect to nonconvex problems as presented in Boyd and Vandenberghe (2006):

- Local solutions are global.
- Very efficient numerical methods to solve CVX-OP exist.
- Initialization is not an issue.
- Convergence rates are guaranteed.
- Can handle efficiently large scale problems.

The conditions that a point w has to satisfy to be a solution of (2.1) are explained in the following paragraphs since they form the basis of the algorithms used to solve the optimization problem.

2.2 Optimality conditions

As mentioned before, every w that satisfies the constraints is called a *feasible point*. Note that at every feasible w there may be some components $j \in \mathbb{N}^{n_H}$ of $H(w)$, i.e., $H_j(w)$, that satisfy $H_j(w) = 0$, those are called *active inequality constraints* $H^{\text{act}}(w)$. Others for which $H_j(w) > 0$ holds, are called *inactive inequality constraints* $H^{\text{inact}}(w)$. The *active set function* for a feasible point w is defined as

$$\tilde{G}(w) = \left(\begin{array}{c} G(w) \\ H^{\text{act}}(w), \end{array} \right) \quad (2.3)$$

i.e., $\tilde{G}(w)$ groups all the constraints that lead to equalities when evaluated at the feasible point w . All the constraints that belong to $\tilde{G}(w)$ are called *active*

constraints. The constraints that are left, i.e., the ones which do not belong to $\tilde{G}(w)$, are called *inactive constraints*.

A *regular point* w is a feasible point for which $\nabla_w \tilde{G}(w)$ is full rank. This property is required, e.g. when solving equality constrained problems obtained from the sub-QP in the sequential quadratic programming algorithm (see Section 2.3.2).

Solving (2.1) implies finding a value w^* that minimizes the cost and satisfies the constraints. In order to formulate the optimality conditions, the *Lagrangian* function is defined

$$\mathcal{L}(w, \lambda, \mu) = F(w) - \lambda^T G(w) - \mu^T H(w), \quad (2.4)$$

with the Lagrange multipliers $\lambda \in \mathbb{R}^{n_G}$ and $\mu \in \mathbb{R}^{n_H}$.

First order optimality conditions

The necessary conditions for a point w^* to be a local solution to (2.1) are summarized in the following theorem due, independently, to Karush (1939) and Kuhn and Tucker (1951). These conditions are widely known as the *first order optimality conditions* or *Karush–Kuhn–Tucker* (KKT) conditions (Nocedal and Wright, 2006).

Theorem 2.2.1 (KKT conditions). *If a regular point² w^* is a local solution to the NLP, then there exist Lagrange multipliers λ^* and μ^* so that the following conditions are satisfied:*

$$\nabla_w \mathcal{L}(w^*, \lambda^*, \mu^*) = 0, \quad (2.5)$$

$$G(w^*) = 0, \quad (2.6)$$

$$H(w^*) \geq 0, \quad (2.7)$$

$$\mu^* \geq 0, \quad (2.8)$$

$$\mu_j^* H_j(w^*) = 0, \quad \forall j = 1, \dots, n_H \quad (2.9)$$

A point that satisfies the KKT conditions is called a *KKT point*. A proof to Theorem 2.2.1 can be found in (Nocedal and Wright, 2006, p. 323). If the NLP is convex, the KKT conditions are sufficient to guarantee a global solution, see e.g., Boyd and Vandenberghe (2006). Equations (2.5)-(2.9) define a set of nonlinear equations known as the *KKT system*.

²This implies linear independent constraint qualification LICQ (Nocedal and Wright, 2006).

Note that, at the solution, the *complementarity condition* (2.9) implies that the Lagrange multipliers μ_j^* for the inactive constraints $H_j^{\text{inact}}(w^*)$ must be zero. For the set of active inequality constraints $H_j^{\text{act}}(w^*) = 0$ it can happen that the μ_j^* are either zero or positive. Algorithms can identify the active set easier if either $\mu_j^* = 0$ or $H_j(w^*) = 0$ but not both. This condition is called *strict complementarity*, i.e., $\mu_j^* > 0$ for all active inequality constraints.

Second order optimality conditions

Consider the linear approximation of the feasible set around a feasible point w :

$$G(w) + \nabla_w G(w)^T d = 0, \quad (2.10)$$

$$H(w) + \nabla_w H(w)^T d \geq 0, \quad (2.11)$$

where $d \in \mathbb{R}^{n_w}$ represents possible directions of the linear approximation. Any direction d that satisfies the linearization is called a *linearized feasible direction*, i.e., directions where the optimizer can move while remaining feasible. Since $G(w) = 0$ and $H^{\text{act}}(w) = 0$, the set of feasible directions is defined as

$$\mathcal{F}(w) = \left\{ d \mid \begin{array}{l} \nabla_w G(w)^T d = 0, \\ \nabla_w H^{\text{act}}(w)^T d \geq 0. \end{array} \right\} \quad (2.12)$$

First order optimality conditions guarantee that at w^* any feasible direction $d \in \mathcal{F}(w^*)$ either increases or keeps the value of the linear approximation of the cost, i.e., $\nabla_w F(w^*)^T d > 0$ or $\nabla_w F(w^*)^T d = 0$. However, for those feasible directions d for which $\nabla_w F(w^*)^T d = 0$, or *undecided directions* (Nocedal and Wright, 2006), the KKT conditions are not informative enough to guarantee an increase of $F(w^*)$. Hence, a second order expansion of the Lagrangian is required to verify that a move along $d \in \mathcal{F}(w^*)$ provides an increase of the cost and retains feasibility, making w^* a local minimum. In this situation, it is necessary to verify second order information for those d that yield $\nabla_w F(w^*)^T d = 0$. The directions that satisfy this condition constitute what is known as the *critical cone* $\mathcal{C}(w^*, \lambda^*, \mu^*)$. Those directions are obtained by differentiating the Lagrangian, with respect to w i.e.,

$$\nabla_w F(w^*)^T d = \lambda^T \nabla_w G(w^*)^T d + \mu^T \nabla_w H(w^*)^T d = 0. \quad (2.13)$$

This condition³ is satisfied for the directions d

$$d \in \mathcal{C}(w^*, \lambda^*, \mu^*) \iff \begin{cases} \nabla_w G(w^*)^T d & = 0 \\ \nabla_w H_j^{\text{act},s}(w^*)^T d & = 0 \quad \forall \mu_j > 0 \\ \nabla_w H_j^{\text{act},w}(w^*)^T d & \geq 0 \quad \forall \mu_j = 0 \end{cases} \quad (2.14)$$

With this definitions the *second order necessary conditions* are given by Theorem 2.2.2.

Theorem 2.2.2 (Second order necessary conditions). *Suppose that a regular point w^* is a local solution to (2.1) with associated Lagrange multipliers λ^* and μ^* that satisfy the KKT conditions, then*

$$d^T \nabla_w^2 \mathcal{L}(w^*, \lambda^*, \mu^*) d \geq 0, \quad \forall d \in \mathcal{C}(w^*, \lambda^*, \mu^*). \quad (2.15)$$

Theorem 2.2.3 (Strong second order sufficient conditions). *If a feasible point w^* with associated Lagrange multipliers λ^* and μ^* , that satisfies the KKT conditions, satisfies also*

$$d^T \nabla_w^2 \mathcal{L}(w^*, \lambda^*, \mu^*) d > 0, \quad \forall d \in \mathcal{C}(w^*, \lambda^*, \mu^*), d \neq 0, \quad (2.16)$$

then w^* is a strict local solution.

2.3 Solving nonlinear programming problems

In this section, well-known numerical methods to tackle problems of the form (2.1) are introduced. These problems can be the result of parameterizing dynamic optimization problems (see Section 2.5). There are basically two large groups of methods to deal with this kind of problems namely, *derivative based* and *derivative-free* methods. However, only derivative based methods are considered here since they are much faster and the functions involved in cost and constraints are assumed to be at least twice continuously differentiable.

2.3.1 Quadratic programming

One of the most popular formulations for optimization problems is a *quadratic programming problem* (QP). There, problems exhibit a quadratic cost and linear equality and inequality constraints. This kind of problems can be cast as:

$$QP: \quad \min_x \quad \frac{1}{2} x^T B x + b x \quad \text{subject to} \quad \begin{cases} Cx + c & = 0, \\ Dx + d & \geq 0, \end{cases} \quad (2.17)$$

³Inactive constraints are not considered since the associated multipliers are zero, thus, they do not contribute to (2.13).

The Lagrangian for the QP problem is defined as

$$\mathcal{L}(x, \lambda_{\text{QP}}, \mu_{\text{QP}}) = \frac{1}{2}x^T Bx + bx - \lambda_{\text{QP}}^T(Cx + c) - \mu_{\text{QP}}^T(Dx + d) \quad (2.18)$$

with KKT conditions

$$\nabla_x \mathcal{L}(x^*, \lambda_{\text{QP}}^*, \mu_{\text{QP}}^*) = Bx^* + b^T - C^T \lambda_{\text{QP}}^* - D^T \mu_{\text{QP}}^* = 0 \quad (2.19)$$

$$Cx^* + c = 0, \quad (2.20)$$

$$Dx^* + d \geq 0, \quad (2.21)$$

$$\mu_{\text{QP}}^* \geq 0, \quad (2.22)$$

$$\mu_{\text{QP}}^*(D_j x^* + d_j) = 0, \quad j = 1, \dots, n_H \quad (2.23)$$

If the Hessian matrix B in the QP is positive semidefinite, $B \succeq 0$, i.e., all its eigenvalues are greater or equal to zero, then the QP is said to be *convex*. This is a quite desired feature in the QP since convexity implies that the KKT conditions are enough to guarantee a global solution (Nocedal and Wright, 2006). Hence, algorithms that attempt to find a KKT point yield a global solution to the problem. Among the most popular methods for solving QPs are *active set* and *interior points* methods (Karmarkar, 1984), (Nesterov and Nemirovski, 1995).

2.3.2 Sequential quadratic programming

In order to find a solution to the NLP (2.1), a common approach is to use *Sequential Quadratic Programming* (SQP). SQP is an iterative method where the NLP is approximated at the current iterate k by a quadratic programming problem of the form

$$QP(w^k) : \min_{\Delta w} \frac{1}{2} \Delta w^T B^k \Delta w + \nabla_w F(w^k)^T \Delta w \quad (2.24)$$

subject to

$$G(w^k) + \nabla_w G(w^k)^T \Delta w = 0, \quad (2.25)$$

$$H(w^k) + \nabla_w H(w^k)^T \Delta w \geq 0. \quad (2.26)$$

where B^k is an approximation of the Hessian of the Lagrangian $\nabla_w^2 \mathcal{L}(w^k, \lambda^k, \mu^k)$. This procedure can be seen as finding a KKT point for the original NLP problem

by obtaining KKT points of the quadratic programming approximations to the NLP, iteratively. Solving the QPs at each iteration, leads to a KKT point $(\Delta w, \lambda_{\text{QP}}^k, \mu_{\text{QP}}^k)$. The update of the estimate for the NLP solution (w^*, λ^*, μ^*) is performed by

$$w^{k+1} = w^k + \alpha^k \Delta w, \quad (2.27)$$

$$\lambda^{k+1} = \lambda^k + \alpha^k (\lambda_{\text{QP}}^k - \lambda^k), \quad (2.28)$$

$$\mu^{k+1} = \mu^k + \alpha^k (\mu_{\text{QP}}^k - \mu^k), \quad (2.29)$$

where α^k is obtained, e.g., by a *backtracking line search* globalization strategy (Nocedal and Wright, 2006). In this document, a globalization strategy based on a L_1 exact penalty function and a watchdog technique is programmed (Leineweber, 1998) for the SQP method used in Chapter 6. The approximation of the Hessian of the Lagrangian B^k is obtained at the current iteration by using the well known Broyden-Fletcher-Goldfarb-Shanno (BFGS) update formula

$$B^{k+1} = B^k - \frac{B^k s^k s^{kT} B^{kT}}{s^{kT} B^k s^k} + \frac{y^k y^{kT}}{y^{kT} s^k}, \quad (2.30)$$

with $s^k = \alpha^k \Delta w$ and $y^k = \nabla_w \mathcal{L}(w^{k+1}, \lambda^{k+1}, \mu^{k+1}) - \nabla_w \mathcal{L}(w^k, \lambda^{k+1}, \mu^{k+1})$.

Remark 2.3.1. An update using BFGS formula does not preserve the sparsity structure of the Hessian obtained with simultaneous optimization approaches. The structure obtained from the parameterization using simultaneous methods allows for updates of the Hessian per blocks, i.e., high-rank updates (Bock and Plitt, 1984), which demands less storage requirements than a full Hessian update and preserves the sparsity pattern. A high-rank update algorithm is applied here so that QP solvers that exploit the structure can be used.

2.3.3 Constrained Gauss-Newton Method

As said before, classical SQP methods require the Hessian of the Lagrangian. However, there are cases where $F(w)$ can be formulated as a quadratic norm on some nonlinear function of the optimization variables i.e., $F(w) = \frac{1}{2} \|R(w)\|_2^2$. In PEP, $R(w)$ corresponds to a residual vector obtained from measuring some distance between the data to fit and the model response,

$$R(w) = [\epsilon_1(w), \epsilon_2(w), \dots, \epsilon_N(w)]^T. \quad (2.31)$$

The gradient and Hessian of the cost can be expressed by:

$$\nabla_w F(w) = \nabla_w R(w)R(w), \quad (2.32)$$

$$\nabla_w^2 F(w) = \nabla_w R(w)\nabla_w R(w)^T + \sum_{i=1}^N \epsilon_i(w)\nabla_w^2 \epsilon_i(w), \quad (2.33)$$

respectively. Normally, the second term in the right hand side of (2.33) is neglected since close to the solution, it is expected that the residuals $\epsilon_i(w)$ are small (Nocedal and Wright, 2006). Hence, the Hessian of the cost is calculated solely from the Jacobian of the residual vector. The approximation of the Hessian of the cost leads to the main feature of Gauss-Newton method where at each major iteration k of the SQP a subproblem of the form

$$LSP(w^k) : \min_{\Delta w} \frac{1}{2} \|R(w^k) + \nabla_w R(w^k)^T \Delta w\|_2^2, \quad (2.34)$$

subject to

$$G(w^k) + \nabla_w G(w^k)^T \Delta w = 0, \quad (2.35)$$

$$H(w^k) + \nabla_w H(w^k)^T \Delta w \geq 0, \quad (2.36)$$

is solved. Hence, no second order information is required and the update of the estimates is performed as in the SQP approach.

The second part of this document concentrates on finding convex approximations to nonconvex optimization problems obtained from parameterization of dynamic optimization problems (DOP). Hence, DOP are introduced in the following section.

2.4 Dynamic optimization problems

A dynamic optimization problem is an optimization problem where the cost and/or the constraints involve the evolution of a time dependent variable⁴ obtained from

⁴Here the time is assumed as independent variable, however, other parameterizations are also possible.

the solution of a dynamic model. A DOP can be cast as

$$\min_{x(\cdot), u(\cdot), p} J(x(\cdot), u(\cdot), p) \text{ s.t. } \begin{cases} (x(0) - x_0) & = & 0, \\ \dot{x}(t) - f(x(t), u(t), p) & = & 0, \quad t \in [0, T], \\ h(x(t), u(t), p) & \geq & 0, \quad t \in [0, T], \\ r^{\text{itr}}(x(T)) & \geq & 0, \\ r^{\text{etc}}(x(T)) & = & 0, \end{cases} \quad (2.37)$$

In a DOP the following building blocks can be distinguished:

- A set of *optimization variables* $x(t) \in \mathbb{R}^{n_x}$, $u(t) \in \mathbb{R}^{n_u}$ and $p \in \mathbb{R}^{n_p}$. Note that depending on the kind of variables to optimize, i.e., controls u or parameters p , the DOP can be classified in an optimal control problem (OCP) or a parameter estimation problem (PEP).
- A *dynamic model* that describes the evolution of the state variables $x(t)$ as a function of controls $u(t)$ and parameters p and the time index t . The complexity of the DOP is, in part, determined by the nature of the model. In this document ordinary differential equations (ODEs) and differential-algebraic equations (DAEs) of the form

$$M\dot{x}(t) = f(x(t), u(t), p), \quad \forall t \in [0, T] \quad (2.38)$$

with $f : \mathbb{R}^{n_x} \times \mathbb{R}^{n_u} \times \mathbb{R}^{n_p} \times \mathbb{R} \rightarrow \mathbb{R}^{n_x}$, are used. $M \in \mathbb{R}^{n_x \times n_x}$ is commonly known as the *mass matrix*⁵. Herein, M is assumed to be a diagonal nonsingular matrix for ODEs and a diagonal singular matrix for a particular class of DAEs called semi-explicit DAEs (Hairer and Wanner, 2002). A desirable feature of the dynamic model is linearity with respect to the decision variables of the DOP. Linearity simplifies the procedures used to solve the model equations and becomes one of the requirements that leads to convexity in the DOP (Boyd and Vandenberghe, 2006).

- A set of constraints on the search space of the optimization variables $h(x(t), u(t), p) \geq 0$, known as the *path constraints*. Additionally, the *inequality terminal constraint* $r^{\text{itr}}(x^T)$ defines a region in the space of the states where the final value of the optimal state trajectory $x^*(T)$ must lie. Likewise, the *equality terminal constraint* $r^{\text{etc}}(x(T))$ defines a point in \mathbb{R}^{n_x} where the final value of the optimal state trajectory must lie. Although the dynamic model can be seen as a constraint as well, it is normally treated in a different manner due to its dynamic nature.
- A cost J that constitutes a *performance measure* of the dynamic model response along the time horizon.

⁵Because its elements can be associated to masses when modeling mechanical systems.

2.4.1 Optimal control problems

Optimal control problems (OCP), constitute a particular class of DOPs where the decision variables are controls $u(t)$. OCPs have been widely studied and for a deep treatment of the classical theory, the reader is referred to Kirk (1970) or Bryson and Ho (1975). In an OCP the performance measure can be cast as

$$J(x(\cdot), u(\cdot)) = \int_0^T L(x(t), u(t)) dt + E(x(T)). \quad (2.39)$$

This Bolza-type objective is composed of a term that accounts for the history of the states and controls evolving along the time horizon T , called the *Lagrange term* L and a terminal cost E known as the *Mayer term*.

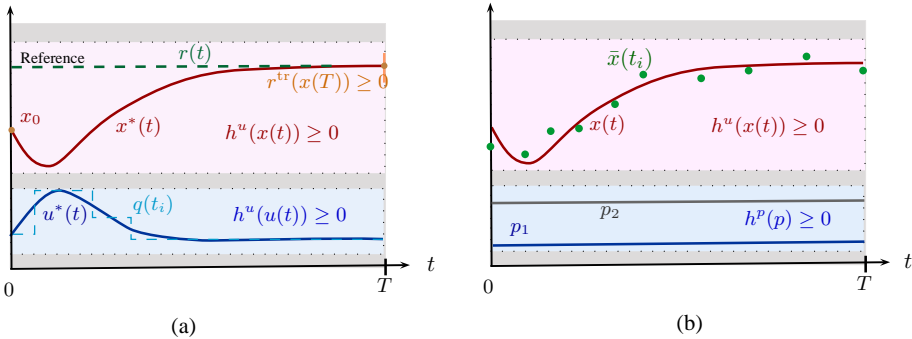


Figure 2.2: Dynamic optimization problem classical scenarios. (a) an optimal control problem, (b) a parameter estimation problem.

The goal in solving an OCP is to find an *admissible control* profile $u^*(t)$ so that the performance measure is minimized. This optimal control must generate a feasible state evolution $x^*(t)$ called the optimal state trajectory. Figure 2.2 illustrates an OCP scenario where the cost is formulated in terms of deviations with respect to a desired reference trajectory $r(t)$. The path constraints are split here in $h^u(u(t)) \geq 0$ and $h^x(x(t)) \geq 0$ so that it is easier to appreciate the search space of those variables. In the context of *Receding Horizon Control* (see Section 2.4.3), the terminal constraint region $r^{\text{tr}}(x(T)) \geq 0$ along with the terminal cost $E(x(T))$ are normally added to the OCP to enforce stability of the finite horizon problem (Findeisen and Allgöwer, 2002).

2.4.2 Parameter estimation problems

A second, widely used class of DOPs consider the model parameters p as optimization variables. For this kind of problem the constraints on the initial state $x(0)$ and the final state $x(T)$ normally disappear. The cost is formulated in terms of a distance measure between some *observation function* of the state trajectories $l(x(t), p)$, and a trajectory measured from a real process $\bar{y}(t)$. Practically, the measurements are performed at specific time instants t^i , hence, the measurement trajectory is by definition a discrete signal, but an integral cost form is used in (2.40) for notational coherence with the OCP. The distance between measurements and the observation function is commonly known as the *model residuals* $\epsilon(t)$. The goal of the PEP solver is to minimize those residuals by finding a feasible set of parameters. A typical performance measure is

$$J(x(t), p) = \int_0^T \|Q^{\frac{1}{2}}(\bar{y}(t) - l(x(t), p))\|_2^2 dt, \quad (2.40)$$

which corresponds to a *least squares cost*. Nevertheless, other kinds of norms, e.g., the L1 norm, have been shown to be less sensitive to *outliers* (Kostina, 2004). Figure 2.2(b) depicts a classical parameter estimation scenario with constraints on the states and the parameters. Here, only time invariant parameters are illustrated for simplicity. The 2-norm in (2.40) exhibits certain advantages with respect to the generation of the second order derivative information that is required for the numerical solution of the PEP: parameterized DOP with nonlinear least squares costs like (2.40) are efficiently tackled by the so called Gauss-Newton method, as explained in Section 2.3.3.

2.4.3 Receding horizon control

A kind of control technique that deserves particular attention due to its wide use is *receding horizon control* (RHC) or *model predictive control* (MPC). This technique is based on the online solution of an open loop OCP at specific time instants along the time evolution of the process to be controlled. Figure 2.3 depicts the main signals in a classic receding horizon strategy (Allgöwer et al., 2004).

In Figure 2.3, at the present time t , the future behavior of the process states, $\hat{x}(t)$, is predicted over a *prediction horizon* T , based on the state information, $x(t)$, and an available dynamic model of the process. The term nonlinear receding horizon control or *nonlinear model predictive control* (NMPC) generally refers to the formulation of predictive control using nonlinear models. A particular feature of the OCPs used in a receding horizon framework is that the control trajectories

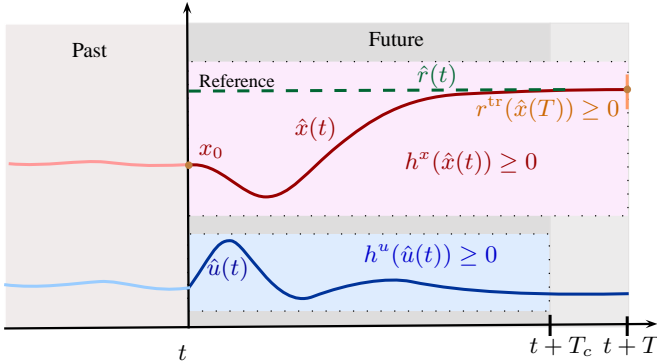


Figure 2.3: Receding horizon control scenario.

are normally allowed to vary during a finite time interval T_c not necessarily equal to the prediction horizon T , i.e., $T_c \leq T$. The time interval T_c is known as the *control horizon*. Based on the prediction of the process behavior, a future control scenario $\hat{u}(t)$ is computed by solving the associated OCP. Ideally, there would be no process disturbances or model uncertainties and the OCP could be solved for infinite horizon. In this case, the optimized control signal $\hat{u}(t)$ could be applied to the process like an open loop control. However, this situation is unrealistic and feedback needs to be incorporated. Therefore, the optimal control $\hat{u}(t)$ is implemented until a new measurement or estimate of the state becomes available. At that point, a new prediction is executed and a new OCP is formulated based on the current state, shifting the entire procedure one step ahead. The main steps of the algorithm are

Algorithm 2.1 Receding horizon control

- 1: At current time t obtain $x(t)$ by measurement or estimation.
 - 2: Solve the OCP, e.g., the DOP in (2.37)
 - 3: Implement $u(t)$ until the new state measurement becomes available.
 - 4: Return to step 1.
-

There is a well developed theory based on *Pontryagin's maximum principle* (Pontryagin, 1962) or *Hamilton-Jacobi-Bellman equation* (Bellman, 1957) that allows to characterize a solution in the infinite dimensional space of controls and states using the necessary optimality conditions so that controls are eliminated. These approaches are known as *indirect methods*. In this document, methods based on a finite dimensional representation of the optimization variables are used. Those methods, known as *direct methods*, are explained in the following section.

2.5 Direct methods for dynamic optimization

The optimal control and the state trajectories lie in an infinite dimensional space in the original continuous time formulation. The key feature of direct methods is the parameterization of time dependent variables in the DOP, i.e., states, controls and possibly model parameters. Once they are parameterized, the dimensionality of the problem is reduced, i.e., the number of decision variables is finite, allowing to formulate the DOP as a *nonlinear programming problem* (NLP) of the form (2.1). Parameterization of the controls is performed using basis functions, normally piecewise functions. However, other kinds of basis functions such as e.g., polynomial or wavelets (Binder et al., 2001) can be used. Figure 2.2 illustrates a possible approximation of the optimal control trajectories $u^*(t)$ using piecewise constant functions $q(t^i)$. Since the finite parameterization constitutes an approximation to the real decision variables, the solution obtained using direct methods is by definition a near optimal solution to the DOP. However, the parameterization can be chosen to approximate the optimal solution to a certain accuracy, e.g., by increasing the number of parameters to describe the solution. Direct methods are preferred when the optimization problem possesses inequality constraints since the indirect methods become difficult to handle in this case, unless information regarding the active constraints is available (Cervantes and Biegler, 1999). Moreover, the resulting NLP can be solved efficiently using state-of-the-art numerical optimization routines. There exist two kind of direct methods, namely *Sequential direct methods* and *Simultaneous direct methods*. These approaches are explained in the following sections.

2.5.1 Sequential methods and direct single shooting

In the sequential direct methods only controls are parametrized and simulation and optimization tasks are performed one after the other so that only the parameterized controls are used as optimization variables. Direct single shooting (DSS) (Sargent and Sullivan, 1978), (Kraft, 1985), (Vassiliadis, 1993), is the most popular sequential approach. In DSS only the infinite dimensional controls are represented by a finite number of parameters along the time horizon, i.e.,

$$u(t) \approx u(t, q), \quad \forall t \in [0, T], \quad (2.41)$$

where the vector q represents the parameters used to approximate $u(t)$, and $u(t, q)$ represents a set of basis functions. A piecewise constant parameterization is obtained by introducing a grid in the time interval $[0, T]$ so that the controls are represented by constant values q^i on each subinterval $[t^i, t^{i+1}]$ of the grid, i.e.,

$$u(t, q) = q^i, \quad \forall t \in [t^i, t^{i+1}], \quad i = [0, \dots, N - 1] \quad (2.42)$$

The states are eliminated from the optimization problem by solving the ODE

$$\dot{x}(t) = f(x(t), u(t, q), p) \quad \forall t \in [t^0, t^N]. \quad (2.43)$$

using a *dynamic equations solver* (DES). Solvers that provide model sensitivities are desired, since first and second order information is normally required for the optimization routines (Biegler, 1984). The state trajectories provided by the dynamic equation solver are used to evaluate cost and path constraints $h(x(t), u(t, q), p)$. The latter are normally sampled at intervals t^i in order to match the introduced grid and to preserve the finite dimensionality of the problem. This procedure leads to the NLP

$$\text{NLP}_{\text{DSS}} : \quad \min_{x(t^0), q, p} \int_0^T L(x(t, x^0, q, p), u(t, q), p) + E(x(t_N)) \quad (2.44)$$

$$\text{subject to } \begin{cases} x(t^0) & = & x^0, \\ h(x(t^i, x^0, q, p), u(t^i, q), p) & \geq & 0 \quad \forall i = 0, \dots, N \\ r(x(t^N, x^0, q, p)) & = & 0. \end{cases} \quad (2.45)$$

Note that the integral term in the cost can be solved as a part of the dynamic model. Hence, the dynamic equations solver is used to evaluate model, cost and to obtain sensitivities of them with respect to the decision variables. Figure 2.4 (a) illustrates the scenario for a DOP which is solved using DSS. The parameters are assumed constant along the time horizon.

Advantages

The main advantage of sequential approaches is the simplicity in the implementation of the method. The NLP obtained is solved in the space of parameterized controls and/or model parameters because the state trajectories are eliminated⁶. This leads to small but dense Jacobian and Hessian matrices in the sub-QPs needed to be solved at each SQP iteration (see Section 2.3). Since the dynamic model is solved apart, state-of-the-art ODE solvers can be used. Particularly, solvers with sensitivity generation capabilities are desired. It is important to note that sensitivity generation is normally the computationally most expensive task in dynamic optimization solvers. Hence, the computation of model sensitivities with respect to the decision variables is crucial for the efficiency of the optimization.

⁶For control problems the initial condition of the states can be eliminated from the decision variables. On the contrary, for parameter estimation problems the initial condition is often part of the degrees of freedom of the DOP.

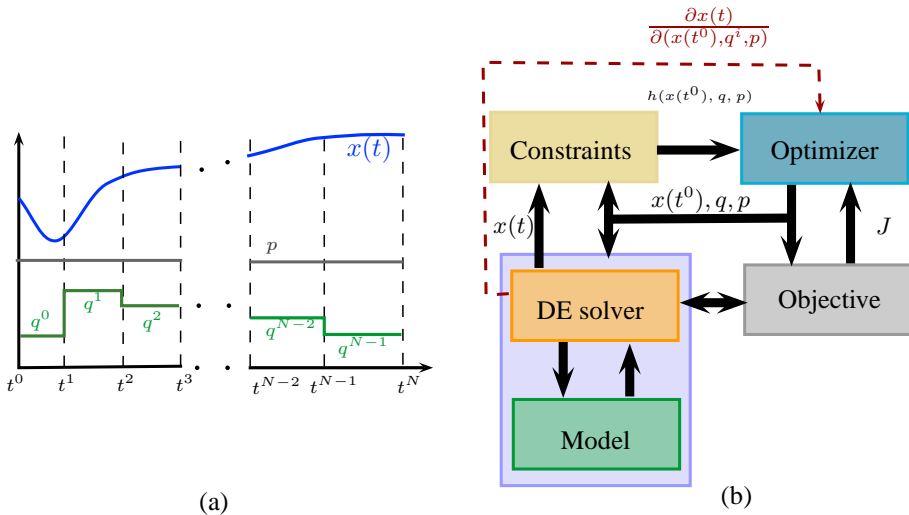


Figure 2.4: Direct single shooting parameterization (a) and a block diagram of the corresponding sequential optimization approach (b).

Disadvantages

The main disadvantage is the sensitivity of the method to initialization, which becomes particularly problematic when the model exhibits unstable modes. Note that path constraints can be violated since the dynamic simulator generates trajectories that may not satisfy the original constraints. This may lead to poor convergence of the NLP. Moreover, the dynamic solver may fail integrating the model along the time horizon due to an improper initialization.

2.5.2 Simultaneous approaches and direct multiple shooting

In simultaneous approaches controls and states are parameterized, allowing the formulation of a NLP in terms of states, control and possibly parameters. Hence, the simulation task needed to determine the state trajectory is coupled to the optimizer so that states, controls and parameters are optimized all together. This allows for controlling the feasibility of the state trajectories and improves convergence rates. Consequently, the dynamic equation is solved simultaneously with the OCP or PEP and a valid state trajectory is only obtained at the end of the optimization task. This total parameterization leads to a large scale NLP. However, there is a lot of structure in the formulation of simultaneous methods, structure that can be exploited by tailored optimization methods (Biegler et al.,

2002). There are mainly two well-developed simultaneous methods, namely, *direct multiple shooting* (DMS) (Bock and Plitt, 1984) and *orthogonal collocation on finite elements* (OCFE) (Biegler, 1984). The former is explained here in detail since it is the basis of the solver used in Chapter 6 for the efficient solution of parameter estimation problems.

DMS can be seen as a hybrid or intermediate step between a sequential approach and a fully parameterized DOP, since a dynamic equation solver is still used. In DMS the time horizon T is divided in N subintervals,

$$t^0 < t^1 < t^2 \dots < t^N = T. \quad (2.46)$$

The process states, control and model parameters are parameterized on each subinterval, $N^i = [t^i, t^{i+1}]$, $i = 0, \dots, N-1$. This means that state trajectories are determined by the state values at shooting nodes $s = [s^0, s^1 \dots s^N]$, the control parameters $q = [q^0, q^1 \dots q^{N-1}]$, local parameters $p = [p^0, p^1 \dots p^{N-1}]$ and the model equations. This parameterization allows the model to be independently integrated from t^i to t^{i+1} , $\forall i = 0, \dots, N-1$. Figure 2.5(a) illustrates the scenario for parameters, controls and states in a DMS formulation. The algorithm optimizes the initial conditions s^i , controls q^i and parameters p^i in each shooting interval N^i . Note that for time invariant models, the parameter vector p is a global variable, i.e., it does not change from one shooting interval to the other. However, to make each subinterval totally independent, local variables p^i are introduced.

Remark 2.5.1. If the global parameter p is kept as a single variable, the obtained NLP leads to a Hessian of the Lagrangian which is nearly block diagonal with doubly-bordered blocks. Applying Hessian updates (see Section 2.3) destroys the sparsity of the Hessian. Hence, special methods are needed to perform Hessian updates (Yokoyama et al., 2008). If local parameters p^i are introduced, as done here, a bigger NLP is obtained but the new Hessian is block diagonal without the double borders. In this form, updates of the Hessian can be easily performed per blocks, preserving the sparse structure, using the so called *high rank updates* (Bock and Plitt, 1984).

In order to guarantee continuity in the solution from t^0 to t^N and to avoid time varying parameters, additional equality constraints are imposed on each subinterval N^i , i.e., (i) the final state value of the subinterval N^i must match the initial state value of the interval N^{i+1} , and (ii) $p^i = p^0$ for all $i = 1, 2, \dots, N-1$. These conditions are illustrated in Figure 2.5(b) through the global constraints block. Following the DMS parameterization, a DOP is reformulated as the NLP

$$\text{NLP}_{\text{DMS}} : \min_{s, q, p} \sum_{i=0}^{N-1} l(s^i, q^i, p^i) + E(s_N), \quad (2.47)$$

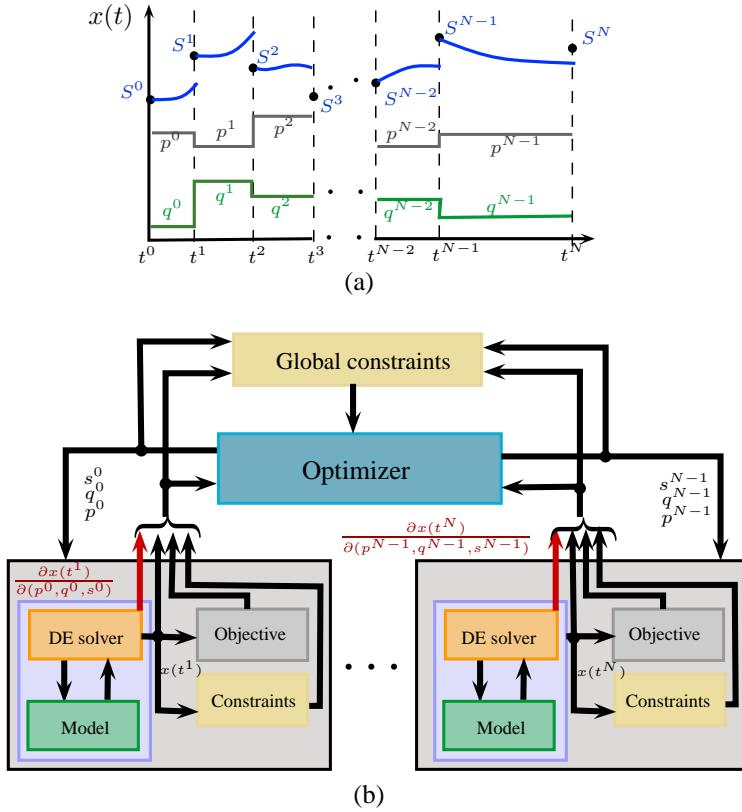


Figure 2.5: Direct multiple shooting (DMS) scenario (a) and a block diagram of the corresponding simultaneous optimization approach (b). Note that in DMS, a dynamic equations solver (DES) is still used.

$$\text{subject to } \begin{cases} (s^0 - x^0 = 0), \\ s^{i+1} - x(t^{i+1}) = 0, & i = 0, \dots, N-1, \\ p^i - p^0 = 0, & i = 1, \dots, N-1, \\ h(s^i, q^i, p^i) \geq 0, & i = 0, \dots, N-1, \\ r^{\text{intr}}(s^N) \geq 0, \\ r^{\text{etc}}(s^N) = 0 \end{cases} \quad (2.48)$$

The cost $l(s^i, q^i, p^i)$ is obtained from the integration of the original cost, e.g., L in (2.39), during the shooting interval i . The dynamic equations solver is used to generate the state value $x(t^i)$ on each shooting interval by integrating the model. In some cases, the solver also provides the model sensitivities (Cervantes and

Biegler, 1999). Note that path constraints $h(s^i, q^i, p^i)$ are normally evaluated at shooting nodes.

Disadvantages

DMS and other simultaneous methods are generally more complex to implement and normally lead to a considerably number of variables when compared with the sequential approaches. Hence, sparse linear algebra solvers needs to be used to efficiently deal with the increased number of variables. An alternative approach is to project the involved variables in a lower dimensional space so that the problem is formulated in a reduced number of optimization variables (Bock and Plitt, 1984).

Advantages

The NLP obtained from DMS and other simultaneous methods, such as collocation, exhibits a lot of structure. This structure can be exploited by sparse methods in optimization (Gill et al., 1984). Moreover, in DMS it is possible to reduce the sparse *quadratic programming* (QP) problems that need to be solved in the sequential quadratic programming iterations (see Section 2.3.2) to dense QPs with the same number of variables as in DSS by a procedure called *condensing* (Bock and Plitt, 1984). Due to this procedure it can be said that the computational effort of DMS and DSS are comparable (Bock and Plitt, 1984), though both approaches are in many variants. One of the significant advantages of simultaneous approaches is the improvement of local convergence (Albersmeyer and Diehl, 2010) and the possibility of providing a better initialization. Because of the state parameterization, the state trajectories can be initialized close to what is expected to be the solution. This is visualized easily in a parameter estimation problem where shooting nodes s^i can be initialized with the available measurements. This kind of initialization combined with the Gauss-Newton method leads to faster convergence to the solution for the PEP (Kostina, 2004). In addition, unstable modes are in general treated in a better form than in DSS since the rapid growth of values is bounded due to shorter integration intervals $[t^i, t^{i+1}]$. Moreover, due to the independent integration in subintervals, the problem can be parallelized. Figure 2.5(b) illustrates that the optimizer receives information of blocks that can run in parallel. Each of those blocks corresponds to one shooting interval, and they are only coupled by the global constraints as previously mentioned.

2.6 Conclusions

In this chapter the bases of parameterized dynamic optimization problems have been introduced, highlighting the advantages of obtaining optimization problems that are convex. Numerical methods based on optimality conditions for the solution of the resulting nonlinear programming problems have been explained. Details on the algorithms are presented since a sequential quadratic programming algorithm is coupled with a dynamic equation solver with sensitivity capabilities as a part of the convex methods used in this thesis. In addition, direct methods for the efficient solution of the parameterized DOP have been presented. It has been discussed that simultaneous optimization methods are in general less sensitive to initialization values and suitable for processes with unstable modes. This chapter has provided basic knowledge on dynamic optimization required for the understanding of the contributions in this dissertation.

Part I

Model structure exploitation for simulation of separation processes

Chapter 3

An equilibrium model for the CIT distillation column

This chapter describes a rigorous *equilibrium model* for distillation in tray based columns with constant pressure drop. The model described in Diehl (2002) is adapted to the particular mixture used in the CIT distillation setup. This setup is described in Section 3.1. Section 3.2 introduces the set of relations that leads to a differential-algebraic equations (DAEs) model. Section 3.3 presents the dynamic simulation results of the proposed DAEs using an off-the-shelf DAE solver. Model states are organized so that sparsity is preserved for simulation tasks. An analysis of model sensitivity with respect to unknown model parameters is performed in Section 3.4 showing that the search space for parameter estimation problems (PEP) can be reduced. Conclusions of the chapter follow in Section 3.5.

3.1 Pilot plant description

Industrial distillation is performed in tray based or packed columns, leading to different approaches for modeling the process. The column studied here is a packed based column. In this kind of systems, the liquid and vapor phases are continuously in contact through the column internals. The experimental setup involves a computer controlled distillation column (see Figure 3.1). The column is about 6 m high and has an internal diameter of 7 cm containing three sections of 960 mm each, with Sulzer CY packing (Sulzer, Winterthur). Each section is subdivided into six smaller packing segments of 160 mm length. This packing has a contact surface of $700 \text{ m}^2/\text{m}^3$. The feed stream containing a mixture of methanol and isopropanol can be introduced into the column between the packed

sections S_1 and S_2 or S_2 and S_3 . Each one of these feeding points has an associated electric heater of maximum 0.25 kW to adjust the temperature of the feed. These heaters are activated or deactivated according to the selected feeding point. At the bottom of the column a reboiler is present containing two electric heaters of maximum 3 kW each. In the reboiler, a part of the liquid is vaporized while the rest is extracted as bottom stream. At the column top a total condenser allows condensing the entire overhead vapor stream, which is then collected in a reflux drum whose volume is maintained constant. A part of the condensed liquid is fed back to the column as reflux, while the remainder leaves the column as the distillate stream.

In this setup the following four variables can be manipulated: the reboiler duty Q_R (kW), the feed rate F (g/min), the duty of the feed heater Q_F (W) and the reflux flow rate L_r (g/min). The distillate flow D (g/min) is adjusted to maintain a constant reflux drum volume. Measurements are available for the reflux flow rate L_r , the distillate flow rate D , the feed flow rate F and twelve temperatures, i.e., the reflux temperature, the temperature at the top of the condenser $T_{s_{11}}$, the temperatures in the center and extremes of each packing section (T_{s_2} to T_{s_9}), the temperature of the feed point T_F , and the temperature in the reboiler T_{s_1} . All actuators and sensors are connected to a Compact Fieldpoint (National Instruments, Austin) with a controller interface cFP-2100 and I/O modules cFP-AIO-610, cFP-AIO-610 and cFP-AI-110. A Labview (National Instruments, Austin) program is developed to control the actuators and to register the variables. There is no online measurement of the concentrations in the distillate and bottom streams but it is possible to measure them offline by sampling the output streams.

Since the CIT distillation column is a packed one, determining the number of separation units or stages is an important issue for the model formulation. The number of stages in a column N , is a design parameter in distillation, so that the higher the number of stages N , the better the separation among the components. In tray based columns is not difficult to determine N from the experimental setup, because each tray can be associated to one stage¹. Here it is not possible to make a direct comparison between stages and trays. However, packing manufacturers provide an equivalent-tray per length of packing material factor or height equivalent per theoretical plate (HETP), (Seader and Henley, 2006). In Dewulf (2009) it is shown that for the particular kind of packing used in the CIT distillation column, the HETP ranges between 8 and 14 per meter of packing material². Since the total length of the packing is 2.8 m, Dewulf (2009) estimates a total of 36 packing stages. Note that for a HETP/m=12 m⁻¹, around 35 theoretical stages are obtained. However, due to an efficiency per tray smaller

¹Note that the number of theoretical trays for a given separation level and the number of physical trays in the setup are related to the tray efficiency.

²This HETP is presented as a function of the F -factor (Seader and Henley, 2006).

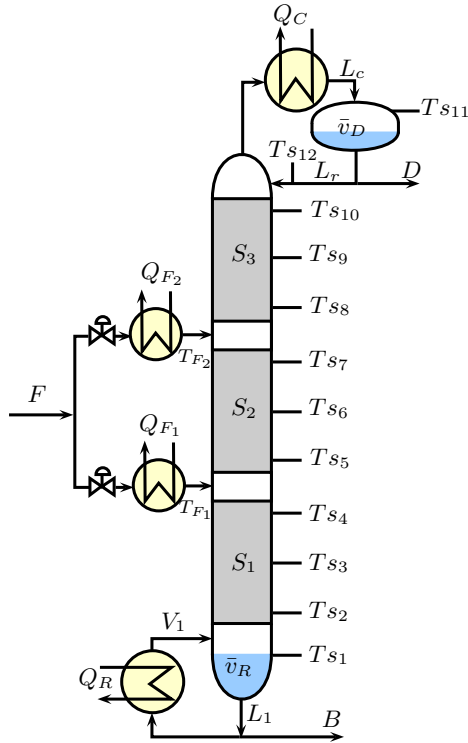


Figure 3.1: General layout of the distillation set-up with the distribution of the temperature sensors.

than one, the real number of stages associated to the real setup has to be bigger. Consequently, a total of 38 stages are assumed in the tray based model for the distillation column. This estimation leads to 12 stages for each one of the 3 packing sections in the column. Since the column is fed just above the first section, the feed is located over the 13th stage, i.e., the reboiler plus the 12 stages of the packing section. This leads to locate the feeding point in the 14th stage, i.e., $N_F = 14$. The second feeding point would be located above the second packing section, i.e., on stage 26.

3.2 Equilibrium based approach for distillation

Most of the models developed for distillation are based on the assumption of *Vapor-Liquid Equilibrium* (VLE) between the phases involved. VLE implies that

in a liquid mixture in contact with its vapor phase, the rates of evaporation and condensation are equal. This is a very rough approximation since in practice VLE is not achieved (Seader and Henley, 2006), (Taylor and Krishna, 1993). VLE possess several advantages when formulating models for distillation with respect to simplicity in the thermodynamic equations. However, it implies physical conditions that may not be satisfied in reality, such as the same temperature for vapor and liquid phase on a stage. The liquid and the vapor leaving a stage may exhibit different temperatures, e.g., superheated vapor and subcooled liquid. These situations are not covered by the VLE approach. Moreover, as mentioned in Seader and Henley (2006), VLE implies relations between liquid and vapor, through the *vapor-liquid distribution ratio* or *K-values*, that do not necessarily describe the real composition values. This mismatch has created the need for artificial modification to the equilibrium equations, introducing artificial concepts such as the stage efficiency. Despite these inconveniences, equilibrium models are widely used due to their simplicity. In the remainder of this chapter, an equilibrium based model is described and simulated, based on the following assumptions

Assumption 3.2.1 (Equilibrium model assumptions).

- Binary mixture.
- Vapor-liquid equilibrium on all the stages,
- Molar vapor holdup negligible,
- Total condenser,
- Saturated liquid feed,
- Constant pressure drops, i.e., ΔP_r for rectifying section and ΔP_s for stripping section,
- Variable tray efficiency per section α_s and α_r ,
- Constant volume holdups in reboiler \bar{v}_R and condenser \bar{v}_D .

Figure 3.2 illustrates the interaction of flows and local variables on an equilibrium stage. Note that each stage j is modeled using the same interaction among the different variables, leading to a highly structured model. Liquid flowing from the stage above at given temperature and composition, vapor rising from the stage below at given temperature and composition, and the feed flow with certain temperature and composition interacts with local holdup, composition and temperature. Consequently, setting the mass balance for one equilibrium stage is enough to build the model, because each set of stage equations is repeated $N - 2$ times in the whole column model.

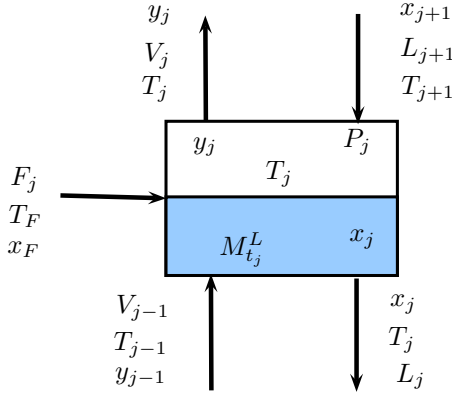


Figure 3.2: Equilibrium stage and the variables involved on its mass and energy balances. Note that the vapor holdup has been neglected. All the variables used have been defined in Section A.4

In the following paragraphs, a set of variables related to the thermodynamic properties of the mixture are used. In order to clarify the notation of the model, those variables have been defined in Section A.4. Moreover, since the vapor holdup is neglected and pressure is assumed constant, the model can be formulated in terms of composition dynamics using

$$M_{i,j}^L = M_{t_j}^L x_{i,j}. \quad (3.1)$$

Likewise,

$$E_j^L = M_{t_j}^L H_j^L, \quad (3.2)$$

is used in the following sections to eliminate energy holdups E_j from the formulation.

The stages at the top and bottom of the column, i.e., the condenser and the reboiler, are especial stages since they normally lead to fewer variables and equations than other sections of the column. Models for those stages are presented independently in the following paragraphs.

3.2.1 Equilibrium partial reboiler

The reboiler is assumed the first stage of the model, i.e., $j = 1$. Due to the neglected vapor molar holdup and the binary mixture assumption, (3.1) can be used to derive an expression for the change of composition of the light component in the liquid phase with respect to time, i.e.,

$$\dot{x}_j = \frac{L_{j+1}(x_{j+1} - x_j) + V_j(x_j - y_j)}{M_{t_j}^L}. \quad (3.3)$$

The energy balance is, in principle, a dynamic equation. However, if the pressure on a stage is assumed constant in time, it is possible to find an explicit expression for \dot{T}_j from Raoult's law, i.e.,

$$\dot{T}_j = G_j \dot{x}_j, \quad (3.4)$$

$$G_j = -\frac{P_1^s(T_j) - P_2^s(T_j)}{\frac{\partial P_1^s(T_j)}{\partial T_j} x_j + \frac{\partial P_2^s(T_j)}{\partial T_j} (1 - x_j)}, \quad (3.5)$$

This expression can be used in combination with (3.2) to transform the dynamic energy balance into an algebraic equation of the form

$$g_{E_j} = V_j ((x_j - y_j)Z_j + H_j^V - H_j^L) - Q - Q_{\text{loss}} \\ + L_{j+1} (H_{j+1}^L - H_1^L - (x_{j+1} - x_j)Z_j), \quad (3.6)$$

$$Z_j = \left(\frac{\partial H_j^L}{\partial x} + \frac{\partial H_j^L}{\partial T} G_j \right), \quad (3.7)$$

where expressions for the partial derivative of liquid enthalpies H_j^L and vapor pressures P_i^s with respect to temperature and composition are given in Appendix A. Equation (3.6) determines the vapor flow V_1 . Q_{loss} is a constant parameter that accounts for the heat losses in the column as presented in Diehl (2002).

Assuming constant volume in the reboiler \bar{v}_R leads to the algebraic equations

$$g_{L_j} = Bv_j^L - L_{j+1} ((x_{j+1} - x_j)Y_j + v_j^L) + V_j ((x_j - y_j)Y_j - v_j^L) \quad (3.8)$$

$$Y_j = \frac{\partial v_j^L}{\partial x} + \frac{\partial v_j^L}{\partial T} G_j,$$

and

$$g_{M_{t_j}} = v_j^L M_{t_j}^L - \bar{v}_R. \quad (3.9)$$

Partial derivatives of the molar volume v_j^L with respect to temperature and composition are given in Appendix A.

Temperature at stage j is calculated from the Raoult's law

$$g_{K_j} = 1 - K_{1,j}x_j - K_{2,j}(1 - x_j) \quad (3.10)$$

with K -values³ obtained from (A.45).

The vapor composition y_j can be calculated using the K -values and the tray efficiencies α_j

$$g_{y_j} = y_j - \alpha_j K_{1,j}x_j. \quad (3.11)$$

with one α for the stripping section and another for the rectifying section, i.e., $\alpha_j = \alpha_s$ for all $j = 1, \dots, N_F$ and $\alpha_j = \alpha_r$ for $j = N_F + 1, \dots, N - 1$.

Pressure in the reboiler is determined from the constant pressure drop in the stripping section ΔP_s , and the pressure of the stage above, as in

$$P_j = P_{j+1} + \Delta P_s. \quad (3.12)$$

This model of reboiler leads to 1 differential and 5 algebraic equations/variables⁴. The equations and variables can be grouped as

$$\mathbf{f}_1 = [g_{L_1}, g_{M_{t_1}}, \hat{x}_1, g_{E_1}, g_{K_1}, g_{y_1}]^T, \quad (3.13)$$

and

$$\mathbf{x}_1 = [B, M_{t_1}^L, x_1, V_1, T_1, y_1]^T, \quad (3.14)$$

respectively.

³In Diehl (2002) the effect of non ideal activity coefficients is neglected, i.e., $\gamma_1 = \gamma_2 = 1$

⁴Note that P can be included as system state. However, since there is an explicit expression for it, it is not included in the state vector \mathbf{x}_j .

3.2.2 Equilibrium stage

The equilibrium stages corresponding to the trays, i.e., $j = 2, \dots, N - 1$, are modeled in the following paragraphs. Total molar holdup and light component composition are defined by total mass and component balances

$$\dot{M}_{t_j}^L = L_{j+1} + V_{j-1} - L_j - V_j + F_j, \quad (3.15)$$

$$\dot{x}_j = \frac{L_{j+1}(x_{j+1} - x_j) + V_{j-1}(y_{j-1} - x_j) + V_j(x_j - y_j) + F(x_F - x_j)}{M_{t_j}^L}, \quad (3.16)$$

respectively.

As in the reboiler, due to the constant pressure assumption, the dynamic energy balance can be cast as the algebraic equation

$$\begin{aligned} g_{E_j} = & L_{j+1} (H_{j+1}^L - H_j^L - Z_j(x_{j+1} - x_j)) \\ & + F_j (H_j^F - H_j^L - Z_j(x_j^F - x_j)) \\ & + V_{j-1} (H_{j-1}^V - H_j^L - Z_j(y_{j-1} - x_j)) \\ & + V_j (H_j^L - H_j^V - Z_j(x_j - y_j)). \end{aligned} \quad (3.17)$$

Liquid flows are calculated from the geometry of the tray. In Diehl (2002) this is performed using the Francis weir formula

$$g_{L_j} = L_j v_{t_j}^L - W_j (v_{t_j}^L M_{t_j}^L - v_j^{\text{ref}}), \quad (3.18)$$

where the weir coefficient W_j and the reference volume per tray v_j^{ref} are model parameters.

Equilibrium temperature for the stage j is determined by (3.10), while vapor composition is calculated from the equilibrium relation modified with tray efficiencies α_j ,

$$g_{y_j} = y_j - \alpha_j \frac{P_1^s(T_j)}{P_j} x_j - (1 - \alpha_j) y_{j-1}. \quad (3.19)$$

Pressure at the stage j is obtained as in the reboiler, by using (3.12). The model of the equilibrium stage involves 2 differential and 4 algebraic equations/variables. They can be arranged as

$$\mathbf{f}_j = [g_{L_j}, g_{K_j}, \dot{x}_j, \dot{M}_{t_j}^L, g_{E_j}, g_{y_j}]^T \quad (3.20)$$

$$\mathbf{x}_j = [L_j, T_j, x_j, M_{t_j}^L, V_j y_j]^T \quad (3.21)$$

3.2.3 Equilibrium condenser

The condenser and the reflux drum are modeled as a whole unit at the top of the column, i.e., $j = N$. A component mass balance, assuming a binary mixture, leads to:

$$\dot{x}_j = \frac{V_{j-1}(y_{j-1} - x_j)}{M_{t_j}^L}. \quad (3.22)$$

Although no energy balance around the condenser is specified in Diehl (2002), an energy balance in the condenser determines the value of the removed heat Q_C , i.e.,

$$g_{E_j} = V_{j-1}H_{j-1}^V - L_jH_j^L + Q_C. \quad (3.23)$$

Q_C is not included as a model state here, but can be calculated explicitly from (3.23) since temperature and composition at the top stage are determined by the model.

Due to the constant volume assumption for the condenser, the distillate flow D and the molar holdup $M_{t_j}^L$ are determined by

$$g_{L_j} = v_{t_j}^L D - V_{j-1} \left((y_{j-1} - x_j)Y_j + v_{t_j}^L \right) + v_{t_j}^L L_j, \quad (3.24)$$

and

$$g_{M_{t_j}^L} = v_j^L M_{t_j}^L - \bar{v}_D, \quad (3.25)$$

respectively. Note that L_N corresponds to the reflux, which is a manipulated variable. Hence, H_N^L must be calculated at the measured reflux temperature T_C . In

Table 3.1: Summary of variables and equations involved in the equilibrium based model proposed in Diehl (2002).

Stage	Variables ^a			Associated equation	Total var./eq.
	name	units	type ^b		
Reboiler $j = 1$	$M_{t_1}^L$	mol	A	(3.9)	6
	x_1	mol/mol	D	(3.3)	
	T_1	K	A	(3.10)	
	V_1	mol/s	A	(3.6)	
	y_1	mol/mol	A	(3.11)	
	B	mol/s	A	(3.8)	
Equilibrium $j = 2, \dots, N - 1$	x_j	mol/mol	D	(3.16)	6(N - 2)
	T_j	K	A	(3.10)	
	$M_{t_j}^L$	mol	D	(3.15)	
	V_j	mol/s	A	(3.17)	
	y_j	mol/mol	A	(3.19)	
	L_j	mol/s	A	(3.18)	
Condenser $j = N$	x_N	mol	D	(3.27)	4
	T_N	mol	A	(3.10)	
	$M_{t_N}^L$	kW	A	(3.25)	
	D	mol/s	A	(3.24)	

^aConsidering a binary mixture

^bD and A stand for differential and algebraic variables, respectively.

Diehl (2002) T_C is not equal to T_N , since T_C normally corresponds to a subcooled liquid, a condition that cannot be described by equilibrium.

Temperature, pressure and vapor composition are determined using (3.10), (3.12) and (3.19), respectively, considering $j = N$. This model of the condenser leads to 1 differential and 3 algebraic equations/variables. Hence, the equations and states for the condenser can be grouped as

$$f_N = [g_{K_N}, \dot{x}_N, g_{M_{t_N}^L}, g_{L_N}]^T, \quad (3.26)$$

$$x_N = [T_N, x_N, M_{t_N}^L, D]^T. \quad (3.27)$$

Table 3.1 summarizes the model states, and the equations that determine those states, for the model presented in Diehl (2002)⁵.

⁵Some of the equations have been modified and analytical expressions for some derivatives of component properties with respect to time have been calculated.

3.2.4 Equilibrium model structure

The presented model leads to $2N - 2$ differential and $4N$ algebraic variables/equations, where N represents the number of stages including reboiler and condenser. Equations and variables can be organized in the particular form

$$\mathbf{f} = [f_1, f_2, \dots, f_{N-1}, f_N]^T, \quad (3.28)$$

$$\mathbf{x} = [x_1, x_2, \dots, x_{N-1}, x_N]^T, \quad (3.29)$$

with the vectors \mathbf{f}_j and $\mathbf{x}_j \forall j = 1, \dots, N$ given by (3.13), (3.20), (3.26) and (3.14), (3.21), (3.27), respectively. This particular form of organizing states and equations leads to a banded structure in the model Jacobian which can be exploited when solving the system. The structure in separation processes is obtained by associating variables involved on a stage with the equations that are determined from energy, mass balance and equilibrium at the same stage. Note that this creates blocks of non-zero entries in the system Jacobian since only a subset of the total states is involved in the equations modeling the stage.

Note also that, although vapor composition y_j can be explicitly determined from (3.11), (3.19), and vapor flows V_j determined from (3.6), (3.17), eliminating those states from the model, destroys the banded structure of the Jacobian. This is easily explained, because (3.19) and (3.17) are recursive equations, i.e., V_j depend on V_{j-1} , T_{j-1} and x_{j-1} and y_j depends on y_{j-1} , x_j and T_j . Due to the recursion required to calculate V_j and y_j explicitly, some of the states involved in the previous $j - 1$ stages need to be used. Hence, the mass balance at stage j would depend on almost all the states involved in the $j - 1$ previous stages. This dependence leads to a Jacobian that is not block diagonal. The dependency is avoided by considering V_j and V_{j-1} , y_j and y_{j-1} as variables that do not depend on each other but satisfy the model equations.

Consequently, although vapor flows and composition can be calculated explicitly leading to a reduced number of model states, in the presented model, they are included as states, because this formulation does not destroy the block diagonal structure of the model Jacobian.

3.3 Dynamic simulation

The equations presented involve a series of parameters that need to be tuned. Table 3.2 summarizes the parameters used in this equilibrium model. Some of the values of those parameters are taken from Diehl (2002), while others are adapted to the CIT distillation column described in Section 3.1. For instance pressure drops

are considerably smaller since a structured packing is used as column internals. The temperature of the reflux T_C , is assumed a measurable disturbance for the model and it is correlated with the removed heat in the condenser and the heat losses in the top stage (Diehl, 2002).

Table 3.2: Initial guess for parameters in the equilibrium model for the CIT column.

	Parameter	Value	Unit	Description
p_1	α_r	0.35		Rectifying section tray efficiency
p_2	α_s	0.62		Stripping section tray efficiency
p_3	Q_{loss}	0.51	kW	Heat losses in the reboiler
p_4	W_{tray}	5.2494	$\text{m}^{-\frac{3}{2}}\text{s}^{-1}$	Tray geometry coefficient
p_5	M^{ref}	0.155×10^{-3}	m^3	Reference volumetric holdup
p_6	ΔP_r	19	Pa	Rectifying section pressure drop
p_7	ΔP_s	25	Pa	Stripping section pressure drop
p_8	P_{top}	101325	Pa	Top pressure
p_9	\bar{v}_R	5×10^{-3}	m^3	Reboiler Liquid volume
p_{10}	\bar{v}_D	2×10^{-3}	m^3	Reflux drum Liquid volume
p_{11}	x_F	0.67	mol/mol	Methanol composition in the feed
p_{12}	M_F^{ref}	0.17	m^3	Reference volume for the feed tray

Table 3.3 illustrates the variables that can be manipulated in the distillation setup. Note that, although top and bottom flows are manipulated variables, they have not been included here since values for those flows are indirectly set by the liquid volumes in the reflux drum and reboiler.

Table 3.3: Manipulated variables in the CIT distillation setup.

	Value	Unit	Description	Control
u_1	4.5	kW	Reboiler duty	Q_R
u_2	80	g/min	Reflux	L_r
u_3	150	g/min	Feed flow	F
u_4	318.15	K	Feed temperature	T_F

In order to run a dynamic simulation, initial values for the model states have to be provided, i.e., stages composition, temperatures, molar holdups, liquid and vapor flows. Here, initialization is performed by interpolating initial values from the model presented in Diehl (2002). However, it is possible to calculate initial values for temperature, compositions and flows from the temperature measurements if

pressure is assumed constant along the column as it is presented in Section 4.3.1. Nevertheless, molar holdups have to be estimated from liquid flows using the Francis weir formula. The resulting DAE does not exhibit stiffness since the fast dynamics due to the vapor holdup have been neglected. Moreover, this assumption allows an easy integration of the DAE using off-the-shelf solvers (Shampine et al., 1999), (Hindmarsh et al., 2005). Figure 3.3 displays the dynamic response of the equilibrium model when a change of 10% is applied to the manipulated variables Q_R and L_r . Note that the model response to a step change in reboiler duty Q_R leads to an instantaneous change in vapor flow. This behavior originates from the lack of equations that properly model the heat transfer between the actuator and the mass of liquid in the reboiler. Equations to model this heat transfer resistance are not considered. Consequently, due to the saturated liquid in the reboiler an increase or decrease of heat immediately changes the vapor flow. Filters can be added to the actuator to mimic the real behavior of the setup. On the other hand, it is possible to notice the asymmetric gain of the process when the manipulated variables are increased or decreased by the same amount.

3.4 Sensitivity analysis of model parameters

The equilibrium model presented uses the set of parameters listed in Table 3.2. Figure 3.4 shows the steady state temperature profile, obtained by simulating the model and sampling the real setup, under the conditions described in Table 3.3. The model temperatures for the N stages have been linearly interpolated to obtain eleven samples corresponding to the sensors in the real setup.

It is clear that the set of model parameters requires a proper tuning to fit the measured profile. Since the set of measurable states is limited to temperatures, and offline measurement of top and bottom compositions, it is convenient to verify if the model parameters can be estimated from the available measurements. A simple procedure to perform this analysis is to calculate the state sensitivities with respect to model parameters. Here, the DAE solver with sensitivity capabilities proposed in Hindmarsh et al. (2005) is used. Figures 3.5 and 3.6 illustrate the time evolution in top and bottom temperature trajectories due to a 10 percent change in the four manipulated variables. These trajectories are compared when a 10 percent change is performed on each one of the 12 parameters considered in the model. The change in temperature profile is calculated from

$$\Delta T_j(t, p_i) \approx \frac{\partial T_j}{\partial p_i}(t) \Delta p_i, \quad (3.30)$$

where i is the index of the parameter and the sensitivity of the temperature at stage j , $\frac{\partial T_j}{\partial p_i}(t)$, is obtained using the solver mentioned above. This procedure

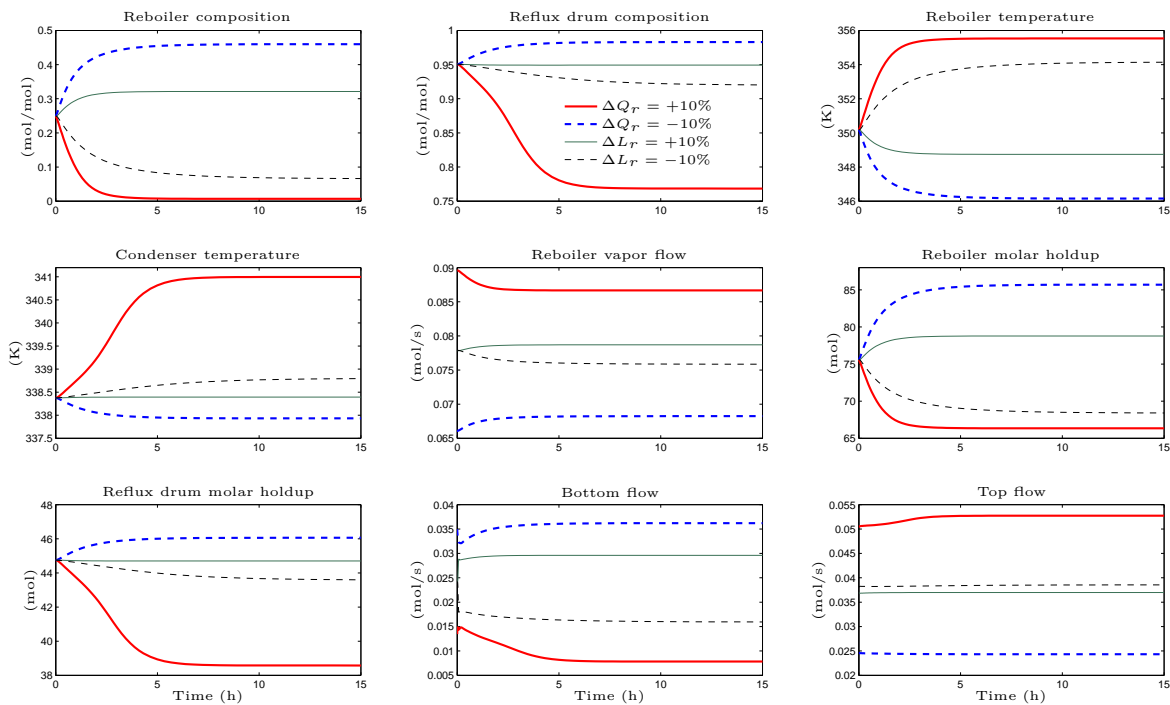


Figure 3.3: Equilibrium model response to 10 percent changes in the reflux and reboiler duty. Note the immediate response of vapor flows to changes in reboiler duty, due to the neglected dynamics of the heat transfer from the actuator. A similar behavior is expected from top and bottom flows due to the perfect volume control assumption.

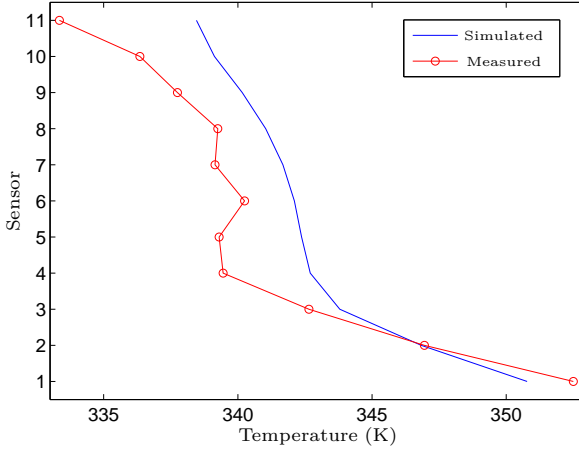


Figure 3.4: Steady state profiles obtained from model and real process under the conditions in Table 3.3.

gives an indication of the parameter influence over the temperature at stage j . As noticed in Figures 3.5 and 3.6, all the parameters related to liquid dynamics, i.e., W_{tray} , M^{ref} , M_F^{ref} , \bar{v}_R and \bar{v}_D only influence the dynamic response.

The total influence of parameter p_i over the temperature profile along the column, i.e., over the N stages, when the four manipulated variables are perturbed, is quantified in the norm

$$\|S_i\| = \frac{1}{4Nk_f} \sum_{m=1}^4 \sum_{j=1}^N \sum_{k=0}^{k_f-1} \|\Delta T_j^m(t_k, p_i)\|_2^2. \quad (3.31)$$

Here, k_f corresponds to the number of integration steps used by the DAE solver to represent the dynamic trajectory of the sensitivities, while m is the number of manipulated variables. The same norm can be applied to other states, e.g., compositions and holdups to study the influence of parameters on those states. Figure 3.7 shows the proposed norm when ΔT and Δx are calculated from 10 percent changes on each one of the 12 parameters independently. Note that parameters such as pressure drops do not have a big influence on the change in temperature. In this particular case, since the pressure drop is relatively low due to the packing material and with respect to the pressure at the top, the change in pressure drop must be considerably high to have noticeable effect on the temperature trajectories. Hence, only a subset of p has a significant influence

on the temperature. Consequently, the set of parameters can be reduced to the following seven: α_r , α_s , Q_{loss} , W_{tray} , M^{ref} , P_{top} and x_F . Volumes in the reboiler and condenser need to change considerably to influence the temperature profiles appreciably.

3.5 Conclusions

This chapter has presented an equilibrium based model for distillation. The necessary dynamic and algebraic equations along with the required thermodynamic correlations have been introduced through the chapter and the included appendices. A particular form of organizing states and equations is proposed so that the resulting model Jacobian is banded and its structure can be easily exploited by nonlinear equations solvers. This structure is obtained by grouping states and equations per stage and clearly associating a state in an stage to the equation that determines it. Moreover, it is concluded that the structure of the problem is preserved if the vapor flow and composition are not eliminated from the model states, as could be done using explicit expressions for those variables. Although the used model is based in previous work (Diehl, 2002), modifications to the existing model are performed so that well documented correlations are used instead of particular ones, allowing for the formulation of a more general model that can be easily employed to represent the behavior of separation of different binary mixtures.

Due to the limited number of measurements available, a sensitivity analysis of models states with respect to parameters is performed. This test allows for a classification of parameters that cannot be identified from steady state data, since their sensitivities vanish in time. Moreover, the test shows that only a reduced set of the proposed model parameters exhibit a high influence on the measurable states. Hence the search space for parameter estimation routines can be reduced from twelve parameters to seven in the proposed model. The non identified parameter values can be set to their initial guesses.

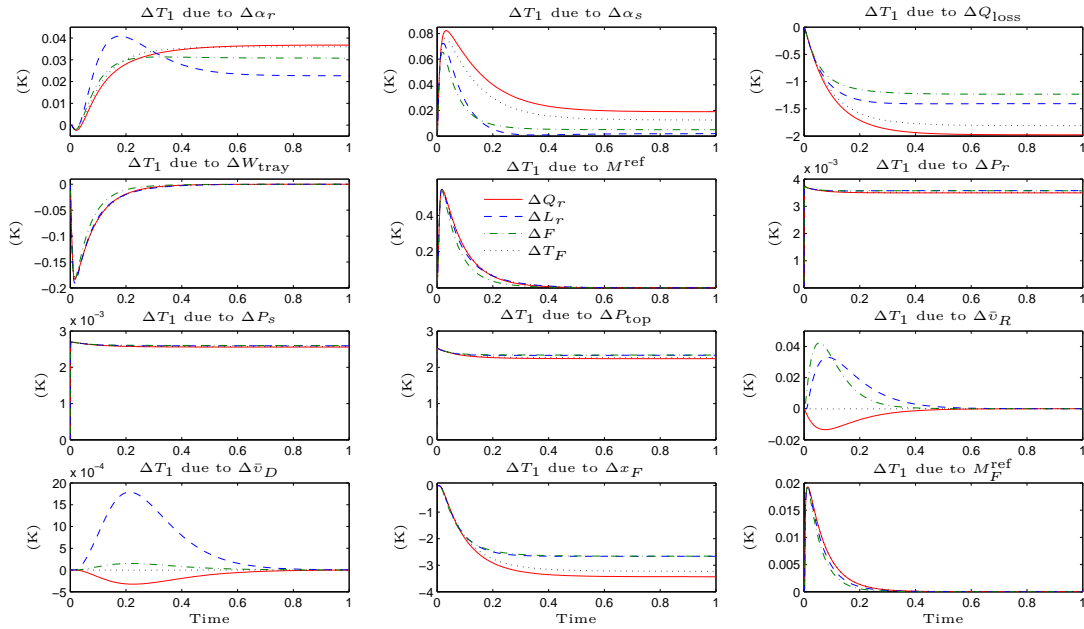


Figure 3.5: Change in bottom temperature response due to 10 percent change in the 4 manipulated variables when the 12 model parameters are perturbed 10 percent over their initial guesses.

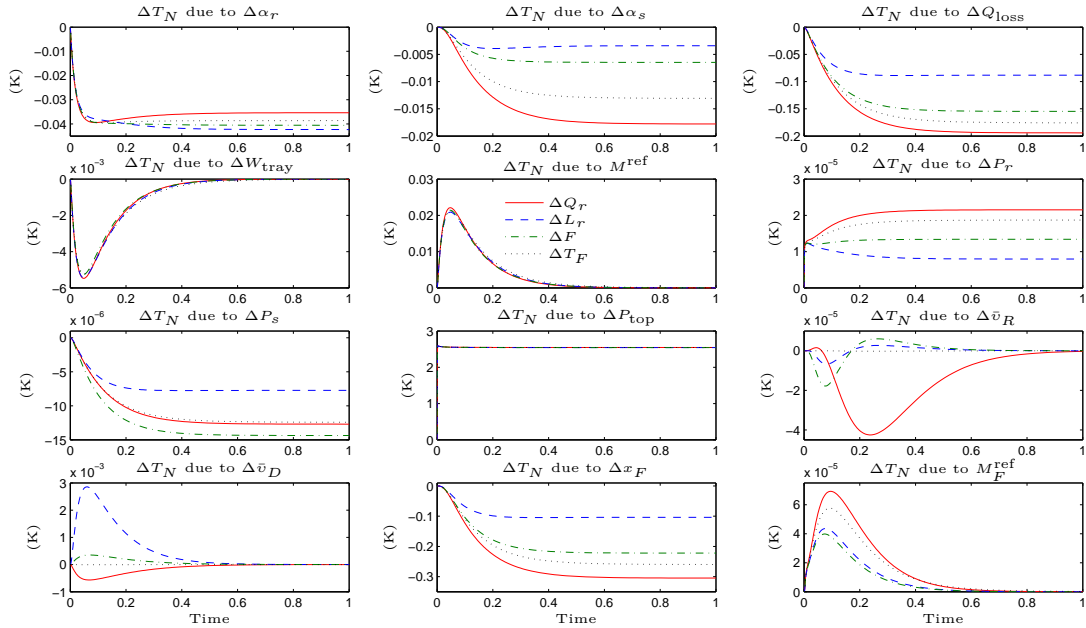


Figure 3.6: Change in condenser temperature due to changes in the 4 manipulated variables when the 12 model parameters are perturbed 10 percent over their initial guesses.

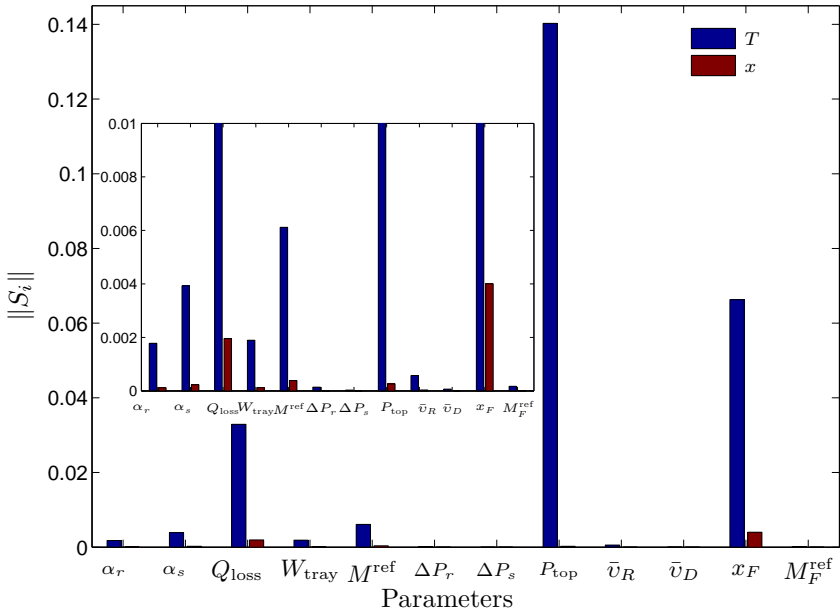


Figure 3.7: Norm on the change of temperature and liquid composition with respect to the 12 model parameters when changes of 10 percent are considered in the four manipulated variables of the model.

Chapter 4

A rate based model for separation in packed columns

This chapter presents the bases for the dynamic simulation and parameter estimation of a *Rate Base Model* (RBM) for distillation in packed columns. The differential-algebraic equations that describe the system are explained in Section 4.1. The number of states required to describe the model is reduced by constraint differentiation and algebraic manipulation in Section 4.2. Nevertheless, the model still involves a large number of differential and algebraic variables. As a first approach to evaluate the model properties, a steady state simulation is performed in Section 4.3, where model structure is exploited to reduce the computational cost involved due to the considerable number of states. In Section 4.4 the parameter estimation problem for the steady estate model is introduced, highlighting the constraints that the parameters need to satisfy in order to obtain state trajectories that are physically possible. Section 4.5 introduces the higher index DAE problem and proposes an index reduction procedure based on model dynamic properties. The reduced index model is simulated using a sparse formulation and a dynamic sensitivity analysis is performed in order to study the influence of model parameters in measurable trajectories. Conclusions to the chapter follow in Section 4.6.

The classical approach for modelling stage-wise columns employs models where the stages are considered in thermodynamic equilibrium. However, this equilibrium-stage approach is not completely valid since, in general, vapor and liquid leaving a stage are not necessarily at the same temperature. To cope with this problem the concept of stage efficiency is introduced. Nevertheless, the stage efficiency method is still deficient when multicomponent processes are analyzed or when the efficiency is relatively low (Seader and Henley, 2006). To this end, mass transfer

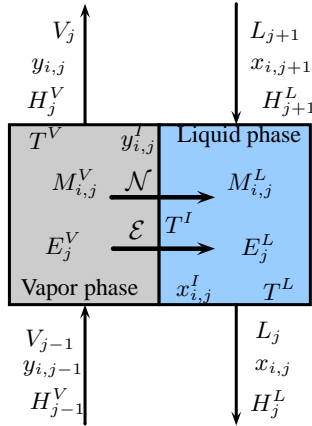


Figure 4.1: Non-equilibrium stage in the rate based model.

considerations are used to more accurately model the interaction between vapor and liquid phases along the column. In this approach, each stage is assumed in mechanical but not thermal equilibrium and it is composed of bulk phases, normally liquid and vapor, that are in contact at the stage interface.

Following a two film theory (Seader and Henley, 2006), a non-equilibrium stage is modeled so that mass and energy transfer are performed between the bulk phases through an interface. This transfer is driven by temperature and composition gradients. This division of the stage in three regions, namely vapor bulk phase, liquid bulk phase and interface, allows the modeling of superheated and subcooled phases. These regions are normally not covered in equilibrium based approaches. Figure 4.1 depicts a non-equilibrium stage in the rate based model (RBM) as proposed by Krishnamurthy and Taylor (1985). Mass and energy transfer between molar holdups in each phase M_j^V , M_j^L and E_j^L , E_j^V is accomplished through the interface by the energy \mathcal{E} and mass \mathcal{N} flows. Independent balances are obtained for each phase, while equilibrium conditions, linking the bulk phases and the interface, are formulated as presented in the following paragraphs.

The model presented in this chapter is based on the following assumptions

Assumption 4.0.1 (Rate based model).

- A binary mixture is considered.
- Each stage is in mechanical equilibrium.
- Bulk phases are perfectly mixed with respect to temperature and composition.

- Vapor-liquid equilibrium is only assumed at the vapor-liquid interface.
- The reboiler and condenser are assumed at thermal and mechanical equilibrium.
- A partial reboiler is modeled.
- The condenser is at atmospheric pressure.
- The pressure drop in the condenser is constant and known.

4.1 The rate based model

A dynamic model is developed, based on the work presented in Kooijman (1995), Taylor and Krishna (1993) and Taylor et al. (1994). Steady state and dynamic simulations are considered here along with the necessary changes to successfully find a solution to both formulations. The packed column is divided in three sections, i.e., (i) reboiler, (ii) non-equilibrium stages and (iii) condenser plus reflux drum. Each one of these sections is modeled in the following paragraphs using dynamic and algebraic equations¹.

4.1.1 Reboiler

A partial reboiler is considered, assuming thermal and mechanical equilibrium. Under these conditions, the equilibrium stage is modeled by the following mass, energy balances and equilibrium equations:

$$\dot{M}_{1,1}^L = L_2 x_{1,2}^I - B x_{1,1}^I - V_1 y_{1,1}^I, \quad (4.1)$$

$$\dot{M}_{2,1}^L = L_2 x_{2,2}^I - B x_{2,1}^I - V_1 y_{2,1}^I, \quad (4.2)$$

$$\dot{E}_1^L = L_2 H_2^L - B H_1^L - V_1 H_1^V + Q_R - Q_1^L, \quad (4.3)$$

$$g_{M_{t_1}^L} = M_{1,1}^L + M_{2,1}^L - M_{t_1}^L, \quad (4.4)$$

$$g_{E_1^L} = M_{t_1}^L H_1^L - E_1^L, \quad (4.5)$$

$$g_{M_{v_1}^L} = B - B^{\text{ref}}, \quad (4.6)$$

¹Inhere, g is used to represent the algebraic constraints.

$$g_{K_{1,1}} = y_{1,1}^I - K_{1,1}x_{1,1}^I, \quad (4.7)$$

$$g_{K_{2,1}} = y_{2,1}^I - K_{2,1}x_{2,1}^I, \quad (4.8)$$

$$g_{S_{y,1}} = y_{1,1}^I + y_{2,1}^I - x_{1,1}^I - x_{2,1}^I, \quad (4.9)$$

$$g_{P_1} = P_2 + \Delta P_2 - P_1. \quad (4.10)$$

This model of the reboiler leads to 3 differential and 7 algebraic equations involving 10 local² variables. The system of equations and the vector of variables can be summarized as:

$$f_1 = [\dot{M}_{1,1}^L \ \dot{M}_{2,1}^L \ \dot{E}_1^L \ g_{M_{t_1}^L} \ g_{M_{v_1}^L} \ g_{E_1^L} \ g_{K_{1,1}} \ g_{K_{2,1}} \ g_{S_{y,1}} \ g_{P_1}]^T, \quad (4.11)$$

and

$$x_1 = [M_{1,1}^L \ M_{2,1}^L \ E_1^L \ M_{t_1}^L \ B \ T_1^L \ y_{1,1}^I \ y_{2,1}^I \ V_1 \ P_1]^T, \quad (4.12)$$

respectively. Liquid and vapor compositions x and y , respectively, are calculated from molar holdups using expressions such as

$$x_{i,j} = \frac{M_{i,j}^L}{M_{t_j}^L}, \quad \forall j = 1, \dots, N, \quad (4.13)$$

$$y_{i,j} = \frac{M_{i,j}^V}{M_{t_j}^V} \quad \forall j = 2, \dots, N-1. \quad (4.14)$$

4.1.2 Non-equilibrium stages

The dynamic equations for the stages $j = 2, \dots, N-1$ are described by the energy and mass balances over the bulk phases for the components $i = 1, 2$

$$\dot{M}_{1,j}^L = L_{j+1}x_{1,j+1} - L_jx_{1,j} + F_j^L x_{1,j}^F + \mathcal{N}_{1,j}, \quad (4.15)$$

$$\dot{M}_{2,j}^L = L_{j+1}x_{2,j+1} - L_jx_{2,j} + F_j^L x_{2,j}^F + \mathcal{N}_{2,j}, \quad (4.16)$$

²The term local here refers to variables that are uniquely determined by the set of equations describing the stage. Although there are more than 10 variables involved, the extra ones are determined by the stages linked to the reboiler by incoming and outgoing flows.

$$\dot{M}_{1,j}^V = V_{j-1}y_{1,j-1} - V_j y_{1,j} + F_j^V y_{1,j}^F - \mathcal{N}_{1,j}, \quad (4.17)$$

$$\dot{M}_{2,j}^V = V_{j-1}y_{2,j-1} - V_j y_{2,j} + F_j^V y_{2,j}^F - \mathcal{N}_{2,j}, \quad (4.18)$$

$$\dot{E}_j^L = L_{j+1}H_{j+1}^L - L_j H_j^L + F_j^L H_{f,j}^L - Q_j^L + \mathcal{E}_j^L, \quad (4.19)$$

$$\dot{E}_j^V = V_{j-1}H_{j-1}^V - V_j H_j^V + F_j^V H_{f,j}^V - Q_j^V - \mathcal{E}_j^V. \quad (4.20)$$

Total holdups are calculated from the geometry of the packing section and the component holdups are given as

$$\mathfrak{g}_{M_{t_j}^L} = M_{1,j}^L + M_{2,1}^L - M_{t_j}^L, \quad (4.21)$$

$$\mathfrak{g}_{M_{t_j}^V} = M_{1,j}^V + M_{2,j}^V - M_{t_j}^V, \quad (4.22)$$

$$\mathfrak{g}_{M_{t_j}^L} = M_{t_j}^L - \frac{\pi}{4}d^2 l h_{t_j}^L c_{t_j}^L, \quad (4.23)$$

$$\mathfrak{g}_{M_{t_j}^V} = M_{t_j}^V - \frac{\pi}{4}d^2 l (\epsilon - h_{t_j}^L) c_{t_j}^V, \quad (4.24)$$

$$\mathfrak{g}_{E_j^L} = E_j^L - \frac{\pi}{4}d^2 l h_{t_j}^L c_{t_j}^L H_j^L, \quad (4.25)$$

$$\mathfrak{g}_{E_j^V} = E_j^V - \frac{\pi}{4}d^2 l (\epsilon - h_{t_j}^L) c_{t_j}^V H_j^V. \quad (4.26)$$

Mass and energy transfer rates between vapor and liquid bulk phases are modeled using gradient driven mass and energy flows along with mass and heat transfer coefficients as proposed in Taylor et al. (1994).

$$\mathfrak{g}_{\mathcal{N}_{1,j}^L} = \mathcal{N}_{1,j} - a^I c_t^L k_j^L (x_{1,j}^I - x_{1,j}) - x_{1,j} (\mathcal{N}_{1,j} + \mathcal{N}_{2,j}), \quad (4.27)$$

$$\mathfrak{g}_{\mathcal{N}_{1,j}^V} = \mathcal{N}_{1,j} - a^I c_t^V k_j^V (y_{1,j} - y_{1,j}^I) - y_{1,j} (\mathcal{N}_{1,j} + \mathcal{N}_{2,j}). \quad (4.28)$$

The energy flow \mathcal{E}_j is calculated from conductive and convective fluxes as:

$$\mathcal{E}_j^V = h_j^V a_j^I (T_j^V - T_j^I) + \sum_{i=1}^2 \mathcal{N}_{i,j} \bar{H}_{i,j}^V, \quad (4.29)$$

$$\mathcal{E}_j^L = h_j^L a_j^I (T_j^I - T_j^L) + \sum_{i=1}^2 \mathcal{N}_{i,j} \bar{H}_{i,j}^L, \quad (4.30)$$

$$g_{\mathcal{E}_j} = \mathcal{E}_j^V - \mathcal{E}_j^L. \quad (4.31)$$

Equilibrium is only assumed at the interface and it is modeled using the K -values:

$$g_{K_{1,j}} = y_{1,j}^I - K_{1,j} x_{1,j}^I, \quad (4.32)$$

$$g_{K_{2,j}} = y_{2,j}^I - K_{2,j} x_{2,j}^I, \quad (4.33)$$

$$g_{S_{x,j}} = x_{1,j}^I + x_{2,j}^I - 1, \quad (4.34)$$

$$g_{S_{y,j}} = y_{1,j}^I + y_{2,j}^I - 1. \quad (4.35)$$

Pressure at each stage is obtained by calculating pressure drops ΔP from particular correlations, such as (A.70), and incorporating them into

$$g_{P_j} = P_{j+1} + \Delta P_{j+1} - P_j. \quad (4.36)$$

A non-equilibrium stage with this formulation leads to 6 differential and 14 algebraic equations/variables. The system of equations and variables is summarized in the vectors:

$$\begin{aligned} \mathbf{f}_j = & [\dot{M}_{1,j}^L \dot{M}_{2,j}^L \dot{E}_j^L g_{M_{t_j}^L} g_{M_{v,j}^L} g_{E_j^L} g_{K_{1,j}} g_{K_{2,j}} g_{S_{x,j}} g_{S_{y,j}} g_{\mathcal{E}_j} g_{N_{1,j}^L} g_{N_{1,j}^V} \\ & g_{E_j^V} g_{M_{t_j}^V} g_{M_{v,j}^V} \dot{M}_{1,j}^V \dot{M}_{2,j}^V \dot{E}_j^V g_{P_j}]^T, \end{aligned} \quad (4.37)$$

and

$$\begin{aligned} \mathbf{x}_j = & [M_{1,j}^L M_{2,j}^L E_j^L M_{t_j}^L L_j T_j^L x_{1,j}^I x_{2,j}^I y_{1,j}^I y_{2,j}^I T_j^I N_{1,j} N_{2,j} T_j^V \\ & M_{t_j}^V V_j M_{1,j}^V M_{2,j}^V E_j^V P_j]^T, \end{aligned} \quad (4.38)$$

$\forall j = 2, \dots, N - 1$, respectively.

4.1.3 Equilibrium condenser

The condenser is modeled using the following static equations.

Energy balance

$$g_{E_{t,N}^L} = V_{N-1}H_N^V - L_cH_c^L + Q_C. \quad (4.39)$$

Equilibrium

$$g_{K_{1,N}} = y_{1,N}^I - K_{1,N}x_{1,N}^I, \quad (4.40)$$

$$g_{K_{2,N}} = y_{2,N}^I - K_{2,N}x_{2,N}^I, \quad (4.41)$$

$$g_{S_1} = x_{1,N}^I + x_{2,N}^I - 1, \quad (4.42)$$

$$g_{S_2} = y_{1,N}^I + y_{2,N}^I - 1. \quad (4.43)$$

Pressure

$$g_{P_N} = P_{\text{atm}} - P_N. \quad (4.44)$$

Vapor composition

$$g_{y_{1,N}} = y_{1,N-1} - y_{1,N}^I, \quad (4.45)$$

Notice that no differential equation is used in this model formulation, leading to 7 algebraic equations/variables. Those variables are summarized in Table 4.1.

Reflux drum

The model is described by the mass and energy balances and total holdup summations:

$$\dot{M}_{1,N}^L = L_c x_{1,N}^I - (L_r + D)x_{1,N}, \quad (4.46)$$

$$\dot{M}_{2,N}^L = L_c x_{2,N}^I - (L_r + D)x_{2,N}, \quad (4.47)$$

$$\dot{E}_N^L = L_c H_N^L - (L_r + D)H_N^L, \quad (4.48)$$

$$g_{M_{t,N}^L} = M_{1,N}^L + M_{2,N}^L - M_{t,N}^L, \quad (4.49)$$

$$g_{E_N^L} = M_{t_N}^L H_N^L - E_N^L, \quad (4.50)$$

$$g_{M_{v_N}^L} = D - D^{\text{ref}}, \quad (4.51)$$

leading to 3 differential and 3 algebraic equations.

The model for the condenser and reflux drum leads to 3 differential and 10 algebraic equations and variables organized as follows

$$\begin{aligned} f_N = & [g_{y_{1,N}} \dot{M}_{1,N}^L \dot{M}_{2,N}^L \dot{E}_N^L g_{M_{t_N}^L} g_{E_N^L} g_{M_{v_N}^L} g_{K_{1,N}} g_{K_{2,N}} \\ & g_{S_{x_N}} g_{S_{y_N}} g_{P_j} g_{E_{t_N}^L}]^T, \end{aligned} \quad (4.52)$$

and

$$\begin{aligned} x_N = & [y_{1,N}^I y_{2,N}^I M_{1,N}^L M_{2,N}^L E_N^L M_{t_N}^L T_N^L D x_{1,N}^I x_{2,N}^I T_N^I \\ & P_N Q_C]^T, \end{aligned} \quad (4.53)$$

respectively.

It has to be mentioned that for steady state simulation (4.6) and (4.51) are modified with

$$g_{M_{v,1}^L} = v_{t_1}^L M_{t_1}^L - \bar{v}_R, \quad (4.54)$$

$$g_{M_{v,N}^L} = v_{t_N}^L M_{t_N}^L - \bar{v}_D, \quad (4.55)$$

respectively (Kooijman, 1995). These modifications account for fixed volumes in the reboiler and condenser. Table 4.1 summarizes the equations and variables used to simulate the model.

4.2 Reduced order rate based model

In this section, a reduction of the number of states required to describe the model behavior is performed. Note that compositions are calculated from molar holdups

Table 4.1: Summary of variables and equations involved in the RBM proposed in Taylor and Krishna (1993).

Stage	Variables ^a			Associated equation	Total var./eq.
	name	units	type ^b		
Reboiler $j = 1$	$M_{1,1}^L$	mol	D	(4.1)	10
	$M_{2,1}^L$	mol	D	(4.2)	
	E_1^L	kW	D	(4.3)	
	M_{t1}^L	mol	A	(4.4)	
	V_1	mol/s	A	(4.5)	
	B	mol/s	A	(4.6)	
	$y_{1,1}$	mol	A	(4.7)	
	$y_{2,1}$	mol	A	(4.8)	
	$T_{1,1}^L$	K	A	(4.9)	
	P_1	Pa	A	(4.10)	
Non-equilibrium $j = 2, \dots, N - 1$	$M_{1,j}^L$	mol	D	(4.15)	$20(N - 2)$
	$M_{2,j}^L$	mol	D	(4.16)	
	$M_{1,j}^V$	mol	D	(4.17)	
	$M_{2,j}^V$	mol	D	(4.18)	
	E_j^L	kW	D	(4.19)	
	E_j^V	kW	D	(4.20)	
	M_{tj}^L	mol	A	(4.21)	
	M_{tj}^V	mol	A	(4.22)	
	V_j	mol/s	A	(4.23)	
	L_j	mol/s	A	(4.24)	
	T_j^L	K	A	(4.25)	
	T_j^V	K	A	(4.26)	
	$\mathcal{N}_{1,j}$	mol/s	A	(4.27)	
	$\mathcal{N}_{2,j}$	mol/s	A	(4.28)	
	T_j^I	K	A	(4.31)	
	$y_{1,j}^I$	mol	A	(4.32)	
	$y_{2,j}^I$	mol	A	(4.33)	
	$x_{1,j}^I$	mol	A	(4.34)	
	$x_{2,j}^I$	mol	A	(4.35)	
	P_j	mol	A	(4.36)	
Condenser $j = N$	T_N^I	K	A	(4.41)	7
	Q_C	kW	A	(4.39)	
	$y_{1,N}^I$	mol	A	(4.45)	
	$y_{2,N}^I$	mol	A	(4.43)	
	$x_{1,N}^I$	mol	A	(4.40)	
	$x_{2,N}^I$	mol	A	(4.42)	
Reflux drum $j = N$	P_N	Pa	A	(4.44)	6
	$M_{1,N}^L$	mol	D	(4.46)	
	$M_{2,N}^L$	mol	D	(4.47)	
	E_N^L	kW	D	(4.48)	
	M_{tN}^L	mol	A	(4.49)	
	T_N^L	K	A	(4.50)	
D	mol/s	A	(4.51)		

^aA binary mixture is considered

^bD and A stand for differential and algebraic variables respectively.

by

$$x_{i,j} = \frac{M_{i,j}^L}{M_{t_j}^L}, \quad \forall j = 1, \dots, N, \quad (4.56)$$

$$y_{i,j} = \frac{M_{i,j}^V}{M_{t_j}^V} \quad \forall j = 2, \dots, N-1, \quad (4.57)$$

and energy holdups could be explicitly determined from total molar holdups and enthalpies using expressions like

$$E_j^p = M_{t_j}^p H_j^p, \quad (4.58)$$

where p denotes the liquid bulk phase ($p = L$), or the vapor bulk phase ($p = V$). If these expressions for holdups are replaced in the differential equations, the whole model can be expressed in a new set of differential variables, i.e., x , y , T^L , T^V , M_t^L and M_t^V . The advantages are that the number of states and algebraic constraints are reduced without losing model structure. The disadvantage is that expressions for the change in enthalpy with respect to time need to be calculated, which can be a tedious task.

Consequently, the number of algebraic variables required for the model can be reduced by properly substituting the presented relations into the original RBM.

4.2.1 Enthalpies and their derivatives

The separation model requires enthalpy relations for vapor and liquid bulk phases. These expressions are composition and temperature dependent.

If the expression (4.58) is substituted in the differential equations involving the change in energy per time unit for the bulk phase p , \dot{E}_j^p , relations of the form

$$M_{t_j}^p \frac{\partial H_j^p}{\partial t} + H_j^p \frac{\partial M_{t_j}^p}{\partial t} = \text{energy balance in stage } j, \text{ phase } p, \quad (4.59)$$

are obtained. On the one hand, expressions for the time derivative of total composition holdups are easily determined from individual component holdups. For the binary case,

$$\dot{M}_t^p = \dot{M}_{1,j}^p + \dot{M}_{2,j}^p, \quad (4.60)$$

$$x_{2,j} = 1 - x_{1,j}, \quad (4.61)$$

$$y_{2,j} = 1 - y_{1,j}, \quad (4.62)$$

hold. On the other hand, expressions for the change of enthalpy with respect to time are obtained by the chain rule, i.e.,

$$\frac{\partial H_j^L}{\partial t} = \frac{\partial H_j^L}{\partial x_{1,j}} \dot{x}_{1,j} + \frac{\partial H_j^L}{\partial T_j^L} \dot{T}_j^L, \quad (4.63)$$

$$\frac{\partial H_j^V}{\partial t} = \frac{\partial H_j^V}{\partial y_{1,j}} \dot{y}_{1,j} + \frac{\partial H_j^V}{\partial T_j^V} \dot{T}_j^V. \quad (4.64)$$

Hence, the model can be expressed in terms of the new differential variables $\dot{x}_{1,j}$, $\dot{y}_{1,j}$, \dot{T}^L , \dot{T}^V , \dot{M}_t^L and \dot{M}_t^V which are linked to the original variables by (4.56), (4.57) and (4.58). The derivation of expressions for the enthalpy derivatives is included in appendix A.

The new reduced order rate based model (RORBM) is formulated only in terms of the light component composition due to the binary mixture assumption, i.e., $x = x_1$, $y = y_1$, $x^I = x_1^I$ and $y^I = y_1^I$. In the following the set of equations describing each stage, with the simplifications proposed, are presented.

4.2.2 Reboiler

With the proper substitutions, the model for the reboiler, $j = 1$, is reduced to:

$$\dot{M}_{t,j}^L = L_{j+1} - B - V_j, \quad (4.65)$$

$$\dot{x}_j = \frac{L_{j+1}(x_{j+1} - x_j) + V_j(x_j - y_j)}{M_{t,j}^L}, \quad (4.66)$$

$$\begin{aligned} \dot{T}_j^L = & \frac{L_{j+1} \left(H_{j+1}^L - H_j^L - \frac{\partial H_j^L}{\partial x} (x_{j+1} - x_j) \right)}{M_{t,j}^L \frac{\partial H_j^L}{\partial T^L}} \\ & + \frac{V_j \left(H_j^L - H_j^V + \frac{\partial H_j^L}{\partial x} (y_j - x_j) \right) + Q_R - Q_L}{M_{t,j}^L \frac{\partial H_j^L}{\partial T^L}}, \end{aligned} \quad (4.67)$$

$$g_{K_{x,1}} = y - K_{1,j}x, \quad (4.68)$$

$$g_{K_{y,1}} = (1 - y) - K_{2,j}(1 - x), \quad (4.69)$$

$$g_{P_1} = P_{j+1} + \Delta P_{j+1} - P_j, \quad (4.70)$$

$$g_{M_{v_1}^L} = B - B^{\text{ref}}. \quad (4.71)$$

Note that B^{ref} in (4.71) is used as a control variable and helps to determine the volumetric holdup of the reboiler. For steady state simulation, (4.71) can be replaced by (4.73)

Further simplifications in the reboiler equations

Although the previous equations for the reboiler describe the dynamics of the system, it is possible to simplify the model even more by assuming a constant volume in the reboiler. If that is the case, (4.65) and (4.71) must be replaced by

$$g_{M_{t_1}^L} = v_{t_j}^L(L_{j+1} - B - V_j) + M_{t_j}^L \left(\frac{\partial v_{t_j}^L}{\partial x_j} \dot{x}_j + \frac{\partial v_{t_j}^L}{\partial T_j^L} \dot{T}_j^L \right) \quad (4.72)$$

$$g_{M_{v_1}^L} = v_{t_1}^L M_{t_1}^L - \bar{v}_R, \quad (4.73)$$

respectively. Note that this kind of assumption transforms $M_{t_1}^L$ in an algebraic variable, since the differential equation corresponding to that variable is converted to an algebraic constraint. It is shown during the dynamic simulation that this kind of assumption presents numerical advantages when solving the model dynamically. Moreover, if this assumption is made, the bottom flow B^{ref} is not a degree of freedom anymore and it is determined by the control loop that allows for a constant volume in the reboiler or, in this case, by the assumption (4.72).

Ordering states and equations in a particular form provides advantages when solving the nonlinear system. Here the following equations and states order is proposed for the reboiler:

$$f_1 = [g_{M_{v_1}^L} \dot{M}_{t_1}^L \dot{x}_1 \dot{T}_1^L g_{K_{1,1}} g_{K_{2,1}} g_{P_1}]^T, \quad (4.74)$$

and

$$\mathbf{x}_1 = [B \ M_{t_1}^L \ x_1 \ T_1^L \ y_1^I \ V_1 \ P_1]^T. \quad (4.75)$$

4.2.3 Non-equilibrium stage

Likewise, the model for a non-equilibrium stage is reduced to the set of differential equations from mass and energy balance

$$\dot{M}_{t,j}^L = L_{j+1} - L_j + \mathcal{N}_{1,j} + \mathcal{N}_{2,j} + F_j^L \quad (4.76)$$

$$\dot{x}_j = \frac{L_{j+1}(x_{j+1} - x_j) + F_j^L(x_j^F - x_j) + \mathcal{N}_{1,j} - (\mathcal{N}_{1,j} + \mathcal{N}_{2,j})x_j}{M_{t_j}^L}, \quad (4.77)$$

$$\begin{aligned} \dot{T}_j^L = & \frac{L_{j+1} \left(H_{j+1}^L - H_j^L - \frac{\partial H_j^L}{\partial x}(x_{j+1} - x_j) \right) + \mathcal{E}_j^L - Q_j^L}{M_{t_j}^L \frac{\partial H_j^L}{\partial T^L}} \\ & + \frac{F_j^L \left(H_{F,j}^L - H_j^L - \frac{\partial H_j^L}{\partial x}(x_j^F - x_j) \right) - \frac{\partial H_j^L}{\partial x} \mathcal{N}_{1,j}}{M_{t_j}^L \frac{\partial H_j^L}{\partial T^L}} \\ & + \frac{(\mathcal{N}_{1,j} + \mathcal{N}_{2,j}) \left(\frac{\partial H_j^L}{\partial x} x_j - H_j^L \right)}{M_{t_j}^L \frac{\partial H_j^L}{\partial T^L}}, \end{aligned} \quad (4.78)$$

$$\dot{M}_{t,j}^V = V_{j-1} - V_j - (\mathcal{N}_{1,j} + \mathcal{N}_{2,j}) + F_j^V, \quad (4.79)$$

$$\dot{y}_j = \frac{V_{j-1}(y_{j-1} - y_j) + F_j^V(y_j^F - y_j) - \mathcal{N}_{1,j} + (\mathcal{N}_{1,j} + \mathcal{N}_{2,j})y_j}{M_{t_j}^L}, \quad (4.80)$$

$$\dot{T}_j^V = \frac{V_{j-1} \left(H_{j-1}^V - H_j^V - \frac{\partial H_j^V}{\partial y}(y_{j-1} - y_j) \right) - \mathcal{E}_j^V - Q_j^V}{M_{t_j}^V \frac{\partial H_j^V}{\partial T^V}}$$

$$\begin{aligned}
& + \frac{F_j^V \left(H_{F,j}^V - H_j^V - \frac{\partial H_j^V}{\partial y} (y_j^F - y_j) \right) + \frac{\partial H_j^V}{\partial y} \mathcal{N}_{1,j}}{M_{t_j}^V \frac{\partial H_j^V}{\partial T^V}} \\
& + \frac{(\mathcal{N}_{1,j} + \mathcal{N}_{2,j}) \left(H_j^V - \frac{\partial H_j^V}{\partial y} y_j \right)}{M_{t_j}^V \frac{\partial H_j^V}{\partial T^V}}, \tag{4.81}
\end{aligned}$$

and the algebraic relations presented in the following paragraphs.

Molar holdups are calculated from the geometry

$$g_{M_{t_j}^L} = M_{t_j}^L - \frac{\pi}{4} d^2 l h_{t_j}^L c_{t_j}^L, \tag{4.82}$$

$$g_{M_{t_j}^V} = M_{t_j}^V - \frac{\pi}{4} d^2 l (\epsilon - h_{t_j}^L) c_{t_j}^V. \tag{4.83}$$

Mass and energy transfer are assumed at the interface

$$g_{\mathcal{N}_j^L} = \mathcal{N}_{1,j} - a^I c_t^L k_j^L (x_j^I - x_j) - x_j (\mathcal{N}_{1,j} + \mathcal{N}_{2,j}), \tag{4.84}$$

$$g_{\mathcal{N}_j^V} = \mathcal{N}_{1,j} - a^I c_t^V k_j^V (y_j - y_j^I) - y_j (\mathcal{N}_{1,j} + \mathcal{N}_{2,j}). \tag{4.85}$$

The energy fluxes \mathcal{E}_j are calculated from conductive and convective fluxes as

$$\mathcal{E}_j^V = h_j^V a_j^I (T_j^V - T_j^I) + \sum_{i=1}^2 \mathcal{N}_{i,j} \bar{H}_{i,j}^V, \tag{4.86}$$

$$\mathcal{E}_j^L = h_j^L a_j^I (T_j^I - T_j^L) + \sum_{i=1}^2 \mathcal{N}_{i,j} \bar{H}_{i,j}^L, \tag{4.87}$$

$$g_{\mathcal{E}_j} = \mathcal{E}_j^V - \mathcal{E}_j^L. \tag{4.88}$$

The interface equilibrium is modeled by

$$g_{K_{1,j}} = y_j^I - K_{1,j} x_j^I, \tag{4.89}$$

$$g_{K_{2,j}} = (1 - y_j^I) - K_{2,j} (1 - x_j^I), \tag{4.90}$$

and the pressure at each stage is obtained from:

$$g_{P_j} = P_{j+1} + \Delta P_{j+1} - P_j. \quad (4.91)$$

Equations and states are organized as

$$\begin{aligned} f_j = & [\dot{x}_j \dot{T}_j^L \dot{M}_{t_j}^L g_{M_{v_j}^L} g_{K_{1,j}} g_{K_{2,j}} g_{\varepsilon_j} g_{N_{1,j}^L} g_{N_{1,j}^V} g_{M_{v_j}^V} \dot{M}_{t_j}^V \\ & \dot{y}_j \dot{T}_j^V g_{P_j}]^T, \end{aligned} \quad (4.92)$$

and

$$x_j = [x_j T_j^L M_{t_j}^L L_j x_j^I y_j^I T_j^I N_{1,j} N_{2,j} V_j M_{t_j}^V y_j T_j^V P_j]^T, \quad (4.93)$$

$\forall j = 2, \dots, N - 1$, respectively.

4.2.4 Equilibrium condenser

The total condenser equations do not change considerably, since no differential variables are involved in its model. However, due to the binary mixture assumption only the light component composition is used in the calculations.

The energy balance leads to

$$g_{E_{t,N}} = V_{N-1} H_N^V - L_c H_N^L + Q_C. \quad (4.94)$$

Equilibrium relations and pressure are described by

$$g_{K_{1,N}} = y_N^I - K_{1,N} x_N^I, \quad (4.95)$$

$$g_{K_{2,N}} = (1 - y_N^I) - K_{2,N} (1 - x_N^I), \quad (4.96)$$

$$g_{y_N} = y_{N-1} - y_N^I, \quad (4.97)$$

and,

$$g_{P_N} = P_{\text{atm}} - P_N, \quad (4.98)$$

respectively.

Reflux drum

The reflux drum model is reduced to

$$\dot{M}_{t_N}^L = L_c - L_r - D, \quad (4.99)$$

$$\dot{x}_N^L = \frac{L_c(x_N^I - x_N)}{M_{t_N}^L}, \quad (4.100)$$

$$\dot{T}_N^L = \frac{L_c \left(H_C^L - H_N^L - \frac{\partial H_N^L}{\partial x} (x_N^I - x_N) \right) - Q_N^L}{M_{t_N}^L \frac{\partial H^L}{\partial T^L}}, \quad (4.101)$$

$$g_{M_{v,N}^L} = D - D^{\text{ref}}, \quad (4.102)$$

where the outflow D^{ref} is a control variable that can be used to set the volumetric holdup in the reflux drum. For steady state simulation, (4.102) is replaced with (4.104).

Further simplifications for the reflux drum

If the volume in the reflux drum is assumed constant, (4.99) and (4.102) must be replaced by

$$g_{M_{t_N}^L} = v_{t_N}^L (L_c - D - L_r) + M_{t_N}^L \left(\frac{\partial v_{t_N}^L}{\partial x_N} \dot{x}_N + \frac{\partial v_{t_N}^L}{\partial T_N^L} \dot{T}_N^L \right) \quad (4.103)$$

and

$$g_{M_{v_1}^L} = v_{t_N}^L M_{t_N}^L - \bar{v}_D, \quad (4.104)$$

respectively³. Note that, as in the reboiler, assumptions of this type transform the liquid molar holdup in the reflux drum into an algebraic variable.

The equations and states in the condenser plus reflux drum are organized as follows

$$f_N^T = [\dot{x}_N \ \dot{T}_N^L \ \dot{M}_{t_N}^L \ g_{E_{t_N}^L} \ g_{M_{v_N}^L} \ g_{K_{1,N}} \ g_{K_{2,N}} \ g_{P_j} \ g_{y_N}], \quad (4.105)$$

³The differential terms in (4.103) may vanish if the volume does not change considerably with temperature and composition.

and

$$\mathbf{x}_N^T = [x_N \ T_N^L \ M_{t_N}^L \ Q_C \ D \ T_N^I \ x_N^I \ P_N \ y_N^I]. \quad (4.106)$$

Table 4.2 summarizes the variables and equations used in the RORBM.

Table 4.2: Summary of variables and equations involved in the reduced order RBM.

Stage	Variables ^{a b}			Associated equation	Total var./eq.
	name	units	type ^c		
Reboiler $j = 1$	$M_{t_1}^L$	mol	D	(4.65)	7
	x_1^L	mol/mol	D	(4.66)	
	T_1^L	K	D	(4.67),(4.68),(4.69)	
	V_1	mol/s	A	(4.67)	
	B	mol/s	A	(4.73)	
	y_1^I	mol	A	(4.69)	
	P_1	Pa	A	(4.70)	
Non-equilibrium $j = 2, \dots, N - 1$	x_j	mol/mol	D	(4.77)	14(N - 2)
	T_j^L	K	D	(4.78)	
	$M_{t_j}^L$	mol	D	(4.76)	
	y_j	mol/mol	D	(4.80)	
	T_j^V	K	D	(4.81)	
	M_j^V	mol	D	(4.79)	
	V_j	mol/s	A	(4.82)	
	L_j	mol/s	A	(4.83)	
	$\mathcal{N}_{1,j}$	mol/s	A	(4.84)	
	$\mathcal{N}_{2,j}$	mol/s	A	(4.85)	
	T_j^I	K	A	(4.88)	
	y_j^I	mol	A	(4.89)	
	x_j^I	mol	A	(4.90)	
	P_j	mol	A	(4.91)	
Condenser $j = N$	T_N^I	K	A	(4.95)	5
	Q_C	kW	A	(4.94)	
	y_N^I	mol/mol	A	(4.97)	
	x_N^I	mol/mol	A	(4.96)	
	P_N	Pa	A	(4.98)	
Reflux drum $j = N$	x_N	mol	D	(4.100)	4
	T_N^L	mol	D	(4.101)	
	$M_{t_N}^L$	kW	D	(4.99)	
	D	mol/s	A	(4.102)	

^aConsidering a binary mixture

^bFour more differential variables/equations are added by introducing a first order filter for each one of the four manipulated variables.

^cD and A stand for differential and algebraic variables, respectively.

On the one hand, the full RBM model in (4.1)-(4.51) uses a total of $6N - 6$ differential and $14N - 8$ algebraic equations/variables, leading to $20N - 14$ equations/variables. On the other hand, the RORBM uses $6N - 6$ differential and $8N - 6$ algebraic equations/variables, i.e., a total of $14N - 12$ equations/variables. Consequently, there is a reduction of $6N - 5$ variables/equations, i.e., approximately 30 percent of the total number of variables for the original model.

4.3 Steady state model simulation

In order to simulate the dynamic model, consistent initial conditions are required, i.e., state values that satisfy the algebraic equations and its derivatives. A consistent initialization is not necessarily a steady state value of the model, however, every steady state value is consistent by definition. The approach followed here is to solve the steady state problem first, in order to find an initial value for the dynamic problem. Although off-the-shelf DAE solvers, such as ode15s (Shampine et al., 1999) and IDAS (Hindmarsh et al., 2005), provide routines to automatically calculate consistent initial values based on Newton iterations, these routines are highly dependent on the initial guess. Moreover, by obtaining the steady state profiles the capabilities of the model to reproduce measured data can be analyzed.

In the following paragraphs an initialization method based on available measurements and physical principles is proposed. This method can be related to *equation tearing* approach (Seader and Henley, 2006). However, here initial values for some states are directly obtained from measurements. Hence, a better initial point is expected.

4.3.1 Initialization of steady state simulation based on temperature measurements

A method to find an initial guess for the state vector in the RBM is proposed here. This method is based in knowledge of the physical process and although similar approaches can be derived for equilibrium models, to the author knowledge, there is no previous reference for its use with rate based models. Particularly, the use of experimental data along with assumptions based on the process behavior are expected to provide small residuals at early iterations when solving the model equations.

It is assumed that numerical values for the following variables are available:

- vapor temperatures at measurement points along the column including condenser and reboiler,
- input, output and re-circulation flows,
- temperature of the surroundings,
- pressure at the top of the column,
- reflux temperature.

Conciliating temperatures measurements with vapor-liquid equilibrium

The first step proposed here is to obtain the temperature of the interface T_j^I , from the available vapor temperature measurements \bar{T}_j^V . Since using equilibrium equations with the temperature measurements \bar{T}_j^V can lead to composition values which are beyond the possible values, the interface temperatures T^I are estimated by finding the closest value to the measurements that satisfy equilibrium. This is accomplished by formulating the convex least squares problem

$$\min_{T^I} \quad \|\bar{T}^V - T^I\|_Q^2, \quad (4.107)$$

$$\text{s.t.} \quad AT^I \geq b, \quad (4.108)$$

$$T_{b_1} \leq T^I \leq T_{b_2}, \quad (4.109)$$

where T^I and $\bar{T}^V \in \mathbb{R}^{11}$. Q is a diagonal matrix defined so that the sixth element of the measurements vector is considered an outlier. This definition is performed for this particular setup, since an abnormal behavior in the sixth sensor has been detected (see Figure 4.2). Although, it can be though that the bias in the measurement corresponding to sensor T_{s_6} is coming from its proximity to the feed heater, i.e, Q_{F_1} (see Figure 3.1), the author believes that despite the heat source can perturb the reading, this is not the origin of the problem. In fact, it would be expected that T_{s_4} and T_{s_5} provide readings with a higher deviation from the

profile than T_{s6} , since they are physically closer to the feed heater. In the problem formulation the matrix

$$A = \begin{pmatrix} -1 & 1 & 0 & 0 & 0 & 0 & 0 & 0 & 0 & 0 & 0 \\ 0 & -1 & 1 & 0 & 0 & 0 & 0 & 0 & 0 & 0 & 0 \\ 0 & 0 & 0 & 0 & -1 & 1 & 0 & 0 & 0 & 0 & 0 \\ 0 & 0 & 0 & 0 & 0 & -1 & 1 & 0 & 0 & 0 & 0 \\ 0 & 0 & 0 & 0 & 0 & 0 & -1 & 1 & 0 & 0 & 0 \\ 0 & 0 & 0 & 0 & 0 & 0 & 0 & -1 & 1 & 0 & 0 \\ 0 & 0 & 0 & 0 & 0 & 0 & 0 & 0 & -1 & 1 & 0 \\ 0 & 0 & 0 & 0 & 0 & 0 & 0 & 0 & 0 & -1 & 1 \end{pmatrix} \quad (4.110)$$

accounts for an increasing temperature profile from condenser to reboiler. Note that no decreasing-temperature constraint has been imposed on the fourth element of T^I since it corresponds to the sensor location where the column is fed, and the temperature there, is directly affected by the temperature of the feed. Bounds T_{b_1} and $T_{b_2} \in R^{11}$ have all their entries equal to the normal boiling points of methanol and isopropanol, respectively. These maximum and minimum values are obtained from Raoult's law with constant pressure and composition ranging from 0 to 1 in a binary mixture.

Figure 4.2 illustrates the vapor phase temperature measurements for a steady state test along with the temperature of the interface obtained by solving the convex optimization problem (4.107)-(4.109). Note that above 340 K there is perfect overlap between the measured profile and the possible equilibrium temperatures since those measurements can be explained by equilibrium equations.

The temperature of the liquid phase is assumed equal to the temperature of the interface for all stages excluding the reflux drum, i.e., $T_j^L = T_j^I, \forall j = 1, \dots, N - 1$. The temperature of the liquid at the reflux drum is known, hence, $T_N^L = T_{\text{reflux}}$. This initialization procedure provides values for the vapor temperatures T^V , the liquid temperatures T^L and the interface temperatures T^I from the available measurements.

Liquid composition initialization

With known values for the interface temperatures T_j^I and a constant pressure profile given by the pressure value at the condenser, the composition can be calculated from Raoult's law assuming constant activity coefficients, $\gamma_1 = \gamma_2 = 1$, i.e.,

$$x_{1,j}^I = \frac{P_j - P_{2,j}^s}{P_{1,j}^s - P_{2,j}^s}, \quad \forall j = 1, \dots, N, \quad (4.111)$$

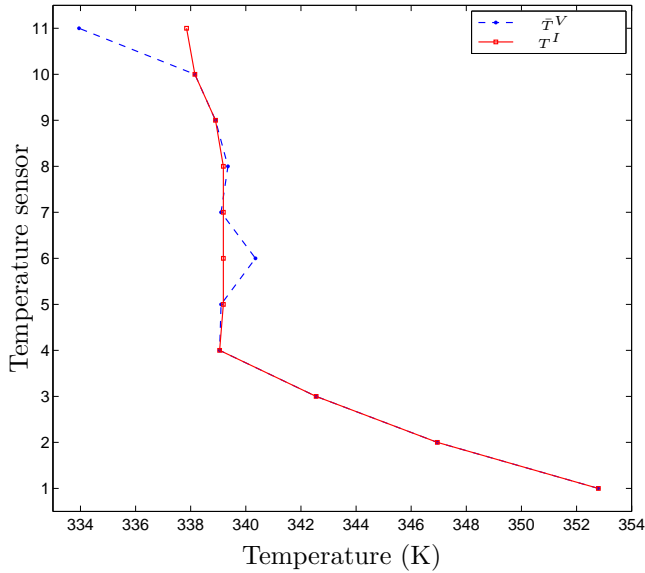


Figure 4.2: Steady state temperature measurements for the vapor phase \bar{T}^V , and the estimated interface temperatures T^I .

with the vapor pressure $P_{i,j}^s$ obtained from (A.71). Likewise, $x_{2,j}^I$ is obtained from the total component molar fraction summation relation. The liquid bulk phase composition is assumed equal to the liquid composition at the interface, i.e., $x_{i,j} = x_{i,j}^I$.

Inflow composition

The composition of the input flow can be determined by experimental measurements. However, here it is assumed to be an unknown parameter to be estimated when the identification problem is formulated. In order to provide an initial guess, the inflow is assumed in its liquid phase with a composition x_F given by

$$x_F = \frac{C_s D(x_{1,N} - x_{1,1})M_2 + F_g x_{1,1}}{F_g + C_s D(x_{1,1} - x_{1,N})(M_1 - M_2)}. \quad (4.112)$$

Equation (4.112) is obtained from a simple total composition balance around the column. Values for the light component composition $x_{1,j}$ are estimated through

(4.111) and the inflow F_g in g/min is a measured variable. M_1 and M_2 represent the components molar mass and $C_s = 60$ s/min is a unit conversion constant. The top product flow D is given in mol/s and it is obtained from the known value D_g in g/min using

$$D = \frac{D_g}{C_s(M_1x_{1,N} + (1 - x_{1,N})M_2)}. \quad (4.113)$$

Calculation of internal flows

The liquid internal flow L_j is assumed to be different for stripping and rectifying sections, i.e., below and above the feeding stage N_F , respectively. Since the reflux is known, it is possible to provide a liquid flow profile by assuming it constant along the rectifying section, an assumption normally made in binary distillation and known as *constant molar overflow*, i.e.,

$$L_N = L_r + D, \quad (4.114)$$

$$L_j = L_r, \quad \forall j = N_F, \dots, N - 1. \quad (4.115)$$

On the other hand, the liquid flow for the stripping section is given by

$$L_j = L_r + F, \quad \forall j = 1, \dots, N_F - 1. \quad (4.116)$$

with F in mol/s calculated from

$$F = \frac{F_g}{C_s(M_1x_{1,N_F} + (1 - x_{1,N_F})M_2)}. \quad (4.117)$$

The bottom flow B in mol/s, is obtained from the available value B_g in g/min, using a relation similar to (4.117). The vapor molar flows V_j are assumed constant through the whole column and are given by

$$V_j = V_1, \quad \forall j = 2, \dots, N - 1, \quad (4.118)$$

$$V_1 = L_1 - B. \quad (4.119)$$

Vapor composition

Values for the composition in the vapor phase are calculated using T^I , $x_{1,j}^I$, $x_{2,j}^I$ and activity coefficients (A.1), (A.2) along with the expressions for the equilibrium

constant (A.45),

$$y_{1,j}^I = K_{1,j}x_{1,j}^I, \quad (4.120)$$

$$y_{2,j}^I = K_{2,j}x_{2,j}^I. \quad (4.121)$$

For initialization, the vapor bulk phase is assumed totally mixed with the interface, i.e., $y_{i,j} = y_{i,j}^I$.

Estimation of heat loss

For the simulation of the model not only states are required, but also some additional tuning parameters. The proposed initialization method provides an initial guess for some of those parameters.

The heat loss coefficient in kW/K for the reboiler can be estimated from an energy balance around this stage with the proper calculation of enthalpies as in (A.16) and (A.19),

$$\psi_R = \frac{-BH_1^L - V_1H_1^V + L_1H_1^L + Q_R}{T_1^L - T_{\text{amb}}}. \quad (4.122)$$

Likewise, the initial value for the heat removed in the condenser Q_C is obtained from the energy balance

$$Q_C = -V_{N-1}H_N^V + (L_{\text{reflux}} + D)H_N^L(T_N^I) \quad (4.123)$$

Note that the liquid leaving the condenser is assumed at temperature T_N^I .

The heat loss coefficient in the reflux drum is obtained from an energy balance around the reflux drum as in

$$\psi_D = \frac{(L_{\text{reflux}} + D)(H_N^L(T_N^I) - H_N^L(T_N^L))}{T_N^L - T_{\text{amb}}}. \quad (4.124)$$

Mass and energy holdups

Mass holdups are used for both, the original and the reduced models presented here. Initial values for those holdups are calculated from the geometry of the packing material and the liquid volumes in the reboiler and reflux drum. Note

that a guess for the liquid volumes in the reboiler \bar{v}_R and reflux drum \bar{v}_D can be determined from the experimental setup. Total molar holdups are obtained from the calculation of liquid and vapor molar densities, c_t^L and c_t^V as in (A.8) and (A.7), respectively.

$$M_{t_1}^L = \bar{v}_R c_{t_1}^L \quad (4.125)$$

$$M_{t_j}^L = \frac{\pi}{4} d^2 l h_{t_j}^L c_{t_j}^L, \quad \forall j = 2, \dots, N-1 \quad (4.126)$$

$$M_{t_N}^L = \bar{v}_D c_{t_N}^L \quad (4.127)$$

Likewise, total vapor holdups are calculated using the packing void fraction e_p , as in

$$M_{t_j}^V = \frac{\pi}{4} d^2 l (e_p - h_{t_j}^L) c_{t_j}^V, \quad \forall j = 2, \dots, N-1. \quad (4.128)$$

Component holdups are easily determined from total holdups and compositions as in

$$M_{i,j}^L = M_{t_j}^L x_{i,j}, \quad \forall j = 1, \dots, N, \quad (4.129)$$

$$M_{i,j}^V = M_{t_j}^V y_{i,j}, \quad \forall j = 2, \dots, N-1, \quad (4.130)$$

Energy holdups are obtained from total molar holdups and molar enthalpy values

$$E_j^L = M_{t_j}^L H_j^L \quad \forall j = 1, \dots, N, \quad (4.131)$$

$$E_j^V = M_{t_j}^V H_j^V \quad \forall j = 2, \dots, N-1. \quad (4.132)$$

Mass transfer fluxes

The proposed initialization method does not provide initial values for the molar transfer rates \mathcal{N}_1 and \mathcal{N}_2 based on model equations. As an alternative, the empirical procedure used in (Taylor and Krishna, 1993, p. 289) is used, i.e., small values are given to \mathcal{N}_1 , \mathcal{N}_2 and a negative sign is used for the molar rate corresponding to the more volatile component, i.e., \mathcal{N}_1 . The negative value is

given to this mass flow since it is going from liquid phase to the vapor phase⁴. Consequently, the transfer rates are defined as $\mathcal{N}_{1,j} = -1 \times 10^{-3}$, $\mathcal{N}_{2,j} = 0.9 \times 10^{-3}$, $\forall j = 2, \dots, N - 1$.

4.3.2 Structure exploitation in the reduced order RBM

Based on the previous initialization procedure, an initial guess for the state vector can be provided for solving either the full steady state RBM or the steady state RORBM. The model can be organized so that the dynamic and algebraic equations and variables are grouped together, i.e., $f = [f_y \ g_z]$ and $x = [y \ z]$ where f_y and g_z group all the dynamic and algebraic equations, respectively, while y and z group all the dynamic and algebraic states, respectively. Although this particular structure is obtained directly from the formulation of balances and equilibrium relations separately, it does not present any advantage when solving the model equations. In order to exploit sparsity in the formulation, the initial vector and the model equations are organized by grouping the variables and equations directly involved on each stage, i.e., $f = [f_1, f_2, \dots, f_{N-1}, f_N]$ and $x = [x_1, x_2, \dots, x_{N-1}, x_N]$ with f_j defined as in (4.11), (4.37) (4.52) and x_j as in (4.12), (4.38) and (4.53). This particular form of organizing variables leads to a sparse and banded pattern in the model Jacobian that can be exploited when solving the model equations.

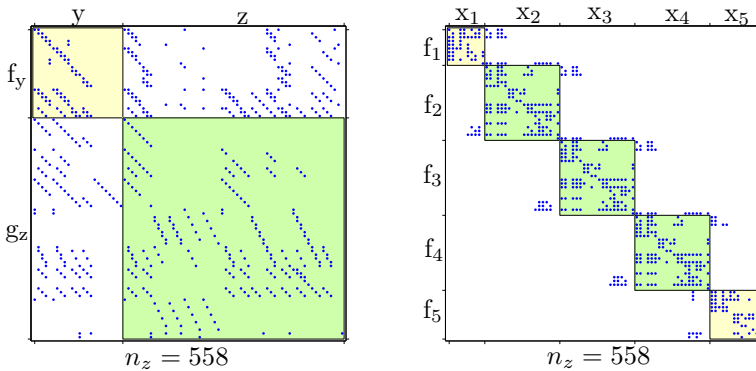


Figure 4.3: System Jacobian for a 5 stages column, reboiler, 3 packing stages and condenser plus reflux drum (right). Note the sparse and banded pattern obtained when a proper ordering of vector and equations is performed (left).

⁴Note that a positive sign convention is assumed for flows entering the liquid phase from the vapor phase, as presented in the mass and energy balance equations.

Figure 4.3 shows the Jacobian $\frac{\partial F}{\partial x}$ for the two kinds of the described equation arrangements. It is clear that the second form presents numerical advantages if sparse linear-algebra solvers are used. Off-the-shelf solvers for nonlinear equations provide options so that the sparsity patterns for the Jacobian can be specified. Providing such patterns, leads to an improvement in the computation time, since first order information can be computed in specific directions for each equation in the model. Since the number of model variables for distillation models scales linearly with the number of stages, providing sparsity patterns is an advantage for columns with several stages. Note that the bandwidth of the reorganized Jacobian does not change with the number of stages, and in this case corresponds⁵ to 20. This bandwidth is employed when solving the sparse system using preconditioned conjugate gradient method PCG (Nocedal and Wright, 2006).

4.3.3 Steady state simulation of the full rate based model

In order to simulate the steady state model response, the set of model parameters shown in Table 4.3 is required. Note that some of these parameters are estimated in the initialization procedure while others are set empirically for the initial test. Manipulated variables are set to the constant values $Q_r = 4.5$ kW, $L_r = 80$ g/min, $F = 150$ g/min and $T_F = 313.15$ K.

The model is solved for $N = 20$, leading to 383 states. Choosing the number of stages is also a design parameter in separation. The number of stages is associated with the number of physical separation units, e.g., trays in the column. Here $N = 20$ is obtained by counting the physical packing stages. As mentioned before the column has 3 packing sections of about 1 m each. Each one of these sections is composed of 6 smaller pieces of packing material leading to a total of 18 packing pieces for the 3 sections. To these 18 stages, the reboiler and condenser plus drum are added leading to a total of 20 stages.

Once the number of stages N is defined and the model parameters are given along with an initial guess for the states, the nonlinear equations can be solved. Since the states correspond to compositions, temperatures, holdups and pressures, among others, they vary widely in different numerical ranges, e.g., composition changes from zero to one mol/mol while pressure is, in the studied case, always around 1×10^5 Pa. Hence, scaling is required for states and model residuals to provide better condition to the matrices obtained in the optimization tasks.

With the proper scaling selected, a nonlinear equation solver is employed. Here, the solver uses a trust-region method with a preconditioned conjugate gradient PCG⁶ linear-algebra solver (Branch and Grace, 2002). Note that the proper

⁵This bandwidth is determined by the stage with the maximum number of variables acting on its equations

⁶Note that this is an iterative method to solve the resulting linear system

scaling provides a better distribution of the eigenvalues of the Jacobian since it improves its condition number. Hence, a small number of iterations is expected when using the CG method (Gill et al., 1984). Table 4.4 illustrates the result when no sparsity pattern is provided. In that case, the solver evaluates the model equations 2688 times to find a solution. On the other hand when the sparse pattern and the bandwidth of the Jacobian are provided, the number of function evaluations drastically decreases. The bandwidth of the Jacobian is used when creating the precondition matrix in the PCG method for the resulting linear subproblems. Results exploiting the sparsity pattern are shown in Table 4.5 where the model equations are only evaluated 161 times to find the solution. This corresponds to an improvement of 94 percent in function evaluations and a decrease from 17.06 s to 1.89 s in the execution time.

Table 4.3: Initial guess for parameters in the rate based model.

	Value	Unit	Parameter	Symbol
p_1	5×10^{-3}	m^3	Liquid volume in the reboiler	\bar{v}_R
p_2	2×10^{-3}	m^3	Liquid volume in the reflux drum	\bar{v}_D
p_3	0.7004	mol/mol	Liquid feed composition	x_F
p_4	0.0	kW/K	Heat losses coefficient for liquid	ψ_L
p_5	0.0	kW/K	Heat losses coefficient for vapor	ψ_V
p_6	0.0215	kW/K	Reboiler losses coefficients	ψ_R
p_7	0.0106	kW/K	Reflux drum losses coefficients	ψ_D
p_8	1		Liquid holdup tuning parameter	C_h
p_9	1		Pressure drop tuning coefficients	$C_{\Delta P}$
p_{10}	1		Liquid mass transfer tuning coefficients	C_{kL}
p_{11}	1		Vapor mass transfer tuning coefficients	C_{kV}

Figure 4.4 illustrates the steady state profile for most of the FRBM states. Mass and energy holdups for the liquid phase present big values when compared to the rest of the column due to the considerable amount of liquid in the top and bottom stages. Note also that the temperature profile is almost the same for the bulk phases and the interface, except for the reflux drum where the liquid phase is expected to be subcooled as it is presented in the figure. The pressure profile is almost constant and has been normalized to atmospheric pressure in order to easily plot it with the composition profiles. These profiles show that the binary mixture in model with the current parameters is not able to reach a high level of separation and leads to highly mixed products in both top and bottom streams. Nevertheless, the experimental setup can achieve top composition close to one. Consequently, it is necessary to tune the parameters in Table 4.3 by formulating a parameter estimation problem (PEP). In general, this first test provides a feasible

Table 4.4: Nonlinear equation solver statistics when no information about the Jacobian pattern is provided in the FRBM

Iteration	Func-count	$\ F(x)\ $	First-order optimality	CG-iterations
0	384	2.61×10^3	1.14×10^4	
1	768	4.37×10^2	6.35×10^3	0
2	1152	1.94×10^1	2.84×10^2	0
3	1536	3.26×10^{-1}	8.97×10^0	0
4	1920	2.35×10^{-4}	7.43×10^{-1}	0
5	2304	1.36×10^{-10}	1.33×10^{-3}	0
6	2688	1.42×10^{-20}	1.15×10^{-8}	0

Table 4.5: Nonlinear equation solver statistics when the Jacobian pattern and its bandwidth are provided in the FRBM

Iteration	Func-count	$\ F(x)\ $	First-order optimality	CG-iterations
0	23	2.61×10^3	1.14×10^4	
1	46	4.37×10^2	6.35×10^3	1
2	69	1.94×10^1	2.84×10^2	1
3	92	3.26×10^{-1}	8.97×10^0	1
4	115	2.35×10^{-4}	7.43×10^{-1}	1
5	138	1.35×10^{-10}	1.32×10^{-3}	1
6	161	1.57×10^{-19}	4.81×10^{-8}	1

steady state value for analysis of model properties and initialization of parameter estimation routines.

4.3.4 Steady state simulation of the reduced order rate based model

In order to check the validity of the reduced order rate based model (RORBM) in steady state, the same procedure, as in the FRBM, for the solution of the resulting nonlinear equations is performed. The initialization vector for the states, obtained previously, can be used considering reduced sizes due to the smaller number of states in the RORBM. Scaling of the model residuals is slightly changed since the model dynamic states are different. This leads to different values in the cost for the initial states with respect to the FRBM. The RORBM is solved on its sparse form by reorganizing the residuals $f^T = [f_1, f_2, \dots, f_{N-1}, f_N]$ according to (4.74), (4.92)

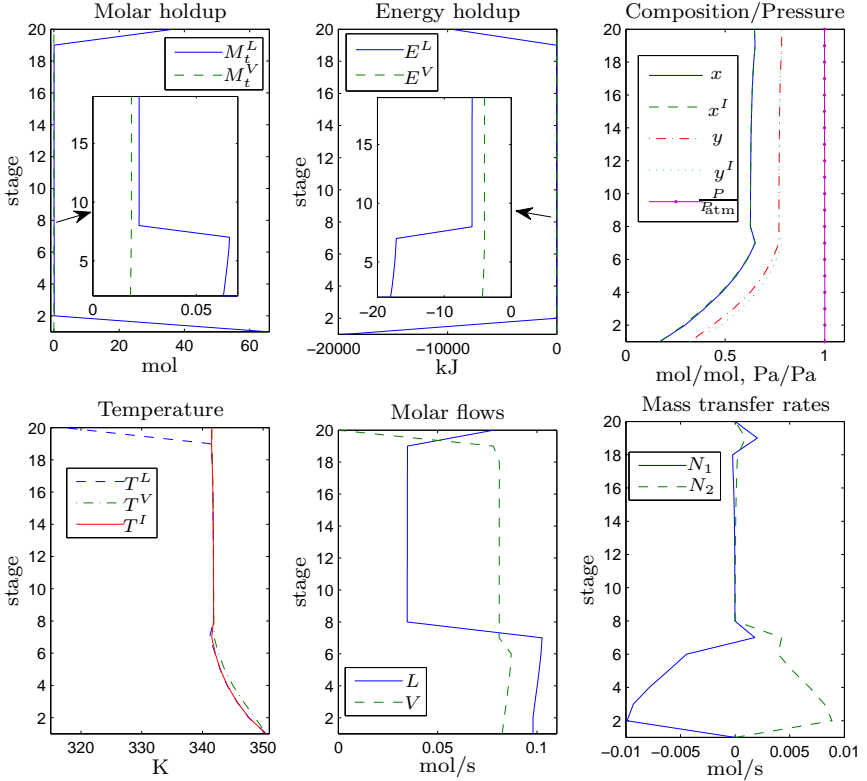


Figure 4.4: Steady state simulation for the full RBM with the parameters given in Table 4.3 and the initial guess obtained by the procedure proposed in Section 4.3.1. Note the big values in energy and mass holdups at the extremes of the profiles due to the considerable amount of liquid in top and bottom stages when compared to the rest of the column. Moreover, the current set of parameters does not allow for a high separation of the mixture as it is done in the real setup.

and (4.105), and the states $x^T = [x_1 \ x_2 \ \dots \ x_{N-1} \ x_N]$ following the definitions in (4.75), (4.93) and (4.106).

The sparsity pattern for the RORBM using two different vector structures is shown in Figure 4.5. Note that, as in the FRBM, by reorganizing the states and equations

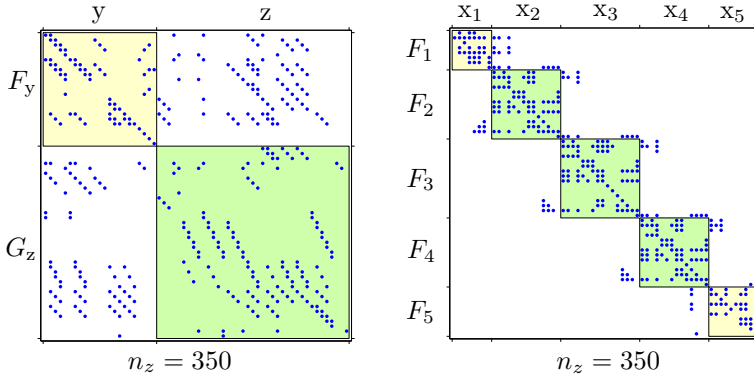


Figure 4.5: System Jacobian for a 5 stages column, reboiler, 3 packing stages and condenser plus reflux drum using the RORBM in its original form (left). Note the sparse and banded pattern in obtained when a proper ordering of vector and equations is performed (right).

appropriately a banded Jacobian can be obtained⁷. The steady state simulation is performed by solving the model equations using the same methods as in the FRBM. Tables 4.6 and 4.7 illustrate the solver statistics while Figure 4.6 displays the steady state simulation results when the parameters in Table 4.3 are used with a model of 20 stages. Note that the profiles obtained exactly match the ones displayed in Figure 4.4, numerically verifying the correctness of the reduced order model. Solving the model equations exploiting the sparsity information leads to 108 function evaluations and a computation time of 0.883 s while the original problem is solved using 1638 function evaluation and 11.96 s. Obtaining a steady state solution is 93 percent more efficient in terms of function evaluations per iteration when the sparse RORBM is used instead of the original FRBM. Hence, the former model is selected for the dynamic simulation, which requires much more computations than solving for the steady state behavior.

Table 4.8 summarizes the computational demand of the full rate based model without exploiting sparsity (FRBM-NSP), the full rate based model exploiting sparsity (FRBM-SP), the reduced order rate based model without exploiting sparsity (RORBM-NSP) and the reduced order rate based model exploiting sparsity (RORBM-SP) in terms of solution time and memory usage. Note the significant improvement in execution time and memory usage when the FRBM-NSP and the RORBM-SP are compared. It has to be mentioned that the solution

⁷The Jacobian in this representation exhibits four states more than in the model presented in Table 4.2. Those four states correspond to first order filters added to the actuators. The addition of these filters is justified in the following sections.

Table 4.6: Nonlinear equation solver statistics when no information about the Jacobian pattern is provided in the RORBM.

Iteration	Func-count	$\ F(x)\ $	First-order optimality	CG-iterations
0	273	1.14×10^3	8.94×10^4	
1	546	2.95×10^2	3.85×10^4	0
2	819	1.43×10^0	1.62×10^3	0
3	1092	3.97×10^{-3}	2.67×10^1	0
4	1365	5.86×10^{-8}	5.95×10^{-2}	0
5	1638	5.62×10^{-17}	6.20×10^{-5}	0

Table 4.7: Nonlinear equation solver statistics when the Jacobian pattern and its bandwidth are provided in the RORBM.

Iteration	Func-count	$\ F(x)\ $	First-order optimality	CG-iterations
0	18	1.14×10^3	8.94×10^4	
1	36	2.95×10^2	3.85×10^4	1
2	54	1.45×10^0	1.62×10^3	1
3	72	3.95×10^{-3}	2.64×10^1	1
4	90	4.10×10^{-8}	5.34×10^{-2}	1
5	108	8.84×10^{-17}	6.86×10^{-5}	1

time, for all the cases, can be further reduced if the model equations are coded using a high level language, e.g., C or pascal and precompiled.

Table 4.8: Performance comparison between the full rate based model and the reduced rate based model when sparsity is exploited.

	FRBM-NSP	FRBM-SP	RORBM-NSP	RORBM-SP
Number of variables	383	383	272	272
Function evaluations	2688	161	1638	108
Execution time (s)	17.6	1.89	11.96	0.883
Memory used ^a (kB)	1146	4.36	578	2.73

^aOnly the number of kilobytes to store the Jacobian in double precision format are considered as indication of the memory usage.

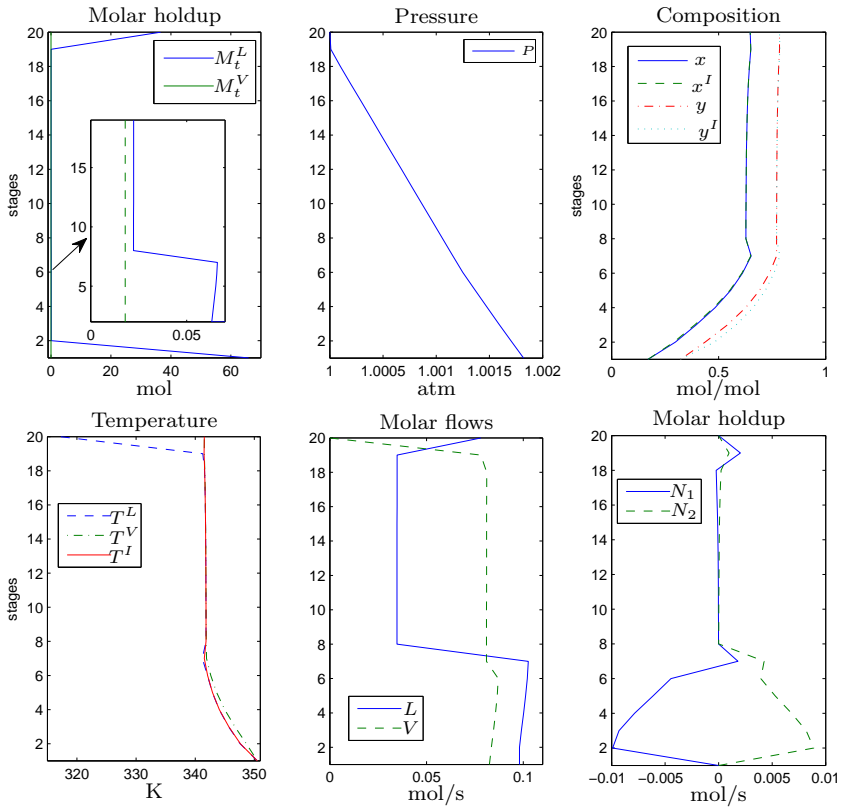


Figure 4.6: Steady state simulation for the RORBM with the parameters given in Table 4.3 and the initial guess obtained by the procedure proposed in Section 4.3.1. The profiles obtained for the RORBM matches the ones obtained with the FRBM in Figure 4.4.

4.3.5 Parameter sensitivity analysis for the steady state reduced order rate based model

As mentioned previously, the set of parameter in Table 4.3 does not induce model profiles that represent properly the real measurements, e.g., the composition profiles given by the model do not reach high levels as it is expected in the real column. Hence, the set of parameters needs to be tuned. Since only temperature measurements are available, it is necessary to verify if the whole set of parameters can be estimated from the real data. It could be possible to attempt an analysis

of the identifiability of model parameters using local observability theory for the nonlinear system, .e.g, linearizing the model around working points and study the observability of the obtained linear systems with classical systems theory. Despite this interesting approach, here the identifiability of the parameters is studied through the sensitivity analysis of state trajectories with respect to the change of the model parameters. Two approaches can be mentioned. On the one hand, it is possible to formulate the PEP considering all the parameters and include some regularization in the cost so that parameters with small or no effect over the model response are close to the regularization value \bar{p}_i . On the other hand, it is possible to make an analysis of the effect of parameters over the model states profiles, i.e., a parameter sensitivity analysis. The advantage of calculating model sensitivities with respect to parameters is that it allows for a classification of parameters, i.e., it provides a criterion for selecting which parameters can be easily estimated from the measurements and which not. Hence, the PEP can be formulated in a reduced search space, i.e., in terms of those parameters with higher sensitivities. This requirement can be translated to check how sensitive the states are to fit with respect to model parameters i.e., to calculate $\partial x/\partial p$. Analytical expressions for sensitivities in the RBM are hard to obtain due to the complexity of the nonlinear equations describing the model. Hence, a numerical method based on finite differences is used. The model sensitivities $\partial x/\partial p$ can be defined as

$$\left. \frac{\partial x}{\partial p} \right|_{\substack{x = x_0 \\ p = p_0}} = \left(\left. \frac{\partial F(x, p)}{\partial x} \right|_{\substack{x = x_0 \\ p = p_0}} \right)^{-1} \left. \frac{\partial F(x, p)}{\partial p} \right|_{\substack{x = x_0 \\ p = p_0}} . \quad (4.133)$$

Since only temperature measurements are available in the real setup, only the parameters which have the highest sensitivity with respect to the model temperature are selected⁸. Note that sensitivities can change depending on the chose of the evaluation point (x_0, p_0) . Figure 4.7 displays an estimation of the sensitivity of vapor and liquid temperatures with respect to model parameters along with sensitivities for the liquid composition at the top and bottom stages⁹. Note that heat loss coefficients and feed composition have a considerable effect on the steady state profiles. Mass transfer coefficients have less influence in the steady state profiles. On the other hand, it is clear that volumes in the reboiler and condenser along with pressure drop and liquid holdup coefficients cannot be estimated from the steady state temperature measurements in the current model.

An important remark here is that some of the parameters mentioned may have no influence on the steady state profile but can be critical for the dynamic behavior. Consequently, this steady state analysis is valid if the final objective is to tune the parameters for a steady state model or to provide initial values for a parameter

⁸Changes in those parameters have the highest effect on the trajectories to fit.

⁹These compositions can be measured offline and integrated to the parameter estimation problem.

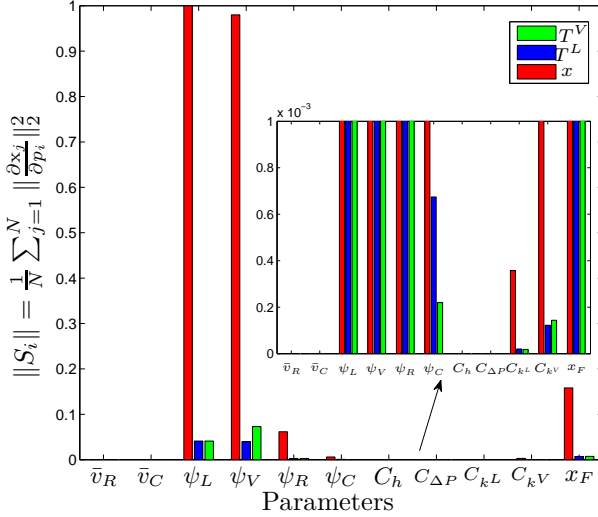


Figure 4.7: Norm on the sensitivity of some model states with respect to the model parameters. Sensitivities are calculated around the pair (x_0, p_0) so that $F(x_0, p_0) = 0$. The values for the sensitivities have been normalized.

estimation problem with a dynamic model. In that case, the parameter estimation can be formulated in two stages as proposed in (Diehl, 2002). Figure 4.7 shows that seven out of eleven model parameters can be estimated from the steady state data obtained from the experimental setup.

4.3.6 Physical constraints on the reduced order rate based model parameters

The presented set of parameters has a physical meaning. However, combination of its positive values could lead to state trajectories that are not physically possible. Although this can be seen as a serious problem, it can be solved by properly constraining the possible values of p . The RORB model does not incorporate any constraint by itself that restricts pairs (y^V, T^V) or (x^L, T^L) to superheated vapor or subcooled liquid regions, respectively. Figure 4.8 (right) displays a case where an initial guess of p leads to a steady state solution that exhibits a vapor temperature in the bulk phase lower than the one at equilibrium for the same vapor composition, i.e., the pair (y^V, T^V) lies below the pair (y^I, T^I) . Physically, this would mean that there would be superheated vapor at a temperature that is below the dew point of the mixture, which is not possible, because it would be liquid. Figure 4.8

(left) displays the same kind of plot when a different p is used. In this case, the steady state trajectories have a physical meaning. These two tests illustrate that it is not enough to guarantee the positiveness of p in the parameter estimation problem but extra constraints must be added to ensure that the pairs (y^V, T^V) lie in the superheated vapor region C_1 and that pairs (x^L, T^L) lie in the subcooled liquid region C_3 . These conditions can be translated into inequality constraints by using the associated partial pressures to each point, i.e., a point (x^L, T^L) is in the subcooled region if the sum of its components partial pressures equals or does not exceed the pressure of the stage. On the other hand a point (y^V, T^V) is in the superheated region if the sum of its component partial pressure equals or exceeds the pressure of the stage. This is translated to the inequalities

$$P_j - \gamma_1(x_j^L)P_1^s(T_j^L)x_j^L - \gamma_2(x_j^L)P_2^s(T_j^L)(1 - x_j^L) \geq 0 \quad \forall j = 2, \dots, N, \quad (4.134)$$

$$\gamma_1(x_j^*)P_1^s(T_j^V)x_j^* + \gamma_2(x_j^*)P_2^s(T_j^V)(1 - x_j^*) - P_j \geq 0 \quad \forall j = 2, \dots, N, \quad (4.135)$$

$$y_j^V(1 - x_j^*) - x_j^*(1 - y_j^V) \frac{\gamma_1(x_j^*)P_1^s(T_j^V)}{\gamma_2(x_j^*)P_2^s(T_j^V)} = 0 \quad \forall j = 2, \dots, N, \quad (4.136)$$

that are obtained from boiling and dew¹⁰ point curves definition (Seader and Henley, 2006) and delimit the region C_2 in Figure 4.8.

Note that evaluating superheated points with the inequality (4.135) implies the solution of the equality (4.136) for x^* , which is a dew point calculation. This inequality poses an embedded root finding problem into the inequality constraints. However, (4.136) can be solved as a part of the model equations by adding x^* to the state vector and (4.136) to the model residuals, so that the inequalities are reduced to (4.134) and (4.135).

4.4 Steady state parameter estimation of the reduced order rate based model

Five experiments for identification and two for validation are used to fit the steady state RORBM to the setup. The manipulated variables are presented in Table 4.9 while the measured steady state profiles for eleven temperature sensors are illustrated in Figure 4.9. Note that the measurement coming from the sensor

¹⁰Note that the fractional expression on the left hand side of (4.136) corresponds to the relative volatility for a binary mixture.

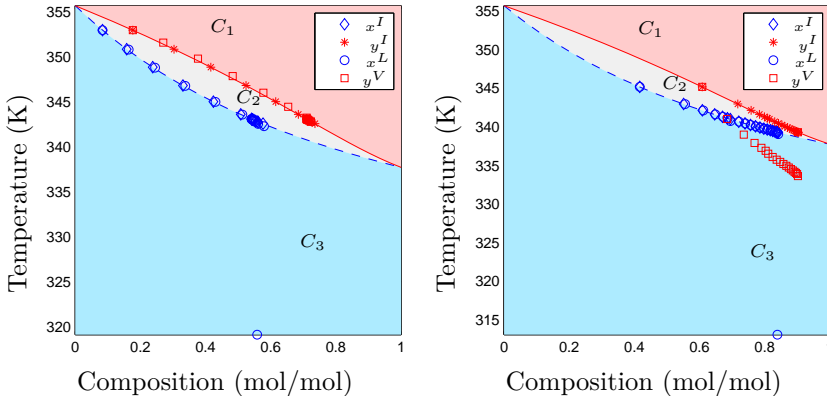


Figure 4.8: Boiling point diagram for the mixture of methanol-isopropanol given by the steady state solution of the RORBM. Regions C_1 and C_3 correspond to superheated vapor and subcooled liquid, respectively. The markers in the plots show temperature-composition pairs obtained with the parameters proposed in Table 4.3 (left) and a perturbed version of them (right). Note the physically inconsistent values obtained in the boiling point diagram for some arbitrary values of $p > 0$ (right).

in the condenser T_{s11} corresponds to a temperature below the boiling point of pure methanol at atmospheric pressure, i.e., $T_{s11} < 338$ K. Hence, assuming that the methanol composition at the top is close to one, it would be difficult for an equilibrium condenser to fit this temperature. Consequently, in the parameter estimation, the measurement coming from the condenser is weighted in a small proportion with respect to the rest of measurements. On the other hand, the PEP is formulated so that the temperature of the liquid phase of the model fits the measurement data. The vapor phase is not used here since measured profiles seem to adjust better to a subcooled liquid phase than to a vapor phase. There is a physical explanation for this, and it is associated with the fact that temperatures are taken at points in the column where the sensor probe can be wetted with liquid falling down through the walls of the column. Hence temperature measurements are lower than the ones predicted by the model vapor phase or equilibrium.

Since only temperature measurements are available, the parameters that have the highest sensitivity with respect to the temperature provided by the model, are selected¹¹. It is important to mention that this approach requires an initialization point for the parameters p_0 and the states x_0 . In the current study, some of the parameters are initialized with the procedure used in Section 4.3.1, while others

¹¹Changes in those parameters have the highest effect on the trajectories to be fitted.

Table 4.9: Steady state experiments used for identification and validation.

Exp ^a	Q_R	L_N	F_{in}	T_F	T_{amb}	D	B
1	4.0	60.0	150	313.15	292.90	70	80
2	4.5	86.0	110	313.15	292.95	70	40
3	4.5	80.0	150	318.15	292.45	70	80
4	4.0	59.0	150	313.15	295.20	70	80
5	4.5	76.5	150	313.15	298.85	70	80
6	4.0	65.0	150	313.15	294.95	70	80
7	4.5	77.2	150	313.15	287.45	70	80

^aApplied power in kW, mass flows in g/min and temperatures in K

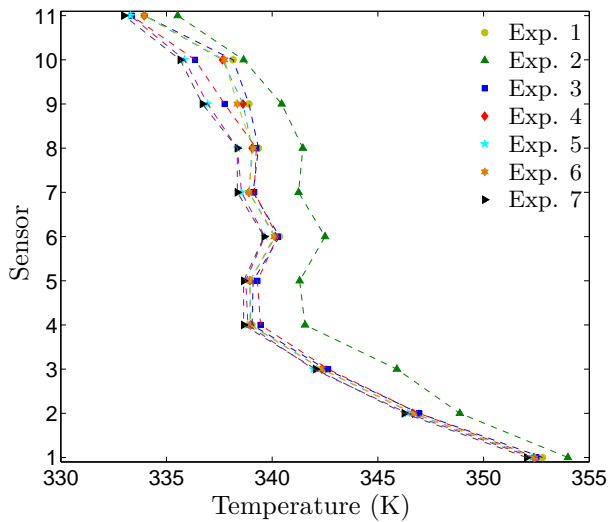


Figure 4.9: Experimental data coming from the 11 sensors located along the column as illustrated in Figure 3.1. Temperature of the subcooled reflux has not been included in the plot but is used in the estimation.

are given a value based on process knowledge.

Table 4.10: Initial and optimized parameters for the steady state RORBM.

Parameter	Initial value	Bounds	Optimum ^a	Units
x_F	0.67	[0.4 0.7]	0.4670	mol/mol
ϕ_L	0.0	[0 5]	2.3	W/K
ϕ_V	0.0	[0 5]	0.0	W/K
ϕ_R	21.6	[0 10]	0.0	W/K
ϕ_D	10.6	[0 10]	8.3	W/K
C_{k^L}	1	[0 3]	0.22	W/K
C_{k^V}	1	[0 3]	2.12	W/K

^aOnly identifiable parameters are optimized.

Since only parameters $\phi_L, \phi_V, \phi_R, \phi_D, C_{k^L}, C_{k^V}$ and x_F have an influence on the temperatures, these parameters are selected to be tuned. Hence, the number of parameters is reduced from eleven to seven. Initial values and bounds for these are presented in Table 4.10. The experiments are performed under different conditions, allowing for different input composition, x_F . Consequently, a different value of x_F is estimated for each of the experiments. This increases the number of parameters again to $N_p = 6 + M$ where M is the number of experiments used for identification. It is important to mention that the neglected parameters are discarded here due to a lack of proper measurements that allow for their estimation.

4.4.1 Problem formulation

The parameter estimation problem can be formulated only in terms of the parameter vector, p , and solved using a Gauss-Newton method (see Section 2.3.3). However, the model equations have to be solved at each Newton-iteration. Consequently, the model equations are introduced as equality constraints and the problem is optimized in parameters and states x at the same time. This is a more efficient approach that preserves sparsity in the optimization, at the cost of increasing the number of optimization variables. Hence, the optimization problem is cast as:

$$\min_{x,p} \|\bar{y} - Cx\|_{Q_x}^2 \text{ subject to } \begin{cases} F(x,p) = 0 \\ x_{\min} \leq x \leq x_{\max} \\ p_{\min} \leq p \leq p_{\max} \end{cases} \quad (4.137)$$

where the vector \bar{y} represents the measurement data, C is a positive-semidefinite diagonal matrix with zero entries in the diagonal corresponding to the states that are not measured and Q_x a weight matrix. Note that this formulation accounts

only for one experiment. In order to use multiple experiments, the optimization vector, the residual vector and the constraints are increased so that

$$\begin{aligned}\tilde{y}^T &= [\bar{y}_1^T, \dots, \bar{y}_M^T], \quad w^T = [x_1^T, \dots, x_M^T, p], \\ F(w)^T &= [F(x_1, p)^T, \dots, F(x_M, p)^T]\end{aligned}\quad (4.138)$$

and the problem is formulated as

$$\min_w \|\tilde{y} - \tilde{C}w\|_{Q_w}^2 \text{ subject to } \begin{cases} F(w) &= & 0 \\ w_{\min} &\leq w \leq & w_{\max} \end{cases} \quad (4.139)$$

with appropriate matrices Q_w , \tilde{C} , and bounds.

Five experiments are used for the estimation task, leading to $N_p = 11$ and a total size of the optimization problem of $M(14N - 12) + N_p$. Due to the structure of the setup, $N = 20$ is selected, yielding an optimization vector $w \in \mathbb{R}^{1351}$. Figure 4.10 (top) illustrates the fitting results for the identification set containing data from the first five experiments presented in Figure 4.9, while Figure 4.10 (bottom) displays the results for the validation set. Note that there is a group of points that lies outside the $\pm 3K$ band around 335 K, those are measurements obtained from the condenser which cannot be totally explained by the model due to the inability to model subcooled liquid. Figure 4.11 shows the boiling point diagrams for the validation set with experiments 6 and 7 in Table 4.9, illustrating the consistency of the results.

4.5 Dynamic simulation

As mentioned previously, the RORBM described in Section 4.2, is used for dynamic simulation. However, writing down the equations that appropriately describe the system dynamics is not a guarantee for obtaining a model that can be simulated dynamically. There exist several numerical problems that need to be considered before being able to run a simulation. Among these typical problems are: (i) a high differentiation index, (ii) model stiffness and (iii) a considerable number of variables to solve for. Distillation models can exhibit these three features. Here, the model size or large scale issue, is addressed by reducing the model from the FRBM to the RORBM and exploiting the reduced model sparsity when possible as it is shown in Section 4.3.4. In the following paragraphs the differentiation index problem is explained and analyzed for the RBM along with the inherent stiffness of the model.

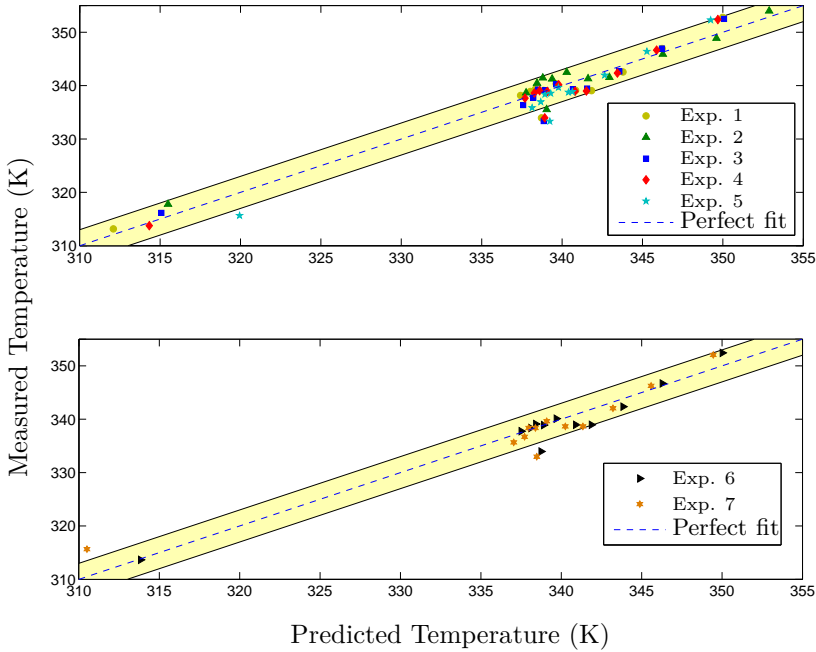


Figure 4.10: Fitted results for five steady state experiments (top), and validation test with two new experiments (bottom). Note that almost all the predicted temperatures lie in a ± 3 K error band.

4.5.1 The differentiation index in DAEs

Since the RBM lies in a particular class of DAEs, namely, semi-explicit DAEs (Hairer and Wanner, 2002), the following definitions are given based on this particular class.

Definition 4.5.1 (Differentiation index). Given a semi-explicit differential algebraic equation of the form:

$$\dot{y} = f(t, y, z), \quad (4.140)$$

$$0 = g(t, y, z), \quad (4.141)$$

with $y \in \mathbb{R}^{n_y}$, $z \in \mathbb{R}^{n_z}$, $f : \mathbb{R}^{n_y} \times \mathbb{R}^{n_z} \times \mathbb{R} \rightarrow \mathbb{R}^{n_y}$ and $g : \mathbb{R}^{n_y} \times \mathbb{R}^{n_z} \times \mathbb{R} \rightarrow \mathbb{R}^{n_z}$. The differentiation index I is defined as the number of times the algebraic constraints

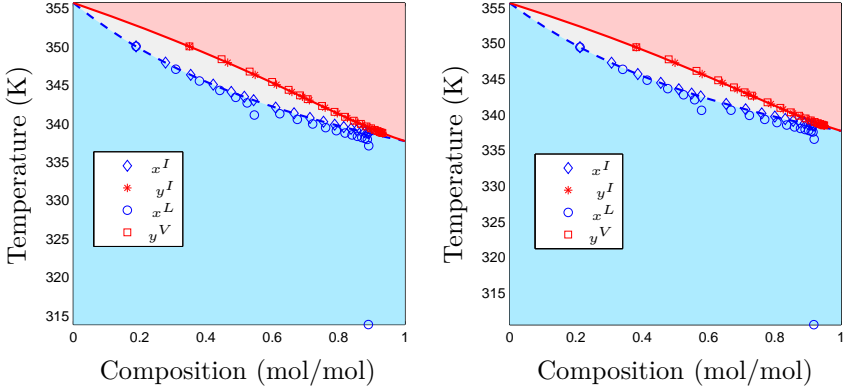


Figure 4.11: Boiling point diagram for the mixture of methanol-isopropanol with states given by the steady state solution of the RORBM. These diagrams correspond to experiment 6 (left) and 7 (right) in Table 4.9 with the tuned parameters. Note the subcooled liquid on both cases, which describes approximately the data of the setup as presented in Figure 4.10(bottom).

$g(y, z, t)$ have to be differentiated with respect to time in order to obtain an explicit expression for the time derivative of the algebraic variables z , i.e., \dot{z} .

The differential index is a measure of how far a DAE lies from an ODE. In fact a DAE could be transformed into an ODE after I differentiations with respect to time and algebraic manipulation, generating what is called the *underlying ODE* (Ascher and Petzold, 1998).

Numerical solvers find a solution to (4.140)-(4.141) by obtaining an expression for the time derivative of the algebraic variables \dot{z} . This set of ODEs can be obtained by differentiating the algebraic constraints with respect to time, leading to

$$\dot{z} = - \left(\frac{\partial g(y, z)}{\partial z} \right)^{-1} \frac{\partial g(y, z)}{\partial y} f(t, y, z). \quad (4.142)$$

It is possible to find a solution to \dot{z} if the Jacobian of the algebraic equations with respect to the algebraic variables $\frac{\partial g(y, z)}{\partial z}$, is nonsingular (Hairer and Wanner, 2002). If that is not the case, the algebraic constraints are differentiated until an index-1 system is obtained, i.e., $I - 1$ times. Off-the-shelf solvers are only capable of dealing with index-1 problems, i.e., $\frac{\partial g(y, z)}{\partial z}$ in (4.142) must be nonsingular. In general, the underlying ODE formed by (4.140) and (4.142) provides a family of solutions that do not necessarily satisfy the original constraints. Hence, in order to achieve the required constraint satisfaction, the correct initialization must be

done, i.e., the initialization of the underlying ODE must be performed considering the original constraints and the derivatives¹² that lead to the underlying ODE.

Definition 4.5.2 (Consistent initialization). An index-1 system of the form (4.140)-(4.141) is consistently initialized iff the initial value $(y(0), z(0))$ satisfies the algebraic constraints, i.e., $g(0, y(0), z(0)) = 0$. For higher-index DAEs, i.e., $I \geq 2$ an initialization vector $(y(0), z(0))$ is consistent iff it satisfies $g(0, y(0), z(0))$ and the $I - 1$ derivatives with respect to time of the algebraic constraints, i.e.,

$$g(0, y(0), z(0)) = 0, \quad (4.143)$$

$$\frac{dg(0, y(0), z(0))}{dt} = 0, \quad (4.144)$$

$$\vdots \quad (4.145)$$

$$\frac{d^{I-1}g(0, y(0), z(0))}{dt^{I-1}} = 0. \quad (4.146)$$

Note that (4.143)-(4.146) $\forall t$ define a manifold, where not only the initial vector lies but the solution of the underlying ODE must lie as well. Consequently, from the family of solutions provided by the underlying ODE only the ones that lie on this manifold are actually solutions of the original DAE.

When a numerical method is applied to the integration of the underlying ODE, a common feature is the drift of the solution trajectories from the manifold defined by the hidden constraints, i.e., the solution of the ODE does not satisfy the original constraint and its $I - 1$ derivatives (Hairer and Wanner, 2002). Hence, reducing the index by differentiation of the constraints is always accompanied by methods for stabilization of the error in the solution. Among the most widely used are Baumgarte's stabilization (Baumgarte, 1972) and projections of the solution on the manifold (Hairer and Wanner, 2002). If the differentiated constraints are just appended to the original set of constraints, the system becomes overdetermined. There exist other methods that attempt to solve the overdetermined system resulting from this index reduction procedure. However, differentiation of constraints can create new differential variables making the solution even more involved. Among the most used methods for overdetermined systems are the least squares minimization applied to the nonlinear equations (Hairer and Wanner, 2002) and the method of the dummy derivatives (Mattsson and Söderlind, 1993). All those methods depart from a DAE reduced to index-1 by differentiation. Pantelides (1988) proposes an algorithm that identifies the minimum set of equations from the DAE that need to be differentiated, so that an

¹²These constraints imposed by the derivatives with respect to time are called the underlying or *hidden constraints*

index-1 system can be obtained for further stabilization with one of the methods mentioned.

4.5.2 Distillation models and the index problem

The DAEs high-index problem has been previously mentioned in several works for different kinds of distillation models, e.g., Pantelides et al. (1988), Gani and Cameron (1992), Kreul et al. (1998), Peng et al. (2003) among others. There are basically two approaches to tackle the problem. On the one hand, the complexity of the model is reduced by making several assumptions that lead to an index-1 DAE. On the other hand, the constraints that need to be differentiated are detected by, e.g., *Pantelides algorithm*. The differentiated constraints are added to the system, leading to an overdetermined model that can be solved by one of the methods mentioned previously. Although this method preserves the original set of variables, it can become involved. The method requires: (i) the implementation of the graph-theory based Pantelides algorithm, (ii) tools to obtain the derivatives of the equations detected by the algorithm and (iii) procedures to solve the overdetermined model dynamically.

The approach used here lies in the first class of the mentioned methods. The index problem for the RORBM is analyzed and the proper assumptions are justified physically and numerically, highlighting the limitations of the resulting model.

Pantelides et al. (1988) traced back the index problem to the appropriate links between vapor flows and pressure drops. Kreul et al. (1998) refers to the index problem and confirms that this appears when there is no relation between pressure drops in a non-equilibrium stage and vapor or liquid flowing through the stage. As it is shown here, this is a necessary condition but it is not the only one that helps to avoid the problem. In general, from the numerical viewpoint, each algebraic variable must appear at least once in the algebraic equations. This avoids what is called *structural singularities*. The flows in a stage, an algebraic variable, must appear in the algebraic equations either through the pressure drops or through the calculation of mass transfer coefficients¹³. Consequently, assuming pressure drops constant or transfer coefficients constant remove the flows from the algebraic equation. Since flows are algebraic variables, this leads to a singular Jacobian $\frac{\partial \mathbf{q}}{\partial \mathbf{z}}$ and to the higher index problem unless extra assumptions are considered. These extra assumptions must imply an extra algebraic equation involving the flows in a stage that were suppressed by assuming, e.g., constant pressure. This is illustrated in the following paragraphs.

¹³Note that both pressure drops and mass and heat transfer coefficients involve the vapor and liquid flows in a stage.

Structural singularity detection

A particular procedure to detect structural singularity problems is proposed in Gani and Cameron (1992) by analyzing the incidence of algebraic variables in the algebraic equations. By analyzing this incidence matrix, it is possible to suggest modifications to the model that avoid the higher index problem. Note that this procedure is restricted to structural singularity, numerical singularities are in general more difficult to avoid by this method. Gani and Cameron (1992) proposes to choose the variables that do not appear in the incidence matrix as degrees of freedom. This approach is certainly effective, however, in practical cases not always the variables that create the higher index can be assumed as given.

In order to check the origins of this higher index problem a simple 3-stages system is analyzed, i.e., only one packing section is assumed and it is modeled using the non-equilibrium equations (4.76)-(4.91), along with the reduced models of reboiler (4.65)-(4.71) and condenser plus reflux drum (4.94)-(4.102). The Jacobian of the nonlinear set of equations, composed of dynamic and algebraic relations, is calculated numerically. Note that the numerical values of the Jacobian change as a function of the states values, however, the purpose of this calculation is to check the structure of the Jacobian and not its numerical values. The equations and states are organized as $f = [f_y \ g_z]^T$ and $x = [y \ z]^T$, respectively, to clearly identify the dynamic and algebraic parts in the Jacobian in the analysis¹⁴.

The results are illustrated in Figure 4.12. Note that, in this model, the pressure drops and the transfer coefficient are calculated as a function of the flows in the stage as suggested in Kreul et al. (1998). However, the DAE system still exhibits a differentiation index bigger than one. It is easy to see that the vapor flow in the reboiler V_1 , does not appear in the algebraic constraints, causing the structural singularity problem. Any other algebraic variable missed in $\frac{\partial q}{\partial z}$ leads to the same structural singularity problem.

Higher index reduction

Once the structural singularity has been detected, there are some options to obtain an index-1 system. In order to reduce the differentiation index of the proposed model, it is required to include all the algebraic variables at least once in the algebraic equations. Hence, assumptions that lead to that inclusion avoid the structural singularity. In this particular case, assuming vapor molar holdup M_2^V , constant solves the problem. This common assumption transforms (4.79) into an algebraic constraint, i.e., shifts the row corresponding to M_2^V , in Figure 4.12,

¹⁴Although, a different organization presents advantages when solving the system of equations, with this form of organizing variables, the analysis of the index problem is easily performed.

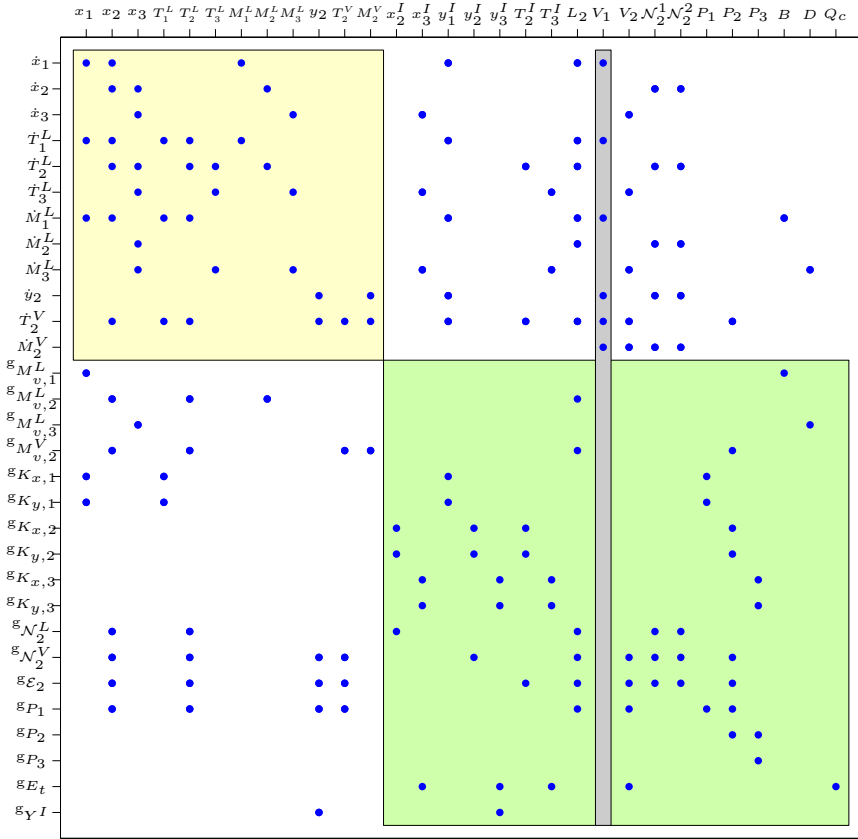


Figure 4.12: Jacobian of a 3 stages distillation system using the RORBM. Note that the Jacobian of the algebraic equations with respect to the algebraic variables lacks of elements in the column corresponding to the reboiler vapor flow V_1 , originating the singularity in $\frac{\partial q}{\partial z}$ and the higher index problem in the DAE.

down to the algebraic part of the Jacobian, allowing for V_1 to appear once in the algebraic constraints. There exists a second effect of this assumption, since the fast dynamics associated with the vapor holdups are being neglected, the stiffness of the DAE is expected to be alleviated. This kind of common assumption reduces on the one hand, the index problem to one and, on the other hand, the stiffness of the whole DAEs system, facilitating the dynamic simulation task.

Detecting structural singularities can be generalized by analyzing the Jacobian of the algebraic constraints with respect to the algebraic variables. A procedure for reducing the index from structural singularity problems is summarized in

Algorithm 4.1.

Algorithm 4.1 Index reduction from structural singularities

- 1: Organize the DAE in the form (4.140)–(4.141)
 - 2: Obtain the incidence matrix (sparsity pattern) of the problem by, e.g., numerical perturbation.
 - 3: Detect the empty columns i_e of the block corresponding to the incidence of algebraic variables z into the algebraic equations g .
 - 4: Identify the variables that originates the structural singularity $z(i_e)$.
 - 5: Scan the rows of the incidence matrix corresponding to the dynamic equations f detecting the ones that contains the variables $z(i_e)$, i.e, $f(z(i_e))$
 - 6: Based on "know-how" of the process evaluate which ones of the $f(z(i_e))$ can be consider as algebraic equations.
-

Note that neglecting the dynamics of one or more of the $f(z(i_e))$ solves the structural singularity problem, but such kind of assumptions have to be determined in agreement with the physical features of the process. Moreover, Algorithm 4.1 does not account for singularities that appear from numerical values of the system equations but for singularities coming from the structure of the equations.

4.5.3 Further simplifications to the RORBM and actuator dynamics

Once the index problem has been solved a simulation of the system, under the assumption of constant molar vapor holdup, can be performed. Note that the dynamic model has as degrees of freedom four manipulated variables, namely L_r , B , D and Q_r . By simple inspection, it is possible to note that the system is not BIBO (bounded input bounded output) stable (Ogata, 2010). If one of these variables is changed, the volumes in the reboiler and condenser can reach saturation. Starting from an equilibrium value, a step in the reboiler power Q_r , induces a higher vapor flow V_1 . If B is not changed, the reboiler volume decreases until it reaches its lower level, i.e., it saturates. At the top of the column, if D and L_r are kept constant, the level in the reflux drum increases since more vapor is flowing through the column. This excess of vapor condensates and induces an increase of liquid volume in the reflux drum until it saturates to its maximum volume. Consequently, the model with these four degrees of freedom is unstable. A very simple approach to avoid this kind of instability is to close loops between liquid volumes in the reboiler and reflux drum with bottom and top flows, respectively (Skogestad, 1997). The dynamics of these liquid loops is, in general, faster than the one associated with temperature and composition. Hence, in many distillation models it is assumed that there exist perfect controllers that keep these volumes constant. In practice, simple PI controllers can be tuned so

that correction for volume variations is rapidly achieved. This perfect control on volumetric holdups in the reboiler and reflux drum is represented by equations (4.72)-(4.73) and (4.103)-(4.104), respectively. The advantages of incorporating these assumptions into the model is an easier simulation, avoiding saturation of variables without the need of considering control loops for the volumes in the top and bottom stages. However, the real dynamics of the liquid loops is merged with the dynamics of the temperature inside the column. As mentioned, if desired, the model can be used without this assumption, however the proper control loops need to be designed and incorporated into the model.

The presented model does not consider the dynamics of the actuators. If a step change is performed in the reboiler duty, the extra heat applied directly propagates to the vapor flow, i.e., the extra heat added, generates an instantaneous change in the vapor flow since the liquid in the reboiler is saturated. Figure 4.13 shows the response of some model states when changes of $\pm 10\%$ in the reboiler duty and the reflux are performed. Although, part of the vapor dynamics have been neglected with the constant molar vapor holdup assumption, there is a very fast response due to the lack of proper modeling for the heat transfer between the actuator and the saturated liquid in the bulk phase.

The real setup exhibits a different behavior. The applied heat takes some time until it is transferred to the surroundings of the actuator and to the vapor due to the heat resistance in the liquid bulk phase, which has not been considered in the model. Similarly, the dynamics of the reflux pump, the feed pump and the feed heater are not considered. Hence, in order to provide a model closer to what is expected in the real setup, first order filters of the form

$$\dot{q}(t) = \frac{1}{\tau}(u(t) - q(t)), \quad (4.147)$$

are added to each one of the command signals. Here, $u(t)$ represents the command sent to the actuator while $q(t)$ accounts for the filtered command signal that reaches the process. The time constants for those filters are tuning parameters that can be easily estimated in the real setup since measurement of slave control loops are available. Table 4.11 displays the extra parameters added to the model, including the tuning value for the fixed vapor molar holdup $\bar{M}_{t_j}^V$. Those parameters are added to the ones presented in Table 4.3, leading to 16 model parameters for the dynamic RORBM.

The four added filters increase the order of the model to $5N-2$ dynamic variables/equations and $9N-3$ algebraic variables/equations¹⁵. The banded Jacobian structure is preserved by allocating these new dynamic states in the

¹⁵Note that $N - 2$ dynamic equations corresponding to $\dot{M}_{t_j}^V$ have become algebraic due to the constant molar vapor holdup assumption.

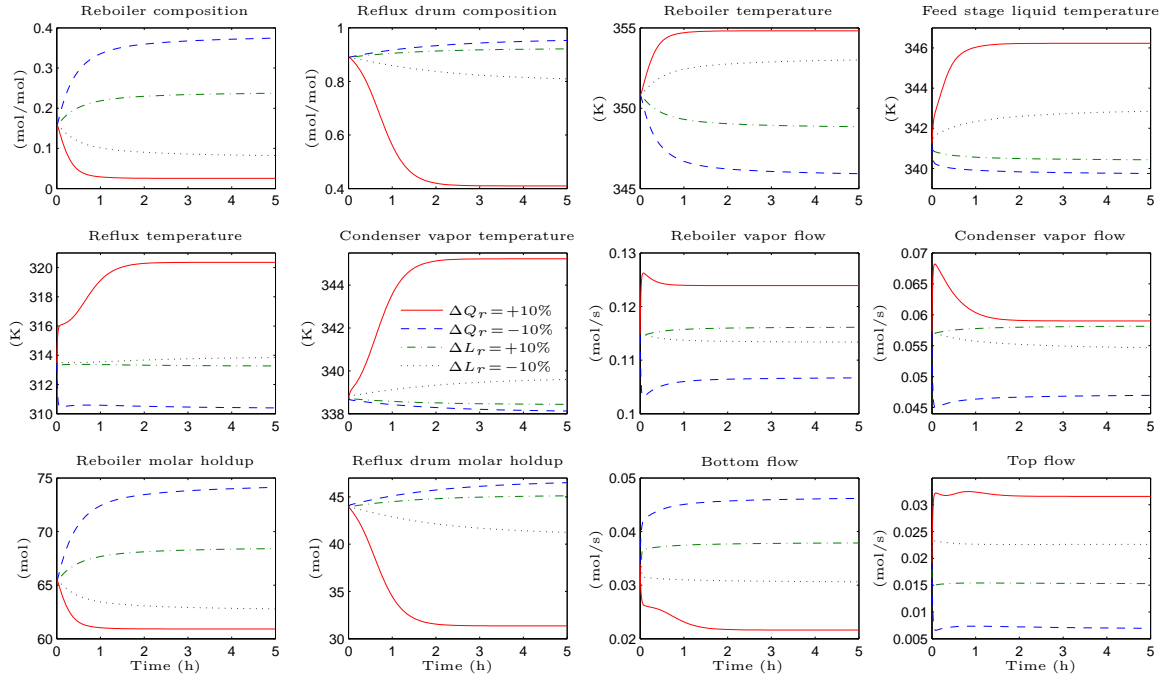


Figure 4.13: RORBM response to $\pm 10\%$ changes in the reboiler duty and the reflux. First order filters have been added to the actuators to model the actuator dynamics

Table 4.11: Actuator related and vapor holdup parameters in the RORBM.

	Value	Unit	Parameter	Symbol
p_{12}	0.018	mol	Molar vapor holdup	$M_{t_j}^V$
p_{13}	180	s	Heater time constant	τ_R
p_{14}	20	s	Reflux pump time constant	τ_{Lr}
p_{15}	20	s	Feed pump time constant	τ_F
p_{16}	90	s	Feed heater time constant	τ_{TF}

reboiler, feed and condenser stages. Jacobian patterns are provided to the DAE solver, achieving an improvement of 63% in the computation time with respect to the dense version of the Jacobian. Note that in online control and estimation the model need to be solved at each sampling instant several times. Hence, the improvement in solving the model has a direct implications on the computation time and memory usage for dynamic optimization algorithms.

4.5.4 Dynamic sensitivity analysis of the RORBM

As noted in Figure 4.13, the steady state value of model compositions for the top stage does not reach the one of a pure component. In the real setup that is approximately the case and the mismatch between the dynamic simulation and the experimental setup is due to non-optimal values for the model parameters. Hence, a dynamic parameter estimation problem needs to be formulated. Note that the formulated model presents 16 parameters. However, the number of parameters that can be estimated, depends on the available state measurements. Since in this particular setup only measurements of temperatures are available, it is necessary to check which parameters can be estimated from those measurements. The analysis performed in the steady state case in Section 4.3.5 can be extended so that the dynamic case is covered. For the index-1 DAE

$$\dot{y} = f(y, z, p, t), \quad (4.148)$$

$$0 = g(y, z, p, t), \quad (4.149)$$

the sensitivities of states $x^T = [y^T \ z^T]$ with respect to parameters p , i.e.,

$$s^T = \frac{\partial x^T}{\partial p} = \left[\frac{\partial y^T}{\partial p} \ \frac{\partial z^T}{\partial p} \right] = [s_y^T \ s_z^T] \quad (4.150)$$

are obtained by solving the DAE

$$\begin{bmatrix} \dot{s}_y \\ 0 \end{bmatrix} = \begin{bmatrix} \frac{\partial f}{\partial y} & \frac{\partial f}{\partial z} \\ \frac{\partial g}{\partial y} & \frac{\partial g}{\partial z} \end{bmatrix} \begin{bmatrix} s_y \\ s_z \end{bmatrix} + \begin{bmatrix} \frac{\partial f}{\partial p} \\ \frac{\partial g}{\partial p} \end{bmatrix}. \quad (4.151)$$

Although the required differentiation could be performed symbolically, the DAE solver with sensitivity generation capabilities presented in Hindmarsh et al. (2005) is used here to obtain and solve (4.151) together with the RORBM. Figures 4.14-4.15 present the sensitivities of temperature trajectories at the top and the bottom of the column as a function of the 16 model parameters. A 10% perturbation is performed in the 4 possible manipulated variables of the setup¹⁶, i.e., Q_r , L_r , F and T_F . The sensitivities can be seen as the gain k in the linear approximation of the states

$$x(p) = x(\bar{p}) + k(p - \bar{p}). \quad (4.152)$$

Consequently, the higher the sensitivity the larger the effects of variation in p over the analyzed state trajectories. On the contrary, lower sensitivities lead to almost no change in the measured states trajectories with respect to changes in the parameters. Hence, parameters with lower sensitivities, i.e., low effect on measured trajectories are difficult to estimate from the available measurements.

In order to use the sensitivities to reduce the search space for the model parameters p , a criterion based on a 2-norm of the form

$$\|S_i\| = \sum_{i=1}^4 \sum_{j=1}^N \sum_{k=0}^{k_f} \frac{\|\frac{\partial x_j}{\partial p_i}(k)\|_2^2}{4k_f N} \quad (4.153)$$

is proposed as an indicator for the relevance of parameters in the estimation procedure. k_f is the number of values used for describing the numerical solution of the sensitivities. N denotes the number of states analyzed, i.e., for the temperature of the liquid or vapor N corresponds to the number of stages and $m = 4$ input variables perturbed. This criterion adds all the contributions of the sensitivities associated to a set of N states with respect to the parameter p_i along one simulation test for the four tests. Figure 4.16 illustrates $\|S_i\|$ for the 16 parameters proposed, when the temperature of the vapor phase, liquid phase and top and bottom concentration are assumed measurable.

Based on the sensitivities it is possible to reduce the search space for the parameter estimation problem. In this case the original vector $p \in \mathbb{R}^{16}$ is reduced to $p_r \in \mathbb{R}^{11}$

¹⁶These signals can be manipulated when gathering data for model identification

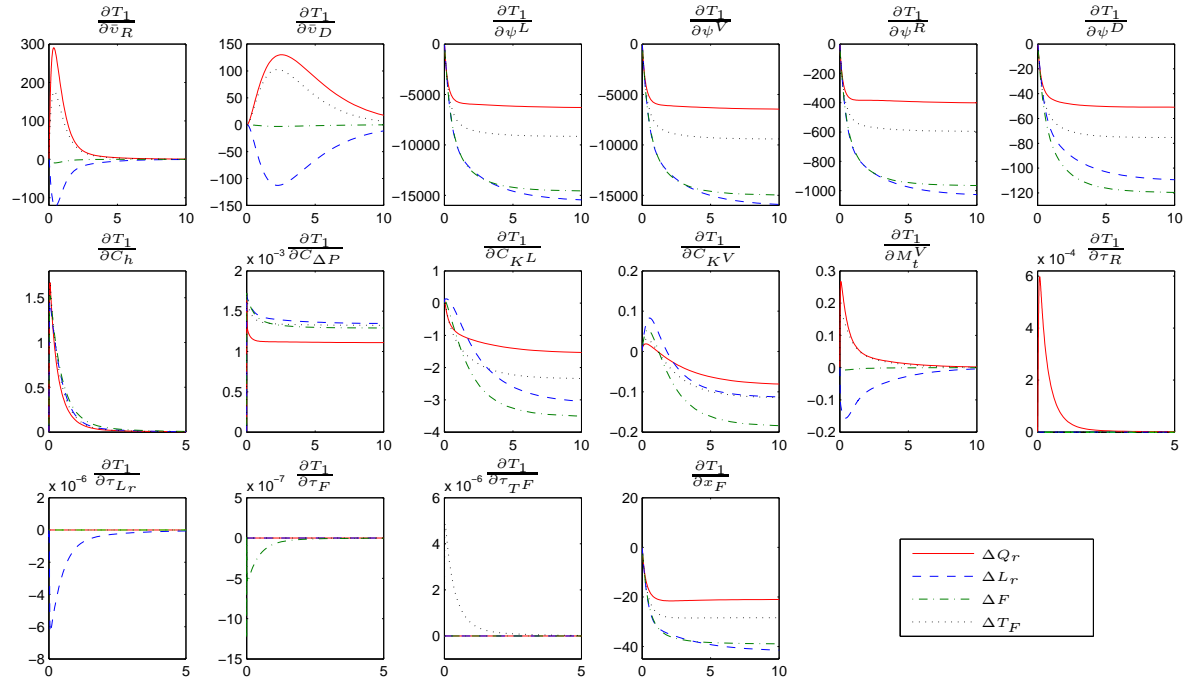


Figure 4.14: Dynamic sensitivities of the bottom temperature with respect to the 16 model parameters, when a change of 10% in the four manipulated variables is performed, i.e., $\Delta Q_r = 10\%$, $\Delta L_r = 10\%$, $\Delta F = 10\%$ and $\Delta T_F = 10\%$.

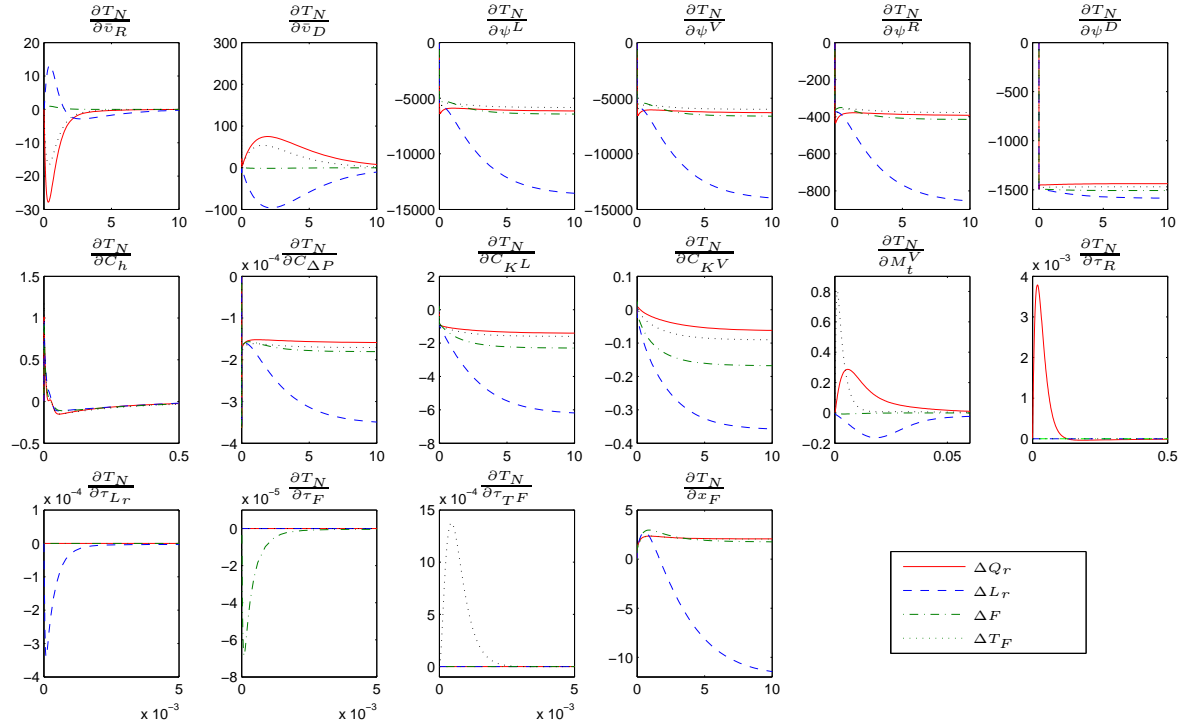


Figure 4.15: Dynamic sensitivities of the top temperature with respect to the 16 model parameters, when a change of 10% in the four manipulated variables is performed, i.e., $\Delta Q_r = 10\%$, $\Delta L_r = 10\%$, $\Delta F = 10\%$ and $\Delta T_F = 10\%$.

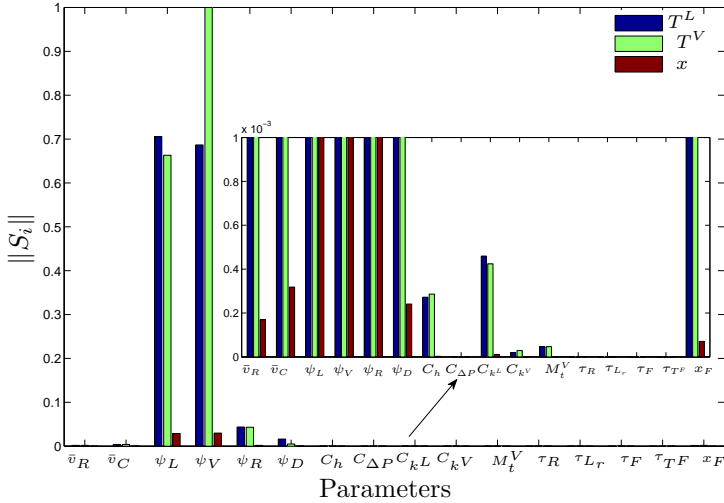


Figure 4.16: Norm on the sensitivity of vapor temperature, liquid temperature and liquid composition with respect to the 16 model parameters when changes of 10% are performed on the four manipulated variables of the model.

as shown in Table 4.12. Note that some of the parameters clearly influence the dynamic and static response while others only the dynamic part. This is a clear difference to be taken into account for the parameter estimation of steady state and dynamic models since only one part of those parameters can be obtained from steady state data.

4.6 Conclusions

In this chapter a rate based model for separation in packed columns has been introduced. It is demonstrated that the number of states involved in the model formulation can be reduced by 30% by manipulating the model states and introducing extra equations involving the enthalpy dynamics. It is shown that both the FRBM and the RORBM are highly structured. This structure is better exploited by reorganizing equations and variables by stage so that a banded Jacobian is obtained for the numerical solution.

Steady state simulations are presented for both models. An initialization method based on available measurements is proposed. This method provides initial values for almost all the states involved in the model and for some of the parameters

Table 4.12: RORBM parameters and its influence on the dynamic and static response.

Parameter	Dynamic	Static	p_r
\bar{v}_R	*		*
\bar{v}_D	*		*
x_F	*	*	*
ψ_L	*	*	*
ψ_V	*	*	*
ψ_R	*	*	*
ψ_D	*	*	*
C_h	*		*
$C_{\Delta P}$			
C_{k^L}	*	*	*
C_{k^V}	*	*	*
M_T^V	*		*
τ_R	*		
τ_{Lr}	*		
τ_F	*		
τ_{TF}	*		

used in model simulation. It is shown that when the initial guess, provided by the method, is used in combination with the structure exploitation of the model equations are solved in a few iterations.

This chapter also provides an analysis of the model parameters, showing that only a reduced set of them can be estimated from the available measurements. Indeed, due to the reduced number of measurement, a steady state sensitivity analysis has shown that steady state data only allow for the estimation of parameters associated to process heat loss in the liquid and vapor phases. The other parameters in the model have no significant influence on the steady state trajectories. Moreover, they are hard to estimate from the steady state measurements of variables such as temperature and concentration in the top and bottom stages.

Additionally, it is shown that positiveness of the proposed parameters is not enough to ensure model state trajectories that are plausible. It can happen that for a particular combination of model parameters the obtained trajectories for vapor and liquid temperature and composition do not lie in the overheated or subcooled regions of a boiling point diagram. Hence, a novel set of constraints on those parameters has been proposed so that the model can provide reasonable results. These constraints are to be used in the formulation of the parameter estimation problem for the reduced set of parameters. It has been noticed that

these constraints must be enforced when trying to fit vapor measurements, since for low temperature measurements the heat loss coefficient can increase leading to vapor lying below the dew point curves, which is physically inconsistent. To the author knowledge there is no previous study of this kind of constraints and their use in parameter estimation of rate based models. The PEP for the steady state RORBM has shown that with the reduced set of measurements from the setup, heat loss coefficients are most likely to be identified.

A dynamic model based on the reduced state procedure is proposed. The high index problem presented in the model is detected by analyzing the model Jacobian. It is shown that the model exhibits a structural singularity since the variable associated with the reboiler vapor flow does not appear in the algebraic equations. Among the possible model assumptions, one that leads to including vapor flow in the algebraic equations is selected. The advantages of this kind of assumption are not only justified numerically but also physically since it also leads to reduce the model stiffness. As in the steady state case, the sensitivity of model states with respect to parameters is studied using a DAE solver with sensitivity capabilities. The dynamic sensitivity analysis shows that some of the parameters neglected in the PEP for the steady state model, influence the dynamic response, such as the volume in the reboiler and reflux drum. The sensitivity analysis also leads to reducing the search space for the parameter estimation problem from 16 to 11 parameters. As in the steady state case, the reduced set of parameters must satisfy positiveness constraints as well as the constraints that define superheated and subcooled regions for temperatures and compositions in the bulk phases. Finally, a reduced state rate based model with a reduced set of parameters is proposed so that the parameter estimation problem can be efficiently formulated in companion with numerical solvers that can exploit the sparsity of this highly structured problem.

Part II

Convexity exploitation in dynamic optimization problems

Chapter 5

A homotopy-based convex approximation of input-affine optimal control problems

In this chapter, a method to solve nonconvex OCP with a particular structure in the cost and constraints is proposed. In particular, a control-affine model structure is assumed together with an objective which penalizes deviations from a desired reference trajectory. Many nonlinear dynamic systems of practical interest present the control-affine structure which enables the applicability of the method. Examples of these kinds of systems arise, for instance, in the chemical industry (e.g., distillation columns and continuous stirred tank reactors -CSTRs), mechanical engineering (e.g., car maneuvering and robot arm manipulators) and power electronics (e.g., DC-DC converters). The convergence to the solution for these OCPs, can be improved by first solving a related convex formulation, which is connected by a homotopy path to the original problem, and using this solution to initialize the original OCP. The proposed technique resembles a *continuation method* for global optimization (Moré and Wu, 2006) where, by means of filtering techniques, the original cost is gradually transformed into a smoother function with fewer local minimizers. An optimization algorithm is then applied to the transformed function, tracing the minimizers back to the original cost.

The chapter is organized as follows: Section 5.1 introduces the main features of the method along with proofs of convergence of the homotopy to its extremes. Section 5.2 presents numerical examples for the method. An application of the method in the context of predictive control is presented in Section 5.3. Conclusions follow in Section 5.5.

5.1 A convex-homotopy based method for the solution of optimal control problems

The approach proposed here deforms the original nonconvex OCP using a homotopy, such that the deformed problem becomes convex, i.e., the original OCP and the convex OCP are *homotopic*. The convex problem is easier to solve and homotopy methods (Watson et al., 1987) may be used to trace back the solution from the deformed problem to the original one. In the following the details of the method are introduced and numerical results are presented for OCP.

A general dynamic optimization problem is introduced in Section 2.4. However, herein the OCP treated is restricted to DOPs with dynamic models that exhibit an input-affine feature and a particular Bolza-type functional, i.e.,

$$\text{OCP} : \min_{x(\cdot), u(\cdot)} \int_0^T \|x(t) - \bar{x}(t)\|_Q^2 dt + \|x(T) - \bar{x}(T)\|_{Q_T}^2, \quad (5.1)$$

subject to

$$\dot{x}(t) = f(x(t)) + g(x(t))u(t), \quad t \in [0, T], \quad (5.2)$$

$$x(0) = x_0, \quad (5.3)$$

$$h(x(t), u(t)) \geq 0, \quad t \in [0, T], \quad (5.4)$$

$$r(x(T)) \geq 0. \quad (5.5)$$

It is assumed that the optimization task involves a desired state trajectory, $\bar{x}(t)$ ($\bar{x}(t) \in C^1$) and no knowledge of a desired input trajectory $\bar{u}(t)$ is provided. Moreover, $\bar{x}(t)$ is considered feasible with respect to the inequality constraints (5.4) and (5.5).

Additionally, the following assumptions are introduced:

Assumption 5.1.1.

1. The sets defined by the inequalities $h(x(t), u(t)) \geq 0$ and $r(x(T)) \geq 0$ are convex (see Definition 2.1.1).
2. The state penalization matrix Q is positive definite and Q_T is positive semi-definite.
3. $f(x(t))$ and $g(x(t)) \in C^1$ and the solution of $\dot{x}(t) = f(x(t)) + g(x(t))u(t)$ is uniquely determined by $u(t)$ and $x(0)$.

Remark 5.1.1. Convexity in the set defined by (5.4) is, e.g., satisfied if the controls and states are constrained by simple bounds, thus (5.4) is a hypercube.

In order to simplify the notation, the norm

$$\|x\|_J^2 = \int_0^T x(t)^T Q x(t) dt + x(T)^T Q_T x(T), \tag{5.6}$$

is introduced. Additionally, as $Q \succ 0$, $x = y$ a.e. if $\|x - y\|_J^2 = 0$.

A homotopy formulation is presented by introducing a pseudo state $x_c(t) \in \mathbb{R}^{n_x}$ and a scalar parameter $\alpha \in (0, 1)$ that interpolates between the original problem ($\alpha \rightarrow 1$) and one of its possible homotopies ($\alpha \rightarrow 0$) as follows:

$$P(\alpha) : \min_{x(\cdot), u(\cdot), x_c(\cdot)} \frac{1}{\alpha} \|x - \bar{x}\|_J^2 + \frac{1}{1 - \alpha} \|x_c - x\|_J^2 \tag{5.7}$$

subject to

$$\dot{x}_c(t) = f(x(t)) + g(x(t))u(t), \quad t \in [0, T], \tag{5.8}$$

$$x_c(0) = x_0, \tag{5.9}$$

$$h(x_c(t), u(t)) \geq 0, \quad t \in [0, T], \tag{5.10}$$

$$r(x_c(T)) \geq 0. \tag{5.11}$$

This augmented parametric OCP defines a family of optimization problems as a function of the parameter α . Other forms of homotopy maps are also possible where the parameter enters linearly or nonlinearly in the problem. Linear homotopy parameters are widely used in root finding problems (Watson, 2001). However, the particular choice proposed here is twofold. On the one hand, the homotopy parameter is restricted to lie in the interval $(0, 1)$. On the other hand, there is an equivalence of the presented formulation with quadratic penalty methods for constrained optimization (Gould, 1989). This equivalence allows showing the convergence conditions of the parametric problem minimizer to the solution of the original OCP. Additionally, consider the related convex problem

$$\text{CVX} : \min_{x_c(\cdot), u(\cdot)} \|x_c - \bar{x}\|_J^2 \tag{5.12}$$

subject to

$$\dot{x}_c(t) = f(\bar{x}(t)) + g(\bar{x}(t))u(t), \quad t \in [0, T], \tag{5.13}$$

$$x_c(0) = x_0, \tag{5.14}$$

$$h(x_c(t), u(t)) \geq 0, \quad t \in [0, T], \tag{5.15}$$

$$r(x_c(T)) \geq 0. \tag{5.16}$$

The following additional technical assumptions on the presented optimization problems are introduced:

Assumption 5.1.2. There exist unique global solutions for the problems OCP (5.1)-(5.5), $P(\alpha)$ (5.7)-(5.11) and CVX (5.12)-(5.16), namely $(x_{\text{ocp}}^*(t), u_{\text{ocp}}^*(t))$, $(x_{P(\alpha)}^*(t), u_{P(\alpha)}^*(t), x_{cP(\alpha)}^*(t))$ and $(x_{c\text{cvx}}^*(t), u_{c\text{cvx}}^*(t))$, respectively.

Assumption 5.1.3.

1. The parametric problem solution $(x_{P(\alpha)}^*(t), u_{P(\alpha)}^*(t), x_{cP(\alpha)}^*(t))$ converges pointwise to $(x_{P(1)}^*(t), u_{P(1)}^*(t), x_{cP(1)}^*(t))$, when α goes to one, i.e.,

$$\lim_{\alpha \rightarrow 1} (x_{P(\alpha)}^*(t), u_{P(\alpha)}^*(t), x_{cP(\alpha)}^*(t)) = (x_{P(1)}^*(t), u_{P(1)}^*(t), x_{cP(1)}^*(t)). \tag{5.17}$$

2. The parametric problem solution $(x_{P(\alpha)}^*(t), u_{P(\alpha)}^*(t), x_{cP(\alpha)}^*(t))$ converges pointwise to $(x_{P(0)}^*(t), u_{P(0)}^*(t), x_{cP(0)}^*(t))$, when α goes to zero, i.e.,

$$\lim_{\alpha \rightarrow 0} (x_{P(\alpha)}^*(t), u_{P(\alpha)}^*(t), x_{cP(\alpha)}^*(t)) = (x_{P(0)}^*(t), u_{P(0)}^*(t), x_{cP(0)}^*(t)). \tag{5.18}$$

Based in the previous assumptions, the following lemmata are introduced:

Lemma 5.1.1 (Convergence of $P(\alpha)$ when $\alpha \rightarrow 1$). *The solution of the parametric problem (5.7)-(5.11) approaches the solution of the original OCP (5.1)-(5.5) in the limit when α goes to one, i.e.,*

$$(x_{P(1)}^*(t), u_{P(1)}^*(t)) = (x_{\text{ocp}}^*(t), u_{\text{ocp}}^*(t)), \quad \forall t \in [0, T] \quad \text{a.e.} \tag{5.19}$$

$$x_{cP(1)}^*(t) = x_{c\text{ocp}}^*(t), \quad \forall t \in [0, T] \quad \text{a.e.} \tag{5.20}$$

Proof. Consider the augmented OCP

$$\min_{x(\cdot), u(\cdot), x_c(\cdot)} \|x - \bar{x}\|_J^2, \tag{5.21}$$

subject to

$$\dot{x}_c(t) = f(x(t)) + g(x(t))u(t), \quad t \in [0, T], \tag{5.22}$$

$$x_c(0) = x_0, \tag{5.23}$$

$$h(x_c(t), u(t)) \geq 0, \quad t \in [0, T], \tag{5.24}$$

$$r(x_c(T)) \geq 0, \tag{5.25}$$

$$x_c(t) = x(t) \quad t \in [0, T], \tag{5.26}$$

whose solution exactly matches the solution of the original problem (5.1)-(5.5), since the added equality constraint (5.26) can be trivially satisfied by the new added variable $x_c(t)$. This additional degree of freedom is introduced in order to provide the same number of optimization variables for the original OCP and the parametric one, $P(\alpha)$.

The proof to Lemma 5.1.1 is presented by reformulating the parametric OCP (5.7)-(5.11) such that the homotopy term penalizing the original cost is factorized, i.e.,

$$P(\alpha) : \min_{x(\cdot), u(\cdot), x_c(\cdot)} \frac{1}{\alpha} (\|x - \bar{x}\|_J^2 + \beta(\alpha)\|x_c - x\|_J^2) \tag{5.27}$$

subject to

$$\dot{x}_c(t) = f(x(t)) + g(x(t))u(t), \quad t \in [0, T], \tag{5.28}$$

$$x_c(0) = x_0, \tag{5.29}$$

$$h(x_c(t), u(t)) \geq 0, \quad t \in [0, T], \tag{5.30}$$

$$r(x_c(T)) \geq 0, \tag{5.31}$$

and

$$\beta(\alpha) = \frac{\alpha}{1 - \alpha}. \tag{5.32}$$

The formulation (5.27) resembles the cost used in quadratic penalty methods (Nocedal and Wright, 2006), where the second term in the right-hand side of (5.27) corresponds to an equality constraint. The scaling factor $\frac{1}{\alpha}$ in (5.27) is neglected since, theoretically, scaling has no effects on the solution. Moreover, for the case

analyzed here, i.e., α increasing towards 1, this factor tends to one. Note that (5.32) defines an equivalence between α going to 1 and β going to $+\infty$.

Now, suppose that $(x_{\text{ocp}}^*(t), u_{\text{ocp}}^*(t), x_{c_{\text{ocp}}}^*(t))$ is a global solution to the OCP (5.21)-(5.26), hence $x_{c_{\text{ocp}}}^*(t) = x_{\text{ocp}}^*(t)$. Suppose also that $(x_{\text{P}(\alpha)}^*(t), u_{\text{P}(\alpha)}^*(t), x_{c_{\text{P}(\alpha)}}^*(t))$ is a global solution to the parametric OCP (5.7)-(5.11). Note that any solution to the OCP (5.21)-(5.26) lies in the feasible set of the parametric OCP, i.e., (5.28)-(5.31) are satisfied by $(x_{\text{ocp}}^*(t), u_{\text{ocp}}^*(t), x_{c_{\text{ocp}}}^*(t)) \forall t \in [0, T]$.

Since $(x_{\text{P}(\alpha)}^*(t), u_{\text{P}(\alpha)}^*(t), x_{c_{\text{P}(\alpha)}}^*(t))$ is a unique global solution of the parametric problem and $\|x_{c_{\text{ocp}}}^* - x_{\text{ocp}}^*\|_J^2 = 0$, the following inequality holds:

$$\|x_{\text{P}(\alpha)}^* - \bar{x}\|_J^2 + \beta(\alpha)\|x_{c_{\text{P}(\alpha)}}^* - x_{\text{P}(\alpha)}^*\|_J^2 \leq \|x_{\text{ocp}}^* - \bar{x}\|_J^2 \tag{5.33}$$

After dividing (5.33) by $\beta(\alpha)$ and re-arranging terms,

$$\|x_{c_{\text{P}(\alpha)}}^* - x_{\text{P}(\alpha)}^*\|_J^2 \leq \frac{1}{\beta(\alpha)} \left(\|x_{\text{ocp}}^* - \bar{x}\|_J^2 - \|x_{c_{\text{P}(\alpha)}}^* - x_{\text{P}(\alpha)}^*\|_J^2 \right), \tag{5.34}$$

is obtained. Following Assumption 5.1.3, taking the limit when α tends to 1 in (5.34), yields

$$\|x_{c_{\text{P}(1)}}^* - x_{\text{P}(1)}^*\|_J^2 \leq \lim_{\alpha \rightarrow 1} \frac{1}{\beta(\alpha)} \left(\|x_{\text{ocp}}^* - \bar{x}\|_J^2 - \|x_{c_{\text{P}(\alpha)}}^* - x_{\text{P}(\alpha)}^*\|_J^2 \right) = 0. \tag{5.35}$$

Due to Assumption 5.1.1, $Q \succ 0$ and $Q_T \succeq 0$, hence, the left-hand-side of inequality (5.35) cannot be negative. Consequently,

$$\|x_{c_{\text{P}(1)}}^* - x_{\text{P}(1)}^*\|_J^2 = 0, \quad \forall t \in [0, T] \quad \text{a.e.} \tag{5.36}$$

This condition corresponds to the additional constraint (5.26) imposed to the augmented OCP in (5.21) with the new variable $x_c(t)$.

Additionally, taking the limit in (5.33) gives

$$\lim_{\alpha \rightarrow 1} \left(\|x_{\text{P}(\alpha)}^* - \bar{x}\|_J^2 + \beta(\alpha)\|x_{c_{\text{P}(\alpha)}}^* - x_{\text{P}(\alpha)}^*\|_J^2 \right) \leq \|x_{\text{ocp}}^* - \bar{x}\|_J^2. \tag{5.37}$$

The nonnegativity of $\beta(\alpha)$ directly implies positiveness of the limit in left-hand side of (5.37), yielding

$$\|x_{P(1)}^* - \bar{x}\|_J^2 \leq \|x_{\text{ocp}}^* - \bar{x}\|_J^2. \tag{5.38}$$

Hence, due to the uniqueness of the solution the following equalities hold,

$$x_{P(1)}^*(t) = x_{\text{ocp}}^*(t), \quad \text{a.e.}, \tag{5.39}$$

$$x_{cP(1)}^*(t) = x_{P(1)}^*(t), \quad \text{a.e.}, \tag{5.40}$$

$$x_{\text{ocp}}^*(t) = x_{c\text{ocp}}^*(t), \quad \text{a.e.} \tag{5.41}$$

and $u_{P(1)}^*$ is uniquely determined by the set of constraints (5.28)-(5.31) which is the same set as the original OCP (5.22)-(5.26). Consequently,

$$(x_{P(1)}^*(t), u_{P(1)}^*(t), x_{cP(1)}^*(t)) = (x_{\text{ocp}}^*(t), u_{\text{ocp}}^*(t), x_{c\text{ocp}}^*(t)), \quad \text{a.e.}, \tag{5.42}$$

meaning that the solution of the parametric OCP (5.7)-(5.11) converges to the solution of the original OCP (5.1)-(5.5) in the limit when α goes to one. \square

Now the other extreme of the parametric DOP is investigated.

Lemma 5.1.2 (Convergence of $P(\alpha)$ when $\alpha \rightarrow 0$). *The solution of the parametric optimization problem $P(\alpha)$ is in the limit, when α goes to zero, equivalent to the solution of the convex optimization problem in (5.12)-(5.16), i.e.,*

$$(x_{cP(0)}^*(t), u_{P(0)}^*(t)) = (x_{\text{cvx}}^*(t), u_{\text{cvx}}^*(t)), \quad \forall t \in [0, T] \quad \text{a.e.}, \tag{5.43}$$

$$x_{P(0)}^*(t) = \bar{x}(t), \quad \forall t \in [0, T] \quad \text{a.e.} \tag{5.44}$$

Proof. The proof of Lemma 5.1.2 follows the same structure as the proof of Lemma 5.1.1. Consider an equivalent formulation of the convex optimization problem (5.12)-(5.16):

$$\min_{x_c(\cdot), u(\cdot), x(\cdot)} \|x_c - \bar{x}\|_J^2 \tag{5.45}$$

subject to

$$\dot{x}_c(t) = f(x(t)) + g(x(t))u(t), \quad t \in [0, T], \tag{5.46}$$

$$x_c(0) = x_0, \tag{5.47}$$

$$h(x_c(t), u(t)) \geq 0, \quad t \in [0, T], \tag{5.48}$$

$$r(x_c(T)) \geq 0, \tag{5.49}$$

$$x(t) = \bar{x}(t), \quad \forall t \in [0, T]. \tag{5.50}$$

whose solution exactly matches the solution of the original convex problem (5.12)-(5.16) since the added equality (5.50) is satisfied by the extra variable $x(t)$.

The parametric OCP is reformulated as:

$$P(\alpha) : \min_{x(\cdot), u(\cdot), x_c(\cdot)} \frac{1}{1-\alpha} (\gamma(\alpha)\|x - \bar{x}\|_J^2 + \|x_c - x\|_J^2) \tag{5.51}$$

subject to (5.28) - (5.31) with

$$\gamma(\alpha) = \frac{1-\alpha}{\alpha}. \tag{5.52}$$

The cost in (5.51) corresponds to a quadratic penalty formulation (Nocedal and Wright, 2006) where the first norm in the cost is considered an equality constraint. Note also that $\gamma(\alpha)$ goes to $+\infty$ as α goes to zero. Again, the scaling factor $\frac{1}{1-\alpha}$ has no influence on the cost in the limit case considered here.

Assume that $(x_{\text{cvx}}^*(t), u_{\text{cvx}}^*(t), x_{c_{\text{cvx}}}^*(t))$ is a unique global solution to the convex OCP (5.45)-(5.50), and $(x_{\text{P}(\alpha)}^*(t), u_{\text{P}(\alpha)}^*(t), x_{c_{\text{P}(\alpha)}}^*(t))$ is a unique global solution to the parametric OCP $P(\alpha)$. Note that any solution to the convex OCP in (5.45)-(5.50) is a feasible trajectory for the parametric OCP $P(\alpha)$ i.e., (5.8) to (5.11) are satisfied by $(x_{\text{cvx}}^*(t), u_{\text{cvx}}^*(t), x_{c_{\text{cvx}}}^*(t)) \forall t \in [0, T]$.

Since the reformulated parametric problem (5.51) exhibits the same structure as the problem in (5.27) in the proof of Lemma 5.1.1, the same procedure presented there can be applied here, leading to:

$$\|x_{\text{P}(0)}^* - \bar{x}\|_J^2 = 0 \tag{5.53}$$

and

$$\|x_{\text{P}(0)}^* - \bar{x}\|_J^2 \leq \|x_{c_{\text{cvx}}}^* - \bar{x}\|_J^2. \tag{5.54}$$

where $(x_{P(0)}^*(t), u_{P(0)}^*(t), x_{cP(0)}^*(t))$ is a limit trajectory according to Assumption 5.1.3. Hence, the following equalities hold

$$x_{cP(0)}^*(t) = x_{c\text{cvx}}^*(t), \quad \text{a.e.}, \tag{5.55}$$

$$x_{P(0)}^*(t) = \bar{x}(t), \quad \text{a.e.}, \tag{5.56}$$

$$x_{\text{cvx}}^*(t) = \bar{x}(t), \quad \text{a.e.}, \tag{5.57}$$

and $u_{P(0)}^*$ is uniquely determined by the set of constraints (5.28)-(5.31) which is the same set in the original convex problem (5.46)-(5.49). Consequently,

$$(x_{P(0)}^*(t), u_{P(0)}^*(t), x_{cP(0)}^*(t)) = (x_{\text{cvx}}^*(t), u_{\text{cvx}}^*(t), x_{c\text{cvx}}^*(t)), \quad \text{a.e.}, \tag{5.58}$$

meaning that the solution of the parametric OCP (5.7)-(5.11) converges to the solution of the original convex OCP (5.12)-(5.16) in the limit when α goes to zero. □

Lemma 5.1.3 (Perfect traceable trajectory $\bar{x}(t)$). *If $\bar{x}(t)$ is a feasible trajectory, with respect to equality and inequality constraints, for some unknown controls $\bar{u}(t)$, i.e., $\dot{x}^{\text{ref}}(t) = f(\bar{x}(t)) + g(\bar{x}(t))\bar{u}(t)$, then $\bar{u}(t)$ is obtained exactly by solution of the convex problem (5.12)-(5.16). Moreover, $(x_{P(\alpha)}^*, u_{P(\alpha)}^*) = (\bar{x}, \bar{u})$ for all $\alpha \in [0, 1]$.*

Proof. If $x_{\text{ocp}}^*(t) = \bar{x}(t)$, $(\bar{x}(t), \bar{u}(t), x_{c\text{ocp}}^*(t))$ is a solution of the OCP (5.21)-(5.26). Moreover, $(\bar{x}(t), u_{\text{ocp}}^*(t), x_{c\text{ocp}}^*(t))$ minimizes the objective of the parametric OCP in (5.7) with function value zero. Due to Assumption 5.1.2, $(x_{P(\alpha)}^*(t), u_{P(\alpha)}^*(t), x_{cP(\alpha)}^*(t)) = (\bar{x}(t), \bar{u}(t), \bar{x}(t))$ for all $\alpha \in [0, 1]$. □

Convergence of the parametric problem solution to the global solution of the original OCP is guaranteed only if we are able to find the global solution for each $P(\alpha)$. This condition is only easily satisfied for the first problem on the homotopy path namely $P(0)$ where a convex problem is addressed as shown in Lemma 5.1.2. In this context, it is proposed to solve the nonconvex OCP with the given structure, by convexifying it through the formulation in (5.7)-(5.11) with $\alpha = 0$. The solution of the convex homotopy is used to initialize successive OCPs when moving α towards 1 in order to recover the original formulation.

Remark 5.1.2 (Increments on the homotopy parameter). With the use of homotopy methods, the question of how to determine the increments of the homotopy parameter arise. Continuation methods increase this value monotonically. However, even with small increments of the homotopy parameter, the zero path cannot be followed if turning points appear. Consequently, practical homotopy methods do not attempt to increase the homotopy parameter monotonically but

allows for decreasing it to track turning points. In order to do so, the zero path is parameterized in terms of its arc length. The parameterization allows for calculating $(\dot{w}, \dot{\alpha})$ from the original system of equations¹ (see (Nocedal and Wright, 2006, pag. 297)) such that dynamic equation solvers can be used track the zero path in the space defined by w and α . Numerical algorithms to efficiently perform this procedures are presented in Watson et al. (1987).

Numerical examples illustrate how the method can be applied in the predictive control frameworks in Section 5.2. It is difficult to guarantee that the method finds a global solution to the nonconvex original problem. However, in view of Lemma 5.1.3, it finds the solution to the nonconvex DOP by solving a simpler convex problem. This situation is presented in Figure 5.1(a). For small values of $\|x - \bar{x}\|_J^2$ the situation in Lemma 5.1.3 is nearly recovered as presented in Figure 5.1(b). Nevertheless, complications can appear for higher values of $\|x - \bar{x}\|_J^2$ such as bifurcations as illustrated in Figure 5.1(c).

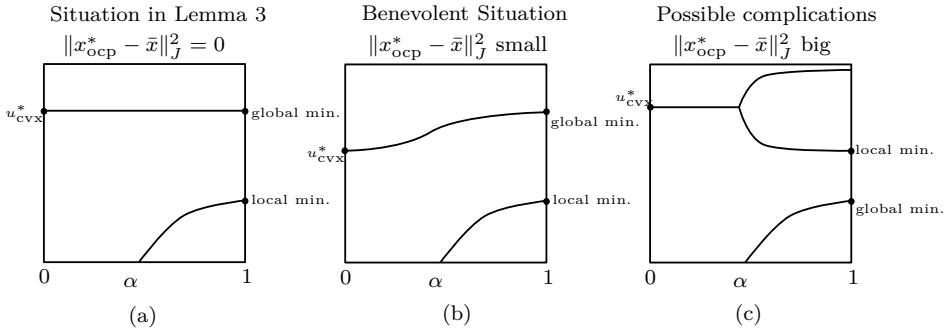


Figure 5.1: Some possible behaviors of the homotopy path in the space (x, u, x_c) . Note that the benevolent situation in (b) is covered with Assumptions 5.1.2 and 5.1.3 for small trajectory changes. However, if Assumption 5.1.2 does not hold, complications like bifurcations or the emergence of a new local minima can appear as in (c).

5.2 Optimal control numerical example

In order to illustrate the applicability of the proposed method to the solution of dynamic optimization problems, the optimal control of a continuous stirred tank reactor (CSTR) is considered. Since the continuous time OCP is an infinite dimensional optimization problem, the decision variables are parameterized in direct solution approaches so that the problem can be formulated as a finite

¹ w accounts for the optimization variables.

dimensional nonlinear programming problem (NLP). Here, it is assumed that the controls are first parameterized by piecewise constant functions and that the model is discretized using finite differences or higher order schemes for its numerical solution. Although direct single shooting is used in the current study, the method can be easily employed in the context of direct multiple shooting (see Section 2.5).

Consider the benchmark problem presented in Sistu and Bequette (1995), where an isothermal CSTR with the Van de Vusse reactions



is analyzed. The CSTR dynamics are governed by the set of nonlinear differential equations

$$\dot{C}_a(t) = \frac{F(t)}{V}(C_{a,0}(t) - C_a(t)) - k_1 C_a(t) - k_3 C_a^2(t), \tag{5.60}$$

$$\dot{C}_b(t) = k_1 C_a(t) - k_2 C_b(t) - \frac{F(t)}{V} C_b(t), \tag{5.61}$$

where $F(t)$ represents the feed flow, while V is the reactor volume. $C_a(t)$ and $C_b(t)$ represent the concentrations of the reactant A and the intermediate B , respectively (see Figure 5.2). Constants k_1 , k_2 and k_3 are reaction rate constants. It is assumed that the reactor volume V , remains constant and that the feed consists of pure A with a concentration $C_{a,0}(t)$. The intermediate concentration $C_b(t)$ is controlled by manipulating the feed rate.

Table 5.1 summarizes the parameters and nominal conditions for this benchmark problem. This particular system exhibits input multiplicity as illustrated in Figure 5.3. Consequently, the formulation of a cost in terms of the errors with respect to a desired trajectory can generate two possible control values. Hence, a local optimization technique can easily be attracted by a local minimum, delivering a suboptimal solution, if it is initialized inappropriately. However, for this particular application, global optimization approaches are able to find a better solution as shown in Long et al. (2006). The approach proposed here suggests a computationally less demanding heuristic to address the problem of finding a global solution to this problem.

Table 5.1: CSTR parameters and nominal conditions.

Parameter	Value
k_1	50 1/h
k_2	100 1/h
k_3	10 L/(gmol.h)
V	1 L
F_{\min}	0 L/h
F_{\max}	200 L/h
\bar{F}	180.95 L/h
$\bar{C}_{a,0}$	10 gmol/L
\bar{C}_a	6.181 gmol/L
\bar{C}_b	1.1 gmol/L

By redefining $x(t) = [C_a(t) \ C_b(t)]^T$ and $u(t) = \frac{F(t)}{V}$, the OCP for the CSTR output concentration can be formulated as in (5.1)-(5.5), with

$$h(x(t), u(t)) = \begin{cases} x(t), \\ u(t), \\ 200h^{-1} - u(t), \end{cases} \tag{5.62}$$

and no terminal region $r(x(T))$. $\bar{x}(t)$ represents the state trajectory and no reference trajectory for the controls is provided. In the numerical solution, the control $u(t)$ is discretized by a piecewise constant discretization with N_u intervals.

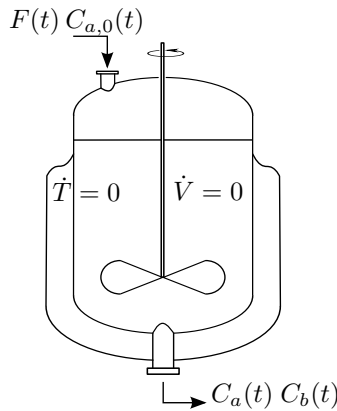


Figure 5.2: Isothermal CSTR.

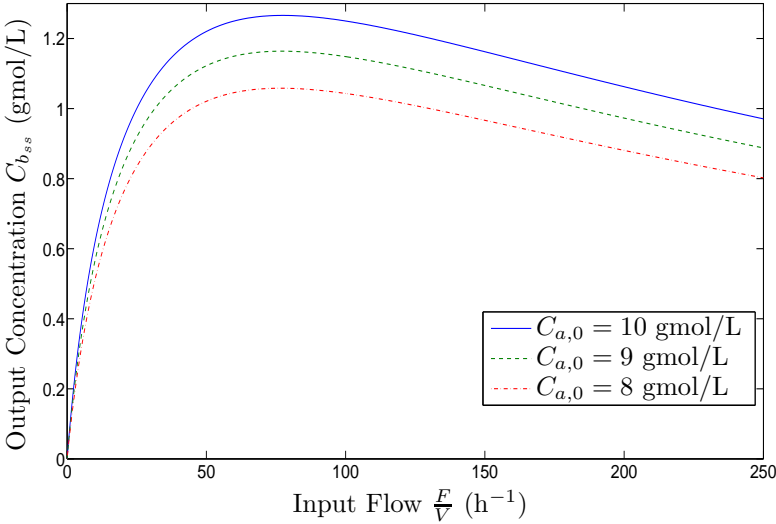


Figure 5.3: Steady state gain for the CSTR process for different values of the input concentration $C_{a,0}$.

The presented nonlinear dynamics is discretized with a sampling rate of 0.002 h (7.2 s) and solved for a prediction horizon $T = 0.06$ h (30 samples) with a constant control along the prediction horizon (Long et al., 2006), i.e., the control horizon, N_u is set to one. The differences between model states and state trajectory are penalized in a different proportion along the time interval $[0, T]$. The discrete version of the penalization matrix Q is set to $diag(1e^{-3} \ 2e^{-1}) L^2/(gmol^2h)$ while Q_T is $diag(1e^{-3} \ 80)L^2/(gmol^2)$.

The cost defined by

$$\psi(u) = \min_{x(\cdot)} \|x - \bar{x}\|_J^2, \quad (5.63)$$

subject to the dynamic equations (5.60) and (5.61) is illustrated in Figure 5.4. It corresponds to the cost to minimize when a step change on the reference trajectory, $\bar{x}(t)$, is performed. The original problem has one global and one local solution. Clearly, if a local optimization technique starts with an initial guess close to the constraints, the solution to the original NLP locks on to the upper bound of $u(t)$ leading to the local minimizer, $u_{lm}(t)$.

The OCP for the CSTR is modified using the proposed approach by introducing the norm on $x_c(t) - x(t)$ and the homotopy parameter α leading to the parametric problem (5.7)-(5.11) with no terminal constraint. Figure 5.5 illustrates the

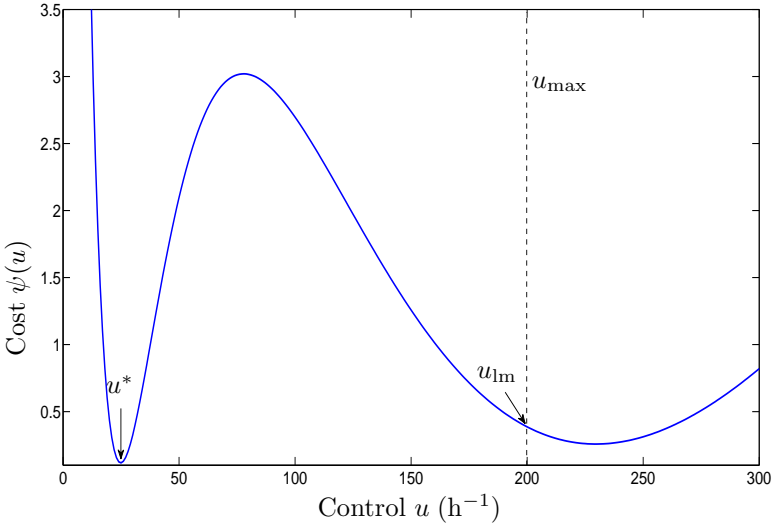


Figure 5.4: Original cost for the CSTR open loop optimal control problem when first optimized over $x(t)$. The value u_{lim} corresponds to the local minimizer

homotopy maps for different values of α in the interval $(0, 1)$. The cost value in (5.7) is first minimized with respect to $x(t)$ and $x_c(t)$. Note that the extremes of the map correspond to a convex function, and to the cost given by the original problem in Figure 5.4, respectively. In this example it is possible to attain the global optimum, if the OCP is convexified with the proposed approach and a local optimization technique is employed for increasing values of α performing each time the initialization with the previously computed optimal solution, i.e., tracking the zero path by a simple continuation method.

Figure 5.6 presents the behavior of $\|x_c - x\|_J^2$ as a function of the homotopy parameter. This norm it tends to zero as α goes to one, recovering the original OCP. This plot corresponds to the values of $\|x_c - x\|_J^2$ on the zero path illustrated in Figure 5.5.

Additionally, the condition presented in Lemma 5.1.3 is illustrated in Figure 5.7, where the problem is assumed in steady state and neither changes in the reference nor disturbances are considered. Following this condition the optimal state trajectory for the OCP satisfies $x_{\text{ocp}}^*(t) = \bar{x}(t)$ meaning that the system remains in steady state. As stated in Lemma 5.1.3, the optimal solution of the original OCP equals the solution provided by the convex cost given by $P(0)$. Hence, in order to obtain the global solution for the original OCP for $x_{\text{ocp}}^*(t) = \bar{x}(t)$ it would be enough to solve the convex OCP $P(0)$. Note that the original OCP for $\alpha = 1$ is

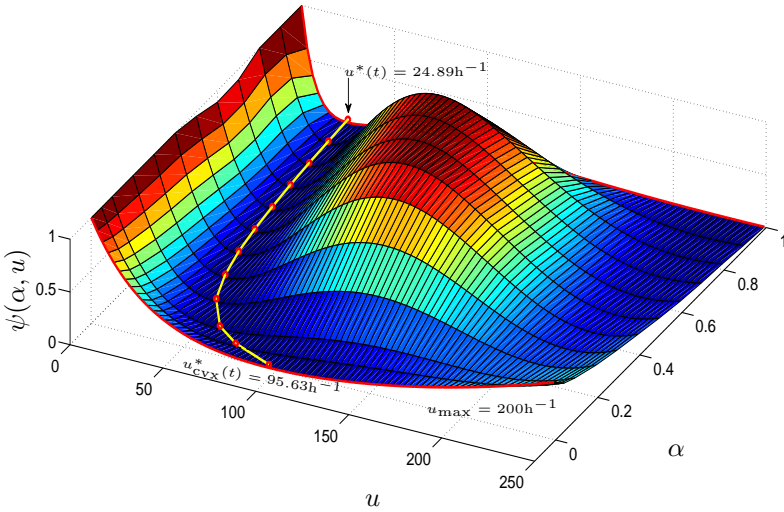


Figure 5.5: Cost functions for a set of the problems between the original OCP and its convex formulation for the CSTR control example when a step change in the reference is performed. The zero path has been obtained by minimizing each one of the parametric OCPs, $P(\alpha)$, for discrete values of α increasing monotonically, leading to $u^*(t)$ when $\alpha \rightarrow 1$.

still highly nonconvex.

5.3 Receding horizon control numerical example

In order to illustrate the applicability of the method in the NMPC framework, a closed loop simulation study is performed. It is important to mention here that a control horizon $N_u = 1$ has been selected only for visualization porpoises, since it is easier to visualize the cost and locate global and local solutions by enumerating the possible control values $u \in \mathbb{R}$. A more realistic case with increased control horizon is presented at the end of the current section. Note that in NMPC, the parameterized OCP has to be solved at each sampling instant. A nonlinear open loop observer is implemented in order to estimate the possible process disturbances and model states. The state reference trajectory is calculated from the desired process output (intermediate concentration $C_b(t)$) and the estimated disturbance as proposed in Rossiter (2003). No knowledge of the input reference trajectory is provided. At each sampling instant the problem is solved first using the homotopy approach with $\alpha = 0$, i.e., the convex problem is addressed, and after, the original

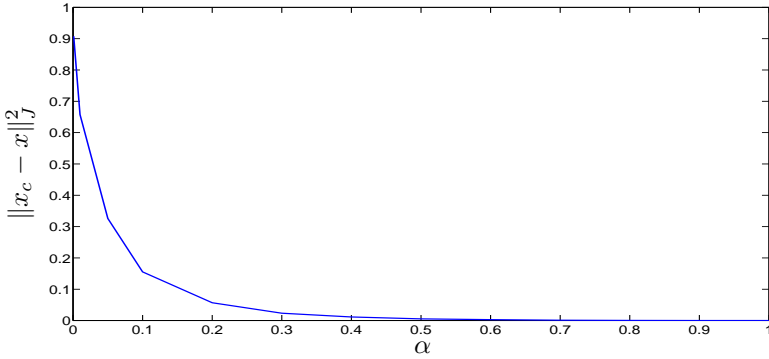


Figure 5.6: Behavior of the norm on $\|x_c - x\|_J^2$ as a function of the homotopy parameter for the CSTR example. This plot corresponds to the zero path values in Figure 5.5

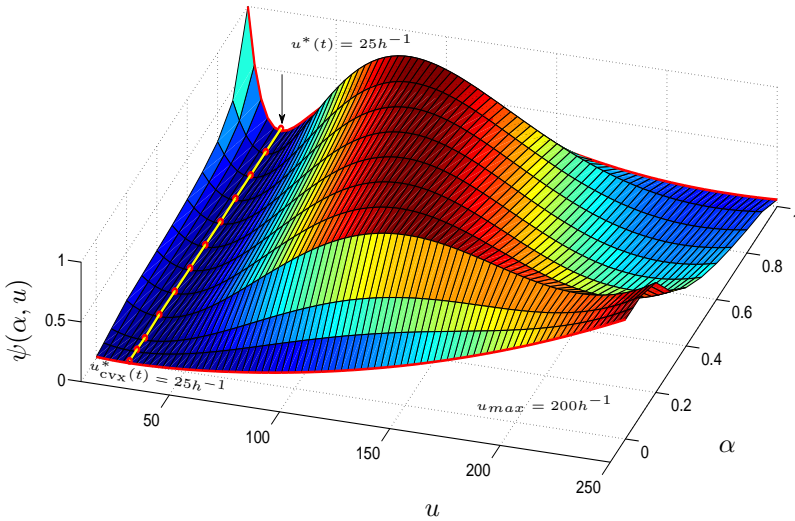


Figure 5.7: Cost functions for a set of the problems between the original OCP and its convex formulation on the homotopy path for the CSTR control example. In this case $x_{ocp}^*(t) = \bar{x}(t)$ leading to $u_{P(\alpha)}^* = u_{ocp}^* \forall \alpha \in (0, 1)$.

NLP ($\alpha = 1$) is solved using as initial guess the solution provided by the convex OCP. Consequently, one quadratic programming problem (QP) and one NLP are solved every 7.2 s. The former one to obtain the initial guess for $u(t)$ and the latter

to refine the approximated solution. Nevertheless, whenever necessary, methods to follow the zero path may be incorporated (Watson et al., 1987). In view of this procedure, it could be possible to think about an algorithm that solves the convex approximation normally and only goes for the NLP when the size of the disturbance $\|x - \bar{x}\|_J^2$ is above a predefined threshold.

In order to evaluate the performance of the closed loop using a NMPC with the presented method, a test scenario is proposed. The test consists of reference changes and disturbance rejection. During the first 0.05 h of simulation, the system reaches steady state. There, the output reference trajectory is changed at 0.15 h and 0.6 h. On the other hand, disturbances are applied by changing the feed concentration at 0.3 h and 0.45 h. Figure 5.8 presents the results for a tracking and disturbance rejection test using both an NLP solver based on sequential quadratic programming (SQP)² and the proposed convexity-based homotopy approach. Both algorithms are initialized with the same initial state $[x_1, x_2]^T = [6.18, 1.1]^T$ gmol/L. On the one hand, to calculate the first control move, the proposed approach does not require an initialization in $u(t)$ since the first problem to solve is convex. On the other hand, the NLP solver requires an initialization which clearly affects the convergence to a solution. In this simulation study, the control is initialized to $u(t) = 180.94\text{h}^{-1}$ which corresponds to the control value for the given initial state. The proposed approach immediately finds the right control, causing the strong change in the control action and the big peak in $C_b(t)$. Note that the homotopy approach finds the global solution while the local optimization technique, which is each time initialized with the previous solution, finds only a local optimum. For the tracking problem, evaluated by performing the changes in reference as mentioned, the NLP locks onto the upper bound of $u(t)$. On the other hand, the homotopy approach finds the global solution as illustrated in the cost function plot. Similar behavior can be noted when evaluating the disturbance rejection properties. When the process is perturbed, the classical technique finds a local solution while the proposed method is able to compute the global solution. Note also that for this cost formulation, a local minimum leads to steady state errors with respect to the reference trajectory.

For the 0.8 h simulation, 400 NLP problems are solved. The test has been executed using a Intel Core 2 Duo microprocessor at 1.6 GHz running a linux distribution with 2 GB of RAM. Figure 5.9 presents the computational demand of the evaluated algorithms. In both cases, the computational demand is below the time constraint of 7.2 s, making the approach feasible for implementation.

The OCP is also solved when increasing the degrees of freedom to $N_u = 30$. Figure 5.10 displays the optimal control provided by the local optimization technique and the proposed method for the case studied in Figure 5.5 but using 30 control moves. The convex initialization combined with the local optimizer is still

²The MATLAB (The Mathworks Inc., Natick, MA.) NLP, the *fmincon* routine is used for this simulation study

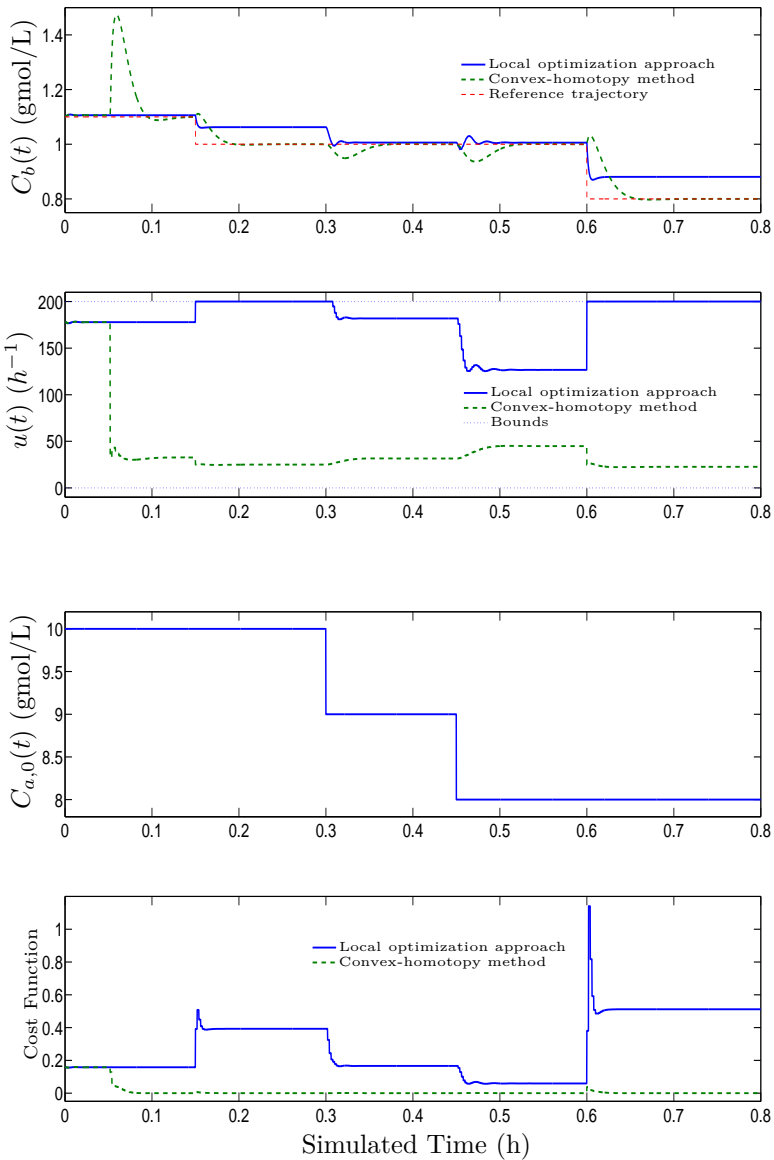


Figure 5.8: Tracking and disturbance test for the NMPC applied to the CSTR using a local optimizer and convexity-based homotopy approach. The problem is solved with a control horizon $N_u = 1$. The convex approach is switched on at $t = 0.05$ hours with the same initialization as in the local approach.

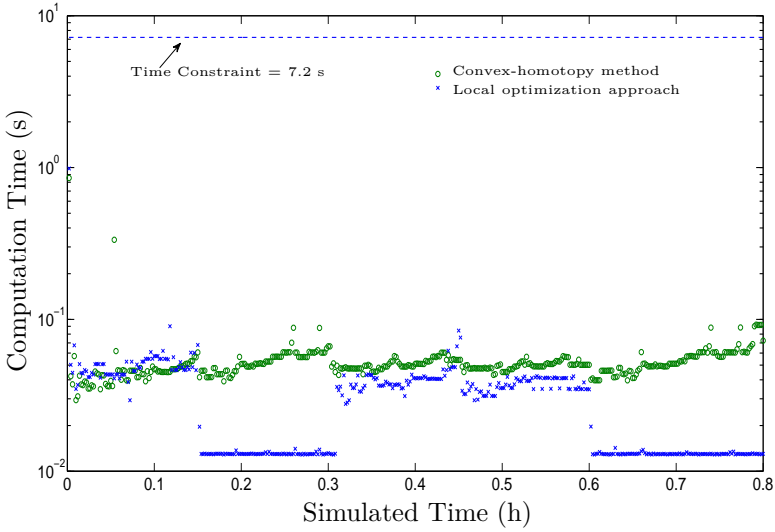


Figure 5.9: Computational demand for the studied test scenario with $N_u = 1$.

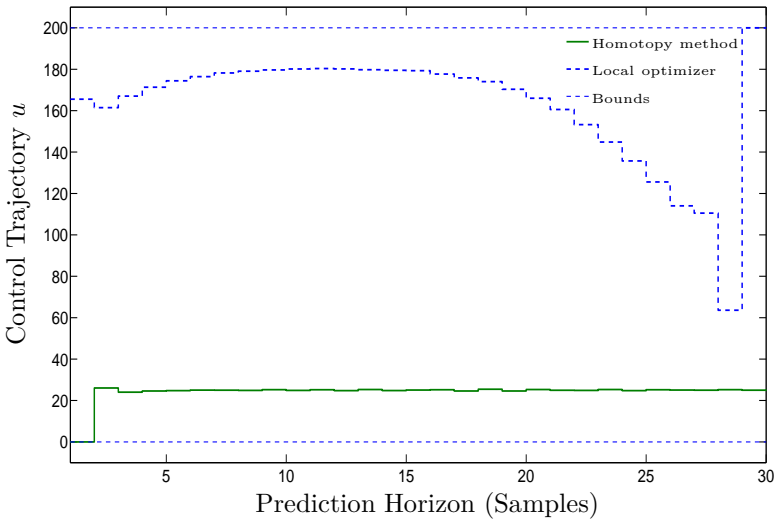


Figure 5.10: Optimal control trajectory provided by the optimization methods when a step change in the reference is performed at 0.15 h. The control horizon is set to $N_u = 30$.

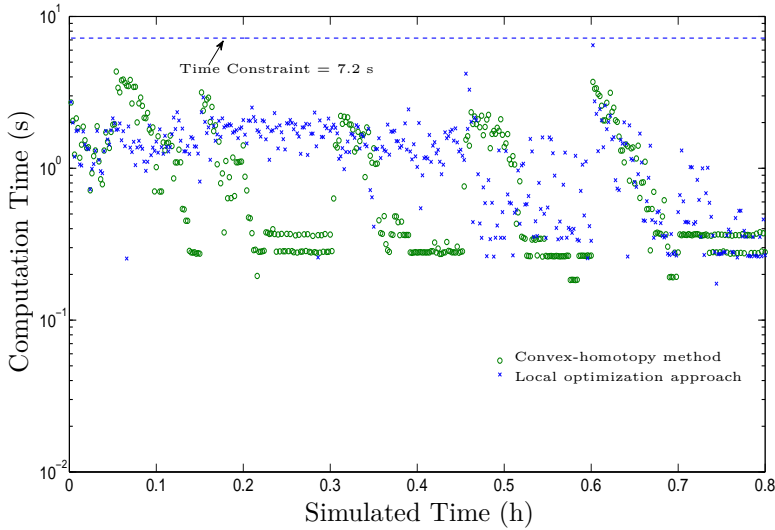


Figure 5.11: Computational cost for the studied test scenario in Figure 5.12 with increased control horizon $N_u = 30$.

able to provide what it is believed to be the global solution with a considerably lower objective³. Additionally, the closed loop behavior of the process is evaluated with the test scenario described previously and an increased control horizon, $N_u = 30$. Figure 5.12 depicts the behavior of the NMPC when input concentration and reference changes are performed. In this case, the proposed method is still able to compute the appropriate control sequence, while the local optimization technique provides an optimal solution which drives the system to the wrong steady state value exhibiting steady state errors. The computational demand of the simulation is presented in Figure 5.11 where the time employed by both algorithms is still smaller than the sampling period T_s of 7.2 s.

5.4 Discussion of the homotopy approach

In general, it is not possible to guarantee continuity of the path of solutions, i.e., the *zero path*. However, continuity of this path and bifurcations on it are directly related to the singularity of the KKT-system jacobian obtained from the finite-dimensional PDOP. Note that the solution of the DOP in the convex and

³For this nonconvex problem in 30 variables it is nearly impossible to verify that the global solution is found.

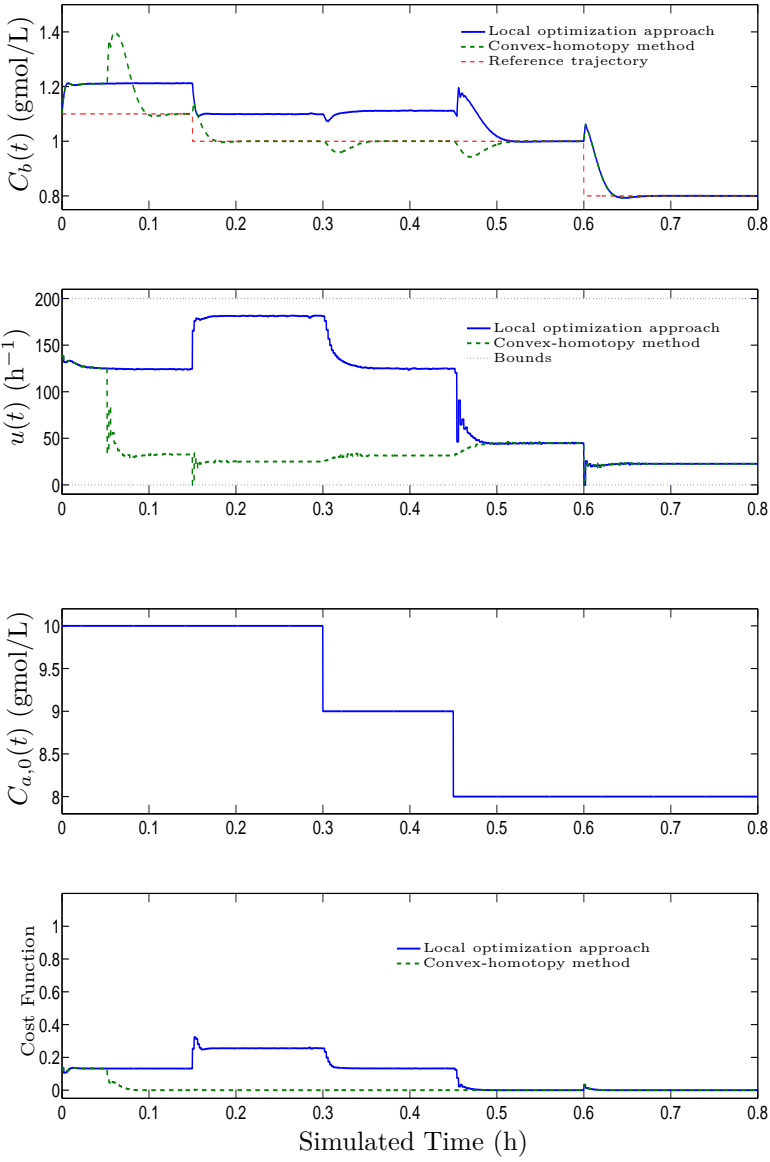


Figure 5.12: Tracking and disturbance test for the NMPC applied to the CSTR using a local optimizer and convexity-based homotopy approach. The problem is solved with a control horizon $N_u = 30$. The convex approach is switched on at $t = 0.05$ hours with the same initial states as in the local approach.

nonconvex extremes correspond to KKT points of the parameterized problems with $\alpha \rightarrow 0$ and $\alpha \rightarrow 1$. If derivative-based local optimization techniques are used, the solutions in between these extreme KKT points are calculated from the KKT-system with embedded α parameter. In view of Theorem 2.3 in Watson (2002), the continuity of the path and the non-existence of bifurcation are guaranteed if the Jacobian of the parameterized KKT-system is nonsingular along the zero path, i.e, along the solutions of the PDOP when α moves from zero to one. If in addition, the zero path is bounded, the path of minimizer from the convex OCP to the nonconvex can be followed, since this condition along with continuity ensure a finite path length (Watson, 2002). Consequently, there is still an open question with respect to the properties of the cost and constraints of the PDOP in order to guarantee non singularity of the KKT system along the zero path. This question remains for future investigations on the convex approximation method.

5.5 Conclusions

In this chapter a homotopy method is presented to initialize nonconvex OCPs arising in optimal control problems where the dynamic model involved is affine in the controls and the objective is a penalty on deviations from a desired state reference. It has been shown that by modifying the nonconvex OCP through a homotopy it is possible to find a convex OCP. The homotopy from the nonconvex to the convex OCP is analyzed as a parametric dynamic optimization problem (PDOP). The necessary assumptions and the proofs of convergence of this PDOP to the original and convex DOPs in the extremes of the homotopy map are provided. Despite the limitation discussed in Section 5.4, the applicability of the method to two particular examples in the field of optimal control is presented. It is shown that the likelihood of finding a global solution to the nonconvex OCP is greatly improved when compared to standard local optimization techniques. Moreover, the validity of the method for NMPC applications has been illustrated through a benchmark problem in chemical process control where the approach is able to find the optimal control trajectory while a classical technique locks onto a local solution. Finally, computational aspects of the method have been addressed in order to illustrate feasibility with respect to implementation. In summary, the presented approach promises to become an attractive heuristic for a smart initialization of a specific class of nonconvex optimal control problems, using the power of convex optimization.

Chapter 6

A near optimal solution to parameter estimation problems with parameter-affine dynamics embedded

Chapter 5 shows that a dynamic optimization problem (DOP) with input-affine dynamics can be recast to obtain a convex DOP through a homotopy. This chapter focuses particularly on parameter estimation problems (PEP) and develops a method to use this convex problem solution either as initialization point of more advanced simultaneous optimization routines, such as Simultaneous Gauss-Newton (SGN), or to perform a refinement of this guess by solving one more convex problem. Since the latter approach provides a suboptimal solution, proofs of the loss of optimality are provided for the method. Moreover, numerical results are presented for the SGN with arbitrary initialization and with the proposed approach using benchmark examples in the chemical and biological fields.

6.1 Convexification of parameter estimation problems with parameter-affine models

Consider the PEP :

$$\min_{x(\cdot), p} \frac{1}{2} \|x(t_i) - \bar{x}(t_i)\|_Q^2 \quad (6.1)$$

subject to

$$\dot{x}(t) = f(x(t)) + g(x(t))p, \quad t \in [0, T], \quad (6.2)$$

$$h(x(t), p) \geq 0. \quad t \in [0, T], \quad (6.3)$$

where the inequality constraints are assumed convex and $Q \succeq 0$, $\forall t \in [0, T]$. The process inputs $u(t)$ that are used to modify the dynamics in (6.2) are assumed known, such that they are not optimization variables and are not explicitly presented in (6.2) for simplicity.

If this problem is deformed using the homotopy approach presented in Chapter 5, it is clear that a convex PEP is obtained. Other well-known procedures leading to convex PEP have been proposed for parameter-affine systems, such as Least Squares Prediction Error Methods (LS-PEM) (Ljung, 2002). Although these methods are widely used, they are sensitive to noisy data and in order to work well in practice, they need to filter the residuals, i.e., noise models have to be proposed as a part of the estimation of parameters. In contrast to this, the approach presented here does not involve the use of arbitrary filters over the residuals and can be shown to be less sensitive to noisy data, leading to less biased results without previous knowledge of the errors' behavior. In order to illustrate this property, one of the PEP examples presented in Bonilla et al. (2008) is used. Consider the attractor introduced by Edward Lorenz in 1963. The dynamics of the Lorenz attractor is governed by a set of differential equations of the form

$$\dot{x}(t) = \sigma(y - x), \quad \dot{y}(t) = x(\rho - z) - y, \quad \dot{z}(t) = xy - \beta z \quad (6.4)$$

where σ , β and ρ are positive parameters. Typical values to illustrate the chaotic behavior of this set of nonlinear equations are $\sigma = 10$, $\beta = 8/3$ and $\rho = 28$. Note that the system presents the parameter affine structure with $p = [\sigma, \rho, \beta]^T$. The multiple time scale evolution and the chaotic behavior of (6.4), is often used to illustrate the internal dynamics of the earth atmosphere (Palmer, 1993) and it has been used as case study for parameter estimation methods as well in Lea et al. (2000) and Annan and Hargreaves (2000).

It is assumed that a sequence containing measurements for all states $\bar{x}(t)$, $\bar{y}(t)$ and $\bar{z}(t)$ at time instants t^i is provided as illustrated in Figure 6.1(b). This sequence is contaminated with colored noise. Thus, it is expected that the LS-PEM without any noise information provides a biased solution (Ljung, 2002).

In order to better visualize the cost functions for the presented approaches, σ and β are considered constant and only ρ is estimated. The NLP is formulated by discretizing the PEP at t^i instants. The obtained cost as a function of $\rho \in [10, 40]$ is presented in Figure 6.2. In this case the initial condition has been assumed fixed. Clearly this cost is non-smooth and contains several local minima due to the high

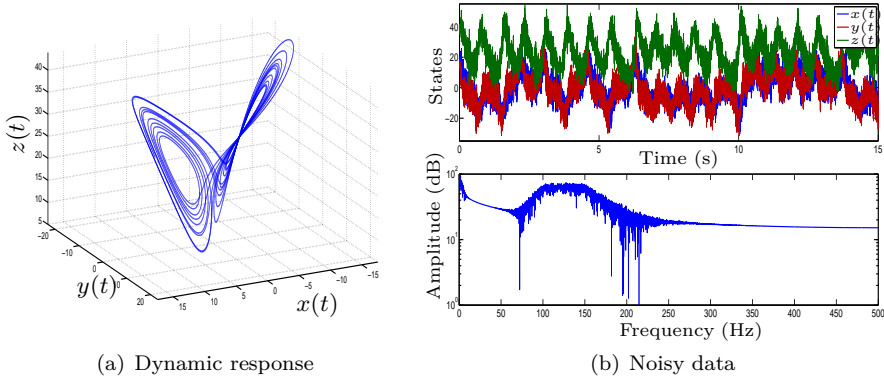


Figure 6.1: Chaotic behavior of Lorenz attractor, $\sigma = 10$, $\beta = 8/3$ and $\rho = 28$ (a), and noisy data used for estimation (b).

sensitivity of model states for values of $\rho > 24$. Consequently, derivative-based techniques hardly find the right solution when initialized far from the optimum. Due to the noise added, and due to the fact that a noise model is not considered, the global solution provided by LS-PEM methods is biased with respect to the optimum. Consequently, it is required to define a filter for the residuals based on the analysis of the noise spectrum of the collected measurements in Figure 6.1(b). For this particular example, it is not difficult to recognize noise in the range 100-150Hz. Hence, a simple approach is to propose a filter with a bandwidth matching this band. Note that this is a heuristic approach and it is not always easy to isolate the noise spectrum from the measured data. A second order bandpass filter is designed and added to each output of the original model. The improved results of the LS-PEM including this filter (LS-PEM+NF) are illustrated in Figure 6.2.

The convex PEP obtained from the homotopy approach is introduced for this parameter estimation problem, by using the Lorenz model (6.4) and the noisy data shown in Figure 6.1(b) with a fixed initial condition. The cost to be optimized, obtained with this formulation, is presented in Figure 6.2 as CVX-H. Similarly to LS-PEM and LS-PEM+NF, the cost is convex. However, the minimum of the convex cost obtained with the homotopy method is less biased w.r.t. the nonlinear least squares (NLS) PEP solution. Note that the plots for all the costs in Figure 6.2 have been scaled for visualization purposes. The same test is run with colored noise in other frequencies, in all cases, the proposed methods showed less bias than its LS-PEM counterpart with and without filter (Bonilla et al., 2008).

Table 6.1 summarizes the optimal values ρ^* for the presented costs considered in the domain of ρ . Additionally, the absolute error $e(\rho)$ with respect to the real value of $\rho = 28$ is presented.

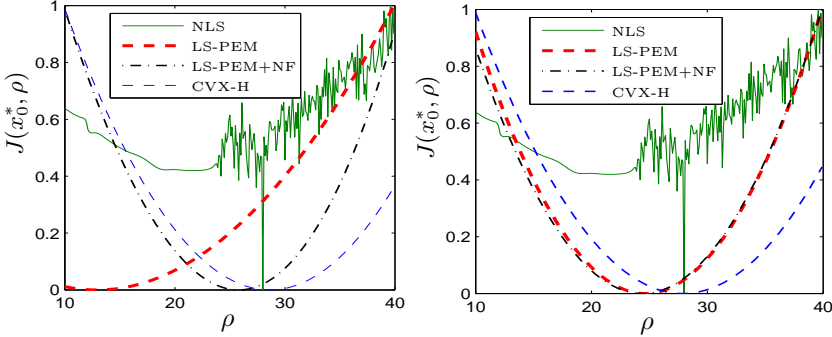


Figure 6.2: Costs for different approaches $\sigma = 10$, $\beta = 8/3$. The data has been contaminated with noise in the range 100 to 150 Hz (left) and 400 to 450 Hz (right).

Table 6.1: Optimum values for the PEP of the Lorenz attractor with $\rho = 28$.

Cost	$\rho^*_{100-150\text{Hz}}$	$e(\rho^*)_{100-150\text{Hz}}$	$\rho^*_{400-450\text{Hz}}$	$e(\rho^*)_{400-450\text{Hz}}$
NLS	28	0.0	28.0	0.0
LS-PEM	24.60	12.14	12.9	53.93
LS-PEM+NF	24.40	12.85	25.8	7.86
LS-CA	27.90	0.36	28.6	2.14

6.2 A 2-step procedure for the solution of estimation problems with parameter-affine dynamics embedded

The solution presented by the convex homotopy can be further improved by simply linearizing the original nonconvex PEP around this minimum. In such a case only two convex problems are solved and the solution is expected to be less biased. Although, the solution is still suboptimal it is possible to provide a measure for the loss of optimality in this procedure. In the following, an assessment of the distance between the real solution to the PEP and the solution provided by the refined convex problem is analyzed. The optimization problem (6.1)-(6.3) and its convex extremes are parameterized under an appropriate discretization method,

leading to:

$$\text{PEP}_{\text{NL}}(\bar{\mathbf{x}}) : \min_{\mathbf{x}} \frac{1}{2} \|\mathbf{x} - \bar{\mathbf{x}}\|_Q^2, \text{ s.t. } \begin{cases} A(\mathbf{x}) - B(\mathbf{x})p - W\mathbf{x} & = 0, \\ h(\mathbf{x}, p) & \geq 0, \end{cases} \quad (6.5)$$

$$\text{PEP}_{\text{CVX}}(\bar{\mathbf{x}}) : \min_{p, \mathbf{x}_c} \frac{1}{2} \|\mathbf{x}_c - \bar{\mathbf{x}}\|_Q^2 \text{ s.t. } \begin{cases} A(\bar{\mathbf{x}}) - B(\bar{\mathbf{x}})p - W\mathbf{x}_c & = 0, \\ h(\mathbf{x}_c, p) & \geq 0 \end{cases} \quad (6.6)$$

where $\mathbf{x} = [x(t_0)^T, x(t_1)^T, \dots, x(t_N)^T]^T$ and $\bar{\mathbf{x}} = [\bar{x}(t_0)^T, \bar{x}(t_1)^T, \dots, \bar{x}(t_N)^T]^T$ correspond to the discrete time model state dynamics and the state measurements, respectively. $A(\mathbf{x})$, $B(\mathbf{x})$ and W represent the nonlinear dynamics of the model along with the discretization method. Q is a positive definite penalization matrix of the appropriate dimensions. If the original NLP is approximated by a QP around the solution obtained by the convex approximation, a problem of the form

$$\text{PEP}_{\text{CVX-REF}}(\bar{\mathbf{x}}) : \min_{p, \mathbf{x}} \frac{1}{2} \|\mathbf{x} - \bar{\mathbf{x}}\|_2^2, \text{ s.t. } \begin{cases} A_L \mathbf{x} - B_L p + b & = 0 \\ H_x \mathbf{x} + H_p p + c & \geq 0, \end{cases} \quad (6.7)$$

is obtained. The model and constraints are linearized around the solution of the convex problem $(\mathbf{x}_{\text{CVX}}^*, p_{\text{CVX}}^*)$.

6.2.1 Loss of optimality

The minimum proposed by the method is a near optimal solution. In this section, an assessment of the distance between this near optimal solution and the solution provided by a fully converged SQP methods is performed. For comparison, consider the unperturbed original PEP where a set of noise-free state measurements $\bar{\mathbf{x}}$ is obtained and no modeling errors are present. In addition, the following assumptions are introduced:

Assumption 6.2.1.

A1 : The functions $A(\mathbf{x})$ and $B(\mathbf{x})$ are twice continuously differentiable.

A2 : There exist a pair $\bar{\mathbf{x}} \in \mathbb{X}$ and $\bar{p} \in \mathbb{P}$ such that $0 = A(\bar{\mathbf{x}}) - B(\bar{\mathbf{x}})\bar{p} - W\bar{\mathbf{x}}$.

A3 : Both problems, $\text{PEP}_{\text{NL}}(\bar{\mathbf{x}})$ and $\text{PEP}_{\text{CVX}}(\bar{\mathbf{x}})$, satisfy the strong second order sufficient conditions (SOSC) in Theorem 2.2.3, strict complementarity and constraint regularity (see Chapter 2) at their solution, $(\bar{\mathbf{x}}, \bar{p})$.

Corollary 1. Under assumptions A2 and A3, the Lagrange multipliers associated with the inequality constraints at the solution $(\bar{\mathbf{x}}, \bar{p})$ are zero, and none of the inequality constraints are active.

Lemma 5.1.3 in Chapter 5 states that the convex approximation provides an exact solution if the measured trajectory can be exactly generated by the model to fit, i.e., $\bar{\mathbf{x}}$ is noise-free and there are no modeling errors. Hence the pair $(\bar{\mathbf{x}}, \bar{p})$ is a solution to the original NLP and to its convex modification for $\bar{\mathbf{x}} = \bar{\bar{\mathbf{x}}}$.

In view of the previous assumptions, the following lemmata can be formulated:

Lemma 6.2.1. *If assumptions 6.2.1 hold, then*

$$\|p_{\text{cvx}}^*(\bar{\mathbf{x}}) - \bar{p}\| = \mathcal{O}(\|\bar{\mathbf{x}} - \bar{\bar{\mathbf{x}}}\|), \tag{6.8}$$

i.e., the distance between the perturbed convex problem solution and the unperturbed one is a function of the size of the perturbation.

Proof. Consider the PEP

$$\min_{p, \hat{\mathbf{x}}} \frac{1}{2} \|\mathbf{x} - \hat{\mathbf{x}}\|_Q^2 \quad \text{s.t.} \quad A(\hat{\mathbf{x}}) - B(\hat{\mathbf{x}})p - W\mathbf{x} = \mathbf{0}, \tag{6.9}$$

which corresponds to the convex problem for unperturbed ($\hat{\mathbf{x}} = \bar{\bar{\mathbf{x}}}$) and perturbed ($\hat{\mathbf{x}} = \bar{\mathbf{x}}$) measurements. Note that the inequality constraints can be neglected for $\hat{\mathbf{x}} = \bar{\bar{\mathbf{x}}}$ due to Corollary 1. Additionally, for sufficiently small perturbations, the inequality constraints remain inactive, this allows to neglect the inequality constraints when $\hat{\mathbf{x}} = \bar{\mathbf{x}}$. Consequently, the convex formulation is reduced to (6.9) for the unperturbed measurement set and in a small neighborhood of it $\|\bar{\bar{\mathbf{x}}} - \bar{\mathbf{x}}\| \leq \epsilon$, $\epsilon > 0$.

The Karush-Kuhn-Tucker (KKT) optimality conditions for (6.9) yield:

$$F(\mathbf{x}^*, p^*, \lambda^*, \hat{\mathbf{x}}) = \begin{bmatrix} Q & \mathbf{0} & -W^T \\ \mathbf{0} & \mathbf{0} & -B(\hat{\mathbf{x}})^T \\ -W & -B(\hat{\mathbf{x}}) & \mathbf{0} \end{bmatrix} \begin{bmatrix} \mathbf{x}^* \\ p^* \\ \lambda^* \end{bmatrix} - \begin{bmatrix} Q\hat{\mathbf{x}} \\ \mathbf{0} \\ -A(\hat{\mathbf{x}}) \end{bmatrix} = \mathbf{0}, \tag{6.10}$$

which provides the solution $(\mathbf{x}^*(\hat{\mathbf{x}}), p^*(\hat{\mathbf{x}}), \lambda^*(\hat{\mathbf{x}}))$ for the perturbed problem $\hat{\mathbf{x}} = \bar{\mathbf{x}}$ and the unperturbed one $\hat{\mathbf{x}} = \bar{\bar{\mathbf{x}}}$. Under the small perturbation condition, the

change in the solutions given a change in the measurement data is given by

$$\begin{aligned} \begin{bmatrix} \frac{\partial \mathbf{x}^*(\hat{\mathbf{x}})}{\partial \hat{\mathbf{x}}} \\ \frac{\partial p^*(\hat{\mathbf{x}})}{\partial \hat{\mathbf{x}}} \\ \frac{\partial \lambda^*(\hat{\mathbf{x}})}{\partial \hat{\mathbf{x}}} \end{bmatrix} &= \begin{bmatrix} Q & \mathbf{0} & -W^T \\ \mathbf{0} & \mathbf{0} & -B(\hat{\mathbf{x}})^T \\ W & -B(\hat{\mathbf{x}}) & \mathbf{0} \end{bmatrix}^{-1} \\ \left\{ \begin{bmatrix} \mathbf{0} & \mathbf{0} & \mathbf{0} \\ \mathbf{0} & \mathbf{0} & -\frac{\partial B(\hat{\mathbf{x}})^T}{\partial \hat{\mathbf{x}}} \\ \mathbf{0} & -\frac{\partial B(\hat{\mathbf{x}})}{\partial \hat{\mathbf{x}}} & \mathbf{0} \end{bmatrix} \begin{bmatrix} \mathbf{x}^*(\hat{\mathbf{x}}) \\ p^*(\hat{\mathbf{x}}) \\ \lambda^*(\hat{\mathbf{x}}) \end{bmatrix} + \begin{bmatrix} Q \\ \mathbf{0} \\ \frac{\partial A(\hat{\mathbf{x}})}{\partial \hat{\mathbf{x}}} \end{bmatrix} \right\}. \end{aligned} \quad (6.11)$$

Due to assumptions A1 to A3, the Jacobian of $F(\mathbf{x}^*, p^*, \lambda^*, \hat{\mathbf{x}})$ is invertible at $(\bar{\mathbf{x}}, \bar{p}, \bar{\lambda})$. Moreover, the perturbed Jacobian remains invertible for small changes in the measurement data $\|\bar{\mathbf{x}} - \hat{\mathbf{x}}\|$. Consequently, the change in the optimal values also depends on the size of the perturbation as can be inferred from the smoothness of the involved functions in (6.11). \square

Theorem 6.2.2. *If Assumptions 6.2.1 are satisfied, then*

$$\|p^*(\bar{\mathbf{x}}) - p_{\text{CVX-REF}}^*(\bar{\mathbf{x}})\| = \mathcal{O}(\|\bar{\mathbf{x}} - \hat{\mathbf{x}}\|^2) \quad (6.12)$$

holds. Equation (6.12) gives an assessment of the distance between the original problem solution and the solution provided by the refined convex approach $p_{\text{CVX-REF}}^(\bar{\mathbf{x}})$ as a function of the size of the perturbation $\|\bar{\mathbf{x}} - \hat{\mathbf{x}}\|$.*

Proof. In order to simplify the notation, the following definitions are introduced:

$$\mathbf{w} = [\mathbf{x}^T, p^T]^T, \quad Q_{\mathbf{w}} = \begin{bmatrix} Q & 0 \\ 0 & 0 \end{bmatrix}. \quad (6.13)$$

Consider the original PEP with the set of perturbed measurements $\bar{\mathbf{x}}$. Following Corollary 1, the original PEP can be formulated as:

$$\text{PEP}_{\text{NL}}(\bar{\mathbf{w}}) : \min_{\mathbf{w}} \frac{1}{2} \|\mathbf{w} - \bar{\mathbf{w}}\|_{Q_{\mathbf{w}}}^2, \quad \text{s.t.} \quad g(\mathbf{w}) = 0. \quad (6.14)$$

Note that Corollary 1 implies that the inequality constraints can be neglected for $\|\bar{\mathbf{x}} - \hat{\mathbf{x}}\|$ small enough. Now, the KKT conditions for the quadratic programming problem:

$$\text{PEP}_{\text{LIN}}(\bar{\mathbf{w}}, \hat{\mathbf{w}}) : \min_{\mathbf{w}} \frac{1}{2} \|\mathbf{w} - \bar{\mathbf{w}}\|_{Q_{\mathbf{w}}}^2, \quad \text{s.t.} \quad g(\hat{\mathbf{w}}) + \nabla g(\hat{\mathbf{w}})^T (\mathbf{w} - \hat{\mathbf{w}}) = 0, \quad (6.15)$$

at the linearization point $\hat{\mathbf{w}}$, are formulated as

$$F(\mathbf{w}, \lambda, \bar{\mathbf{w}}, \hat{\mathbf{w}}) = \begin{bmatrix} Q_{\mathbf{w}}(\mathbf{w} - \bar{\mathbf{w}}) + \nabla g(\hat{\mathbf{w}})\lambda \\ g(\hat{\mathbf{w}}) + \nabla g(\hat{\mathbf{w}})^T(\mathbf{w} - \hat{\mathbf{w}}) \end{bmatrix} = \mathbf{0}, \quad (6.16)$$

where λ represents the Lagrange multipliers for the equality constrained problem. This set of equations provides a solution $\mathbf{w}_{\text{LIN}}^*(\bar{\mathbf{w}}, \hat{\mathbf{w}})$ as a function of the linearization point and the set of measurements.

For sufficiently small perturbations $\|\bar{\mathbf{x}} - \bar{\bar{\mathbf{x}}}\|$ and considering Assumptions 6.2.1, it is possible to establish the following relations

$$A : \|\mathbf{w}^*(\bar{\mathbf{w}}) - \mathbf{w}_{\text{LIN}}^*(\bar{\mathbf{w}}, \bar{\bar{\mathbf{w}}})\| = \mathcal{O}(\|\bar{\mathbf{w}} - \bar{\bar{\mathbf{w}}}\|^2) \quad (6.17)$$

and

$$\|\mathbf{w}_{\text{LIN}}^*(\bar{\mathbf{w}}, \bar{\bar{\mathbf{w}}}) - \bar{\bar{\mathbf{w}}}\| = \mathcal{O}(\|\bar{\mathbf{w}} - \bar{\bar{\mathbf{w}}}\|) \quad (6.18)$$

Equation (6.17) states that the solution provided by the first-order predictor $\mathbf{w}_{\text{LIN}}^*(\bar{\mathbf{w}}, \bar{\bar{\mathbf{w}}})$ differs from the real solution $\mathbf{w}^*(\bar{\mathbf{w}})$ by $\mathcal{O}(\|\bar{\mathbf{w}} - \bar{\bar{\mathbf{w}}}\|^2)$ as presented in (Diehl, 2002, Theorem 3.6 and Section 3.4.1). Equation (6.18) is a result of perturbation analysis of optimization problems (Robinson, 1980) under Assumption A1 to A3 and can easily be proved by linearizing the original problem around the unperturbed solution.

Considering (6.17) and (6.18), Theorem 6.2.2

$$C : \|\mathbf{w}^*(\bar{\mathbf{w}}) - \mathbf{w}_{\text{LIN}}^*(\bar{\mathbf{w}}, \mathbf{w}_{\text{cvx}}^*)\| = \mathcal{O}(\|\bar{\mathbf{w}} - \bar{\bar{\mathbf{w}}}\|^2) \quad (6.19)$$

is proven by showing that the distance between the first-order predictor solution $\mathbf{w}_{\text{LIN}}^*(\bar{\mathbf{w}}, \bar{\bar{\mathbf{w}}})$ and the solution provided by $\mathbf{w}_{\text{LIN}}^*(\bar{\mathbf{w}}, \mathbf{w}_{\text{cvx}}^*)$ is of second-order in $\|\bar{\mathbf{w}} - \bar{\bar{\mathbf{w}}}\|$, i.e.,

$$B : \|\mathbf{w}_{\text{LIN}}^*(\bar{\mathbf{w}}, \bar{\bar{\mathbf{w}}}) - \mathbf{w}_{\text{LIN}}^*(\bar{\mathbf{w}}, \mathbf{w}_{\text{cvx}}^*)\| = \mathcal{O}(\|\bar{\mathbf{w}} - \bar{\bar{\mathbf{w}}}\|^2). \quad (6.20)$$

Note that in this proof what is basically used is an inequality triangle, i.e., A&B \Rightarrow C. Consequently C is proved by proving B. In order to do so, consider the series expansion of the linear predictor solution around the minimizer

provided by the convex problem using the perturbed set of measurements¹,

$$\begin{aligned} \mathbf{w}_{\text{LIN}}^*(\bar{\mathbf{w}}, \mathbf{w}_{\text{cvx}}^*) &= \mathbf{w}_{\text{LIN}}^*(\bar{\mathbf{w}}, \bar{\bar{\mathbf{w}}}) + \frac{\partial \mathbf{w}_{\text{LIN}}^*(\bar{\mathbf{w}}, \hat{\mathbf{w}})}{\partial \hat{\mathbf{w}}} \Big|_{\hat{\mathbf{w}}=\bar{\bar{\mathbf{w}}}} (\mathbf{w}_{\text{cvx}}^* - \bar{\bar{\mathbf{w}}}) \\ &\quad + \mathcal{O}(\|\mathbf{w}_{\text{cvx}}^* - \bar{\bar{\mathbf{w}}}\|^2). \end{aligned} \tag{6.21}$$

The term

$$\frac{\partial \mathbf{w}_{\text{LIN}}^*(\bar{\mathbf{w}}, \hat{\mathbf{w}})}{\partial \hat{\mathbf{w}}} \Big|_{\hat{\mathbf{w}}=\bar{\bar{\mathbf{w}}}} (\mathbf{w}_{\text{cvx}}^* - \bar{\bar{\mathbf{w}}}) \tag{6.22}$$

is investigated in detail. By evaluating (6.16) at the solution $(\mathbf{w}_{\text{LIN}}^*, \lambda_{\text{LIN}}^*)$,

$$F(\mathbf{w}_{\text{LIN}}^*, \lambda_{\text{LIN}}^*, \bar{\mathbf{w}}, \hat{\mathbf{w}}) = 0, \tag{6.23}$$

and applying the implicit function theorem, it is possible to obtain an expression for the first factor in (6.22),

$$\frac{\partial \mathbf{w}_{\text{LIN}}^*(\bar{\mathbf{w}}, \hat{\mathbf{w}})}{\partial \hat{\mathbf{w}}} = -[\mathbb{I} \ 0] J(\hat{\mathbf{w}})^{-1} \frac{\partial F}{\partial \hat{\mathbf{w}}}, \tag{6.24}$$

with

$$J(\hat{\mathbf{w}}) = \frac{\partial F(\mathbf{w}_{\text{LIN}}^*, \lambda_{\text{LIN}}^*, \bar{\mathbf{w}}, \hat{\mathbf{w}})}{\partial (\mathbf{w}_{\text{LIN}}^*, \lambda_{\text{LIN}}^*)} = \begin{bmatrix} Q_{\mathbf{w}} & \nabla g(\hat{\mathbf{w}}) \\ \nabla g(\hat{\mathbf{w}})^T & 0 \end{bmatrix},$$

and

$$\frac{\partial F}{\partial \hat{\mathbf{w}}} = \begin{bmatrix} \nabla^2 g(\hat{\mathbf{w}}) \lambda_{\text{LIN}}^* \\ \nabla^2 g(\hat{\mathbf{w}}) (\mathbf{w}_{\text{LIN}}^* - \hat{\mathbf{w}}) \end{bmatrix}. \tag{6.25}$$

Equation (6.24) is obtained by considering that $\frac{\partial \bar{\bar{\mathbf{w}}}}{\partial \hat{\mathbf{w}}} = 0$, i.e., the measurement data does not depend on the linearization point. Assuming A3, and the invertibility of $J(\bar{\bar{\mathbf{w}}})$, at the linearization point $\hat{\mathbf{w}} = \bar{\bar{\mathbf{w}}}$, $J(\bar{\bar{\mathbf{w}}})^{-1}$ and $\nabla^2 g(\bar{\bar{\mathbf{w}}})$ become constants yielding

$$\frac{\partial \mathbf{w}_{\text{LIN}}^*(\bar{\mathbf{w}}, \hat{\mathbf{w}})}{\partial \hat{\mathbf{w}}} \Big|_{\hat{\mathbf{w}}=\bar{\bar{\mathbf{w}}}} = \mathcal{O} \left(\left\| \begin{bmatrix} \lambda_{\text{LIN}}^*(\bar{\mathbf{w}}, \bar{\bar{\mathbf{w}}}) \\ \mathbf{w}_{\text{LIN}}^*(\bar{\mathbf{w}}, \bar{\bar{\mathbf{w}}}) - \bar{\bar{\mathbf{w}}} \end{bmatrix} \right\| \right). \tag{6.26}$$

¹This linear predictor is the model used in the first SQP iteration.

Note that $\mathbf{w}_{\text{LIN}}^*(\bar{\mathbf{w}}, \bar{\mathbf{w}}) - \bar{\mathbf{w}}$ corresponds to the distance between the unperturbed solution $\bar{\mathbf{w}}$ and the perturbed one provided by the use of a linear predictor in the constraints. This distance is given by (6.18) and leads to

$$\frac{\partial \mathbf{w}_{\text{LIN}}^*(\bar{\mathbf{w}}, \hat{\mathbf{w}})}{\partial \hat{\mathbf{w}}} \Big|_{\hat{\mathbf{w}}=\bar{\mathbf{w}}} = \mathcal{O}(\|\bar{\mathbf{w}} - \bar{\mathbf{w}}\|). \quad (6.27)$$

Hence, combining (6.27) and Lemma 6.2.1 yields

$$\frac{\partial \mathbf{w}_{\text{LIN}}^*(\bar{\mathbf{w}}, \hat{\mathbf{w}})}{\partial \hat{\mathbf{w}}} \Big|_{\hat{\mathbf{w}}=\bar{\mathbf{w}}} (\mathbf{w}_{\text{cvx}}^* - \bar{\mathbf{w}}) = \mathcal{O}(\|\bar{\mathbf{w}} - \bar{\mathbf{w}}\|^2). \quad (6.28)$$

Consequently, (6.21) is rewritten by using (6.28) leading to

$$\mathbf{w}_{\text{LIN}}^*(\bar{\mathbf{w}}, \mathbf{w}_{\text{cvx}}^*) = \mathbf{w}_{\text{LIN}}^*(\bar{\mathbf{w}}, \bar{\mathbf{w}}) + \mathcal{O}(\|\mathbf{w}_{\text{cvx}}^* - \bar{\mathbf{w}}\|^2), \quad (6.29)$$

i.e., the solutions $\mathbf{w}_{\text{LIN}}^*(\bar{\mathbf{w}}, \mathbf{w}_{\text{cvx}}^*)$, and $\mathbf{w}_{\text{LIN}}^*(\bar{\mathbf{w}}, \bar{\mathbf{w}})$ are identically apart from second order perturbations. \square

6.2.2 A numerical example

Theorem 6.2.2 is numerically corroborated by formulating the PEP of an harmonic oscillator using different experiments (Bonilla et al., 2008). In each one of these experiments, a state sequence, contaminated with Gaussian noise with different variances, is generated. The distance between the solution to the PEP (6.5), provided by a nonlinear optimizer, and the solution proposed by the linearization of the original problem around p_{CVX}^* , i.e., (6.7), is calculated along with the size of the perturbation with respect to the noise-free data. Figure 6.3 (bottom) illustrates that the distance between the actual solution $p^*(\bar{\mathbf{x}})$ and the one provided by solving the two convex least squares problems sequentially, i.e., (6.7) after (6.6), is of second order in the size of the perturbation. Note that a second order polynomial accurately fits the data corresponding to the six experiments. In addition, the method is evaluated on the Lotka-Volterra model using a similar approach, showing also that the loss of optimality is of second order in the size of the perturbations (Bonilla et al., 2009).

In the following, the presented convex approximation is combined with a simultaneous optimization algorithm in order to provide an initialization-free estimation methodology for parameter-affine models.

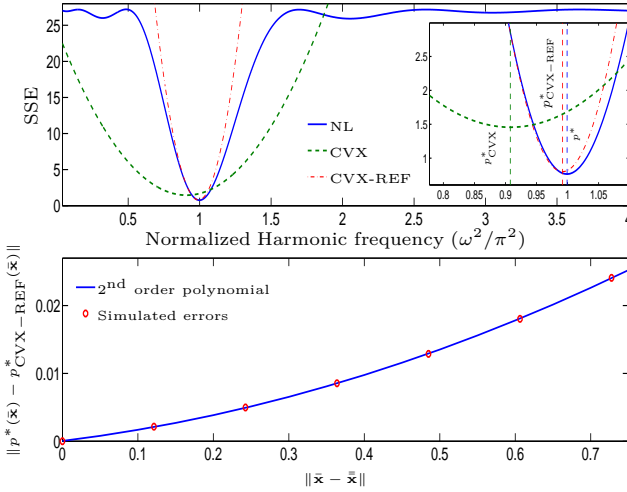


Figure 6.3: Cost functions generated by the PEP of a harmonic oscillator when a noisy state sequence is measured (top). NL corresponds to the original problem formulation while CVX to the convex approach. The plot in the bottom illustrates that the errors in the solution provided by the proposed approach are of second order in the size of the perturbations.

6.3 Automatic initialization for PEP in simultaneous optimization

The approach proposed in Section 6.2 can be used in combination with simultaneous optimization methods to provide an initialization-free procedure for parameter estimation with parameter-affine dynamic models. Note that in Simultaneous Gauss-Newton (SGN) (see Section 2.3.3), the shooting nodes are initialized with the available measurements, improving the convergence (Kostina, 2004). However, it is still necessary to provide an initial guess for the parameter vector to be optimized. The proposed initialization approach complements this set of available state measurements by providing an initial guess to the parameters and avoiding an arbitrary initialization.

A dynamic optimization solver using DMS parameterization is programmed in MATLAB (The Mathworks Inc, Natick, MA). The first-order information required to build the Jacobians of the cost and inequality constraints can be obtained by several methods (finite differences, automatic differentiation or symbolic calculations). However, due to the static characteristic of the cost in least

squares problems and the inequality constraints, these Jacobians can be easily calculated by finite differences². On the other hand, the Jacobian of the equality constraints, imposed by the dynamic model, is obtained, in this document, by using the dynamic equation solver with sensitivity generation capabilities proposed in Hindmarsh et al. (2005). The SQP and SGN algorithms presented in Chapter 2 are coupled with the ODE solver, and sensitivities are used to build the sparse sub-QPs at each major iteration of the SQP or SGN methods. Figure 6.4 shows the sparsity patterns in the Jacobian matrices presented in (2.34)-(2.36). These patterns are obtained when using multiple shooting parameterization for an LS-PEP involving a dynamic model with 2 states, 3 parameters, 4 measurement points and bound constraints on the parameters. The sparse and banded structures in the formulation can be either exploited by sparse solvers or a condensing strategy can be applied in order to reduce the size of the matrices. This procedure leads to a smaller least squares problem involving dense matrices as described in Bock and Plitt (1984).

In the following, the multiple shooting parameterization is used to estimate the parameters in two benchmark case studies. Comparative results are illustrated for an arbitrary initialization against an initialization based on the solution of the convex modification introduced in Section 6.2.

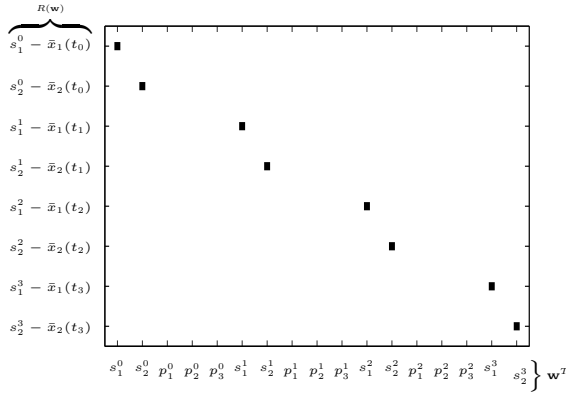
6.3.1 Lotka-Volterra equations

Consider the Lotka-Volterra model independently introduced by Alfred J. Lotka in 1925 and Vito Volterra in 1926. The nonlinear differential equations (6.31)-(6.32) describe the time evolution of the population density for two species in a biological system, i.e., a predator $x_2(t)$ and its prey $x_1(t)$. The dynamic behavior of this interaction is characterized by the following parameters:

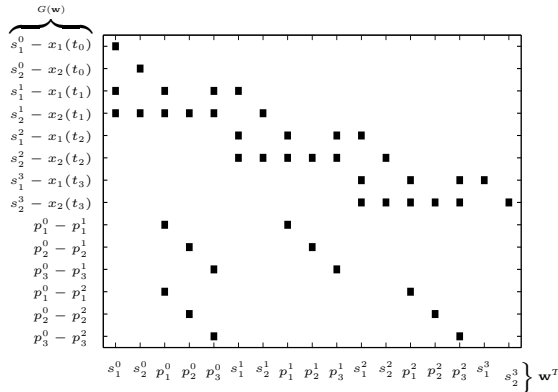
- α : The intrinsic rate of prey population increase,
- β : The predation rate coefficient,
- γ : The reproduction rate of predators per 1 prey eaten,
- δ : The predator mortality rate,

leading to a parameter vector $p = [\alpha, \beta, \gamma, \delta]^T$. Equations (6.31)-(6.32) exhibit two fixed points $[0, 0]$ and $[\alpha/\beta, \gamma/\delta]$. The first one corresponds to a saddle point while the second one to a center-stable, generating periodic solutions with an amplitude depending on the initial values. The oscillatory behavior of this pair of nonlinear equations is illustrated in Figure 6.5, where a set of noisy state measurements is obtained by simulating the model with nominal parameters $p = [0.6, 0.5, 0.7, 0.4]^T$, $x(t_0) = [1, 0.5]^T$ and adding Gaussian noise with a

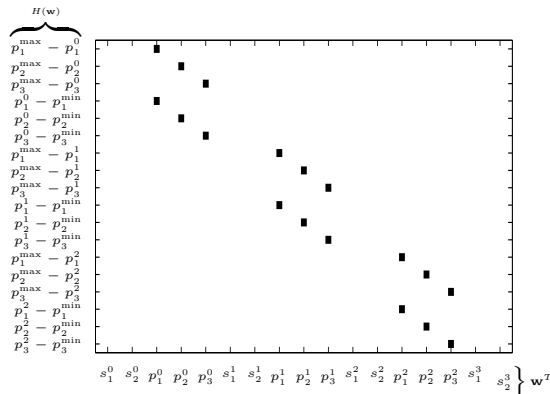
²Note that an integral cost can be embedded into the dynamic equations of the model.



(a) Residuals cost Jacobian $\nabla R(\mathbf{w})^T$



(b) Equality constraints Jacobian $\nabla G(\mathbf{w})^T$



(c) Inequality constraints Jacobian $\nabla H(\mathbf{w})^T$

Figure 6.4: Sparsity patterns for the Jacobians in a multiple shooting parameterization. In this example, the non-zero entries of the cost residuals Jacobian, and the equality and inequality constraints Jacobian are illustrated.

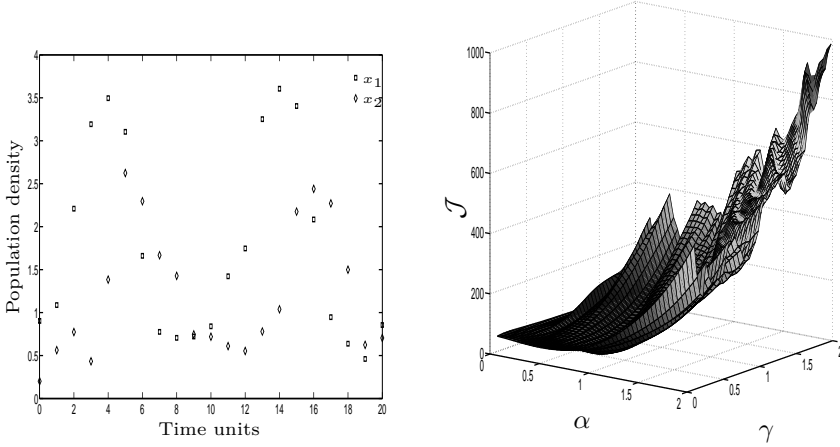


Figure 6.5: Data set for the PEP of the Lotka-Volterra model generated by simulating the model with nominal parameters $p = [0.6, 0.5, 0.7, 0.4]^T$, $x(0) = [1, 0.5]$ and adding Gaussian noise with a variance $\sigma^2 = 0.05$ (left). SSE as a function of the variation of parameters α and γ for the PEP (right). The parameters β , δ and the initial condition are constant and equal to their original values, i.e., $\beta = 0.5$, $\delta = 0.4$ and $[x_1(t_0), x_2(t_0)]^T = [1, 0.5]^T$.

variance $\sigma^2 = 0.05$. This benchmark problem can be found in Floudas et al. (1999) where only two of the four parameters are estimated.

Although, the system (6.31)-(6.32) is parameter-affine, the estimation of the parameter vector p is not a simple task. The PEP can be formulated as:

$$\min_{p, x(\cdot)} \mathcal{J} = \frac{1}{2} \sum_{i=0}^{20} \sum_{j=1}^2 (x_j(t_i) - \bar{x}_j(t_i))^2 \quad (6.30)$$

subject to

$$\dot{x}_1(t) = \alpha x_1 - \beta x_1 x_2, \quad (6.31)$$

$$\dot{x}_2(t) = -\gamma x_2 + \delta x_1 x_2, \quad (6.32)$$

$$0 \leq \alpha, \beta, \gamma, \delta \leq 2, \quad (6.33)$$

where $\bar{x}(t_i)$ represents the noisy state measurements in Figure 6.5. The contaminated data sequence is used to evaluate the cost (6.30) when the pair $[\alpha \ \gamma]$

changes while the parameters β and δ remain constant and equal to their original values. Figure 6.5 (right) presents the obtained nonconvex cost as a function of the varied parameters for a fixed initial condition $[x_1(t_0), x_2(t_0)]^T = [1, 0.5]^T$. Note that in this case a local minimum can be easily attained by the arbitrary initialization of the problem.

The PEP is parameterized using the DMS approach by introducing shooting nodes at each measurement point. In this example 21 shooting nodes are optimized along with the four model parameters α , β , γ and δ . Initialization of the parameter vector p is arbitrarily performed first by setting the initial guess to the center of the hyperbox defined by the bounds constraints (6.33), i.e., $p^0 = [1, 1, 1, 1]^T$. This initialization leads to an optimal value $p^* = [0.6700, 0.5455, 0.6288, 0.3501]^T$. In a second test, the initialization is performed with the value $p_{\text{CVX}}^* = [0.6343, 0.483, 0.5617, 0.288]^T$, corresponding to the solution of the convex optimization problem described by

$$\min_{p, x_c(\cdot)} \tilde{\mathcal{J}} = \frac{1}{2} \sum_{i=0}^{20} \sum_{j=1}^2 (x_{cj}(t_i) - \bar{x}_j(t_i))^2 \quad (6.34)$$

subject to

$$\dot{x}_{c1}(t) = \alpha \bar{x}_1 - \beta \bar{x}_1 \bar{x}_2, \quad (6.35)$$

$$\dot{x}_{c2}(t) = -\gamma \bar{x}_2 + \delta \bar{x}_1 \bar{x}_2, \quad (6.36)$$

$$0 \leq \alpha, \beta, \gamma, \delta \leq 2, \quad (6.37)$$

and leads to the same optimum obtained with the arbitrary initialization. Table 6.2 summarizes algorithm parameters along with the results obtained with both approaches and Figure 6.6 illustrates the performance of both approaches, where it is possible to appreciate the faster convergence of the SGN method with the convex initialization. Note that already in the second iteration, the continuity conditions in the DMS are almost totally satisfied.

6.3.2 Complex batch reaction

The batch reaction of formaldehyde, A , and sodium p -phenol sulfonate, B , exhibits a complex dynamic scheme with four intermediates, C, D, F and G , and a final product, E . All the reactions follow second order kinetics and are modeled as proposed in Ingham et al. (2000). Table 6.3 lists the reactions, their reaction rate constants and their nominal values.

Table 6.2: Algorithm parameters for the Lotka-Volterra PEP using arbitrary and convex initialization approaches.

Parameter	Arbitrary	Convex
TOL_{SQP}	1×10^{-10}	1×10^{-10}
$ATOL_{ODE}$	1×10^{-6}	1×10^{-6}
$RTOL_{ODE}$	$[1, 1] \times 10^{-4}$	$[1, 1] \times 10^{-3}$
$KKT_{TOL}(p^*)$	5.8486×10^{-11}	3.7386×10^{-11}
$\mathcal{J}(p^*)$	0.80318	0.80318
N_{Iter}	11	6

In order to simplify the notation, the concentration of the reactants, products and intermediates, A to G are represented by $x_1(t)$ to $x_7(t)$, respectively, and the parameter vector is defined as $p = [k_1, \dots, k_8]^T$. The parameter estimation problem can be cast as

$$\min_{p, x(\cdot)} \mathcal{J} = \frac{1}{2} \sum_{i=0}^{10} \sum_{j=1}^7 (x_j(t_i) - \bar{x}_j(t_i))^2 \tag{6.38}$$

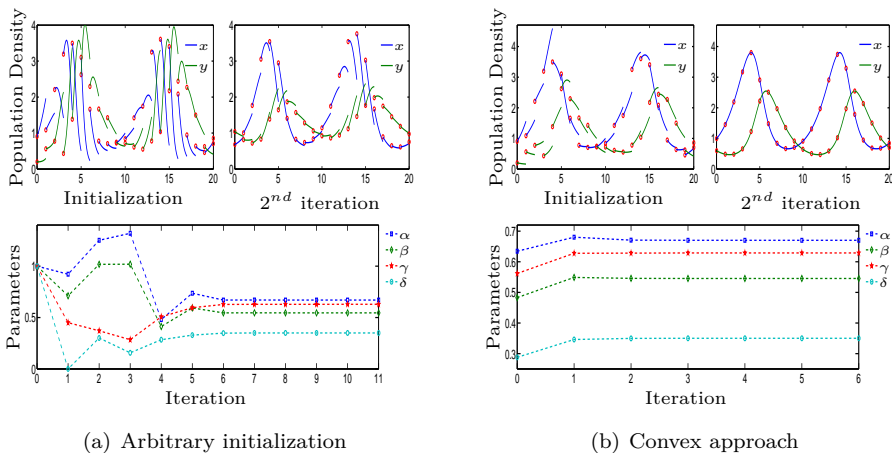


Figure 6.6: Convergence results for the simultaneous Gauss-Newton method applied to the PEP in the Lotka-Volterra model. The optimization is performed using an arbitrary initialization (a) and the proposed convex approach (b).

Table 6.3: Reaction rates for the batch reaction of formaldehyde with sodium p-phenol sulfonate.

Reaction	Rate coefficient	Nominal value (m ³ /kmol s)
A+B→C	k_1	0.16
A+C→D	k_2	0.05
C+D→E	k_3	0.15
B+D→F	k_4	0.14
C+C→F	k_5	0.03
C+B→G	k_6	0.058
A+G→F	k_7	0.05
A+F→E	k_8	0.05

subject to

$$\dot{x}_1(t) = -k_1x_1x_2 - k_2x_1x_3 - k_7x_1x_7 - k_8x_1x_6, \tag{6.39}$$

$$\dot{x}_2(t) = -k_1x_1x_2 - k_4x_2x_4 - k_6x_3x_2, \tag{6.40}$$

$$\begin{aligned} \dot{x}_3(t) = & k_1x_1x_2 - k_2x_1x_3 - k_3x_3x_4 - 2k_5x_3^2 \\ & - k_6x_3x_2, \end{aligned} \tag{6.41}$$

$$\dot{x}_4(t) = k_2x_1x_3 - k_3x_3x_4 - k_4x_2x_4, \tag{6.42}$$

$$\dot{x}_5(t) = k_3x_3x_4 + k_8x_1x_6, \tag{6.43}$$

$$\dot{x}_6(t) = k_4x_2x_4 + k_5x_3^2 + k_7x_1x_7 - k_8x_1x_6, \tag{6.44}$$

$$\dot{x}_7(t) = k_6x_3x_2 - k_7x_1x_7, \tag{6.45}$$

$$0 \leq k_1, k_2, \dots, k_8 \leq 1, \tag{6.46}$$

$$0 \leq x_1, \dots, x_7. \tag{6.47}$$

Figure 6.7(left) depicts the noisy state measurements $\bar{x}(t_i)$, obtained when (6.39) to (6.45) are simulated with the initial condition $x(t_0) = [0.15, 0.1, 0, 0, 0, 0, 0]^T$. This data set has been contaminated with Gaussian noise with standard deviation

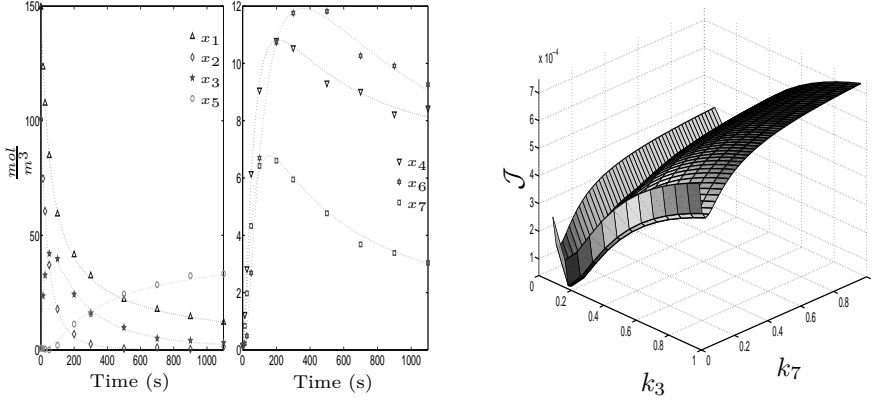


Figure 6.7: Data for the formaldehyde-sodium p-phenol sulfonate reaction PEP, generated by contaminating the model states with Gaussian noise with standard deviation $\sigma = 1 \times 10^{-3}$ for x_1, x_2, x_3 and x_5 and $\sigma = 2.23 \times 10^{-4}$ for x_4, x_6 and x_7 (left), and SSE as a function of the variation of parameters k_1 and k_3 (right). The remaining parameters and the initial condition are fixed to their nominal values.

$\sigma = 1 \times 10^{-3}$ for x_1, x_2, x_3 and x_5 and $\sigma = 2.23 \times 10^{-4}$ for x_4, x_6 and x_7 ³.

Figure 6.7(right) illustrates the nonconvex cost (6.38) when 6 parameters are fixed and the initial condition is set to the one introduced previously. It is not difficult to see that despite the linearity in the parameters, the optimization problem becomes nonconvex due to the nonlinearity in the states.

The PEP (6.38)-(6.46) is parameterized using the DMS approach and solved with initialization of the shooting nodes at the measurement points and arbitrarily setting $p^0 = [1, 1, 1, 1, 1, 1, 1, 1]^T$. In this case, it takes eight iterations to reach the optimum $p^* = [162.03, 41.13, 142.57, 32.87, 44.71, 57.46, 50.33, 54.91]^T \times 10^{-3}$. In order to improve convergence rate and avoid arbitrary initialization, the proposed approach is applied and the convex problem

$$\min_{p, x_c(\cdot)} \tilde{\mathcal{J}} = \frac{1}{2} \sum_{i=0}^{10} \sum_{j=1}^7 (x_{c_j}(t_i) - \bar{x}_j(t_i))^2 \quad (6.48)$$

subject to:

$$\dot{x}_{c_1}(t) = -k_1 \bar{x}_1 \bar{x}_2 - k_2 \bar{x}_1 \bar{x}_3 - k_7 \bar{x}_1 \bar{x}_7 - k_8 \bar{x}_1 \bar{x}_6, \quad (6.49)$$

³Different levels of noise are used due to different amplitudes in the states trajectories

Table 6.4: Algorithm parameters for the complex batch reaction PEP using arbitrary and convex initialization approaches.

Parameter	Arbitrary	Convex
TOL_{SQP}	1×10^{-10}	1×10^{-10}
$ATOL_{ODE}$	1×10^{-6}	1×10^{-6}
$RTOL_{ODE}$	$[1, 1] \times 10^{-4}$	$[1, 1] \times 10^{-4}$
$KKT_{TOL}(p^*)$	9.8354×10^{-11}	1.556×10^{-11}
$\mathcal{J}(p^*)$	1.6996×10^{-5}	1.6996×10^{-5}
N_{Iter}	8	4

$$\dot{x}_{c2}(t) = -k_1 \bar{x}_1 \bar{x}_2 - k_4 \bar{x}_2 \bar{x}_4 - k_6 \bar{x}_3 \bar{x}_2, \quad (6.50)$$

$$\begin{aligned} \dot{x}_{c3}(t) = & k_1 \bar{x}_1 \bar{x}_2 - k_2 \bar{x}_1 \bar{x}_3 - k_3 \bar{x}_3 \bar{x}_4 - 2k_5 \bar{x}_3^2 \\ & - k_6 \bar{x}_3 \bar{x}_2, \end{aligned} \quad (6.51)$$

$$\dot{x}_{c4}(t) = k_2 \bar{x}_1 \bar{x}_3 - k_3 \bar{x}_3 \bar{x}_4 - k_4 \bar{x}_2 \bar{x}_4, \quad (6.52)$$

$$\dot{x}_{c5}(t) = k_3 \bar{x}_3 \bar{x}_4 + k_8 \bar{x}_1 \bar{x}_6, \quad (6.53)$$

$$\dot{x}_{c6}(t) = k_4 \bar{x}_2 \bar{x}_4 + k_5 \bar{x}_3^2 + k_7 \bar{x}_1 \bar{x}_7 - k_8 \bar{x}_1 \bar{x}_6, \quad (6.54)$$

$$\dot{x}_{c7}(t) = k_6 \bar{x}_3 \bar{x}_2 - k_7 \bar{x}_1 \bar{x}_7, \quad (6.55)$$

$$0 \leq k_1, k_2, \dots, k_8 \leq 1, \quad (6.56)$$

$$0 \leq x_{c1}, \dots, x_{c7}, \quad (6.57)$$

is solved first. The obtained solution $p_{CVX}^* = [112.6, 30.4, 125.6, 0, 42.4, 33.7, 30.5, 49.9]^T \times 10^{-3}$ is used to initialize the SGN algorithm, leading to the same optimal value previously presented. Table 6.4 summarizes some of the algorithm parameters along with the parameter optimization results for this case study.

Figure 6.8 illustrates the evolution of the iterations for the methods with arbitrary initialization and the proposed approach. The state evolution of the intermediate compounds is not presented for clarity in the visualization. Note also that while convergence is achieved after the fourth iteration when the problem is arbitrarily initialized, the SGN with the proposed convex initialization method already attains convergence after the first iteration. Consequently, the advantage of the presented methodology lies not only in improving the convergence speed but in the fact that no arbitrary initialization is performed and the initial value is calculated by solving

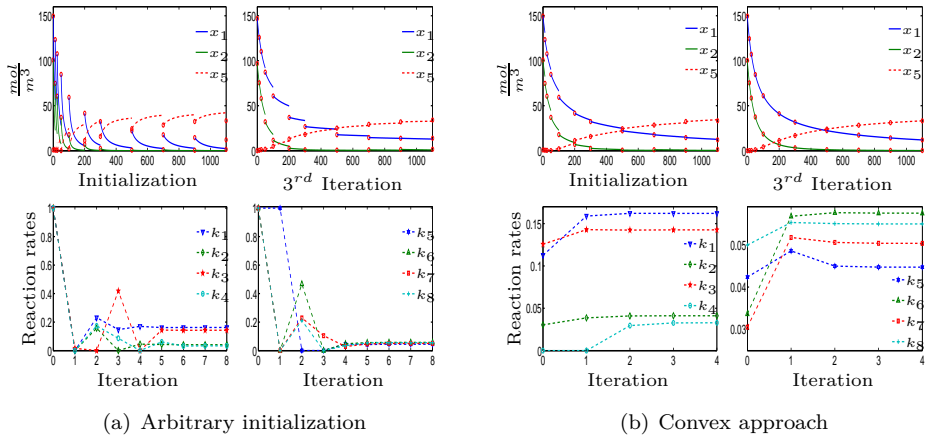


Figure 6.8: Convergence results using the simultaneous Gauss-Newton algorithm for the PEP of the reaction rates in the reaction of formaldehyde with sodium p-phenol sulfonate. The figure illustrates the time evolution for the state trajectory using an arbitrary initialization (a) and the convex approach (b) along with the parameters convergence.

a related convex problem.

6.4 Conclusions

In this chapter a suboptimal solution to the PEP with parameter affine dynamic models has been proposed. The method relies on the convex approximation to the PEP by considering full state measurements and further linearization of the original nonconvex PEP around the convex PEP solution. It has been proven that the loss of optimality in the suboptimal solution is of second order in the size of perturbations in the state trajectory from data perfectly reproduced by the model, i.e., a solution to the NL-PEP with zero cost. Moreover, the proposed approach implies only the solution of two convex problems, improving the computational requirements w.r.t. a fully converged SQP method.

Additionally, the application of the approach with more advanced optimization techniques has been presented. The method is used in order to provide an initial guess for the parameters in a SGN algorithm coupled with a DE solver with sensitivity capabilities. Three benchmark examples have been studied, illustrating that the method reduces the number of iteration required to converge to a solution when compared with an arbitrary initialization. The advantages of the method not

only lie in improving convergence properties but also in the fact that no previous knowledge of an initial guess for the parameter vector is required, allowing an automatic initialization by solving a convex PEP.

One of the limitations of the method is the applicability to a reduced set of dynamic models, namely parameter affine, or models which can be reformulated in that form, e.g.,

$$\dot{x}(t) = \Gamma(x) + \Upsilon(x)M(p), \quad (6.58)$$

where $M(p)$ is a diffeomorphism. An extension of the method in its current form to a more general class of systems, where the dynamic is not affine in the parameters, is not viable. Note that in that case, although state measurements might be available for performing the convex approximation, the resulting equality constraint imposed by the model is not affine in the parameters to estimate. Hence, the PEP is still nonconvex, and the same initialization requirements as in the original NLP problem would be necessary to obtain a solution.

Chapter 7

General conclusions and future work

7.1 Concluding remarks

Along this dissertation, the problem of exploiting structure for simulation purposes and convexity, in dynamic optimization, for a particular class of chemical processes has been treated. Emphasis is put on a class of dynamic models which appear often in chemical industry, namely, input/parameter-affine models. Dynamic optimization problems dealing with these kinds of models are normally considered as nonconvex optimization problems. However, in this document, it has been shown that it is possible to find convex approximations to these problems by using available references/measurements of the process to be controlled/estimated. Moreover, the efficiency of the optimization routines can be improved if the structure of model with respect to the optimization variables is exploited, particularly when hundreds of optimization variables are involved. Distillation has been chosen in this document showing that this popular chemical process, as many stagewise chemical applications, is highly structured. Detecting this structure in advance facilitates not only simulation but optimization tasks as well and leads to more efficient online computation for control and estimation problems.

In the first part of the dissertation a distillation models are introduced. With respect to this part, the following conclusions are presented:

- An existing distillation model based on vapor-liquid equilibrium is reformulated so that the thermodynamic correlations used for calculation of the mixture properties can be easily referenced to the existing literature. This

allows for adaptability of the model for the separation of different binary mixtures. Moreover, it is shown that simplifying model equations may lead to destroy the banded patterns in the model Jacobian. Consequently, the model is formulated such that sparsity can be exploited at the simulation level, in order to alleviate the use of a considerable number of states in the description.

- A rate based model for separation in packed columns is proposed. This model accounts for mass transfer on each stage and it is able to describe the vapor-liquid interaction along the column without the use of artificial concepts such as the stage efficiency. However, it leads to a considerable increase of the number of variables required for process simulation. It is illustrated that it is possible to perform a model reduction on the basis of constraint differentiation and algebraic manipulation. Nevertheless, even with a reduced model, the distillation process generally leads to higher index differential-algebraic equations (DAEs) which make them impossible to simulate with off-the-shelf-solvers. For this particular formulation, the index problem can be associated to structural singularities and solved by neglecting the dynamics of the vapor holdup on each stage as it is detailed in Chapter 4. In general, it is shown that structural singularities, hence, the index problem, appear if there is no correlation between pressure drops or mass transfer coefficients in a stage with flows coming in and out in the same stage.
- Model structure can be also exploited by looking how the variables interact in the model formulation. In this dissertation, rigorous distillation models have been studied. It has been shown that by a simple reorganization of variables and equations a sparse and banded structure in the model Jacobian is obtained. Despite the large number of model states involved in this kind of formulation, it is illustrated numerically that providing this structure to a numerical solver reduces the computational requirements for simulation. These sparse and banded structures can be exploited in parameterized dynamic optimization problems (DOPs) when the states are not eliminated from the optimization task.
- It is concluded that for the estimation problems involving the models presented in Chapters 3 and 4 the search space for the parameters can be reduced since, due to the limited set of measurements, only a subset of the total model parameters can be estimated. This allows for minimizing efforts in the estimation task. These results can be the bases of a more detailed analysis on instrumentation required to estimate particular parameters.

With respect to the convex exploitation in DOPs, the following conclusions are presented:

- An homotopy method to approximate a nonconvex dynamic optimization problem with a convex DOP has been proposed. It has been proven in Chapter 5 that the proposed parametric DOP leads to the original optimal control problem (OCP) in one extreme and to the convex OCP in the other extreme. For particular examples, simple continuation methods lead to the solution of the original OCP and the method can be used to improve convergence in a OCP formulation.
- Despite the uncertainty for the continuity of the zero path in the homotopy method presented in Chapter 5, it has been shown in Chapter 6 that the convex extreme of the DOP can be exploited for initialization tasks in simultaneous optimization, where it improves convergence with respect to an arbitrary initialization. Moreover, the convex initialization delivers a solution that can be refined by simple linearization. It has been proven that the loss of optimality for this 2-step approach is of second order in the size of the modeling and measurement errors in the parameter estimation problem (PEP).

The sparse formulation of the rigorous dynamic rate based model presented in this thesis can be used for prediction and adapted to model more advanced separation process, such as reactive adsorption where separation is performed far from equilibrium (Kenig and Seferlis, 2009). Concerning the applicability of the methods developed in the second part of the thesis, despite the fact that they require estimation of the full state vector, there are processes where this requirement can be achieved. However, these processes lie mainly in mechanical and electrical fields where acceleration, velocity and position or voltage and currents can be easily measured.

7.2 Future work

In the following paragraphs some possible directions for future research are proposed:

Simulation of high index rate based models In order to provide a model that can be simulated with off-the-shelf solver, the vapor holdup dynamics of the system have been neglected. This is clearly explained in Chapter 4 and justified using the structural singularity analysis of an incidence matrix. However, there are methods that attempt to solve the system by detecting the constraints that need to be differentiated (Pantelides, 1988) and adding additional variables and constraints to the DAE (Mattsson and Söderlind, 1993). These methods provide an augmented DAE with index-1. The advantage of having an index 1 RBM

without neglecting vapor holdup, is its applicability for modeling columns where pressure dynamics plays an important role. Pressure has a high impact on the quality of the separation when using temperatures as an indication of composition (Sloley, 2001). This condition is specially noticed in low pressure columns.

Efficient parameter estimation using dynamic RBMs In Bonilla et al. (2011) the steady state PEP of a RBM for the CIT distillation column is proposed using multiple experiments. There, a sparse formulation is used by stacking constraints related to each test and keeping model states as optimization variables for all the experiment scenarios. This leads to a problem with 1940 variables for a 20-stages RBM. A future direction to explore is to address the dynamic PEP using the direct multiple shooting (DMS) parameterization for the multiple experiment case. This leads to a large scale PEP where the sparsity patterns of the RBM Jacobian need to be exploited using sparse QP solvers. Moreover, the initialization method explained in Section 4.3.1 can be used to provide a guess for the model states in the NLP. Note that the sensitivity analysis for the RBM in Section 4.5.4 yields that most of the identifiable parameters are affine in the model, e.g., heat losses. The proposed method in Chapter 6 can be used along with the initialization in Section 4.3.1 to obtain a convex PEP which provides an initial guess for the parameters which are affine in the model equations, reducing the arbitrary initialization to those parameters who cannot be estimated by the method. In this case improvements in the convergence are expected as presented in the numerical examples shown in Chapter 6.

Continuity of the zero path for the homotopy method. As mentioned in Chapter 5, the homotopy method still lacks clear conditions on the nature of the functions involved in the DOP in order to guarantee continuity and finite length of the zero path. A possible research direction would be to characterize the constraints $h(x, u)$ and the nature of $f(x)$ and $g(x)$ in the model $\dot{x}(t) = f(x) + g(x)u(t)$ such that singularities of the KKT system for the parametric DOP in (5.7)-(5.11) are avoided along the zero path. As explained in Chapter 5, if this is guaranteed and the path has a finite arc length, it is possible to use well developed methods (Watson et al., 1987) to track the path of minimizers from the convex problem to the original DOP.

Feedback linearization for convex formulation of DOP. Along this dissertation a particular class of dynamic model has been assumed, namely input/parameter affine models. The nonconvexity has its origin in the structure of these models, since cost and constraint have been assumed convex. A classical approach to deal with the control of input affine models is *feedback linearization* (Isidori, 1989). Although it is not included in the present dissertation, it was explored in the

beginning of this research as a possible alternative to convexification of input-affine dynamic models. In this kind of method states and inputs $(x(t), u(t))$ are mapped to a different space $(z(t), v(t))$ through a nonsingular transformation $\Phi(x)$, the advantage is that the dynamic system becomes linear in the new space of variables, the disadvantage is that constraint and cost have to be mapped as well, possibly translating the nonconvexity to constraints and cost and leading to a problem of the form

$$\begin{aligned} \text{OCP} : \min_{z(\cdot), v(\cdot)} \int_0^T \|\Phi^{-1}(z(t)) - \Phi^{-1}(z^{\text{ref}}(t))\|_Q^2 dt \\ + \|\Phi^{-1}(z(T)) - \Phi^{-1}(z^{\text{ref}}(T))\|_{Q_T}^2, \end{aligned} \quad (7.1)$$

subject to

$$\dot{z}(t) = Az(t) + Bv(t), \quad t \in [0, T], \quad (7.2)$$

$$z(0) = T(x_0), \quad (7.3)$$

$$h^z(z(t), x(t)) \geq 0, \quad t \in [0, T], \quad (7.4)$$

$$r^z(z(T)) \geq 0, \quad (7.5)$$

where the inequality constraints functions $h^z(z(t), x(t))$ and $r^z(z(T))$ are obtained by mapping the original constraint in x , u into the space of z , v , using the mentioned transformation.

It is clear that introducing a nonlinear transformation $\Phi(x)$ affects the convexity of the constraints and cost, i.e., even for simple bound constraints and quadratic cost, the DOP in the new space (z, v) leads to nonlinear constraints, possibly nonconvex. Following this direction, the research question arise:

- Are there nonsingular transformations $\Phi(x)$ such that the nonlinear input affine system is transformed into a linear one and the constraint and cost in the space of z , v remain convex?. The kind of nonlinearities handled in $f(x)$ and $g(x)$ have to be well identified and reduced to specific cases. It is possible to analyze first the simple unconstrained case with quadratic cost, and gradually add complexity in the constraints of inputs and states.
- In the general case where the transformation $\Phi(x)$ leads to nonconvex inequality constraints and cost in the space of (z, v) , it is worth to solve the NLP in the space of (z, v) and not in the space of (x, u) ? Notice that now a linear model is obtained but the problem includes nonconvex constraints and cost.

- Is it possible to find convex relaxations to the nonconvex inequality constraints such that a sequential convex programming method can be used to solve the nonconvex problem in the space of (z, v) ? Is it an advantage in the efficiency of the method with respect to solving the parameterized DOP in its original space (x, u) with the nonlinear model?

Appendix A

Correlations for calculation of thermodynamic properties

The purpose of the current appendix is to provide the necessary correlations to calculate the physical properties of a binary mixture. All the correlations used have been properly referenced to the literature such that the sources can be easily located and the correlation coefficients can be modified when dealing with different mixtures.

A.1 Correlations for binary mixtures

The physical properties of the components are presented here in alphabetical order. The index i corresponds to the component ($i = 1$, for methanol and $i = 2$ for isopropanol). The stage subindex, j , has been omitted for simplicity in the notation but it is clear that the correlations apply for each of the one stages considered in the model.

A.1.1 Activity Coefficients

The activity coefficients γ_i for the binary mixture are calculated using the Wilson model (Wilson, 1964):

$$\ln(\gamma_1) = -\ln(x_1 + \Lambda_{12}x_2) + \quad (\text{A.1})$$

$$x_2 \left(\frac{\Lambda_{12}}{x_1 + \Lambda_{12}x_2} - \frac{\Lambda_{21}}{x_2 + \Lambda_{21}x_1} \right),$$

$$\ln(\gamma_2) = -\ln(x_2 + \Lambda_{12}x_1) - \quad (\text{A.2})$$

$$x_1 \left(\frac{\Lambda_{12}}{x_j + \Lambda_{12}x_2} - \frac{\Lambda_{21}}{x_2 + \Lambda_{21}x_1} \right).$$

In general, the binary interaction parameters Λ , are function of the mixture temperature. However, here they are assumed constant with the temperature and calculated from the activity coefficients at infinite dilution as presented in Gmehling and Onken (1977), i.e., for methanol and isopropanol, $\gamma_1^\infty = 1.22$, $\gamma_2^\infty = 1.37$, respectively, and Λ_1 and Λ_2 must satisfy

$$\ln(\gamma_1^\infty) = 1 - \ln(\Lambda_{12}) - \Lambda_{21}, \quad (\text{A.3})$$

$$\ln(\gamma_2^\infty) = 1 - \ln(\Lambda_{21}) - \Lambda_{12}, \quad (\text{A.4})$$

as proposed in Seader and Henley (2006). This procedure leads to $\Lambda_{12} = 1.2914$ and $\Lambda_{21} = 0.5454$, for a mixture of methanol and isopropanol.

A.1.2 Density of the mixture

The mass and molar densities of the mixture for the liquid and vapor phases at each stage are calculated based on the total molar volume of the bulk phase v_t provided in section A.1.15, i.e.,

$$\rho_t^V = M^V c_t^V \quad (\text{kg/m}^3), \quad (\text{A.5})$$

$$\rho_t^L = M^L c_t^L \quad (\text{kg/m}^3), \quad (\text{A.6})$$

and,

$$c_t^V = \frac{1}{v_t^V} \quad (\text{mol/m}^3), \quad (\text{A.7})$$

$$c_t^L = \frac{1}{v_t^L} \quad (\text{mol/m}^3), \quad (\text{A.8})$$

A.1.3 Diffusion coefficients

The vapor phase binary diffusion coefficient is calculated as proposed in Seader and Henley (2006) using the Fuller, Schettler and Giddings correlation¹

$$D^V = 0.00143 \times 10^{-4} \frac{TV^{1.75}}{M_{ab}PV_{ab}} \quad (\text{m}^2/\text{s}) \quad (\text{A.9})$$

where V_{ab} is determined from the atomic volumes of elements in the components (Seader and Henley, 2006), i.e.,

$$V_{ab} = (V_a^{\frac{1}{3}} + V_b^{\frac{1}{3}})^2 \quad (\text{m}^2) \quad (\text{A.10})$$

$$V_a(\text{CH}_4\text{O}) = 15.9 + 4 \times 2.31 + 6.11, \quad (\text{A.11})$$

$$V_b(\text{C}_3\text{H}_8\text{O}) = 3 \times 15.9 + 8 \times 2.31 + 6.11 \quad (\text{A.12})$$

$$M_{ab} = \sqrt{\frac{2}{\frac{1}{M_1} + \frac{1}{M_2}}} \quad (\text{kg/kmol}) \quad (\text{A.13})$$

with the pressure and temperature given in atmospheres and Kelvin, respectively.

The binary liquid diffusion coefficient ($D_{AB} = D_{BA}$) is calculated using the Wilke-Chang technique (A.14) and the Vignes relation (A.15) for infinite dilution (Reid et al., 1987) with $\phi_i = 1.9$ $i = 1, 2$. The pure component liquid viscosity is obtained from (A.77) and transformed to centipoises cP to be used in (A.15).

$$D_j^L = D_{1,2}^L{}^{x_2} D_{2,1}^L{}^{x_1}, \quad (\text{A.14})$$

$$D_{a,b}^L = 7.4 \times 10^{-12} \frac{(\phi_a M_a)^{\frac{1}{2}} T^L}{\eta_a^L v_b^{0.6}}. \quad (\text{m}^2/\text{s}) \quad (\text{A.15})$$

M_a is the molecular weight of solvent a in kg/kmol. Molar volumes for pure components v_i are given by (A.66) and calculated at normal boiling temperature T_{b_i} for the component i as illustrated in Table A.1.

¹Reid et al. (1987) provides an alternative formulation using a collision integral for diffusion, however, that formulation is more involved.

A.1.4 Enthalpies of the bulk phase

In order to calculate heat balances, enthalpies of the mixture for vapor and liquid phases are required. The enthalpy for the vapor phase is calculated as an averaged quantity from the vapor enthalpy of the pure species (Seader and Henley, 2006):

$$H^V = y_1 H_{p_1}^V + y_2 H_{p_2}^V \quad (\text{kJ/mol}), \quad (\text{A.16})$$

where the pure component enthalpies $H_{p_i}^V$ are obtained as functions of the ideal-gas species molar enthalpy $H_{0,i}^V$ and the heat of formation ΔH_i^f , i.e.,

$$H_{p_i}^V = \Delta H_i^f + H_{0,i}^V \quad (\text{A.17})$$

The ideal-gas molar enthalpy of the pure species i is obtained by integrating the vapor molar heat capacity C_P^V with respect to the vapor temperature:

$$\begin{aligned} H_{0,i}^V = & A_i(T^V - T_0) + \frac{1}{2}B_i(T^{V^2} - T_0^2) + \\ & \frac{1}{3}C_i(T^{V^3} - T_0^3) + \frac{1}{4}D_i(T^{V^4} - T_0^4), \quad (\text{kJ/mol}) \end{aligned} \quad (\text{A.18})$$

with the coefficients used to calculate the molar vapor heat capacity as shown in Tables A.2 and A.3 and $\Delta H_1^f = -200.67$ kJ/mol, $\Delta H_2^f = -272.42$ kJ/mol and $T_0 = 298.15$ K.

On the other hand, the liquid phase enthalpy is calculated as a function of the pure component enthalpies and the heat of mixing ΔH^{mix} (Sandler, 1999):

$$H^L = x_1 H_{p_1}^L + x_2 H_{p_2}^L + \Delta H^{\text{mix}}, \quad (\text{kJ/mol}) \quad (\text{A.19})$$

where the pure component liquid enthalpies H_i^L are given as a function of pure component enthalpies for the vapor phase and the heat of vaporization:

$$H_{p_i}^L = H_{p_i}^V - \Delta H_i^{\text{vap}}. \quad (\text{A.20})$$

Simplified models often require expressions which involve the changes of enthalpy with respect to composition and temperature. Those expressions are presented here.

$$\frac{\partial H^V}{\partial T^V} = C_{P_m}^V \quad (\text{kJ}/(\text{mol.K})), \quad (\text{A.21})$$

$$\frac{\partial H^V}{\partial y} = H_{p_1}^V - H_{p_2}^V \quad (\text{kJ/mol}). \quad (\text{A.22})$$

Changes in liquid enthalpy with respect to liquid temperature and composition are given by

$$\frac{\partial H^L}{\partial T^L} = x \left(C_{P,1}^V - \frac{\partial \Delta H_1^{\text{vap}}}{\partial T^L} \right) + (1-x) \left(C_{P,2}^V - \frac{\partial \Delta H_2^{\text{vap}}}{\partial T^L} \right) \quad (\text{kJ}/(\text{mol.K})), \quad (\text{A.23})$$

$$\frac{\partial H^L}{\partial x} = H_{p_1}^L - H_{p_2}^L + \frac{\partial \Delta H^{\text{mix}}}{\partial x} \quad (\text{kJ/mol}), \quad (\text{A.24})$$

respectively.

A.1.5 Heat of mixing

The heat of mixing ΔH^{mix} is calculated from correlations for the particular mixture of methanol-isopropanol as proposed in Christensen (1982):

$$\Delta H^{\text{mix}} = \frac{x_1(1-x_1)(-302.6 - 126(1-2x_1) - 8(1-2x_1)^2)}{1 \times 10^3} \quad (\text{kJ/mol}) \quad (\text{A.25})$$

with

$$\frac{\partial \Delta H^{\text{mix}}}{\partial x_1} = \frac{128x_1^3 - 948x_1^2 + 1441.2x_1 - 436.6}{1 \times 10^3} \quad (\text{A.26})$$

A.1.6 Fractional Liquid Holdup

Two correlations have been considered for the calculation of the fractional liquid holdup in the packing. On the one hand, Bravo et al. (1986) propose a simple correlation, as a function of the *Froude number* Fr , i.e.,

$$h_t^L = C_h Fr^{0.5}. \quad (\text{A.27})$$

This correlation can be tuned to experimental data using the parameter C_h . Equation (A.27) is valid below the loading point where the liquid holdup does

not depend on the gas velocity. The dimensionless Froude number is determined from the liquid speed u^L and the equivalent diameter of the packing channel² d_{eq} .

$$Fr = \frac{u^L{}^2}{d_{eq}g} \quad (\text{A.28})$$

On the other hand, Billet and Schultes (1993) propose the correlation

$$h_t^L = 12 \left(\frac{Fr^L}{Re^L} \right)^{1/3} \left(\frac{a_h}{a} C_h Fr^L{}^{0.1} \right)^{\frac{2}{3}}, \quad (\text{A.29})$$

with

$$\frac{a_h}{a} = Re^L{}^{0.15} \quad \text{if } Re^L < 5, \quad (\text{A.30})$$

$$\frac{a_h}{a} = 0.85 Re^L{}^{0.25} \quad \text{if } Re^L \geq 5, \quad (\text{A.31})$$

and the *Reynolds number*

$$Re^L = \frac{u^L \rho^L}{a_p \eta^L}, \quad (\text{A.32})$$

to predict liquid holdup in structured packing. This correlation is used in Bonilla et al. (2011) for the parameter estimation in a steady state rate based model with C_h obtained from experimental data.

Although this correlation is tested on more than fifty kind of packings by Billet and Schultes (1993), it is considered too complex for the set of equations already formulated in this model. Hence, the simpler approach based on the work of Bravo et al. (1986) is considered for the development of the dynamic model. Nevertheless, (A.29) can be used instead of (A.27) if desired, with the proper changes in pressure drops and the calculation of the mass transfer coefficients.

The relation used in (A.27) agrees with the equation used to determine the pressure drop proposed by the same author.

²Bravo et al. (1986) assumes $d_{eq} = S$, with S given in Table A.3

A.1.7 Heat Capacities

Vapor and liquid³ heat capacities of the mixture are mole-fraction averaged and calculated from pure component heat capacities (Perry and Green, 1985):

$$C_{Pm}^V = y_1 C_{P,1}^V + (1 - y_1) C_{P,2}^V \quad \text{kJ}/(\text{mol.K}), \quad (\text{A.33})$$

$$C_{Pm}^L = x_1 C_{P,1}^L + (1 - x_1) C_{P,2}^L \quad \text{kJ}/(\text{mol.K}). \quad (\text{A.34})$$

Expressions for liquid and vapor heat capacities of pure components are obtained from Daubert and Danner (1989) and Sandler (1999), respectively. The values are given by the polynomial

$$C_{P,i}^p = A_i + B_i T^p + C_i T^{p^2} + D_i T^{p^3}, \quad (\text{A.35})$$

with $p = V, L$. The polynomial coefficients for methanol, $i = 1$ and isopropanol $i = 2$ for the liquid and vapor phases are presented in Tables A.2 and A.3.

Specific heat capacities for the bulk phase can be calculated from the molar mass of the mixture, M^p , (A.55):

$$C_P^p = \frac{C_{Pm}^p}{M^p} \quad \text{with } p = V, L \quad (\text{kJ}/\text{kg.K}) \quad (\text{A.36})$$

A.1.8 Heat Losses

Heat losses are assumed functions of the bulk phase temperature at the stage and the temperature of the surroundings i.e.,

$$Q^L = \psi_{QL} (T_j^L - T_{\text{amb}}) \quad (\text{kW}) \quad (\text{A.37})$$

$$Q^V = \psi_{QV} (T_j^V - T_{\text{amb}}) \quad (\text{kW}) \quad (\text{A.38})$$

and tuned experimentally using heat loss coefficients ψ_{QL} and ψ_{QV} in (kW/K) .

³The procedure neglects heat of mixing effects for the liquid heat capacity calculation.

A.1.9 Heat of vaporization

The heat of vaporization for pure components ΔH_i^{vap} is calculated using the correlation

$$\Delta H_i^{\text{vap}} = A_i \left(1 - \frac{T^L}{T_{c_i}} \right)^{\left(B_i + C_i \frac{T^L}{T_{c_i}} \right)} \quad (\text{kJ/mol}) \quad (\text{A.39})$$

presented in Daubert and Danner (1989). The changes of ΔH^{vap} with respect to temperature are given by

$$\frac{\partial \Delta H_i^{\text{vap}}}{\partial T^L} = \Delta H_i^{\text{vap}} \frac{B_i T_{c_i} + C_i \left(T^L + \log \left(\frac{T_{c_i} - T^L}{T_{c_i}} \right) (T^L - T_{c_i}) \right)}{T_{c_i} (T^L - T_{c_i})}. \quad (\text{A.40})$$

A.1.10 Heat transfer coefficients

Heat transfer coefficients h^V and h^L are calculated using the Chilton-Colburn analogy between heat and mass transfer (Seader and Henley, 2006):

$$h^V = k^V c_t^V C_P^V \left(\frac{Sc^V}{Pr^V} \right)^{\frac{2}{3}} \quad (\text{A.41})$$

$$h^L = k^L c_t^L C_P^L \left(\frac{Sc^L}{Pr^L} \right)^{\frac{1}{2}} \quad (\text{A.42})$$

where the Schmidt and the Prandtl numbers are function of the bulk phase viscosity η , density ρ and conductivity λ among others.

$$Sc^p = \frac{\eta^p}{\rho^p D^p} \quad p = L, V, \quad (\text{A.43})$$

$$Pr^p = \frac{C_P^p \eta^p}{\lambda^p} \quad p = L, V. \quad (\text{A.44})$$

A.1.11 K -values

The K -values are calculated using the *Modified Raoult's Law* (Seader and Henley, 2006):

$$K_i = \gamma_i \frac{P_i^s}{P}, \quad (\text{A.45})$$

where γ_i and P_i^s represent the activity coefficients and the vapor pressure for the species i .

A.1.12 Mass transfer coefficients

The correlations proposed by Bravo and Fair (1982) for structured packings are used here to calculate the mass transfer coefficients in the liquid and vapor phases. The mass transfer coefficient for the vapor phase is defined as

$$k^V = \frac{Sr^V D^V}{d_{\text{eq}}}, \quad (\text{m/s}). \quad (\text{A.46})$$

The equivalent diameter of the packing channel d_{eq} is given by

$$d_{\text{eq}} = Bh_c \left(\frac{1}{B + 2S} + \frac{1}{2S} \right) \quad (\text{m}) \quad (\text{A.47})$$

where B , h_c and S are packing-dependent channel parameters shown in Table A.3 for the particular type of packing.

The liquid mass transfer coefficient is calculated using a *penetration model* (Taylor and Krishna, 1993), based on the correlations proposed by Bravo and Fair (1982),

$$k^L = 2 \left(\frac{D^L u_e^L}{\pi S} \right)^{\frac{1}{2}} \quad (\text{m/s}). \quad (\text{A.48})$$

The Sherwood number, Sr , is calculated according to the Johnstone and Pigford (1942) correlation

$$Sr^V = 0.0338 Re^V{}^{0.8} Sc^V{}^{0.333}. \quad (\text{A.49})$$

The vapor phase Reynolds number

$$Re^V = \frac{\rho^V (u_e^L + u_e^V) d_{\text{eq}}}{\eta^V}, \quad (\text{A.50})$$

is defined as a function of the effective velocities for the vapor and liquid phases u_e^V and u_e^L , respectively by

$$u_e^V = \frac{u^V}{\epsilon \sin \theta} \quad (\text{m/s}). \quad (\text{A.51})$$

$$u_e^L = \frac{3\Gamma}{2\rho^L} \left(\frac{(\rho^L)^2 g}{3\eta^L \Gamma} \right)^{\frac{1}{3}} \quad (\text{m/s}). \quad (\text{A.52})$$

where Γ is the liquid flow rate per unit length of packing perimeter

$$\Gamma = \frac{\rho^L u^L}{P_\phi} \quad (\text{kg/s.m}). \quad (\text{A.53})$$

and the packing perimeter P_ϕ is determined as in Taylor and Krishna (1993)

$$P_\phi = \frac{4S + B}{Bh} \quad (\text{m/m}^2), \quad (\text{A.54})$$

A.1.13 Molar Mass

The molar mass of bulk phases is calculated as a composition average of molar masses for pure components

$$M^V = y_1 M_1 + y_2 M_2 \quad (\text{kg/mol}), \quad (\text{A.55})$$

$$M^L = x_1 M_1 + x_2 M_2 \quad (\text{kg/mol}) \quad (\text{A.56})$$

$$(\text{A.57})$$

A.1.14 Partial Molar Enthalpies

In order to calculate the energy flows \mathcal{E} , the changes of enthalpy with respect to composition in the liquid and vapor phases $\bar{H}^L = \partial H^L / \partial x$, $\bar{H}^V = \partial H^V / \partial y$ are required. The partial molar quantities are, in general, not equal to the pure molar quantities (Sandler, 1999). Hence, for the liquid phase, partial molar properties are calculated as:

$$\bar{H}_1^L = H_{p_1}^L + \Delta H^{\text{mix}} - x_2 \frac{\partial \Delta H^{\text{mix}}}{\partial x_2} \quad (\text{kJ/mol}) \quad (\text{A.58})$$

$$\bar{H}_2^L = H_{p_2}^L + \Delta H^{\text{mix}} - x_1 \frac{\partial \Delta H^{\text{mix}}}{\partial x_1} \quad (\text{kJ/mol}) \quad (\text{A.59})$$

with,

$$\frac{\partial \Delta H^{\text{mix}}}{\partial x_1} = \frac{x_2(8(2x_1 - 1)^2 - 252x_1 + \frac{2143}{5})}{1000}$$

$$-\frac{x_1 x_2 (64x_1 - 284)}{1000} \quad (\text{kJ/mol}) \quad (\text{A.60})$$

$$\frac{\partial \Delta H^{\text{mix}}}{\partial x_2} = \frac{x_1 (8(2x_1 - 1)^2 - 252x_1 + \frac{2143}{5})}{1000}. \quad (\text{A.61})$$

On the other hand, the calculation of the partial molar property for the vapor phase, leads to:

$$\bar{H}_1^V = H_{p_1}^V \quad (\text{kJ/mol}), \quad (\text{A.62})$$

$$\bar{H}_2^V = H_{p_2}^V. \quad (\text{A.63})$$

A.1.15 Molar Volumes

The molar volume for the vapor phase is calculated as proposed in Taylor and Krishna (1993)

$$v_t^V = \frac{RT^V}{P} \quad (\text{m}^3/\text{mol}), \quad (\text{A.64})$$

with $R = 8.314472 \text{ J}/(\text{mol}\cdot\text{K})$. On the other hand, liquid molar volumes are calculated as averaged values using pure component quantities as proposed in Daubert and Danner (1989):

$$v_t^L = x_1 v_1^L + x_2 v_2^L \quad (\text{m}^3/\text{mol}) \quad (\text{A.65})$$

with

$$v_i^L = \frac{B_i^{1+(1-\frac{T^L}{C_i})^{D_i}}}{A_i}, \quad i = 1, 2. \quad (\text{m}^3/\text{mol}) \quad (\text{A.66})$$

Changes in molar volume with respect to temperature and composition are given by

$$\frac{\partial v_t^L}{\partial T} = x \frac{\partial v_1^L}{\partial T^L} + (1-x) \frac{\partial v_2^L}{\partial T^L} \quad (\text{m}^3/(\text{mol}\cdot\text{K})), \quad (\text{A.67})$$

$$\frac{\partial v_t^L}{\partial x} = v_1^L - v_2^L \quad (\text{m}^3/\text{mol}), \quad (\text{A.68})$$

respectively, with

$$\frac{\partial v_i^L}{\partial T^L} = - \frac{D_i \log(B_i) \left(1 - \frac{T^L}{C_i}\right)^{D_i-1} B_i \left(\left(1 - \frac{T^L}{C_i}\right)^{D_i+1}\right)}{A_i C_i}. \quad (\text{A.69})$$

A.1.16 Pressure Drop

There are several approaches to calculate the pressure drop in structural packing. Among the most used are the ones by Bravo et al. (1986) and Billet and Schultes (1999). Due to the simplicity in the equations, the former is used in the current formulation, i.e.,

$$\Delta P = \left(0.171 + \frac{92.7}{Re^V}\right) \left(\frac{\rho^V u_e^{V^2}}{d_{eq}}\right) \left(\frac{1}{1 - C_3 \sqrt{Fr}}\right)^5 \quad (\text{Pa}), \quad (\text{A.70})$$

with⁴ $d_{eq} = S$ and $C_3 = 3.38$. The equation is expected to be valid below the loading point. The Froude and Reynolds numbers are calculated as in (A.28) and (A.50), respectively. This pressure drop formulation matches the formulae proposed by the same author for the mass transfer coefficients and the fractional liquid holdup.

A.1.17 Vapor pressures

Vapor pressures are required for the calculation of K -values. They are obtained from an extended Antoine equation as presented in Daubert and Danner (1989):

$$P_i^s = \exp\left(A_i + \frac{B_i}{TV} + C_i \ln(TV) + D_i T^{V E_i}\right), \quad (\text{Pa}) \quad (\text{A.71})$$

and their derivatives with respect to temperature are calculated as:

$$\frac{\partial P_i^s}{\partial T^V} = \left(-\frac{B_i}{T^V{}^2} + \frac{C_i}{T^V} + \frac{D_i T^{V E_i} E_i}{T^V}\right) P_i^s, \quad (\text{Pa/K}) \quad (\text{A.72})$$

⁴The value for C_3 corresponds to Sulzer BX packing

A.1.18 Viscosity

The viscosity of the vapor phase at low pressure is determined using an approximation obtained from Chapman-Enskog kinetic theory (Reid et al., 1987)

$$\eta_t^V = \frac{y_1 \eta_1^V}{y_1 + y_2 \phi_{12}} + \frac{y_2 \eta_2^V}{y_2 + y_1 \phi_{21}}. \quad (\text{A.73})$$

In order to reduce the complexity of the expression (A.73), ϕ_{ij} is calculated using the Hering and Zipperer approximation (Reid et al., 1987),

$$\phi_{12} = \left(\frac{M_2}{M_1} \right)^{\frac{1}{2}} = \frac{1}{\phi_{21}}. \quad (\text{A.74})$$

The pure component viscosities for the vapor phase are calculated as proposed in Daubert and Danner (1989)

$$\eta_i^V = \left(\frac{A_i T^{V B_i}}{1 + \frac{C_i}{T^V}} \right), \quad i = 1, 2. \quad (\text{Pa.s}). \quad (\text{A.75})$$

The viscosity of the liquid phase is obtained by applying the mixing rule proposed in (Reid et al., 1987)

$$n^L = n_1^{L x_1} n_2^{L x_2} \quad (\text{Pa.s}), \quad (\text{A.76})$$

where the pure component liquid viscosity is calculated using the correlations proposed in Daubert and Danner (1989)

$$\eta_i^L = \exp \left(A_i + \frac{B_i}{T^L} + C_i \ln(T^L) \right), \quad i = 1, 2. \quad (\text{A.77})$$

A.1.19 Velocities of liquid and vapor

Velocities for the liquid and vapor streams are calculated from molar flows V , L , the molar volume of the bulk phases and the cross section area of the column A_c , as presented in

$$u^V = \frac{Vv_t^V}{A_c} \quad (\text{m/s}) \quad (\text{A.78})$$

$$u^L = \frac{Lv_t^L}{A_c} \quad (\text{A.79})$$

A.1.20 Thermal conductivities

The thermal conductivity coefficients for the mixture in the vapor and liquid phases are calculated as in Taylor and Krishna (1993), i.e.,

$$\lambda^V = y_1\lambda_{p_1}^V + y_2\lambda_{p_2}^V, \quad (\text{kW}/(\text{m.K})) \quad (\text{A.80})$$

$$\lambda^L = x_1\lambda_{p_1}^L + x_2\lambda_{p_2}^L, \quad (\text{kW}/(\text{m.K})) \quad (\text{A.81})$$

where the pure component conductivities λ_{p_i} are given by the correlations proposed in Daubert and Danner (1989):

$$\lambda_{p_i}^V = \frac{A_i T^{V B_i}}{1 + \frac{C_i}{T^V} + \frac{D_i}{T^V{}^2}} \quad i = 1, 2 \quad (\text{kW}/(\text{m.K})) \quad (\text{A.82})$$

$$\lambda_{p_i}^L = A_i + B_i T^L + C_i T^{L^2} \quad i = 1, 2 \quad (\text{kW}/(\text{m.K})) \quad (\text{A.83})$$

Note that the coefficients for pure liquid and vapor conductivities have not the same values, they are given similar names for simplicity in the formulation, but are clearly differentiated in Tables A.2 and A.3.

A.2 Pure components properties and coefficients

Pure component properties such as molar mass, M_i , normal boiling point⁵ T_{b_i} and critical temperature T_{c_i} for the methanol, $i = 1$, and isopropanol, $i = 2$ are shown in Table A.1.

Correlation coefficients for all the thermodynamic properties of pure components introduced in Section A.1 are summarized in Tables A.2 and A.3. These coefficients

⁵Normal boiling points are, by definition, calculated at atmospheric pressure.

Table A.1: Component parameters for the binary mixture.

Component ^a	Formula	M_i (g/mol)	ρ_i (kg/m ³) ^b	T_{b_i} (K)	T_{c_i} (K)
methanol	CH ₄ O	32.042	0.07918	337.851	512.58
isopropanol	C ₃ H ₇ OH	60.096	0.0786	355.41	508.31

^a $i = 1$ for methanol and $i = 2$ for isopropanol

^bCalculated at ambient temperature $T = 25^\circ C$.

are obtained mainly from Daubert and Danner (1989), Reid et al. (1987) and Sandler (1999). Hence, those sources can be used as references when a different mixture is being analyzed.

A.3 Structural parameters for sulzer CY packing

The geometry parameters for the particular class of structured packing are obtained from Kister (1992) and Sulzer Chemtech technical data. These parameters describe the geometry of the channels on each packing section. Details of the description are presented in Bravo et al. (1986) and Taylor and Krishna (1993).

Table A.2: Pure component coefficients for different properties of methanol CH_4O , ($i = 1$)

Property	A_i	B_i	C_i	D_i	E_i	Equation
Liquid heat capacity	1.076×10^2	-3.8060×10^{-1}	9.79×10^{-4}			(A.35)
Vapor heat capacity	19.038×10^{-3}	9.146×10^{-5}	-1.218×10^{-8}	-8.034×10^{-12}		(A.35),(A.18)
Heat of vaporization	5.270×10^1	3.766×10^{-1}	0.0			(A.39)
Liquid molar volume	2.3080×10^3	2.7192×10^{-1}	5.1258×10^2	2.3310×10^{-1}		(A.66)
Vapor pressure	1.0993×10^2	-7.4713×10^3	13.988	1.5281×10^{-2}	1.0	(A.71)
Liquid viscosity	-7.2880	1.0653×10^3	-6.6570×10^{-1}			(A.77)
Vapor viscosity	3.0663×10^{-7}	6.9655×10^{-1}	2.05×10^2			(A.75)
Liquid thermal conductivity	2.837×10^{-4}	-2.81×10^{-7}	0	0		(A.83)
Vapor thermal conductivity	-7.7630×10^{-3}	1.0279	-7.436×10^7	6.77×10^9	0	(A.83)

Table A.3: Pure component coefficients for different properties of isopropanol C_3H_8O , ($i = 2$)

Property	A_i	B_i	C_i	D_i	E_i	Equation
Liquid heat capacity	4.664×10^2	-4.1086	1.4506×10^{-2}	-1.4126×10^{-5}		(A.35)
Vapor heat capacity	3.321×10^{-3}	35.573×10^{-5}	-20.987×10^{-8}	48.368×10^{-12}		(A.35),(A.18)
Heat of vaporization	5.698×10^1	8.700×10^{-2}	3.007×10^{-1}			(A.39)
Liquid molar volume	1.18×10^3	2.6475×10^{-1}	5.0831×10^2	2.43×10^{-1}		(A.66)
Vapor pressure	92.935	-8.1771×10^3	-10.031	3.9988×10^{-6}	2.0	(A.71)
Liquid viscosity	-8.2300	2.2822×10^3	-9.8495×10^{-1}			(A.77)
Vapor viscosity	1.9993×10^{-7}	7.2330×10^{-1}	1.78×10^2			(A.75)
Liquid thermal conductivity	2.029×10^{-4}	-2.2780×10^{-7}	0	0		(A.83)
Vapor thermal conductivity	-80.642×10^{-3}	-1.4549	-6.0442×10^2	0		(A.82)

Table A.4: Geometry parameters of Sulzer CY packing (Kister, 1992).

θ (deg)	S_c (mm)	h_c (mm)	B (mm)	ϵ^6	a_p (m^2/m^3)
45	6.3	4.5	9.0	0.85	700

A.4 List of properties and variables used in distillation models

P	Pressure
T^p	Temperature in the phase p
x	Composition of the light component in the liquid phase
y	Composition of the light component in the vapor phase
M_t^p	Total molar holdup of the phase p
L	Liquid molar flow
V	Vapor molar flow
E^p	Energy holdup in the phase p
γ_i	Activity coefficient of component i
Λ_i	Binary interaction parameter
ρ_t^p	Mass density of the phase p
c_t^p	Molar densities for phase p
v_t^p	Molar volumes of phase p
D^p	Diffusion coefficients for phase p
H^p	Enthalpies for phase p
ΔH^{mix}	Heat of mixing
h_t^L	Fractional liquid holdup
$C_{P,m}^p$	Molar heat capacities of phase p
C_P^p	Heat capacities phase p
Q^p	Heat losses for phase p
ΔH_i^{vap}	Heat of vaporization for component i
h^p	Heat transfer coefficients for phase p
K_i	Vapor-liquid ratio for the i component
P_i^s	Vapor pressure for the i component
k^V	Mass transfer coefficients for phase p
M_t^V	Molar holdups for phase p
\bar{H}^V	Partial molar enthalpies for phase p
ΔP_j	Pressure drop
η_t^V	Viscosity for phase p
u^V	Velocities for phase p
λ^V	Thermal conductivities for phase p

Bibliography

- J. Albersmeyer and M. Diehl. The lifted newton method and its application in optimization. *SIAM*, 20:1655–1684, 2010.
- F. Allgöwer, R. Findeisen, and Z. Nagy. Nonlinear model predictive control: from theory to application. *Journal of the chinese institute of chemical engineers*, 35(3):299–315, 2004.
- J. Annan and J. Hargreaves. Efficient parameter estimation for a highly chaotic system. *Tellus*, 56:520–526, 2000.
- U. M. Ascher and L. R. Petzold. *Computer methods for ordinary differential equations and differential-algebraic equations*. SIAM Publications, 1998.
- J. Baumgarte. Stabilization of constraints and integrals of the motion in dynamical systems. *Computer methods in applied mechanics and engineering*, 1(1):1–16, 1972.
- R. E. Bellman. *Dynamic programming*. Princeton university press, 1957.
- L. T. Biegler. Solution of dynamic optimization problems by successive quadratic programming and orthogonal collocation. *Computers & chemical engineering*, 8(3/4):243–248, 1984.
- L. T. Biegler, A. M. Cervantes, and A. Wachter. Advances in simultaneous strategies for dynamic process optimization. *Chemical Engineering Science*, 57(4):575–593, 2002.
- R. Billet and M. Schultes. A physical model for the prediction of liquid hold-up in two-phase countercurrent columns. *Chemical Engineering & Technology*, 16(6):370–375, 1993.
- R. Billet and M. Schultes. Prediction of mass transfer columns with dumped and arranged packings. *Trans IChemE*, 77:498–504, 1999.
- T. Binder, A. Cruse, C. Cruz-Villar, and W. Marquardt. *Computer and Chemical Engineering Journal*, 24:1201–1207, 2001.

- H. Bock and K. Plitt. A multiple shooting algorithm for direct solution of optimal control problems. In *Proc. 9th IFAC world congress*, pages 246–247, Budapest, Hungary, July 1984.
- J. Bonilla, M. Diehl, B. De Moor, and J. Van Impe. A nonlinear least squares estimation procedure without initial parameter guesses. In *Proceedings of the 47th IEEE Conference on Decision and Control*, pages 5519–5524, Cancún, México, December 2008.
- J. Bonilla, M. Diehl, F. Logist, B. De Moor, and J. Van Impe. A convex approximation for parameter estimation involving parameter-affine dynamic models. In *Joint 48th IEEE Conference on Decision and Control and 28th Chinese Control Conference*, pages 4670–4675, Shanghai, China, December 2009.
- J. Bonilla, F. Logist, B. De Moor, and J. Van Impe. Parameter estimation of a rigorous rate base model for distillation in packed columns. In *18th World Congress of the International Federation of Automatic Control*, 2011. Accepted.
- S. Boyd and L. Vandenberghe. *Convex Optimization*. Cambridge University Press, Cambridge, first edition, 2006.
- S. Boyd, C. Crusius, and A. Hansson. Control applications of nonlinear convex programming. *Journal of process control*, 8(5-6):313–324, 1998.
- M. A. Branch and A. Grace. *Optimization Toolbox User's Guide, Version 2*. 24 Prime Park Way, Natick, MA 01760-1500, 2002.
- J. L. Bravo and J. R. Fair. Generalized correlation for mass transfer in packed distillation columns. *Industrial Engineering Chemical Research*, (21):162–170, 1982.
- J. L. Bravo, J. A. Rocha, and J. R. Fair. Pressure drop in structured packing. *Hydrocarbon processing*, pages 45–49, March 1986.
- A. E. Bryson and Y. C. Ho. *Applied optimal control: optimization, estimation and control*. Taylor & Francis, 1975.
- A. Cervantes and L. T. Biegler. Optimization strategies for dynamic systems. In C. Floudas and P. Pardalos, editors, *Encyclopedia of optimization*. Kluwer Academic Publishers, Dordrecht, 1999.
- B. Chachuat, A. B. Singer, and P. I. Barton. Global solution of dynamic optimization and mixed-integer dynamic optimization. *Industrial Engineering Chemical Research*, 45(25):8373–8392, 2006.
- J. Christensen. *Handbook of heats of mixing*. Wiley, 1982.

- T. E. Daubert and R. P. Danner. *Physical and thermodynamic properties of pure chemicals*. Taylor & Francis Inc., 1989.
- B. Demeulenaere, J. Swevers, and J. D. Schutter. A convex optimization framework for dynamic balancing of planar linkages. In *Proceedings of the international conference on noise and vibration*, 2004.
- S. Dewulf. Ontwerp en analyse van een mechanistisch model voor de cit-destillatietoren (in dutch). Master's thesis, Department of Chemical Engineering, Katholieke Universiteit Leuven, 2009.
- M. Diehl. *Real time optimization for large scale non-linear processes*. PhD thesis, Interdisziplinäres Zentrum für Wissenschaftliches (IWR), University of Heidelberg, 2002.
- M. Diehl, I. Uslu, R. Findensen, S. Schwarzkopf, F. Allgöwer, H. G. Bock, T. Bürner, E. D. Gilles, A. Kienle, J. P. Schölder, and E. Stein. *Real-Time optimization for a large scale process: Nonlinear model predictive control of a high purity distillation column*, chapter Online optimization of large scale systems, pages 363–383. Springer, 2001.
- S. Engell. Feedback control for optimal process operation. *Journal of process control*, 17:203–219, 2007.
- R. Findeisen and F. Allgöwer. An introduction to nonlinear model predictive control. In *21st Benelux meeting on systems and controls.*, 2002.
- P. Flatby, S. Skogestad, and P. Lundström. Rigorous dynamic simulation of distillation columns based on UV-flash. In *IFAC symposium ADCHEM*, 1994.
- C. A. Floudas, P. M. Pardalos, C. S. Adjiman, W. R. Esposito, Z. H. Gumus, S. T. Harding, J. L. Klepeis, C. A. Meyer, and C. A. Schweiger. *Handbook of test problems in local and global optimization*. in nonconvex optimization and its applications. Kluwert Academic Publishers, Dordrecht, The Netherlands, 1999.
- R. Gani and I. Cameron. Modelling for dynamic simulation of chemical process: the index problem. *Chemical engineering science*, 47 (5):1311–1315, 1992.
- R. Gani, C. A. Ruiz, and I. T. Cameron. A generalized model for distillation columns-I: Model description and applications. *Computers & chemical engineering*, 10:181–198, 1986.
- P. E. Gill, E. D., W. Murray, M. A. Saunders, and M. H. Wright. Sparse matrix methods in optimization. *SIAM Journal of scientific statistical computing*, 5: 562–589, 1984.
- J. Gmehling and U. Onken. *Vapor-Liquid equilibrium data collection, Organic Hydroxy Compounds: Alcohols*. DECHEMA, Chemistry Data Series, 1977.

- N. Gould. On the convergence of sequential penalty function methods for constrained minimization. *SIAM Journal of numerical analysis*, 26(1):107–128, 1989.
- I. E. Grossmann and A. W. Westerberg. Research challenges in process system engineering. *AIChE Journal*, 46(9):1700–1703, 2000.
- M. Guo, S. Wang, J. Repke, and G. Wozny. Nonequilibrium model and parameter estimation on three-phase distillation in a packed column. In *Proceedings of the 5th world congress on intelligent control and automation*, 2004.
- E. Hairer and G. Wanner. *Solving ordinary differential equations II: Stiff and differential-algebraic problems*. Springer series in computational mathematics, 2002.
- M. P. Harold and B. A. Ogunnaike. Process engineering in the evolving chemical industry. *AIChE Journal*, 46(11):2123–2127, 2000.
- A. C. Hindmarsh, P. N. Brown, K. E. Grant, S. L. Lee, R. Serban, D. E. Shumaker, and C. S. Woodward. SUNDIALS: Suite of nonlinear and differential/algebraic equation solvers. *ACM Transactions on mathematical software*, 31(3):363–396, 2005.
- R. Horst and H. Tuy. *Global optimization: Deterministic approaches*. Springer-Verlag, Berlin, 3rd edition, 1996.
- H. Ingham, I. J. Dunn, E. Heinze, and J. E. Přenosil. *Chemical engineering dynamics: An Introduction to modelling and computer simulation*. Wiley-VCH, Weinheim, Germany, second edition, 2000.
- A. Isidori. *Nonlinear control systems*. Springer-Verlag, 1989.
- H. F. Johnstone and R. L. Pigford. Distillation in a wetted wall column. *Transactions of the american institute of chemical engineers*, (38):25–51, 1942.
- S. Karacan, H. Hapoglu, and M. Alpbaz. Multivariable system identification and generic model control of a laboratory scale packed distillation column. *Applied thermal engineering*, 27:1017–1028, 2007.
- N. Karmarkar. A new polynomial-time algorithm for linear programming. *Combinatorica*, 4:373–395, 1984.
- W. Karush. Minima of functions of several variables with inequalities as side conditions. Master’s thesis, Department of mathematics. Chicago University, 1939.
- E. Kenig and P. Seferlis. Modeling reactive absorption. *Chemical Engineering Progress*, pages 65–73, January 2009.

- R. Krishnamurthy and R. Taylor. A nonequilibrium stage model for multicomponent separation processes: Part I model description and method of solution. *AIChE Journal.*, 31(3):449–456, 1985.
- D. Kirk. *Optimal control theory: An introduction*. Prentice Hall, 1970.
- H. Z. Kister. *Distillation design*. McGraw-Hill, 1992.
- H. A. Kooijman. *Dynamic nonequilibrium column simulation*. PhD thesis, Clarkson University, 1995.
- E. Kostina. Robust parameter estimation in dynamic systems. *Optimization and engineering*, 5(4):461–484, 2004.
- D. Kraft. On converting optimal control problems into nonlinear programming problems. In K. Schittkowski, editor, *Computational mathematical programming.*, volume F15 of *NATO ASI*, pages 261–280. Springer, 1985.
- L. U. Kreul, A. Górak, C. Dittrich, and P. I. Barton. Dynamic catalytic distillation: Advanced simulation and experimental validation. *Computer & chemical engineering journal*, 22:371–378, 1998.
- H. W. Kuhn and W. Tucker. Nonlinear programming problems. In J. Neyman, editor, *Second Berkeley symposium on mathematical statistics and probability*, 1951.
- D. J. Lea, M. R. Allen, and T. W. N. Haine. Sensitivity analysis of the climate of a chaotic system. *Tellus*, 52(A):523–532, 2000.
- D. B. Leineweber. *Efficient reduced SQP methods for optimization of chemical process described by large sparse DAE models*. PhD thesis, Interdisziplinäres Zentrum für Wissenschaftliches Rechnen (IWR). University of Heidelberg, 1998.
- L. Ljung. Prediction error estimation methods. *Circuits systems signal processing*, 21(1):11–21, 2002.
- C. E. Long, P. K. Polisetty, and E. P. Gatzke. Nonlinear model predictive control using a global optimization approach. *Journal of process control*, 16:365–643, 2006.
- Z. Lukszo, M. Weijnen, R. Negenborn, B. D. Schutter, and M. Ilić. Challenges for process system engineering in infrastructure operation and control. In W. Marquardt and C. Pantelides, editors, *16th European symposium on computer aided process engineering and 9th international symposium on process systems engineering*, volume 21 of *Computer-Aided Chemical Engineering*, pages 95–100. Elsevier, 2006.

- S. E. Mattsson and G. Söderlind. Index reduction in differential-algebraic equations using dummy derivatives. *SIAM journal of scientific computing*, 14(3):677 – 692, 1993.
- G. McCormick. Computability of global solutions to factorable nonconvex programs: part I - convex underestimating problems. *Mathematical programming*, 10(1):147–175, 1976.
- J. Moré and Z. Wu. Global continuation for distance geometry problems. *SIAM Journal on optimization*, 7(3):814–836, 2006.
- Y. Nesterov and A. Nemirovski. *Interior points polynomial methods in convex programming*. SIAM Publications, Philadelphia, 1st edition, 1995.
- J. Nocedal and S. Wright. *Numerical optimization*. Springer, New York, second edition, 2006.
- K. Ogata. *Modern control engineering*. Prentice Hall, 2010.
- T. N. Palmer. Extended range atmospheric prediction and the Lorenz models. *American meteorological society*, 74(1):49–55, 1993.
- C. C. Pantelides. Consistent initialization of differential-algebraic systems. *SIAM Journal of scientific statistical computing*, 9(2):213–231, 1988.
- C. C. Pantelides, D. Gritsis, K. R. Morrison, and R. W. H. Sargent. The mathematical modelling of transient systems using differential-algebraic equations. *Computers and chemical engineering*, 12(5):449–454, 1988.
- J. Peng, T. F. Edgar, and R. B. Eldridge. Dynamic rate-base and equilibrium models for packed reactive distillation column. *Chemical Engineering Science*, 58:2671–2680, 2003.
- R. H. Perry and D. Green. *Perry's chemical engineers' handbook*. McGraw-Hill, 1985.
- L. S. Pontryagin. *The Mathematical Theory of Optimal Processes*. Interscience publishers, New York, 1962.
- R. C. Reid, J. M. Prausnitz, and B. E. Poling. *The properties of gases and liquids*. McGraw-Hill, New York, fourth edition, 1987.
- S. M. Robinson. Generalized equations and their solution, part II: Application to nonlinear programming. MRC Technical summary report 2048, University of Wisconsin, Madison, 1980.
- J. A. Rossiter. *Model-based predictive control, a practical approach*. CRC Press, USA, first edition, 2003.

- S. I. Sandler. *Chemical and engineering thermodynamics*. Wiley & Sons, Inc., 1999.
- R. W. H. Sargent and G. R. Sullivan. The development of an efficient optimal control package. *Optimization techniques: lecture notes in control and information sciences*, 7:158–168,, 1978.
- J. D. Seader and E. J. Henley. *Separation process principles*. Wiley & Sons, Inc., 2006.
- L. F. Shampine, M. W. Reichelt, and J. A. Kierzenka. Solving index-1 DAEs in MATLAB and Simulink,. *SIAM Review*, 41(3):538–552, 1999.
- A. B. Singer and P. I. Barton. Global optimization with nonlinear ordinary differential equations. *Journal of global optimization*, 34(2):159–190, 2006.
- P. B. Sistu and B. W. Bequette. Model predictive control of processes with input multiplicities. *Chemical engineering science*, 50(6):921–936, 1995.
- S. Skogestad. Dynamics and control of distillation columns - a critical survey. In *IFAC-symposium DYCORN 92*, April 1992.
- S. Skogestad. Dynamics and control of distillation columns - a tutorial introduction. *Trans IChemE*, 75:539–562, 1997. A6 special issue: Distillation.
- A. Sloley. Effectively control column pressure. *Chemical engineering progress*, pages 39–48, January 2001.
- R. Taylor and R. Krishna. *Multicomponent mass transfer*. Wiley & Sons, Inc., New York, 1993.
- R. Taylor, H. A. Kooijman, and J.-S. Hung. A second generation nonequilibrium model for computer simulation of multicomponent separation process. *Computer & chemical engineering journal*, 18(3):205–217, 1994.
- V. Vassiliadis. *Computational solution of dynamic optimization problems with general differential-algebraic constraints*. PhD thesis, University of London, London. UK., 1993.
- D. Verscheure, B. Demeulenaere, J. Swevers, J. D. Schutter, and M. Diehl. time-optimal path tracking for robots: a convex optimization approach. *IEEE Transactions on automatic control*, 54:2318–2327, 2009.
- J. B. Waller and J. M. Böling. Multi-variable nonlinear MPC of an ill-conditioned distillation columns. *Journal of process control*, 15:23–29, 2005.
- L. T. Watson. Theory of globally convergent probability-one homotopies for nonlinear programming. *SIAM Journal of optimization*, 11(3):761–780, 2000.

- L. T. Watson. *Encyclopedia of optimization*, chapter Globally convergent homotopy methods, pages 353–358. Kluwer Academic Publishers, 2001.
- L. T. Watson. Probability-one homotopies in computational science. *Journal of computational and applied mathematics*, 140:785–807, 2002.
- L. T. Watson, S. C. Billups, and A. P. Morgan. Hompack: A suite of codes for globally convergent homotopy algorithms. *ACM Transactions on mathematical software.*, 13(3):281–310, 1987.
- G. M. Wilson. Vapor-Liquid equilibrium XI: A new expression for the excess free energy of mixing. *Journal of the American Chemical Society*, 86:127–130, 1964.
- B. Wittgens and S. Skogestad. Evaluation of dynamic models of distillation columns with emphasis on the initial response. *Modeling, identification and control*, 21:83–103, 2000.
- N. Yokoyama, S. Suzuki, and T. Tsuchiya. Convergence acceleration of direct trajectory optimization using novel Hessian calculation methods. *Journal of optimization theory and applications*, 136:297–319, 2008.

Curriculum vitae



Julián Eduardo Bonilla Alarcón was born in Buenavista (Sucre), Colombia in 1980. He went to Colegio Nacional San Simón (Ibagué, Colombia) where he graduated in 1995 with honors. He received his degree as Electronics Engineer (*meritorious*) with the design and implementation of a fuzzy logic controller on a field programmable gate array, from the Universidad Distrital Fco. José de Caldas (Bogotá, Colombia) in April 2001. From January 2002 until June 2005 he was teacher at the electronics departments of Universidad Antonio Nariño and Universidad de Ibagué (Ibagué, Colombia).

In February 2006 he obtained his master degree (M.Sc.) in process control from the Universidad de Ibagué (Ibagué, Colombia) in agreement with the Katholieke Universiteit Leuven and Universiteit Gent (Belgium). From July 2005 until February 2007 he was research cooperater at the Department of Electrical Energy Systems and Automation (EESA) Universiteit Gent (Gent, Belgium) where he worked in the predictive control of power electronics drives under the supervision of prof. R. De Keyser. From March 2007 until May 2011 he pursued a PhD degree in engineering at the Katholieke Universiteit Leuven (Belgium) under the main supervision of prof. J. Van Impe. The results of this research are summarized in this dissertation. Since June 2011 he works as controls engineer in the Controls and Power Electronics Center of Excellence at General Electric Global Research (Munich, Germany).

Publications by the author

Journal papers

International

- J. Bonilla, M. Diehl, F. Logist, B. De Moor, J. Van Impe, A convexity-based homotopy method for nonlinear optimization in model predictive control. *Optimal control applications and methods*, Vol 31 (5), p. 393–414, 2010.
- J. Bonilla, M. Diehl, F. Logist, B. De Moor, J. Van Impe. An automatic initialization procedure in parameter estimation problems with parameter-affine dynamic models. *Computers and Chemical Engineering*, 34, 953–964, 2010.
- J. Bonilla, F. Logist, J. Degrève, B. De Moor, and J. Van Impe. Rate based model for distillation in packed columns: Sensitivity analysis and structure exploitation. *Submitted to Computers and Chemical Engineering*, 2011.
- J. Bonilla, F. Logist, J. Degrève, B. De Moor, and J. Van Impe. Rate based model for distillation in packed columns: Dynamic simulation and the index problem. *Submitted to Chemical Engineering Science*, 2011.

National

- J. Bonilla, M. Megarejo and V. Grisales. Design of a fuzzy controller on programmable cells (in spanish). In *Revista Científica*, Universidad Distrital Fco. Jose De Caldas. Centro de Investigaciones y Desarrollo Científico. ISSN 0124-2253 . Bogotá-Colombia. August 2001.

Conference papers

International

- J. Bonilla, F. Logist, B. De Moor, and J. Van Impe. Parameter estimation of a rigorous rate based model for distillation in packed columns. *In proceedings of the 18th World Congress of the International Federation of Automatic Control*, Milan-Italy, August 2011.
- J. Bonilla, M. Diehl, F. Logist, B. De Moor, and J. Van Impe. A suboptimal solution to nonconvex optimal control problems involving input-affine dynamic models. *20th European Symposium on Computer Aided Process Engineering-ESCAPE20*, Ischia-Italy, 2010.
- J. Bonilla, M. Diehl, F. Logist, B. De Moor, and J. Van Impe. A convex approximation for parameter estimation involving parameter-affine dynamic models. *In Joint 48th IEEE Conference on Decision and Control and 28th Chinese Control Conference*, p. 4670–4675, Shanghai-China, December, 2009.
- J. Bonilla, M. Diehl, B. De Moor, J. Van Impe. A nonlinear least squares estimation procedure without initial parameter guesses. *In Proceedings of the 47th IEEE Conference on Decision and Control* pp. 5519–5524, Cancún-Mexico, December 2008.
- D. Plaza, R. De Keyser, J. Bonilla. Model Predictive and Sliding Mode Control of a Boost Converter. *In proceedings of the International Symposium on Power Electronics, Electrical Drives, Automation and Motion, SPEEDAM*, pp 37–42, Ischia-Italy 2008.
- J. Bonilla, R. De Keyser. Nonlinear Model Predictive Control for a DC-DC converter: A NEPSAC approach. *In proceedings of the European Control Conference ECC07*, pp 1634–1641. Koss-Greece 2007.
- J. Bonilla, R. De Keyser, M. Diehl and J. Espinosa. Fast NMPC of a DC-DC converter: An Exact Newton Real-Time Iteration Approach. *In proceedings of the 7th IFAC Symposium on Nonlinear Control Systems NOLCOS*. pp. 194–199, Pretoria-South Africa, 2007.
- R. De Keyser, J. Bonilla and C. Ionescu. A comparative study of several control techniques applied to a boost converter. *IEEE 10th International Conference on Optimization of Electrical and Electronic Equipment OPTIM*. pp. 71–78. Brasov-Romania 2006. ISBN 973-635-704-X.
- J. Bonilla, M. Melgarejo and V. Grisales. Genetic Tuned FPGA based PD fuzzy LUT controller. *Proceedings of 10th IEEE international Conference*

on fuzzy Systems, pp. 1084 – 1087. Melbourne-Australia, 2001. Cod 0-7803-7293-X.

- J. Bonilla, M. Melgarejo and V. Grisales . Design and Implementation of a FPGA-based fuzzy controller (in spanish). In proceedings of the VII workshop IBERCHIP-IWS2001, Montevideo-Uruguay 2001.

National

- J. Bonilla and A. Muñoz. Preliminary aspects to modeling and controlling an aerobic waste water bioreactor. in VII congreso de la Asociación Colombiana de Automática ACA (in spanish). Ibagué-Colombia. November 2004. ISBN 958-8028-39-6.
- A. Gutierrez, I. Ramirez, J. Bonilla, and A. Muñoz. Identification and multivariable control of a coffee dryer prototype . in VII congreso de la Asociación Colombiana de Automática ACA (in spanish). Ibagué-Colombia. November 2004, ISBN 958-8028-39-6.

Conference abstracts

- D. Ugrjumova, G. Vandersteen, R. Pintelon, B. Huyck, J. Bonilla, F. Logist and J. Van Impe. Identification of distillation columns using multisine excitation. *Book of abstracts of the 30th Benelux Meeting on Systems and Control*. Lommel-Belgium. 2011.
- J. Bonilla, F. Logist, M. Diehl, B. De Moor, and J. Van Impe. A Convex Approximation for Parameter Estimation Involving Parameter-Affine Dynamic Models, *14th Belgian-French-German Conference on Optimization*. Leuven-Belgium, September 14-18, 2009.
- J. Bonilla, F. Logist, M. Diehl, B. De Moor, and J. Van Impe. (2009). An initialization procedure for parameter estimation problems using simultaneous Gauss-Newton method. *Book of abstracts of the 28th Benelux Meeting on Systems and Control*. 28th Benelux Meeting on Systems and Control. Spa-Belgium, March 16-18, 2009.
- J. Bonilla, M. Diehl, B. De Moor, and J. Van Impe. Convexity-based method for the initialization of optimal control problems. *Book of abstracts 27th Benelux Meeting on Systems and Control: vol. 27*. Benelux Meeting on Systems and Control. Heeze-The Netherlands, March 2008, p. 130, Abstract No. ThP03-4.

- J. Bonilla, M. Diehl, B. De Moor, and J. Van Impe. A convexity-Based Homotopy Method for Nonlinear Optimization in Model Predictive Control. *Book of abstracts of the International Conference on Nonconvex Programming. International Conference on Nonconvex Programming.* Rouen-France, December 17-21, 2007.
- J. Bonilla, R. De Keyser, M. Diehl. Fast NMPC of a DC-DC Converter. *In Czech-French-German conference on optimization CFG07.* Heidelberg-Germany. 2007.
- J. Bonilla, R. De Keyser. Model Predictive Control Applied to Power Electronic Drives: A simulation study. *26th Benelux Meeting on Systems and Control.* Lommel -Belgium. 2007.

Arenberg Doctoral School of Science, Engineering & Technology

Faculty of Engineering

Department of Chemical Engineering

Research group BioTeC

W. de Croylaan 46, 3001 Leuven-Belgium